HYDRAULIC MODELLING OF A HORIZONTAL SUBSURFACE FLOW CONSTRUCTED WETLAND

UNIVERSITY OF THE
WITWATERSRAND,
JOHANNESBURG

Ricky Bonner

A dissertation submitted to the Faculty of Engineering and the Built Environment, University of the Witwatersrand, Johannesburg, in fulfilment of the requirements for the degree of Master of Science in Engineering.

Johannesburg 2016

Declaration

I declare that this dissertation is my own unaided work. It is being submitted for the degree of Master of Science in Engineering to the University of the Witwatersrand, Johannesburg. It has not been submitted before for any degree or examination to any other University.

_____

Ricky Bonner

15th day of November, 2016

Summary

Horizontal subsurface flow constructed wetlands (HSSF CWs) are being considered in South Africa as an alternative waste water treatment technology which is low in capital costs and typically requires less operational infrastructure when compared to conventional treatment technologies. HSSF CWs may thus be a potential solution for solving the challenge of ensuring reliable access to clean water for rural communities whose municipalities may not be able to afford the construction of a waste water treatment plant as well as not being able to supply sufficient technical expertise for the operation thereof. Proper design of HSSF CWs requires a detailed investigation into the hydraulic behaviour as it has a direct effect on the treatment performance in these systems.

In this study, three available hydraulic modelling methodologies for HSSF CWs were compared and these are the impulse, step change integral and step change derivative modelling methodologies. Hydraulic data were generated from planted and unplanted pilot scale HSSF CWs using residence time distribution (RTD) studies and the modelling results using each methodology were compared. It was found that each methodology was capable of suggesting a different hydraulic behaviour for the same system being studied and since it is not possible to evaluate an analytical answer to the problem independently it was not possible to determine which modelling methodology was the most accurate. Practical limitations of the experiments used to feed hydraulic data to the respective methodologies were also highlighted. Despite a well-designed sampling regime it was not possible to capture sufficient data surrounding the peak of the impulse response curve and may have impacted negatively on the modelling results. No such difficulties were encountered with the step change tracer experiments. The mathematical techniques which each methodology employs were also critically assessed. It was found that numerical differentiation in the step change derivative modelling approach introduced noise into the RTD curve and may have affected subsequent results. Ultimately each methodology has its own associated strengths and weaknesses and choice of methodology may be dictated by other factors such as cost to set up the hydraulic experiment as well as equipment availability.

Tasks two and three of this dissertation dealt with how Biomimicry can be used as a tool to develop more sustainable HSSF CW designs and hydraulic modelling processes. In task two, hydraulic data generated from the first task were used to develop estimates of the velocity profiles inside a

planted HSSF CW to identify regions most prone to clogging, a phenomenon which would be a serious concern for rural communities whose sole water treatment system would be the CW. Biomimetic design principles were combined with the modelling results to develop a modular system design allowing for sections of the CW to be removed for cleaning while still allowing for continuous treatment of the waste water.

Task three explored the use of heat as a hydraulic tracer. Heat is considered more environmentally friendly when compared to chemicals as tracers as the CW can equilibrate to ambient conditions post study and the effluent does not require dedicated disposal infrastructure. Heat is non-conservative in these systems and processes such as absorption by the subsurface media and loss to the surroundings distort the hydraulic response curve from which the hydraulic behaviour cannot be directly obtained. In this study a mathematical model was developed which maps a heat tracer response curve to one which would be obtained if a conservative chemical tracer were used. It was tested by conducting a combined heat-chemical tracer study on an unplanted laboratory-scale HSSF CW and the predicted chemical response curve was compared with the actual experimental response curve. The model performed satisfactorily indicated by a 5% and 6% relative difference in the Peclet number (Pe) and mean of the RTD respectively. In each of these chapters, an abstract is provided which summarizes the main findings of the study.

To my family

And my dearest Rivki

Acknowledgements

I wish to thank the following people for their support and assistance:

- Professor Craig Sheridan for his outstanding support and supervision;
- Dr. Uwe Kappelmeyer and Lara Aylward for their guidance and support;
- The staff at the School of Chemical and Metallurgical Engineering;
- The NRF-DAAD joint research initiative; and
- Golder Associates.

Contents

Table of Figures

List of Tables

Nomenclature

α_l	Longitudinal solute dispersivity
α_t	Transverse solute dispersivity
$\alpha_{f/s}$	Interfacial mass transfer coefficient
A_s	Superficial surface area
AR_w	Aspect ratio
a_v	Interfacial surface area
β_l	Longitudinal thermal dispersivity
β_t	Transverse thermal dispersivity
$C(t)$	Concentration of dye at time t
C^*	Background concentration
$C_{initial}$	Initial wetland tracer concentration
C_{inlet}	Wetland inlet tracer concentration
C_{max}	Concentration of chemical dye as $t \to \infty$
C_{out}	Outlet concentration
C_{pf}	Fluid specific heat capacity
C_{ps}	Solid specific heat capacity
$C_{p,gravel}$	Specific heat capacity of gravel
$C_{p,water}$	Specific heat capacity of water
c_i	Parameter i in 4-parameter logistics equation
$\delta_{pinewood}$	Thickness of pinewood
$\delta_{polystyrene}$	Thickness of polystyrene
$\delta_{pond\ liner}$	Thickness of pond liner
D	Chemical dispersion coefficient
$D_{heat,f}$	Heat dispersion in fluid phase
D_m	Molecular diffusion coefficient
D_n	Dimensionless dispersion number
D_p	Mean solid particle diameter
ε	Packed bed porosity
η	Dynamic viscosity
e	Effective volume utilization
$E(t)$	Residence time distribution function
$erfc$	Complementary error function
$F(t)$	Cumulative distribution function
γ	Zero order production coefficient
$h_{f/s}$	Interfacial heat transfer coefficient

H	Packed bed depth
h	Hydraulic head
h_{air}	Convective heat transfer coefficient of air
h_{water}	Convective heat transfer coefficient of water
J	Dispersive flux
K	Hydraulic conductivity
K_d	Distribution coefficient
k_{rate}	Reaction rate constant
k_{gravel}	Thermal conductivity of gravel
k_s	Solid thermal conductivity
k_{water}	Thermal conductivity of water
k_0	System thermal conductivity
$k_{pinewood}$	Thermal conductivity of pinewood
$k_{polystyrene}$	Thermal conductivity of polystyrene
$k_{pond\ liner}$	Thermal conductivity of pond liner
Λ	Hydraulic efficiency factor
λ_T	Heat dispersion coefficient
L	Packed bed length
μ	First order decay coefficient
M_0	Mass of tracer injected in impulse experiment
ΔM	Mass of tracer leaving system between t and $t + \Delta t$
N	Number of equally sized CSTRs placed in series
Pe	Peclet number
ρ_f	Fluid density
ρ_s	Solid density
ρ_b	Bulk density
ρ_{gravel}	Gravel density
ρ_{water}	Water density
R	Chemical retardation factor
R_T	Thermal retardation factor
Re_p	Reynolds number for packed beds
σ^2	Variance
σ_θ^2	Normalized variance
S	Adsorbed solid concentration
SC	Short circuiting ratio
τ	Nominal residence time
Θ	Normalized time
$E(\Theta)$	Normalized residence time distribution function
$F(\Theta)$	Normalized cumulative distribution function

t	Time
$\bar{t}_m$	Mean of residence time distribution
T	Temperature
T_a	Ambient temperature
T_f	Fluid temperature
$T_{initial}$	Initial wetland temperature
T_{inlet}	Wetland inlet temperature
T_s	Solid temperature
u	Pore water velocity
u_s	Superficial velocity
U_{wall}	Wall heat transfer coefficient
$\dot{v}$	Volumetric flow rate
$\dot{v}_a$	Volumetric flow rate through active region
$\dot{v}_b$	Bypass volumetric flow rate
$\dot{v}_r$	Recycle volumetric flow rate
V	Working volume of reactor
V_p	Plug flow volume
V_m	Mixed flow volume
V_{eff}	Working volume minus dead volume of reactor
V_{total}	Total volume of reactor
W	Packed bed width
x	Distance

Acronyms

DEA	Department of Environmental Affairs
DST	Department of Science and Technology
IMWaRU	Industrial and Mining Water Research Unit
IWA	International Water Association
NASA	National Aeronautics and Space Administration
SANBI	South African National Biodiversity Institute
WISA	Water Institute of Southern Africa
CW	Constructed wetland
HSSF CW	Horizontal subsurface flow constructed wetland
SF CW	Surface flow constructed wetland
SSF CW	Subsurface flow constructed wetlands
VF CW	Vertical flow constructed wetland
BOD	Biological oxygen demand
COD	Chemical oxygen demand
DOM	Dissolved organic matter
POM	Particulate organic matter
RTD	Residence time distribution
PFR	Plug flow reactor
CSTR	Continuously stirred tank reactor
TIS	Tanks in series model
GA	Genetic algorithm
PE	Polyethylene
HDPE	High density polyethylene
PVC	Polyvinyl chloride

1. Introduction

South Africa is currently facing water supply and quality challenges (Hedden and Cilliers, 2014). The development of necessary water treatment technology is thus of utmost importance, with national government providing support for the improvement of water quality and supply infrastructure (Tibane and Vermeulen, 2013). This is evidenced by the fact that the Department of Science and Technology (DST) is in the process of defining a niche for it to support the ecological infrastructure work being performed by the Department of Environmental Affairs (DEA) and the South African National Biodiversity Institute (SANBI). Biomimicry is being looked at closely by the DST as a potential tool for developing innovative ecologically-integrated water treatment solutions (Dama-Fakir *et al.*, 2012). Biomimicry can be classified as an applied science which involves the careful study of nature's systems, designs and processes to derive inspiration for the purposes of solving human problems (El-Zeiny, 2012). Nature has developed unique ways of solving problems which humans are encountering today (Zarro, 2014). The mechanisms which animals, plants and microbes currently use are the products of millions of years of rigorous testing (Bar-Cohen, 2006).

One of the main challenges in a South African context is to develop infrastructure that allows for easy and reliable access to clean water for rural communities (Majuru *et al.*, 2012). Horizontal subsurface flow constructed wetlands (HSSF CWs) are an attractive solution to the problem since they are a low-cost alternative to conventional waste water treatment systems (Paing and Voisin, 2005; Park, 2009) and hence their applicability is currently being explored (Ochieng *et al.*, 2010). Like other packed bed reactors, the hydrodynamic behaviour of these systems has been simplified as being ideal plug flow (Werner and Kadlec, 2000). This implies that every parcel of waste water spends the same amount of time inside the system. The subsurface is, however, heterogeneous in nature. The presence of complex plant root structures; the growth of bacterial biofilms within the wetland matrix; the entrapment of suspended solids and the precipitation of heavy metals originating from the feed wastewater cause clogging within different regions of the subsurface media and results in both spatially and temporally-dependent flow resistance (Sheoran and Sheoran, 2006; Suliman *et al.*, 2006a; Knowles *et al.*, 2011). The variation in flow resistance creates non-uniform flow velocity profiles and, hence, different pockets of water reside within the

system for different lengths of time, giving rise to a residence time distribution (RTD) and a mean of the RTD which is smaller than or equal to the ideal theoretical residence time (Levenspiel, 1999). Pollutant degradation models built on the ideal plug flow assumption have, thus, proved to be in the large part inaccurate (Marsili-Libelli and Checchi, 2005; Galvão *et al.*, 2010; Sheridan *et al.*, 2014a), since there is no way of incorporating the varying lengths of time spent by different pockets of waste water in contact with elements of the system which can facilitate their degradation. This may lead to the installation of an under-sized CW and an unsatisfactory production performance. Consequently, a pilot scale reactor is built beforehand and an RTD study is conducted to develop a reactor model accounting for the non-ideal flow behaviour which when coupled with kinetic data can facilitate more accurate sizing of the reactor equipment (Lima and Zaiat, 2012; Rüdisüli *et al.*, 2012).

There are three available RTD modelling methodologies for CWs and these are the impulse, step change integral and step change derivative approaches. The first approach requires data generation from an impulse response experiment whereas the latter two require data generation from a step change experiment. The first task of this dissertation was to provide a comparison of the three available modelling approaches by generating hydraulic data from pilot-scale HSSF CWs at the Industrial and Mining Water Research Unit (IMWaRU) facility at the University of the Witwatersrand, Johannesburg. The study would serve as a comprehensive reference that would assist designers in selecting the most appropriate methodology in future hydraulic studies on CWs.

Different management strategies have been developed to remediate the effects of clogging inside HSSF CWs, with two of the most prominent being excavation and washing of the bed media as well as in-situ application of cleaning chemicals such as hydrogen peroxide (Nivala *et al.*, 2012). Current CW design dictates that excavation and washing requires the whole system to be taken offline for extended periods of time (Nivala *et al.*, 2012). In-situ application of cleaning chemicals poses health and safety risks to local community members and the long-term effects which the chemicals have on wetland performance are still unknown (Nivala and Rousseau, 2009). The second task of this dissertation was to demonstrate the development of a Biomimetic CW design based on the hydraulic data obtained from the pilot-scale HSSF CWs at the IMWaRU facility in task 1. Biomimicry design principles facilitate designs which are able to adapt to changing conditions and may assist in developing a system in which an effective clogging management

strategy is integrated ensuring minimal downtime for clogging remediation and hence a more reliable water treatment facility for rural communities.

RTD studies require the addition of a soluble and inert chemical tracer into the CW feed to track the flow of waste water through the system (Chazarenc *et al.*, 2003). The long-term effects which these chemicals have on the living organisms inside the system are still relatively unknown and the effluent from the study requires dedicated disposal infrastructure. Heat has not been used previously as a tracer in CWs due to its non-conservative behaviour. However it is considered a more environmentally friendly alternative to conventional chemical tracers as the system can rapidly equilibrate to ambient conditions post-study. The third task of this dissertation was to explore the use of heat as a tracer in HSSF CWs.

1.1 Dissertation structure

This dissertation comprises six chapters. The first chapter is an introduction and the second consisting of a literature study. The three chapters which follow have each been written in the form of a scientific paper with the intention of publication in peer-reviewed journals. There is thus an overlap between the literature study presented in Chapter 2 and the literature studies presented in each of the papers and we request the readers' indulgence for this. If a paper has been submitted to a journal or has been published it has been indicated as such. The final chapter of the dissertation comprises an overall discussion and conclusion.

2. Background

2.1 What are wetlands?

Wetlands are complex ecosystems and are a transition between terrestrial and aquatic environments (Mitsch and Gosselink, 1993; Stottmeister *et al.*, 2003). Such systems typically contain soil, macrophytes and various bacteria which work as a functional unit to improve the quality of ground and surface water (Galletti *et al.*, 2010; Marchand *et al.*, 2010). A variety of physical, chemical and biological processes are used to purify the influent water (Trang *et al.*, 2010; Fan *et al.*, 2013). Physical removal processes include settling and sedimentation of heavy metals and suspended solids (Sheoran and Sheoran, 2006; El-Sheikh *et al.*, 2010). Chemical removal processes include the adsorption of metallic cations and phosphorus (Drizo *et al.*, 1999; Del Bubba *et al.*, 2003). Biological removal processes typically rely on the activity of the microorganisms present within the wetland system (Vymazal, 2007). These processes are primarily responsible for the removal of organic carbon and nitrogen from the waste water (Vohla *et al.*, 2007; Faulwetter *et al.*, 2009).

2.2 Historical development of wetlands

At the turn of the twentieth century natural wetlands were used as convenient sites for sewage water disposal due to their capabilities of storing large amounts of nutrients and toxic substances (Gopal, 1999; Vymazal, 2011). Kadlec *et al.* (2009) cite a series of such systems in North America. Relevant examples include the Brillion Marsh in Wisconsin which received municipal discharge since 1923 and the discharge of municipal water to a natural cypress swamp in Florida since 1939. The sentiment towards wetlands at this stage even caused some to hold the view that the systems were of no utilitarian value and it would be preferable to convert them into something more useful such as agricultural land (Mitsch and Gosselink, 1993; Patten, 1990).

It was only in the 1950's when Dr. Käthe Seidel of the Max Plank Institute discussed the potential benefits of constructing wetlands for water purification (Wallace, 2004). Her initial experiments entailed invesitgating the use of the common bulrush for purposes of pollutant removal (Brix, 1997). The results indicated a good potential for heavy metal and phenol degredation as well as pathogen removal (Seidel, 1964; Seidel, 1966). The experiments became more advanced in the 1960s with full-scale testing of systems used to treat domestic waste water, urban runoff and waste water from different industrial processes (Brix, 1994). Dr. Seidel's ideas inspired the development

of the *Lelystad Process* in The Netherlands in the late 1960s which essentially was a wetland system used to treat waste water from a camping site near Elburg (Jong, 1976). The work performed in Europe attracted interest from North America and the National Aeronautics and Space Administration (NASA) began experimenting with gravel-based wetland systems (Wolverton *et al.*, 1976). The work was expanded on by other researchers and it was found that bulrushes were effective in removing suspended solids, biological oxygen demand (BOD) and nitrogen (Gersberg *et al.*, 1983; Gersberg *et al.*, 1984; Gersberg *et al.*, 1986). Different designs of wetland systems were then developed such as the *Marsh Pond Meadow* which consisted of a lateral-flow marsh planted with cattails in a sand medium, a pond and a meadow planted with canary grass (Brix, 1994). Today, state-of-the-art CWs are being developed across the globe with an example being the wetland built in Glaslough, Ireland which was commissioned in 2007 (Scholz, 2011). The system is designed to treat sewage and has a design capacity of 1750 inhabitants. The system consists of a pumping station, two sludge cells used to remove solids and five vegetated cells for the purpose of general water quality improvement.

2.3 Types of constructed wetlands

CWs can be classified according to the dominant macrophyte present, the wetland hydrology and the substrate matrix employed (Vymazal, 2010; Pedescoll *et al.*, 2015). In Figure 2.1 a breakdown is provided of the possible types of CWs.

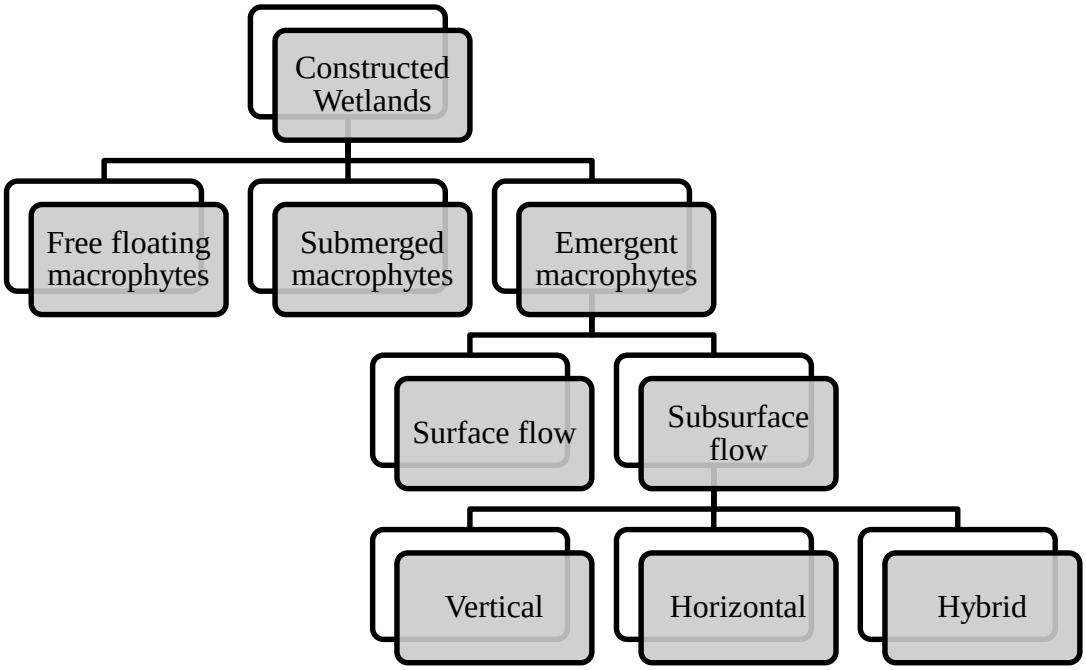

Figure 2.1: Types of CW configurations according to dominant macrophyte, flow regime and wetland matrix

2.3.1 Classification according to type of macrophyte

Plants have proven to be an important part of wetland systems since they facilitate a variety of removal mechanisms necessary for water purification (Brix, 1987; Wu *et al.*, 2011). Wetland plants can be classified under three categories: free-floating, submerged and emergent (Dhote and Dixit, 2009; Bakker *et al.*, 2013).

Free-floating macrophytes

A free-floating macrophyte's entire body except the plant roots are situated above the surface of the water (Van de Moortel *et al.*, 2010; Headley and Tanner, 2012). An illustration of free-floating macrophytes in a CW is provided in Figure 2.2.

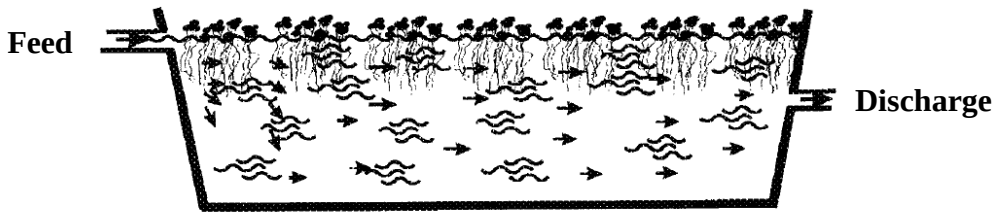

Figure 2.2: Free-floating macrophytes in CW. Adapted from Stottmeister *et al.* (2003)

Two of the most common species employed in CWs are *Eichhornia crassipes* (water hyacinth) and *Pistia stratiotes* (water lettuce) (Nahlik and Mitsch, 2006; Marchand *et al.*, 2010; Mufarrege *et al.*, 2010).

Submerged macrophytes

The submerged macrophyte's entire body is situated below the water surface and the whole body conseqeuntly plays an important role in contaminant removal (Dhote and Dixit, 2009; Chen, 2011). *Potamogeton crispus* and *Littorella uniflora* are two of the most commonly used submerged macrophytes in CWs (Dordio and Carvalho, 2013; Zhao *et al.*, 2014). An illustration of wetlands employing these particular species is provided in Figure 2.3.

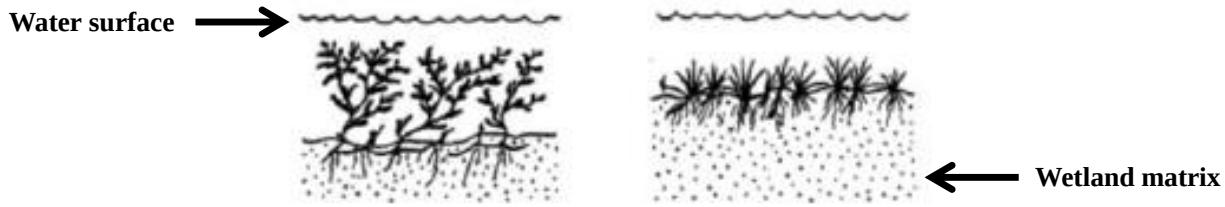

Figure 2.3: Illustration of CWs employing *Potamogeton crispus* (left) and *Littorella uniflora* (right). Adapted from Headley and Tanner (2012)

Emergent macrophytes

Emergent macrophytes are firmly rooted in the soil, but emerge to different heights above the surface of the water. The roots thus play an important part in absorbing heavy metals from soil sediment (Dhote and Dixit, 2009). *Typha latiofolia* and *Phragmites carka* are examples of emergent macrophytes (Li *et al.*, 2013; Chatterjee, 2014). A wetland utilizing emergent macrophytes is illustrated in Figure 2.4.

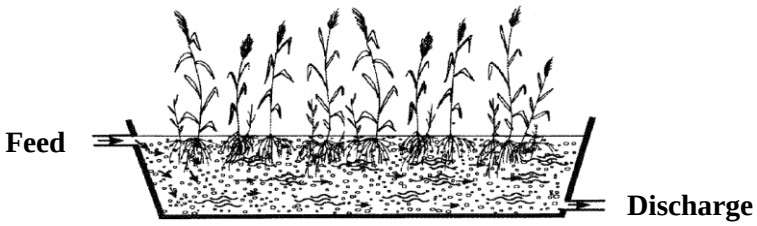

Figure 2.4: Emergent macrophyte wetland system. Adapted from Stottmeister *et al.* (2003)

2.3.2 Classification according to hydraulic regime

Surface flow constructed wetlands

A schematic of a surface flow constructed wetland (SF CW) is provided in Figure 2.5.

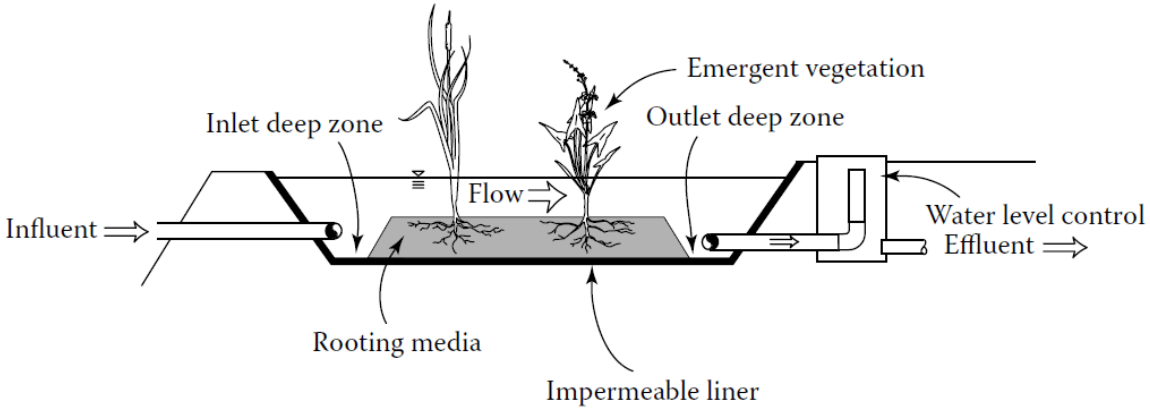

Figure 2.5: An SF CW. Taken from Kadlec (2009)

An SF CW typically consists of emergent vegetation rooted in a sediment at the bottom of the system. Water flows over the sediment and is exposed to the atmosphere (Lim *et al.*, 2001; Ghermandi *et al.*, 2007). The water level is controlled by use of a siphon breaker at the system outlet. Besides water purification, SF CWs provide ancillary benefits such as the potential for aquaculture and a habitat for various forms of amphibious wildlife (Kadlec, 2009). However, the exposed water surface and typically low flow rates make surface flow systems susceptible to insect vectors and odours from the polluted water are difficult to control due to lack of covering (Bondurant, 2010; Leverenz *et al.*, 2010). Another drawback of the surface flow system is the loss of water due to excessive evapotranspiration in the summer months (Kivaisi, 2001). Kadlec *et al.* (2009) note that a lack of thermal insulation for the water in the colder winter months result in a

decrease in nitrogen removal efficiency since the majority of the removal mechanisms depend on biological activity and hence warmer temperatures.

SF CWs can be used as part of an integrated water treatment system or as an independent treatment technology (Chen, 2011). In an integrated treatment system, sedimentation and biological processes are used as primary and secondary treatments followed by the SF CW as a tertiary treatment or polishing unit (Wallace and Knight, 2006). A study performed by Lesley *et al.* (2008) showed that surface flow systems can be used for polishing acid mine drainage waste water due to high iron and manganese removal rates. Such systems can also be used as a tertiary treatment step in polishing food processing and pharmaceutical waste water (Masi *et al.*, 2002; Li *et al.*, 2014).

Subsurface flow constructed wetlands

In contrast to an SF CW, the waste water flows through the granular medium containing emergent macrophytes thereby preventing the water from being exposed to the atmosphere (Ávila *et al.*, 2010; Saeed and Sun, 2012). Whilst flowing through the granular medium, the waste water comes into contact with biofilms, plant roots and rhizomes which facilitates pollutant removal (Garcia *et al.*, 2010; Saeed *et al.*, 2012). Subsurface flow constructed wetlands (SSF CWs) can be further classified as either vertical or horizontal flow (Zurita *et al.*, 2009; Ranieri *et al.*, 2013).

Vertical flow constructed wetlands

A schematic of the vertical flow constructed wetland (VF CW) is provided in Figure 2.6. In VF CWs, wastewater is distributed at the surface and flows downward through the vegetation and substrate until it reaches the bottom layer where it is collected and transported out of the system (Giraldi *et al.*, 2010; Lavrova and Koumanova, 2010).

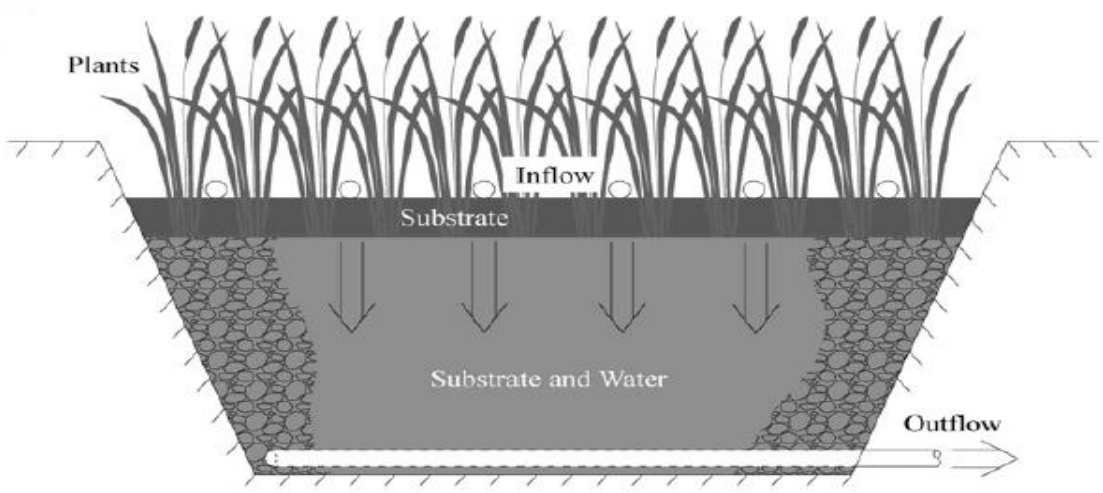

Figure 2.6: VF CW. Taken from Li *et al.* (2014)

VF CWs are attractive because of their low surface area requirements when compared to horizontal subsurface flow constructed wetlands (HSSF CWs) (Matamoros *et al.*, 2007). They have also proven to be effective in removing suspended solids from wastewater due to the pronounced gravitational effects which promote settling and sedimentation as well as enhanced aerobic conditions which result in high rates of biological degradation (Kantawanichkul *et al.*, 1999; Johansen *et al.*, 2002; Saeed *et al.*, 2012). A drawback of the VF CW is its inability to remove phosphorus from waste water due to insufficient binding capacity of the available granular media (Brix and Arias, 2005; Prochaska and Zouboulis, 2006).

Horizontal subsurface constructed wetlands

In HSSF CWs, waste water enters through an inlet or inlet distribution network on one side of the wetland after which it flows horizontally through the substrate media and then exits on the other side (Ríos *et al.*, 2009; Liolios *et al.*, 2012). Bed depth is typically between 0.6 and 1.0 m and the bottom of the bed is sloped downwards to prevent water from flowing across the surface of the system (Haberl *et al.*, 2003). A diagram of an HSSF CW is presented in Figure 2.7. Dissolved oxygen concentrations are typically low in HSSF CWs due to the highly compacted soil and vegetation covering, ultimately giving rise to anaerobic conditions (Camacho *et al.*, 2007; Ávila *et al.*, 2013). HSSF CWs are typically operated under lower flow rates than SF CWs due to the higher area requirements and maintenance costs associated with the subsurface design (Kadlec *et*

al., 2009). Such wetland systems have historically been designed for secondary or tertiary treatment of municipal waste water and domestic sewage, with a pre-treatment unit such as a settling tank being required to prevent high concentrations of suspended solids from entering the system which may cause clogging (Vymazal, 2002).

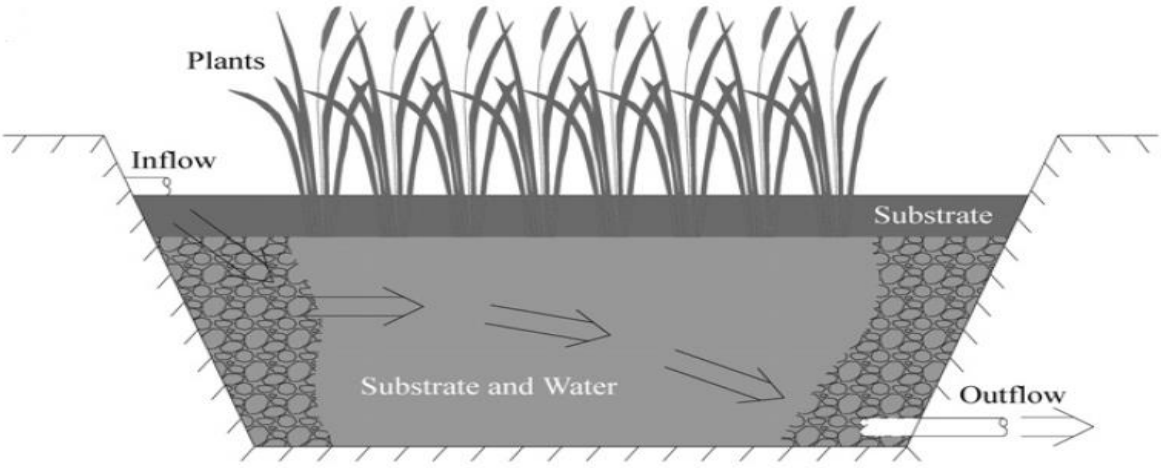

Figure 2.7: Schematic of HSSF CW. Taken from Li *et al.* (2014)

2.4 Waste water pollutant removal mechanisms in HSSF CWs

2.4.1 Nitrogen transformation and removal

Agricultural runoff, industrial and municipal waste water discharge as well as nitrous oxide emissions from fossil fuel energy generation plants pollute surface and groundwater with nitrogenous compounds (Vitousek *et al.*, 1997; Ochoa-Hueso *et al.*, 2011). Organic nitrogen pollutants include aromatics and amino acids (Rosal *et al.*, 2010; Ali *et al.*, 2012). Inorganic nitrogen pollutants found in water resources include ammonium, nitrate, nitrite, dinitrogen gas, nitrous oxide and ammonia (Deblonde *et al.*, 2011; Hassard *et al.*, 2015). Many of these pollutants can damage aquatic and terrestrial life and substances containing nitrites are suspected carcinogens (Taylor *et al.*, 2005; Barlow and Schlatter, 2010). Consequently, nitrogen removal from waste waters using CWs is an extensively researched topic (Vymazal and Kröpfelová, 2009).

Nitrification

Nitrification is the biological oxidation of ammonium to nitrate, with nitrite as an intermediate (Vymazal, 2007; Burgin and Hamilton, 2007). The process can be described using the following reaction steps:

$$NH_4^+ + 1.5O_2 \rightarrow NO_2^- + 2H^+ + H_2O$$ Equation 2.1

$$NO_2^- + 0.5O_2 \rightarrow NO_3^-$$ Equation 2.2

The first reaction step is performed by aerobic bacteria which derive energy from the oxidation of ammonium to nitrite and use carbon dioxide as a carbon source (Hauck, 1984; Tanner *et al.*, 2012). The second step involves the activity of nitrite-oxidising bacteria to convert nitrite to nitrate (Kim *et al.*, 2010). Oxygen is supplied to the nitrifying bacteria via two methods, namely diffusion from the atmosphere to the subsurface layers of the system and translocation from the atmosphere to the rhizome via plant structure (Van de Moortel *et al.*, 2010; Yalcuk *et al.*, 2010). Since the diffusion of oxygen is approximately $3x10^5$ times smaller in water than in air (Verberk *et al.*, 2011), translocation of oxygen via vegetation is the primary method for oxygen supply to the nitrifying bacteria. Albuquerque *et al.* (2009) note, however, that oxygen supply via the rhizomes is consumed rapidly since there is competition for oxygen with other aerobic bacteria. Conseuqently, nitrfication rates are low in HSSF CWs with values between 0.01 and 2.15 g N m^{-2} d^{-1} being reported in literature (Reddy and D'angelo, 1997; Tanner *et al.*, 2002). The optimum temperature for the process to occur is between 30 ºC and 40 ºC and between a pH of 6.6 and 8.0 (Tchobanoglous and Burton, 1991; Paul and Clark, 1996).

Denitrification

Denitrification is the process in which nitrate is converted to dinitrogen gas via a series of intermediates such as nitric oxide and nitrous oxide (Jetten *et al.*, 1997; Vymazal, 2007; Mander *et al.*, 2011):

$$2NO_3^- \rightarrow 2NO_2^- \rightarrow 2NO \rightarrow N_2O \rightarrow N_2$$

The overall reaction depciting the process is provided as follows (Hauck, 1984):

$$6(CH_2O) + 4NO_3^- \rightarrow 6CO_2 + 2N_2 + 6H_2O$$ Equation 2.3

The process occurs under anaerobic conditions with organic compounds being utilized by bacteria as a carbon source (Wen *et al.*, 2010) and nitrogen being used as an electron acceptor instead of oxygen (Fleming-Singer and Horne, 2002; Noorvee *et al.*, 2007; Vymazal, 2007). Jakubaszek and Wojciech (2014) report that for 1 g of nitrate being converted to nitrogen gas, 0.7 g of carbon are required for the bacteria to perform the process. Optimal pH for the process is between 7 and 7.5 whereas optimal temperatures lie between 20 ºC and 25 ºC (Reddy *et al.*, 2014).

Nitrification has shown to be the rate-limiting step of the complete transformation of nitrate to nitrogen gas in HSSF CWs due to limited oxygen availability (Bezbaruah and Zhang, 2005). Consequently, extensive research has been performed to develop hybrid systems which induce favourable conditions for both nitrification and dentrification in different areas of the system. Mechanical aeration in the initial stages of the wetland is one such technique and has been explored by Nivala *et al.* (2007). Tanner *et al.* (2012) has experimented with utilizing different combinations of wetland systems with internal recycle loops. A VF CW in the hybrid system provides sufficient oxygen levels for nitrification while an HSSF CW with a recycle loop provides anaerobic conditions and contact with carbon-rich feed water to ensure denitrying bacteria can thrive. Ammonium removal efficiencies were increased from 61% to 98-99.8% and total nitrogen removal efficiencies were increased from 49% to 58-95% when the hybrid systems were employed.

Ammonia volatilization

Ammonia volatilization is a physical process which consists of four sequential steps (Kadlec *et al.*, 2009):

1. Dissociation: ammonium ions are in equilibrium with un-ionized ammonia (NH_3);
2. Diffusion of ammonia to the water-air interface;
3. Volatilization: ammonia is transferred across the water-air interface; and
4. Ammonia is transferred from the water-air interface to the bulk air.

Ammonia losses are significant at a pH above 9, at which point the ratio of ammonium ions to ammonia in solution is roughly 1:1 (Vymazal, 2007). Since the process is dependent on diffusion of ammonia to the water-air interface and diffusion is temperature-dependent (Johnson, 2010), the overall conversion rate of ammonium ions to ammonia gas is higher at elevated temperatures.

Ammonia volatilization rates are typically between 0.27 and 0.5 g N m^{-2} day^{-1}, and constitute a small portion of the total nitrogen removal in HSSF CWs (Poach *et al.*, 2002).

Ammonification

Ammonification is the process in which organically bound nitrogen in the form of peptides, proteins and nucleic acids (Abou-Elela *et al.*, 2013) are biologically converted into ammonia using a series of oxidative and reductive deamination reactions (Scholz and Lee, 2005; Vymazal, 2007; Saeed and Sun, 2012). The oxidative transformation scheme of the organic nitrogen to ammonia is provided by Savant and De Datta (1982) as follows:

$$\text{Amino acids} \rightarrow \text{Imino acids} \rightarrow \text{Keto acids} \rightarrow NH_3$$

The reductive transformation scheme is provided by Rose (1976):

$$\text{Amino acids} \rightarrow \text{saturated acids} \rightarrow NH_3$$

The oxidative conversion process proceeds much faster than the reductive conversion process (Vymazal, 2007). It would thus typically be the case in HSSF CWs that the rate of ammonification is higher near the surface of the wetland where there are higher levels of dissolved oxygen for the aerobically-driven process to occur and lower rates of ammonification towards the bottom of the wetland where dissolved oxygen levels are much lower. According to Reddy *et al.* (1984) other factors which affect the ammonification rate include temperature, pH, carbon:nitrogen ratio in the wetland system and soil structure. Optimal temperatures for ammonification are between 40 ºC and 60 ºC whereas optimal pH lies between 6.5 and 8.5 (Vymazal, 1995).

Annamox Process

The annamox process describes the anaerobic oxidation of ammonium ions to nitrogen gas (Mulder *et al.*, 1995; Zhang *et al.*, 2011). Nitrate ions can be used as electron acceptors (Vymazal, 2007):

$$5NH_4^+ + 3NO_3^- \rightarrow 4N_2 + 9H_2O + 2H^+ \qquad \text{Equation 2.4}$$

Nitrite ions can also be used as electron acceptors for the process (Van de Graaf *et al.*, 1995):

$$NH_4^+ + NO_2^- \rightarrow N_2 + 2H_2O \qquad \text{Equation 2.5}$$

According to Sliekers *et al.* (2002), approximately 1.9 g O_2 are required for every 1 g of ammonium in the wetland system. A recent study performed by Coban *et al.* (2015) revealed that annamox activity is low in HSSF CWs and consequently plays a minor role in the overall nitrogen transformation process.

Ammonia adsorption

Ammonium ions can be loosely bound onto the surface of soil or gravel sediments in HSSF CWs (Lee *et al.*, 2009). The amount of ammonia adsorbed onto the solid matrices is in equilibrium with the amount of ammonia in solution and hence the nitrification activity within the wetland directly affects the adsorption rate (Vymazal, 2007). Ammonia adsorption rate is also dependent on the type of sediment, nature and amount of soil organic matter as well as the presence of vegetation (Savant and De Datta, 1982).

Plant uptake

Macrophytes are capable of absorbing nitrogen from wastewater and incorporating the nutrient into their biomass structures (Wu *et al.*, 2011). The two forms of nitrogen which are most commonly absorbed are ammonia and nitrate (Vymazal, 2007). Nitrogen uptake by plants is highly dependent on the plant growth rate and nitrogen concentration in the wastewater (Garcia *et al.*, 2010). Konnerup *et al.* (2009) investigated nitrogen uptake in HSSF CWs utilizing *Canna* and *Heliconia*. The mean nitrogen uptake rate for *Canna* was determined to be 0.23 g m^{-2} day^{-1} while for *Heliconia* the uptake rate was 0.03 g m^{-2} day^{-1} and it was estimated that plant uptake into the aboveground biomass accounted for 41% and 12% of total nitrogen removal, respectively.

2.4.2 Phosphorus transformation and removal

Phosphorus is present in HSSF CWs in the form of phosphates which can be organically and inorganically bound to other compounds (Vymazal, 2007). Inorganic phosphorus-containing compounds include orthophosphate and polyphosphate (Cade-Menun and Paytan, 2010). Organically bound phosphorus compounds can be classified according to two different groups, namely those which are easily decomposable and those which biodegrade over a long period of time (Dunne and Reddy, 2005). Easily biodegradable organic compounds include nucleic acids and phospholipids while refractory organic compounds include inositol phosphates and phytin (Reddy *et al.*, 1999).

Adsorption

Soluble inorganic phosphates are transferred from the soil-pore interface to the surface of the soil matrix via adsorption (Huett *et al.*, 2005; Vohla *et al.*, 2011). Adsorption rates are dependent on the granular medium's texture, grain size distribution, iron, calcium, magnesium and aluminium content (Garcia *et al.*, 2010) as well as environmental factors such as redox potential and pH (Vymazal, 2005). As a general rule, the higher the iron, calcium, magnesium and aluminium content the higher the adsorption capacity becomes as a result of more reactive iron, aluminium, magnesium and calcium hydroxide groups on the granular surface (Drizo *et al.*, 1997; Shenker *et al.*, 2005). Adsorbed phosphate can be released back into the water under reducing conditions due to the reductive dissolution of ferric and managenese phosphate minerals (Young and Ross, 2001; Palmer-Felgate *et al.*, 2010). According to Lüderitz and Gerlach (2002) phosphates can also be adsorbed onto humic substances produced as a result of vegetation breakdown.

Sustainable phosphate adsorption in HSSF CWs is, however, a major concern since organic matter clogs the granular pores and adsorption sites become staurated with phosphates within the space of a few months (Arias *et al.*, 2001; Garcia *et al.*, 2010). Hedström (2006) thus recommends utilizing a pre-treatment unit and a substrate with a high sorption capacity to prolong succesful phosphate adsoprtion.

Chemical precipitation

Phosphates can also react with minerals containing iron, aluminium, calcium and magnesium to precipitate out of solution as amorphous and crystalline solids (Vymazal, 2007; Mateus *et al.*, 2012). The pH and redox conditions of the system dictate which compounds precipitate out of the waste water. In acidic-oxidised conditions, insoluble iron and aluminium phosphate compounds are formed while under alkaline-reduced conditions, insoluble calcium and magnesium phosphates dominate (Garcia *et al.*, 2010). Phosphate precipitation can be stimulated by injecting metal complexes into the feed water or granular medium. Ferric chloride, calcium hydroxide and caclium carbonate have proven to be effective (Reddy and D'angelo, 1997; Ann *et al.*, 1999; Esser *et al.*, 2004).

Microbial removal

There exists no permanent phosphorus removal sink since bacteria can only take up and store phosphorus and cannot biologically convert the substance into a gas which can be released from

the system (Garcia *et al.*, 2010). As a result, extent of removal is typically low in HSSF CWs since the phosphorus is released back into the water once the micro-organisms die off. A study performed by Mander *et al.* (2003) revealed that of the 52.8 kg of phosphorus retained in the wetland system over a period of 5 years, only 4.4% could be attributed to microbial removal. Research has shown that microbial uptake of organic phosphorus occurs in the aerobic upper layers of the HSSF CW whereas microbial-facilitated conversion of organic to inorganic phosphorus occurs in the anaerobic bottom layers of the system (Edwards *et al.*, 2006).

Plant uptake

Plant uptake of phosphorus varies according to plant species, climate and the phosphorus loading rate (Garcia *et al.*, 2010). Storage in vegetation can be short or long-term, depending on the plant species employed, plant decomposition rate as well as translocation between the belowground and aboveground biomass (Vymazal, 2007). Plant uptake accounts for a small proportion of the overall removal of phosphorus in HSSF CWs (Davies and Cottingham, 1993) . A study conducted by Edwards *et al.* (2006) on a five years old HSSF CW planted with *Phalaris arundinacea* revealed that plant uptake only accounted for 1.5% of the phosphorus input to the system. Gottschall *et al.* (2007) investigated nutrient removal in a CW treating agricultural waste water. The dominant plant species in the system were *Typha latifolia* and *Typha angustifolia.* Plant uptake only accounted for 5% of total phosphorus removal.

2.4.3 Metal removal

Metal removal in HSSF CWs can occur via a variety of processes including sedimentation, filtration, chemical precipitation, adsorption, microbial activity as well as interactions with vegetation (Hafeznezami *et al.*, 2012).

Chemical precipitation

Metals such as iron, aluminium and manganese precipitate out of the water and are deposited in the wetland in the form of oxides or hydroxides (Woulds and Ngwenya, 2004). Precipitation processes are dependent on pH, redox conditions and the presence of aerobic and anaerobic bacteria (Nelson *et al.*, 1981; Goulet and Pick, 2001; Allende *et al.*, 2012). Manganese removal is typically difficult to achieve because it precipitates as an hydroxide at a pH of 8. However, with the help of oxidising bacteria the removal process can occur at a much lower pH (Stumm and

Morgan, 1981). Iron is removed from the waste water first by oxidising ferrous to ferric iron, after which ferric iron hydrolyses at a pH of 3.5 (Sheoran and Sheoran, 2006).

Anaerobic conditions in the bottom layers of the CW promote the growth of sulphate reducing bacteria (Sheoran and Sheoran, 2006). These bacteria convert sulphate in the waste water to hydrogen sulphide which in turn reacts with heavy metals such as copper, lead, cadmium, zinc, nickel, iron and manganese to form insoluble metal sulphides (Stein *et al.*, 2007).

Adsorption

Adsorption of metal ions onto the substrate surface is an important mechanism for removing metals from waste water in HSSF CWs (Marchand *et al.*, 2010). Factors affecting the adsorption rate depends on the type of metal adsorbed, competition for available sites with other metals as well as pH (Machemer and Wildeman, 1992; Seo *et al.*, 2008). Adsorption capacity of the substrate in particular generally increases with increasing clay and organic matter content (Sheoran and Sheoran, 2006).

Sedimentation and filtration

Sedimentation of metals in HSSF CWs is facilitated by vegetation and subsurface media as they decrease water flow rates and increase hydraulic retention time (Lee and Scholz, 2007). Sedimentation of metals is enhanced by flocculant formation (Marchand *et al.*, 2010). Flocculant formation rates are high under alkaline conditions, a strong presence of suspended solids, high ionic strength and high algal density (Matagi *et al.*, 1998). The extent of filtration and sedimentation within the CW can be determined by measuring the cumulative metal concentration in the granular medium over extended periods of time (Garcia *et al.*, 2010). In Table 2.1 a summary is provided of the studies performed investigating metal removal by sedimentation in HSSF CWs.

Table 2.1: Summary of cumulative sediment metal concentrations found in various HSSF CWs

Study	Gschlößl and Stuible (2000)	(Gschlößl and Stuible, 2000)	Vymazal and Krása (2003)	Lesage *et al.* (2007)
Waste water type	Sewage	Sewage	Sewage	General domestic
Surface area (m^2)	500	940	3224	1300
Years of operation	10	10	3	3
Granular medium	Sand/gravel	Sand	Crushed rock (8-16 mm)	Gravel (5-10 mm)
Plant species	*Phragmites* sp. *Typha* sp.	*Phragmites* sp. *Typha* sp.	*Phragmites australis*, *Phalaris arundinacea*	*Phragmites australis*,
Average metal concentrations (mg/kg DW)				
Cu	65.5	80	494	151.5
Zn	207.5	271	1029.5	499.5
Cd	1.95	2.15	85.25	1.35
Ni	18.5	49.5	179.05	37
Cr	22.5	148.5	N/A	33.5
Pb	14.5	48.65	230.5	88
Mn	N/A	N/A	941.5	604
Fe	N/A	N/A	700	29404.5

Gschlößl and Stuible (2000) found large amounts of copper and manganese in the sediments of the two CWs which they examined and may be indicative of high sedimentation and filtration efficiency. These two metals were found in particularly high concentrations near the inlet of the wetland and in the organic layers on the sediment surface. This trend of high metal accumulation near the inlet and a decrease in accumulation with longitudinal distance was also reported by Vymazal and Krása (2003) as well as Lesage *et al.* (2007) in their respective studies.

Interactions with vegetation

Plants are capable of absorbing a variety of metals including iron, manganese, zinc, copper, cadmium, chromium and lead as demonstrated by Salt *et al.* (1995). Bonanno and Giudice (2010) investigated the bio-accumulation of heavy metals in different organs of the emergent macrophyte *Phragmites australis*. The results indicated that the roots and rhizomes were more effective than the stem and leaves in bio-accumulation. These results correlate with those found in another study by Weis and Weis (2004). Manganese, zinc, lead and copper concentrations were highest in all of

the plant's organs. Cadmium and chromium were the most difficult to bio-accumulate, indicated by the fact that their concentrations were lowest in all of the plant's organs. Chromium is toxic to plants, inducing metabolic stress (Mohanty and Patra, 2011). This explains the low accumulation levels in the plant when compared to the other metals in the waste water. Cadmium, too, is highly toxic since it facilitates the release of free radicals which damage membranes and lipids within the plant structure resulting in plant death (Foyer *et al.*, 1994; Divan *et al.*, 2009). Copper and manganese have been shown to be important for plant nutrition (Siedlecka *et al.*, 2001; Baldantoni *et al.*, 2004), thus explaining their relatively high levels of accumulation in this particular study.

The contribution of plant accumulation to the overall metal removal rate in HSSF CWs is questionable (Garcia *et al.*, 2010). Lim *et al.* (2001) and Lim *et al.* (2003) found that plant uptake made a negligible contribution towards total metal removal and accounted for less than 3% of the total metal removal for copper, cadmium, lead and zinc respectively. Yadav *et al.* (2012) investigated the extent of chromium, copper, nickel, zinc and cobalt accumulation in the plant species *Typha angustifolia*. The results indicated that uptake by the plant was a major removal mechanism for all of the investigated metals. Bio-accumulation of metals in plants depends on numerous environmental factors such as pH, redox potential, concentration of metals in the water and sediment as well as the structure and composition of the sediment (Sundareshwar *et al.*, 2003; Deng *et al.*, 2004). Soda *et al.* (2012) found a positive correlation between plant uptake of a particular metal and its corresponding aqueous concentration.

Besides bio-accumulation, macrophytes indirectly affect other metal removal processes occurring within HSSF CWs. Plants excrete organic matter into the rhizosphere, a process referred to as rhizodeposition (Nguyen, 2003). The presence of available organic matter stimulates microbial activity and hence microbial metal removal processes play a role. Radial oxygen loss and excretion of protons from plant roots, however, tend to acidify and oxidise the rhizosphere, resulting in the oxidation and subsequent mobilization of metal sulphides (Jacob and Otte, 2003).

2.4.4 Organics transformation and removal

Two techniques can be used to determine the quantity of organic matter to be removed from influent waste water, namely the chemical oxygen demand (COD) and biochemical oxygen demand (BOD) (Delzer and McKenzie, 2003). BOD is a measure of the amount of oxygen that bacteria will consume while decomposing organic matter under aerobic conditions while COD

does not differentiate between biologically available and inert organic matter and consequently is a measure of the total oxygen required to oxidize all organic matter into carbon dioxide and water (Masters and Ela, 2008). HSSF CWs can receive internal and external loading of organic matter (Nguyen, 2000), with external loading originating from the waste water and internal loading from plant and microbial decomposition within the wetland. The three dominant organic removal processes in HSSF CWs are aerobic and anaerobic decomposition as well as filtration (Kadlec *et al.*, 2000).

Organic matter present in HSSF CWs can be classified as dissolved (DOM) and particulate (POM), with the transformation and removal mechanisms being different for each case (Garcia *et al.*, 2010).

Particulate organic matter

POM is retained in the system primarily via the physical process of filtration (Vymazal and Kröpfelová, 2009). Retention of POM usually occurs within the first third of the wetland, as noted by Behrends *et al.* (2007). Research conducted by Tanner (2001) suggested that the filtration process is dominant in the root zone of the HSSF CW. The retained organic matter disintegrates and is converted into DOM which further undergoes a series of biochemical degredation reactions, depending on local system conditions.

Dissolved organic matter

DOM from the influent waste water and that produced from the disintegration of POM can be decomposed via aerobically or anaerobically-facilitated processes (Garcia *et al.*, 2010). Aerobic degradation is performed by aerobic heterotrophic bacteria which use oxygen as a final electron acceptor (Vymazal and Kröpfelová, 2009):

$$C_6H_{12}O_6 + 6O_2 \rightarrow 6CO_2 + 6H_2O + \text{energy} \qquad \text{Equation 2.6}$$

Oxygen transfer rates in HSSF CWs are typically low, as noted by Rousseau *et al.* (2007) who estimated it to be approximately 0.7 g O_2 m^{-2} day^{-1}. Consequently, aerobic degradation pathways are not prominent.

Anaerobic degradation is thus the dominant transformation pathway for DOM in HSSF CWs and is a multi-step process, as shown in Figure 2.8.

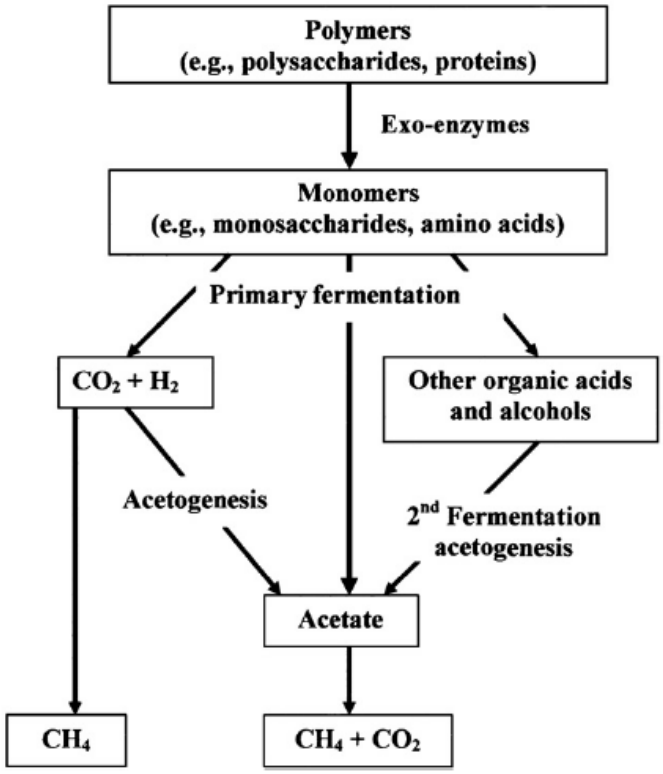

Figure 2.8: Schematic overview of the anaerobic degradation of DOM in HSSF CWs. Taken from Vymazal & Kröpfelová (2009)

The first step of the process entails the microbial conversion of complex soluble polymers into simpler monomers such as amino acids (Megonikal *et al.*, 2004). These amino acids then undergo fermentation to produce primarily fatty acids, alcohols as well as hydrogen and carbon dioxide. Sulphate-reducing bacteria then convert the fatty acids into carbon dioxide, water and hydrogen sulphide:

$$CH_3COOH + H_2SO_4 \rightarrow 2CO_2 + 2H_2O + H_2S$$ Equation 2.7

Methanogenic bacteria also convert fatty acids as well as carbon dioxide and hydrogen into methane:

$$CH_3COOH + 4H_2 \rightarrow 2CH_4 + 2H_2O$$ Equation 2.8

$$4H_2 + CO_2 \rightarrow 2CH_4 + 2H_2O$$ Equation 2.9

2.5 Modelling HSSF CW performance

Modelling of the various waste water treatment processes discussed in Section 2.4 is an integral task when designing an HSSF CW. The rate at which these degradation reactions occur, referred to as the treatment kinetics (Sheridan *et al.*, 2014b), directly determines the size of the CW. Historically HSSF CW sizing has been performed by combining prior knowledge of kinetic data with an appropriate hydraulic model, much like the sizing process used for other types of chemical reactors (Fogler, 1999). The hydraulic model either assumes an ideal plug flow reactor (PFR) in which the waste water moves as a plug through the wetland with no dispersion or on the other extreme as a continuously stirred tank reactor (CSTR) in which the concentration of the waste water constituents is uniform throughout the system. The sizing process requires computation of the nominal residence time of fluid, shown in Equation 2.10 and is fed into the PFR or CSTR model equations presented in Equation 2.13 and Equation 2.14 respectively.

$$\tau = \frac{V}{\dot{v}} \qquad \text{Equation 2.10}$$

$$V = HWL\varepsilon \qquad \text{Equation 2.11}$$

Where ε is the subsurface media porosity defined as the ratio of open pore space to total wetland volume (Kadlec *et al.*, 2009):

$$\varepsilon = \frac{V}{V_{total}} \qquad \text{Equation 2.12}$$

$$C_{i,out} = C_{i,in} e^{-k_{rate}\tau} \qquad \text{Equation 2.13}$$

$$C_{i,out} = \frac{C_{i,in}}{(1+k_{rate}\tau)} \qquad \text{Equation 2.14}$$

The PFR and CSTR models have shown to be an over-simplification of the actual hydraulic processes occurring inside HSSF CWs (Werner and Kadlec, 2000) and consequently may lead to an incorrectly sized HSSF CW when used in the design phase of the project.

2.6 Factors contributing to non-ideal hydraulic behaviour in HSSF CWs

HSSF CWs are structurally complex (Brovelli *et al.*, 2011) and thus there are many factors which influence the hydraulic flow patterns of water, resulting in non-ideal hydraulic behaviour. Some of the factors contributing to non-ideality include:

1. Spatially varied grain size distributions of subsurface media (García *et al.*, 2004);
2. Clogging of sediment pores (Pedescoll *et al.*, 2011);
3. Positioning of inlet and outlet ports as well as wetland shape (Suliman *et al.*, 2006b; Wörman and Kronnäs, 2005); and
4. Basin topography (Conn and Fiedler, 2006);

Factors 1 and 2 induce spatial variation of flow resistance inside the subsurface media hence preventing the waste water from flowing as an idealized plug through the system. Hydraulic conductivity (K) is the physical parameter which is used to describe the ease with which waste water can flow through certain regions of an HSSF CW (Klute, 1986) and is defined in Equation 2.15 (Coulson and Richardson, 1991):

$$\dot{v} = KA_s \frac{dh}{dx} \qquad \text{Equation 2.15}$$

Hydraulic conductivity is a function of the media porosity, particle shape, particle size distribution, particle arrangement and the tortuosity (Kadlec *et al.*, 2009). Extensive research has been performed for the purpose of developing appropriate correlations between hydraulic conductivity and these physical parameters. One such correlation was developed by Ergun (1952) and is provided in Equation 2.16.

$$K = \frac{\rho g \varepsilon^3 D_p^2}{150(1-\varepsilon^2)\eta} \qquad \text{Equation 2.16}$$

2.6.1 Heterogeneous subsurface media

Subsurface media used in HSSF CWs are typically heterogeneous in nature and are found to have large grain size distributions (Suliman *et al.*, 2006b). By referring to Equation 2.16, it can be seen that regions containing smaller grain sizes have lower hydraulic conductivities when compared to regions with larger grain sizes. Waste water would thus flow with higher velocity through regions containing larger grain sizes and disrupt the ideal plug flow scenario. This observation has been confirmed by researchers (Werner and Kadlec, 2000) and has led to the development of different filling strategies prior to wetland operation aimed at enhancing homogeneity of subsurface media in order to approach ideal plug flow conditions as close as possible (Suliman *et al.*, 2007).

2.6.2 Wetland clogging

Wetland clogging is typically caused by the following processes (Kadlec *et al.*, 2009):

- Deposition of suspended solids at the system inlet;
- Deposition of organic compounds, which are resistant to microbial degradation, at the system inlet;
- Chemical precipitation;
- Introduction of organic matter to the system which encourages growth of microbial biofilms in the plant rhizosphere;
- Growth of plant roots within the packed media; and
- Gas bubble dynamics

Deposition of suspended solids and organic compounds resistant to degradation

Continual loading of organic and inorganic matter throughout the lifespan of the CW results in the accumulation of sediments and refractory organic material, particularly near the inlet of the system (Kadlec *et al.*, 2009). Detailed models describing exactly how these suspended solids accumulate in the packed media have been developed, with an example being the transport model built by Yao *et al.* (1971). A visual demonstration of the model is provided in Figure 2.9. The underlying assumption of this model is the acknowledgement of a relatively large spherical particle on the surface of the packed media which is referred to as a collector, whose purpose is to facilitate the collection of suspended solids from the bulk flow of water. Three diferent processes can facilitate collection of suspended solids namely interception, sedimentation and diffusion. During interception the suspended solid comes into contact with the collector as a result of its own large size. During sedimentation the suspended solid will follow a different trajectory to the bulk flow of water because of its size and experiences larger gravitational force. Whilst flowing through the packed media the particle can come into random contact with other particles. This results in Brownian movement and hence diffusion, which can force the particle to come into contact with the collector.

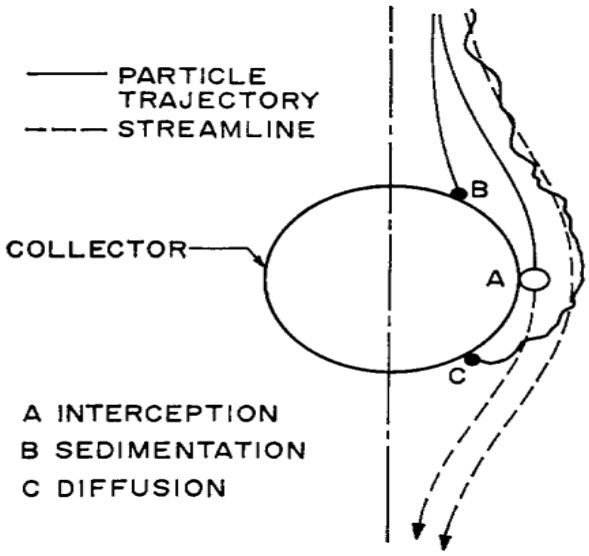

Figure 2.9: Demonstration of transport model. Taken from Yao et al. (1971)

Tanner *et al.* (1998) investigated organic matter accumulation over a period of five years in four gravel bed HSSF CWs used to treat farm dairy waste water. The CW receiving the highest organic loading of 5.8 g m^{-2} d^{-1} experienced the most significant reduction in media porosity. Caselles-Osorio *et al.* (2007) conducted similar experiments on six full-scale HSSF CWs used for sanitation puproses of small towns in northeastern Spain. Results indicated that there was significantly more solids accumulation near the inlet than the outlet, with an average of 30 kg of dry matter per m^2 being collected near the inlet and an average of 7 kg of dry matter per m^2 being collected near the outlet. Hydraulic conductivity was lower near the inlet than near the outlet, with an average hydraulic conductivity of 2 m/day being recorded near the inlet and 106 m/day near the outlet.

Biofilm formation

Researchers such as Suliman *et al.* (2006a) have shown that biofilm formation may impact the hydraulics of CWs and their growth is dependent primarily on the amount of organic matter in the feed to the system. Other experiments, such as those performed by Dupin and McCarty (2000), showed that the development of microbial colonies greatly depended on pH.

Plant root growth

According to Lockhart (1999), plant morphology in the rhizosphere is strongly dependent on redox conditions and as such preferentially develop their roots in the upper layers of the wetland where redox conditions are favourable for root growth. This process tends to create preferential flow

paths, or channeling, in the lower layers of the system where a limited presence of roots presents less obstruction to flow of water. According to IWA (2001) a macrophyte stand can contain between 500-5000 g of material per m^2 of subsurface roots and rhizomes. McIntyre and Riha (1991) used greenhouses with macrophytes rooted in sand to test the hydraulic conductivity with time. They found that the hydraulic conductivities in vegetated and non-vegetated systems decreased with time, but vegetated systems experienced a far greater reduction of 55% as opposed to a 41% reduction in non-vegetated systems. These reductions in hydraulic conductivity were a result of porosity reduction due to plant root growth and biofilm development in the rhizosphere. Baird *et al.* (2004) reported that CWs containing *Phragmites australis* had hydraulic conductivities that were half the magnitude of unplanted CWs.

Gas bubble formation

Methanogensis generates methane gas bubbles in the lower layers of the HSSF CW (Maltais-Landry *et al.*, 2009). The gas bubbles rise and become trapped within the system, especially in densely packed areas of soil and plant roots (Glaser *et al.*, 2004; Kellner *et al.*, 2005). When these bubbles coalesce and their collective diameter exceeds that of the soil pores, blockage of the pores occurs and tends to reduce the hydraulic conductivity of the system dramatically (Beckwith and Baird, 2001).

2.6.3 Wetland shape

Deep zones have been excavated within CWs in order to promote settling and sedimentation efficiency (Koskiaho, 2003). However, research has shown that increasing CW depth may have a negative impact on hydraulics by enhancing non-ideal flow behaviour (Holland *et al.*, 2004). Another design parameter affecting hydraulic behaviour is the CW aspect ratio defined in Equation 2.17:

$$AR_w = \frac{L}{W} \qquad \text{Equation 2.17}$$

A high AR_w is recommended as it enhances the probability of achieving near plug-flow conditions (Crites, 1994; Wörman and Kronnäs, 2005). Rules of thumb for optimal AR_w vary according to researcher, with Thackston *et al.* (1987) recommending a ratio of 5-10:1 whereas Reed *et al.* (1995) recommends a ratio of 1-4:1. According to Su *et al.* (2009) increasing AR_w over 5:1 causes a diminishing benefit in the improvement of hydraulic behaviour.

2.6.4 Inlet-outlet port structure

The structuring of inlet and outlet ports have been shown to affect the hydraulics in HSSF CWs (Chazarenc *et al.*, 2003). Situating inlet and outlet ports towards the top of the wetland bed tends to induce a hull-shaped flow profile (Sheridan *et al.*, 2014a). Near plug flow conditions may be achieved by installing inlet and outlet ports at multiple depths or by placing inlet ports towards the bottom of the bed and outlet ports near the top as recommended by Suliman *et al.* (2006b).

2.7 Using RTD studies to quantify hydraulic behaviour of HSSF CWs

A residence time distribution (RTD) study is a method used for tracking waste water as it passes through an HSSF CW and can be used by engineers to ascertain the flow characteristics of the system (Headley and Kadlec, 2007). The study entails passing a soluble, inert tracer through the system which follows the same flow pattern as the waste water. The resultant tracer RTD can then be used to determine the apparent volume of the HSSF CW and the degree of mixing. Tracer studies can also be used to determine the internal flow paths inside the system by injecting tracer at the inlet and monitoring tracer concentration using sampling ports at a multitude of positions (Suliman *et al.*, 2006a). This can be conducted along longitudinal, lateral and vertical profiles (Headley and Kadlec, 2007). Two possible methods for conducting the tracer study are to introduce either a step or impulse of tracer at the inlet of the CW, after which the concentration of tracer is continuously monitored at the system outlet. A summarized flow diagram of the tracer test is provided in Figure 2.10.

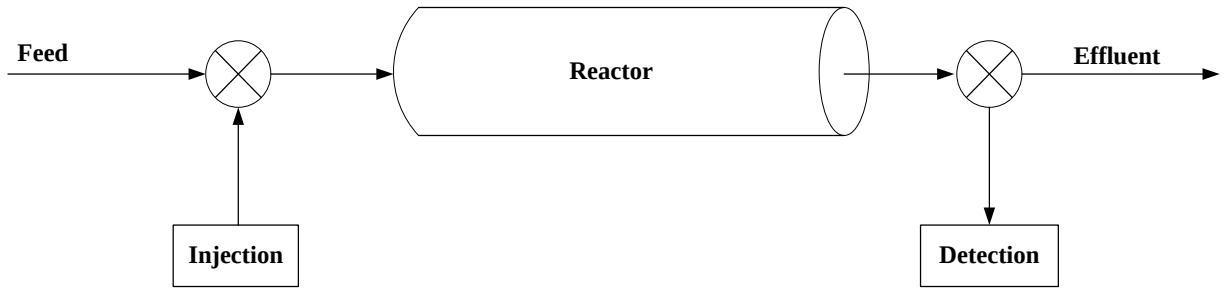

Figure 2.10: Flow diagram of the RTD study depicting injection and detection points

2.7.1 Impulse response tracer study

In the impulse response tracer study a mass of tracer is introduced as an impulse into the wetland feed with the concentration at the outlet being continuously measured as a function of time (Giraldi *et al.*, 2009). The generic concentration-time curves associated with the impulse tracer study are provided in Figure 2.11. The response is modified at the system outlet due to non-ideal hydraulic processes occurring within the CW.

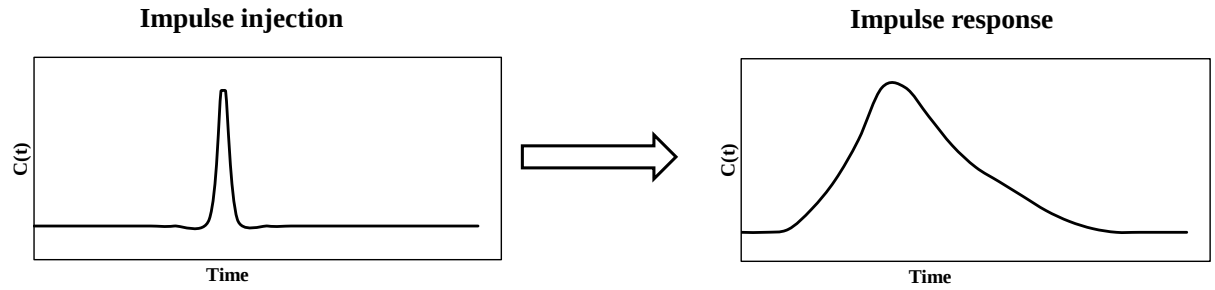

Figure 2.11: Generic schematic of impulse injection and impulse response of a wetland system

The mathematical development for the determination of the RTD function, $E(t)$, using the impulse tracer study is described according to the methodology annotated by Fogler (1999).

The amount of tracer leaving the reactor between time t and $t + \Delta t$:

$$\Delta M = C(t)\dot{v}\Delta t \qquad \text{Equation 2.18}$$

Dividing Equation 2.18 by the total tracer material injected into the reactor:

$$\frac{\Delta M}{M_0} = \frac{C(t)\dot{v}\Delta t}{M_0} \qquad \text{Equation 2.19}$$

$E(t)$ is then defined according to Equation 2.20:

$$E(t) = \frac{\dot{v}C(t)}{M_0} \qquad \text{Equation 2.20}$$

By combining Equation 2.19 and Equation 2.20:

$$\frac{\Delta M}{M_0} = E(t)\Delta t \qquad \text{Equation 2.21}$$

As can be deduced from Equation 2.21, $E(t)$ describes how much time different fluid elements spend within the CW and consequently the quantity $E(t)\Delta t$ represents the fraction of fluid exiting the system which has spent between time t and $t + \Delta t$ inside the reactor. By writing Equation 2.18 in differential form and then integrating, Equation 2.22 is obtained:

$$M_0 = \int_0^\infty \dot{v} C(t)\, dt \qquad \text{Equation 2.22}$$

By substituting Equation 2.22 into Equation 2.20 and assuming a constant volumetric flow rate employed during the tracer study:

$$E(t) = \frac{C(t)}{\int_0^\infty C(t)dt} \qquad \text{Equation 2.23}$$

The denominator in Equation 2.23 represents the area under the concentration-time curve from the tracer experiment, as illustrated in Figure 2.12.

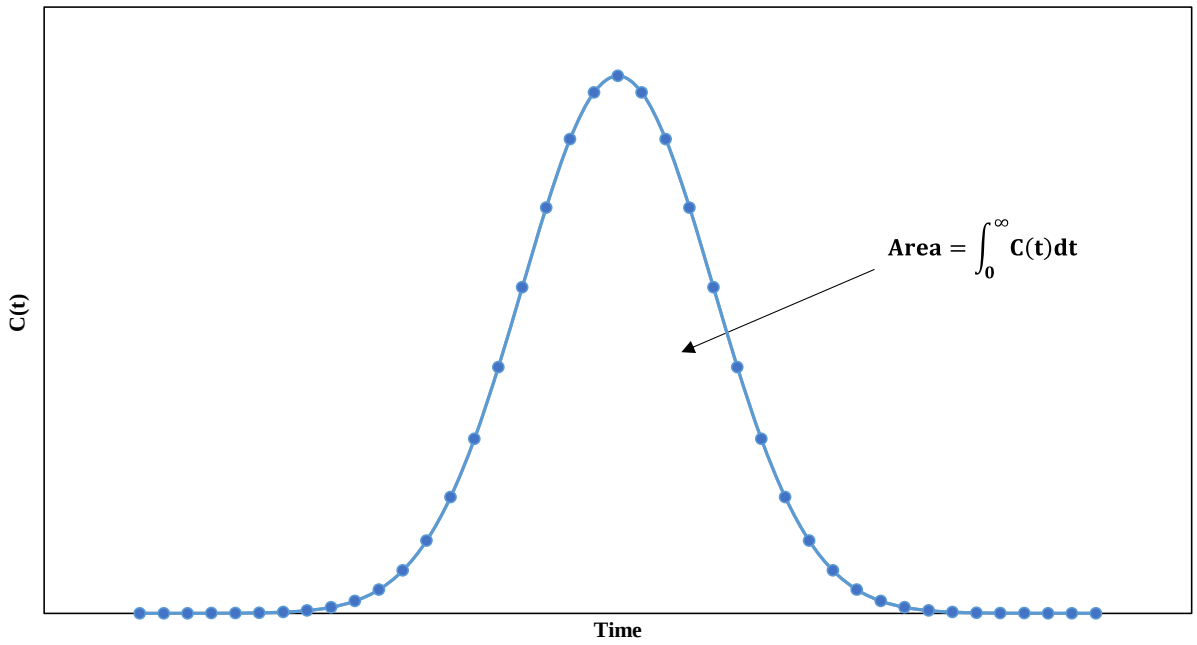

Figure 2.12: Area under concentration-time curve from impulse response tracer study

The area under the curve in Figure 2.12 can be evaluated using numerical integration techniques, such as Simpson's rule. Since the RTD curve represents the fraction of fluid exiting the system which has spent between time t and $t + \Delta t$ inside the reactor, the concept can be expanded on to deduce that 100% of the tracer resides in the reactor between time of injection and as $t \rightarrow \infty$:

$$\int_0^\infty E(t)dt = 1$$ Equation 2.24

The mean of the RTD function is then calculated using $E(t)$ as shown in Equation 2.25:

$$\bar{t}_m = \int_0^\infty tE(t)dt$$ Equation 2.25

The variance of the RTD curve provides an indication of the spread of tracer as it flows through the system (Drummond *et al.*, 2012) and is calculated using Equation 2.26 (Jackson *et al.*, 2012).

$$\sigma^2 = \int_0^\infty t^2E(t)dt - \bar{t}_m^2$$ Equation 2.26

The actual experimental recovery of tracer is determined using Equation 2.27:

$$\%\ \text{recovery} = \frac{\dot{v}\int_0^\infty C(t)dt}{M_0} \times 100$$ Equation 2.27

The advantages and disadvantages of the impulse response tracer study are listed in Table 2.2.

Table 2.2: Summary of advantages and disadvantages of impulse response tracer study (Teefy, 1996)

Advantages	Disadvantages
Smaller quantity of tracer required compared to step change response tracer study	Danger of missing peak of response curve
Less infrastructure required for tracer addition compared to step change response study	Difficult to determine correct quantity of tracer to be added to system
	Experiment repeatability is a problem

Case studies involving the use of the impulse response tracer study on HSSF CWs

The impulse response is the more widely implemented technique for conducting hydraulic studies on HSSF CWs due to lower tracer mass requirements and hence lower associated costs (Headley and Kadlec, 2007). The technique has been applied to a variety of systems in different industries. Ríos *et al.* (2009) evaluated changes in flow patterns of pilot-scale HSSF CWs used for secondary treatment of domestic waste water in southwest Columbia using the hydraulic tracer Rhodamine WT. Three different units were used which varied according to the dominant vegetation present. The first unit was planted with *Phragmites australis*, the second with *Heliconia psittacorum* and the third was unplanted. In this study, the impulse response tracer study successfully assisted the

researchers with identifying relationships between biological growth of roots and stems and the subsurface hydrodynamics. Another important study involving the use of the impulse response tracer study was performed by Seeger *et al.* (2013) on different types of HSSF CWs used to treat groundwater contaminated with BTEX, the fuel additive MTBE and ammonium. In this case fluorescein was chosen as a tracer due to its detection at low concentrations; it is toxicologically safe; it is resistant to biodegradation as well as its low sorption potential to gravel, quartz media and plants inside CWs. Two of the systems contained gravel as the system sediment, with one being populated by *Phragmites australis* and the other unplanted, while the other two used hydroponic root mats and varied according to the water level employed. The various wetland configurations are shown in Figure 2.13.

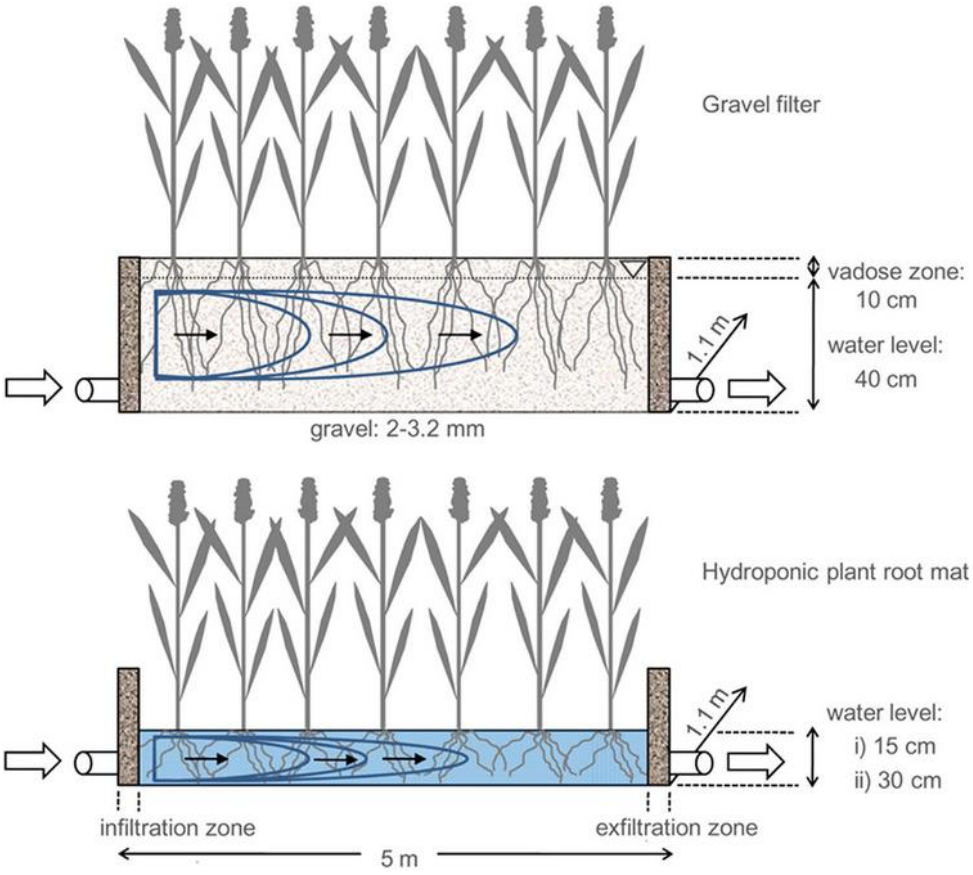

Figure 2.13: Various wetland configurations studied by Seeger *et al.* (2013)

Following tracer addition, water was sampled in a multitude of locations within the CWs and assisted in developing localized hydraulic indices which highlighted preferential flow paths as well as stagnant zones. The results of the hydraulic study were coupled with regular contaminant

sampling to identify the relationship between hydraulic behaviour and contaminant removal efficiency.

2.7.2 Step change response tracer study

In the case of a step change experiment, tracer is continuously introduced into the feed pipe until the effluent is indistinguishable from the feed (Fogler, 1999). The generic concentration-time curves for the step change tracer study are provided in Figure 2.14.

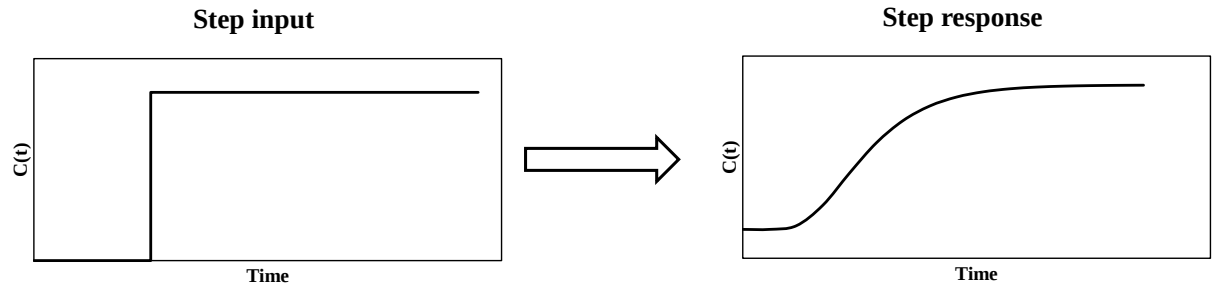

Figure 2.14: Generic concentration-time curves for the step-change tracer technique

The outlet concentration of tracer can be related to the cumulative distribution function, $F(t)$, using Equation 2.28 (Fogler, 1999):

$$F(t) = \left[\frac{C(t)}{C_{max}}\right] \qquad \text{Equation 2.28}$$

Step change integral modelling methodology

In this approach the mean of the RTD is determined directly from the $F(t)$ curve as shown in Equation 2.29 and in Figure 2.15.

$$\bar{t}_m = \int_0^\infty [1 - F(t)]dt \qquad \text{Equation 2.29}$$

The variance of the RTD is then determined using Equation 2.30:

$$\sigma^2 = 2\int_0^\infty t[1 - F(t)]dt - \bar{t}_m^2 \qquad \text{Equation 2.30}$$

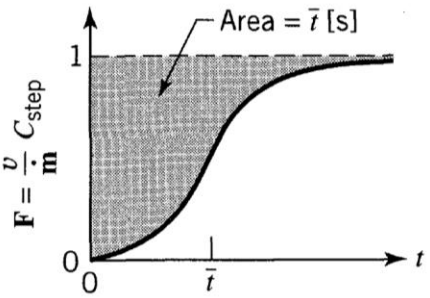

Figure 2.15: Determining the mean of the RTD by computing the area above the F(t) curve. Taken from Levenspiel (1999)

Step change derivative modelling methodology

The step-change derivative methodology requires differentiating the $F(t)$ curve to obtain the $E(t)$ curve as shown in Equation 2.31 and in Figure 2.16.

$$E(t) = \frac{dF(t)}{dt} \qquad \text{Equation 2.31}$$

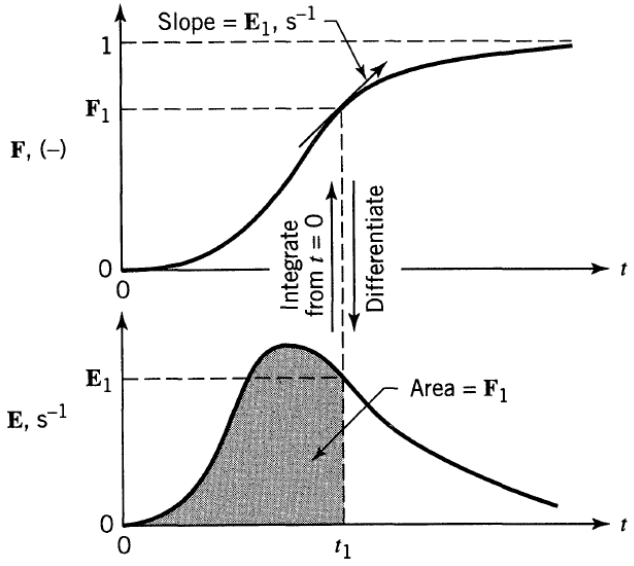

Figure 2.16: The relationship between the RTD function, $E(t)$, and the cumulative distribution function, $F(t)$. Taken from Levenspiel (1999)

Once the $E(t)$ curve is obtained Equation 2.25 and Equation 2.26 are then used to determine the mean and the variance of the RTD, respectively.

The advantages and disadvantages of the step-change response are provided in Table 2.3 (Teefy, 1996; Fogler, 1999).

Table 2.3: Summary of advantages and disadvantages of step change response

Advantages	Disadvantages
The total amount of tracer used in the experiment does not need to be known	Larger quantities of tracer are required when compared to impulse response
No danger of missing concentration peak at the system outlet	Differentiation of the F(t) curve to obtain the E(t) curve may lead to large errors when computing mean and variance of RTD data
	Possible difficulties associated with maintaining a constant tracer concentration in the feed

Applications of step change experiment in HSSF systems in literature

The step change tracer experiment has not been applied to as many HSSF CWs when compared to the impulse response experiment. The most notable study was that performed by Suliman *et al.* (2006a), who utilized step change tracer studies with bromide as a tracer to evaluate the effect of biological growth on hydraulic performance of HSSF CWs utilizing different types of subsurface media. One of the wetlands were packed with lightweight aggregates, commonly known as Filtralite-P. The medium consisted of clay particles which enhance phosphorus sorption and nitrogen removal (Zhu *et al.*, 1997; Adam *et al.*, 2005). The other wetland was packed with shell sand, which mainly consisted of calcium carbonate and magnesium carbonate produced by shells, snails and algae. Step change tracer studies were conducted during the initial phase of wetland operation to determine the inital hydraulic behaviour of each system. Soy broth, ammonium chloride, potassium nitrate as well as a phosphate-based solution were then passed through each of the wetlands for a period of four months to stimulate biological growth on the packed media. The hydraulic studies were then repeated and assisted the researchers with identifying light weight aggregates to be more resistant to biological fouling when compared to the shell sand.

2.7.3 Normalizing the E(t) and F(t) curves

The reversible property of flow in the laminar flow region makes it possible to normalize the E(t) and F(t) curves with respect to time. This is useful for comparing hydraulic data generated at different experimental flow rates and comparing hydraulic performance of systems with different

volumetric capacities (Wahl *et al.*, 2010; Lange *et al.*, 2011). The data set is normalized by converting it into dimensionless variables as is shown in Equation 2.32 through Equation 2.34 (Fogler, 1999).

$$\theta = \frac{t}{\bar{t}_m} \qquad \text{Equation 2.32}$$

$$E(\theta) = \bar{t}_m E(t) \qquad \text{Equation 2.33}$$

$$F(\theta) = F(t) \qquad \text{Equation 2.34}$$

Where θ represents the number of reactor volumes of fluid which have flowed through the system at a particular point in time.

2.7.4 Interpretation of RTD function

The figures used in this section have been limited to the RTD function $E(t)$. The discussion can be extended to include the cumulative distribution function $F(t)$ by noting the relation between these two functions provided in Equation 2.31.

Short-circuiting behaviour

Short-circuiting behaviour within the system occurs when there is a pathway through which water is accelerated and thus travels at a higher rate compared to the rest of the water body. The system will then also comprise of dead zones, in which the water flows at a much slower pace. Short-circuiting is characterized by a horizontal shift of the RTD curve and the development of a long tail representing slow elimination of tracer from the dead zones, as shown in Figure 2.17. The subsequent shift decreases the mean of the RTD (Alcocer *et al.*, 2012).

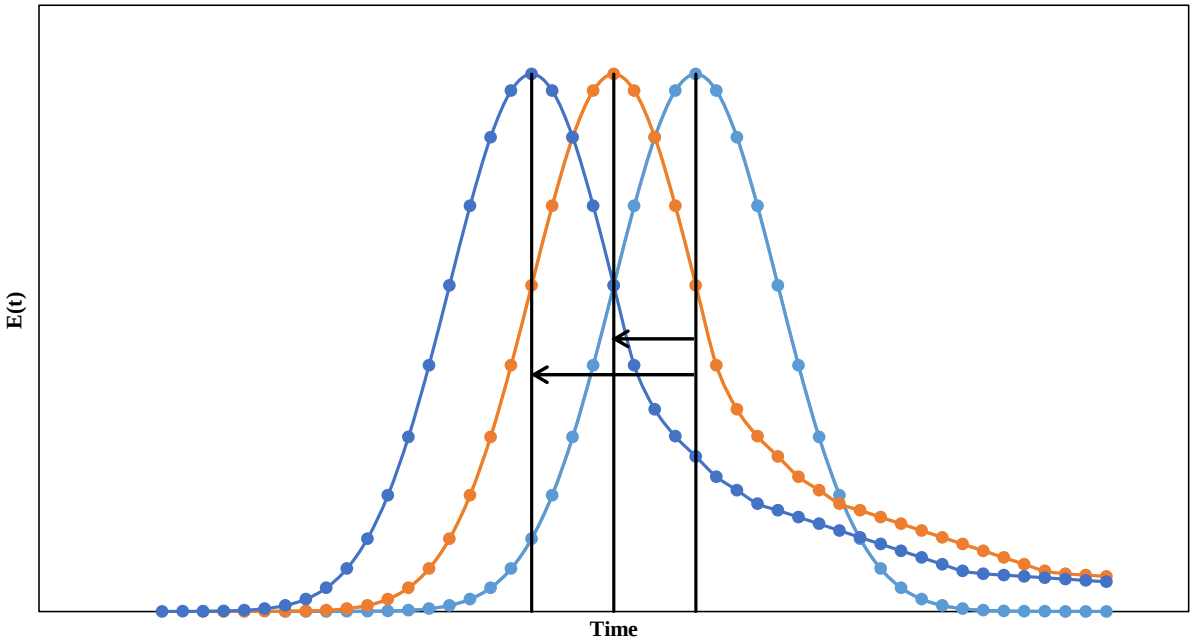

Figure 2.17: Effect of short-circuiting on RTD curve

The degree of short-circuiting inside an HSSF CW can be quantified using Equation 2.35 (Persson, 2000):

$$SC = \frac{t_{16}}{\bar{t}_m} \qquad \text{Equation 2.35}$$

Where t_{16} represents the time for passage of the 16th percentile of tracer through the outlet port. The higher the value of the short-circuiting coefficient, the lower the degree of short-circuiting and vice versa.

Internal recirculation

Internal recirculation of fluid may cause a multi-modal RTD curve and tends to induce an oscillatory output since the tracer exits in highly concentrated clumps at staggered intervals (Fogler, 1999). In Figure 2.18 a visual of the bimodal distribution is presented.

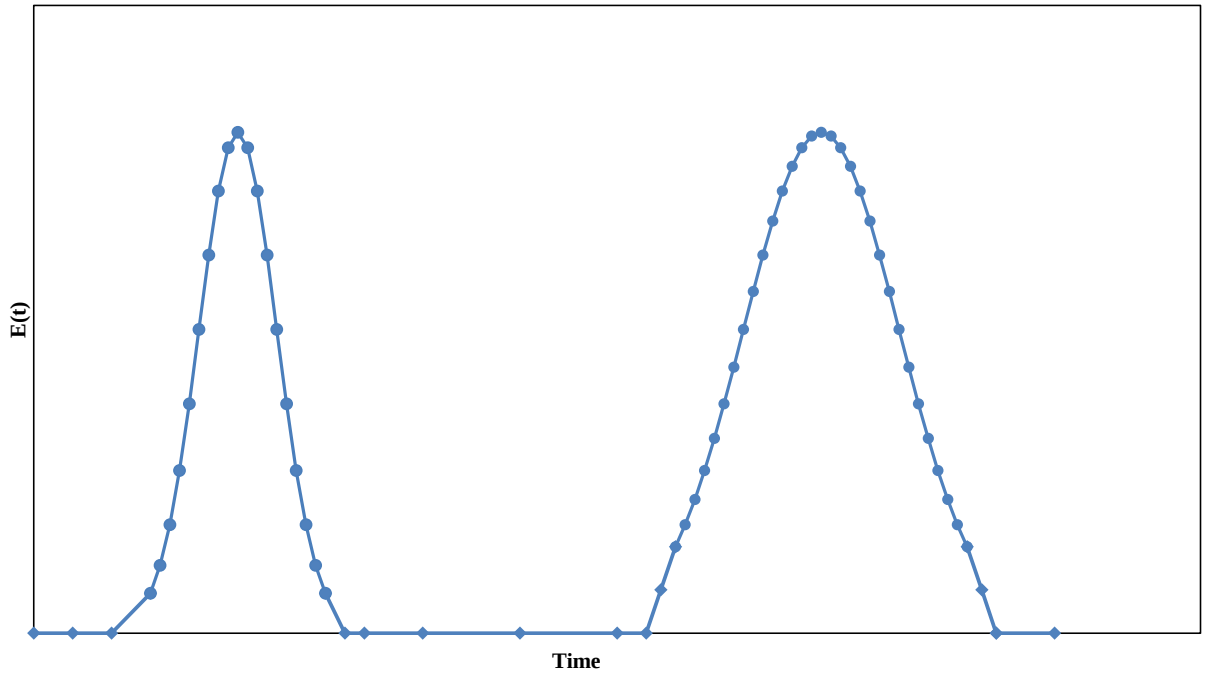

Figure 2.18: RTD output for system with internal recirculation of fluid

2.7.5 Deriving reactor model characteristics from RTD data

Effective volume utilization

The effective volume ratio indicates how much of the reactor volume is being utilized to provide the necessary contact between the fluid and bed matrix. The portion of the reactor which is not being used for this purpose is considered dead volume (Albertini *et al.*, 2012). It is calculated using Equation 2.36 (Thackston *et al.*, 1987):

$$e = \frac{\bar{t}_m}{\tau} = \frac{V_{eff}}{V} \qquad \text{Equation 2.36}$$

Thackston *et al.* (1987) developed a correlation relating the aspect ratio of an HSSF CW with the effective volume utilization:

$$e = 0.84\left[1 - \exp^{(-0.59AR_w)}\right] \qquad \text{Equation 2.37}$$

The convolution integral

In this method the RTD function, $E(t)$, is combined with data pertaining to CW inlet concentration to predict corresponding outlet concentrations. This is a particularly useful approach for determining the conversion of chemical species inside the CW assuming a first order reaction rate is applicable (Sheridan *et al.*, 2014b). The logic is depicted in Figure 2.19.

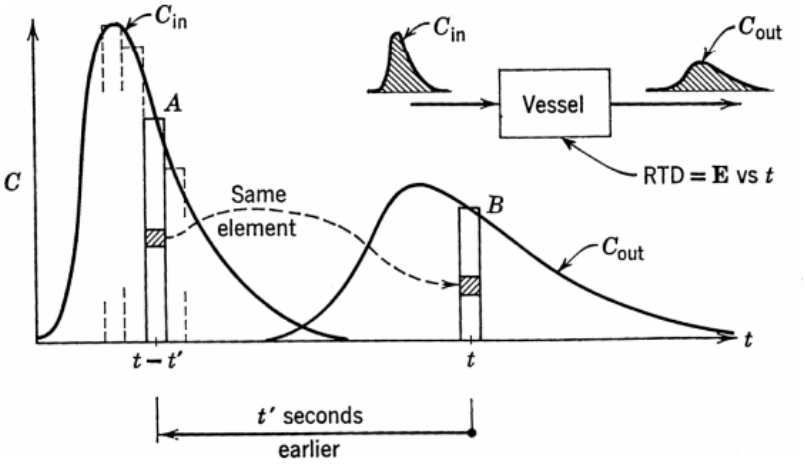

Figure 2.19: The convolution integral. Taken from Levenspiel (1999)

By performing a mass balance on tracer about to leave at time t:

$$C_{out}(t) = \int_0^t C_{in}(t')E(t-t')dt'$$

Which can be better represented using Equation 2.38:

$$C_{out}(t) = C_{inlet} * E(t) \qquad \text{Equation 2.38}$$

The conceptual thinking behind the methodology was developed for the impulse response experiment from which the $E(t)$ curve is directly determined. The method holds for the case of the step change response experiment by converting $F(t)$ to $E(t)$ using Equation 2.31.

Compartment models

Compartment models combine PFRs and CSTRs in a configuration which will best estimate the RTD response curve obtained from the HSSF CW. The total CW volume is expressed as follows (Levenspiel, 1999):

$$V = V_{eff} + V_d$$ Equation 2.39

The effective volume may comprise both plug flow and mixed flow regions:

$$V_{eff} = V_p + V_m$$ Equation 2.40

The total volumetric flow rate $\dot{v}$ may comprise an active volumetric flow rate through plug flow and mixed flow regions $\dot{v}_a$, a bypass flow rate $\dot{v}_b$ and a recycle flow rate $\dot{v}_r$. The approach used when building these models is as follows:

1. Obtain HSSF CW response curve from RTD study;
2. Compare shape of actual response curve with generic response curves associated with different reactor configurations;
3. Determine which reactor configuration best estimates the HSSF CW being studied; and
4. Determine V_{eff}, V_p and V_m as well as $\dot{v}_a$, $\dot{v}_b$ and $\dot{v}_r$ (where appropriate).

Selected reactor configurations and their associated response curves are presented in Figure 2.20.

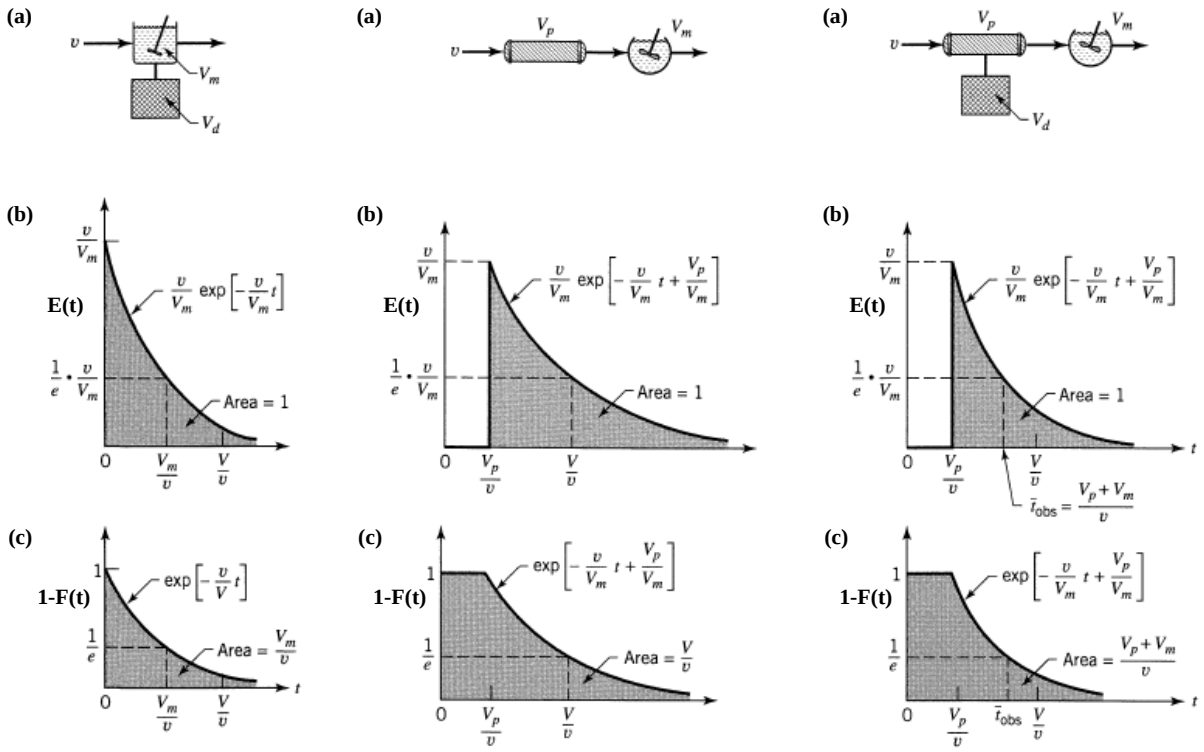

Figure 2.20: Possible reactor configurations and their associated response curves. Adapted from Levenspiel (1999)

Tanks in series model

In the tanks in series (TIS) model, the RTD data from the tracer study is analyzed to determine the number of ideal equally sized CSTRs placed in series that will best estimate the RTD response obtained from the HSSF CW being studied. A demonstration of this rationale is provided in Figure 2.21.

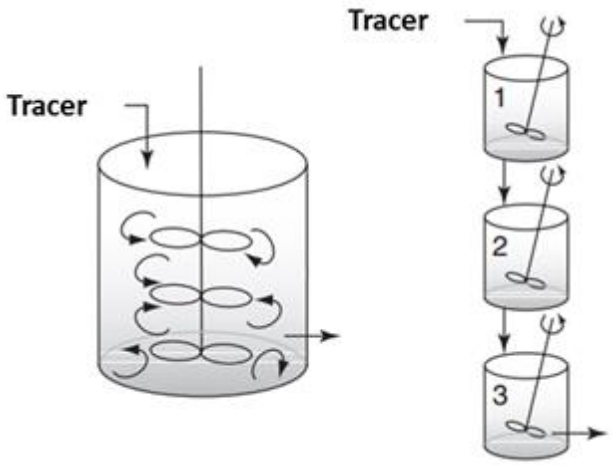

Figure 2.21: Tanks in series model demonstrated for the ideal reactor on the left using a series of idealized tanks in series shown on the right. Taken from Fogler (2005)

The number of CSTRs to be placed in series can be determined from the dimensionless variance σ_θ^2.

By re-writing Equation 2.26 in terms of dimensionless variables:

$$\sigma_\theta^2 = \int_0^\infty (\theta - 1)^2 E(\theta) d\theta \qquad \text{Equation 2.41}$$

Equation 2.41 can be simplified to produce Equation 2.42 as is discussed in Fogler (2005).

$$\sigma_\theta^2 = \int_0^\infty \theta^2 E(\theta) d\theta - 1 \qquad \text{Equation 2.42}$$

By performing a material balance on N CSTRs in series and incorporating the RTD function, it can be shown that:

$$E(\theta) = \frac{N(N\theta)^{N-1}}{(N-1)!} e^{-N\theta} \qquad \text{Equation 2.43}$$

By substituting Equation 2.43 into Equation 2.42 and through further simplification:

$$\sigma_\theta^2 = \frac{1}{N} \qquad \text{Equation 2.44}$$

The relationship between the required number of tanks in series and the shape of the normalized RTD curve is provided in Figure 2.22. As $N \rightarrow 1$, the hydrodynamics approach completely mixed

flow. As N → ∞, the degree of dispersion tends to zero and thus the hydrodynamics approach ideal plug flow behaviour.

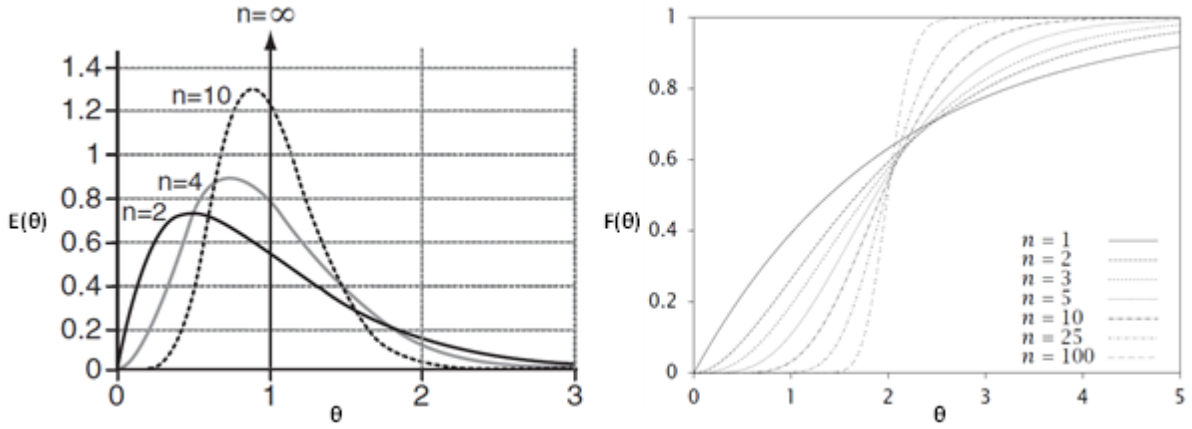

Figure 2.22: Normalized E(t) (left) and F(t) (right) curves for different values of N (Fogler, 1999)

Hydraulic efficiency

Hydraulic efficiency is used to evaluate the hydraulic performance of non-ideal reactors, with ideal plug flow systems being 100% efficient (Wahl *et al.*, 2010). The hydraulic efficiency can be described as the capacity of a reactor to utilize its entire volume by uniformly distributing flow to maximize residence time (Holland *et al.*, 2004). One of the most commonly used relations is that provided by Persson *et al.* (1999) and is shown in Equation 2.45.

$$\Lambda = e\left(1 - \frac{1}{N}\right) \qquad \text{Equation 2.45}$$

Advective-dispersive transport model

The advective-dispersive transport model, which is also referred to as the plug flow with dispersion model, entails quantifying hydrodynamic dispersion by fitting the response curve to the solution of the partial differential equation describing movement of a chemical tracer inside the subsurface media (Šimůnek *et al.*, 2003). The non-steady state continuity equation is developed by considering a shell of thickness Δx as shown in Figure 2.23.

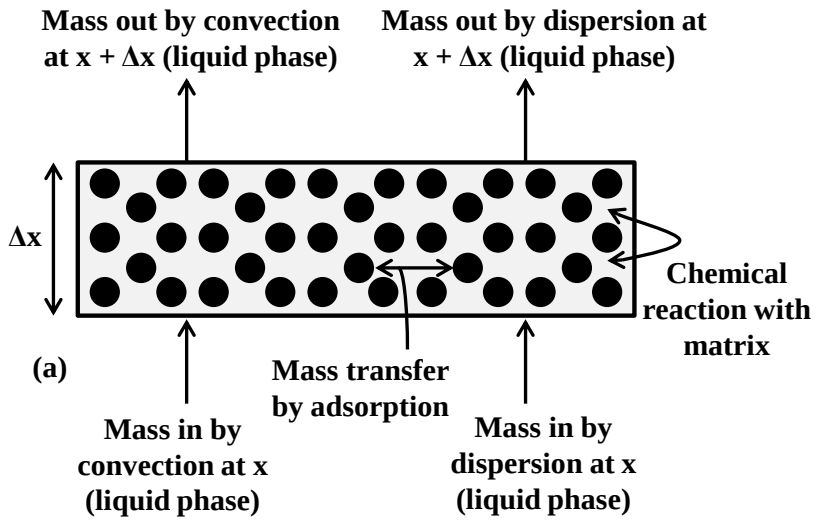

Figure 2.23: Transport processes of chemical tracer in representative shell

The generalized form of the continuity equation in the liquid and solid phase is provided in Equation 2.46 and Equation 2.47 respectively.

(Rate of tracer accumulated) = (Rate of tracer entering shell) – (Rate of tracer leaving shell) – (Rate of tracer lost to gravel matrix) – (Rate of tracer decay) Equation 2.46

(Rate of tracer accumulated) = (Rate of tracer entering shell) – (Rate of tracer leaving shell) + (Rate of tracer gained from liquid phase) Equation 2.47

Details of each of the terms in Equation 2.46 and Equation 2.47 are presented in Table 2.4.

Table 2.4: Mathematical description of transport phenomena in shell for chemical tracer

Liquid phase	**Chemical tracer**
Tracer accumulated in shell during Δt	$\varepsilon HW\Delta x\left[C_{\|t+\Delta t} - C_{\|t}\right]$
Tracer entering shell by convection during Δt	$u\varepsilon HW\Delta t C_{\|x}$
Tracer exiting shell by convection during Δt	$u\varepsilon HW\Delta t C_{\|x+\Delta x}$
Tracer entering shell by dispersion during Δt	$\varepsilon HW\Delta t J_{\|x}$
Tracer exiting shell by dispersion during Δt	$\varepsilon HW\Delta t J_{\|x+\Delta x}$
Interactions with gravel matrix during Δt	$HW\Delta x\Delta t\alpha_{f/s}a_v[C - \rho_b S]$
Sink/decay during Δt	$HW\Delta x\Delta t[\varepsilon\mu C - \varepsilon\gamma]$
Solid phase	**Conservative tracer**
Tracer accumulated in shell during Δt	$HW\Delta x\rho_b\left[S_{\|t+\Delta t} - S_{\|t}\right]$

Tracer entering shell by dispersion during Δt	
Tracer exiting shell by dispersion during Δt	
Interactions with liquid phase during Δt	$HW\Delta x\Delta t\alpha_{f/s}a_v[C-\rho_b S]$

Substituting the transport terms presented in Table 2.4 into Equation 2.46 and dividing by $HW\Delta x\Delta t$ yields:

$$\varepsilon\frac{[C_{|t+\Delta t}-C_{|t}]}{\Delta t}=-u\varepsilon\frac{[C_{|x+\Delta x}-C_{|x}]}{\Delta x}-\varepsilon\frac{[J_{|x+\Delta x}-J_{|x}]}{\Delta x}-\alpha_{f/s}a_v[C-\rho_b S]-HW\Delta x\Delta t[\varepsilon\mu C-\varepsilon\gamma]$$

Equation 2.48

Taking the limit as Δt and Δx tend to zero:

$$\varepsilon\frac{\partial C}{\partial t}=-u\varepsilon\frac{\partial C}{\partial x}-\varepsilon\frac{\partial J}{\partial x}-\alpha_{f/s}a_v[C-\rho_b S]-\varepsilon\mu C+\varepsilon\gamma$$

Equation 2.49

Substituting Equation 2.50 for dispersive transport (Levenspiel, 1999) yields the chemical tracer continuity equation in the liquid phase in Equation 2.51.

$$J_x=-D\frac{\partial C}{\partial x}$$

Equation 2.50

$$\varepsilon\frac{\partial C}{\partial t}=-u\varepsilon\frac{\partial C}{\partial x}+D\varepsilon\frac{\partial^2 C}{\partial x^2}-\alpha_{f/s}a_v[C-\rho_b S]-\varepsilon\mu C+\varepsilon\gamma$$

Equation 2.51

Total hydrodynamic dispersion is a function of molecular diffusion as well as mechanical dispersion, which occurs as a result of the fluid flowing through channels of different geometries and hydraulic conductivity (Bons *et al.*, 2013). Mechanical dispersion of fluid in the subsurface media can occur in both the longitudinal and transverse directions (Delgado, 2007). This leads to the formulation of the chemical dispersion coefficient in Equation 2.52 (Rau *et al.*, 2012).

$$D=\varepsilon D_m+u[\alpha_l+\alpha_t]$$

Equation 2.52

Where α_l and α_t are defined as the longitudinal and transverse solute dispersivity, respectively. Hydrodynamic dispersivity is a function of the subsurface media heterogeneity and is, in essence, the physical property which an RTD study attempts to evaluate.

Substituting the transport terms presented in Table 2.4 into Equation 2.47 and dividing by $HW\Delta x\Delta t$ yields:

$$\rho_b \frac{[S_{|t+\Delta t} - S_{|t}]}{\Delta t} = \alpha_{f/s} a_v [C - \rho_b S] \quad \text{Equation 2.53}$$

Taking the limit as Δt tends to zero yields the tracer continuity equation in the solid phase in Equation 2.54.

$$\rho_b \frac{\partial S}{\partial t} = \alpha_{f/s} a_v [C - \rho_b S] \quad \text{Equation 2.54}$$

Combining the liquid and solid phase continuity equations provides Equation 2.55:

$$\frac{\partial C}{\partial t} + \frac{\rho_b}{\varepsilon}\frac{\partial S}{\partial t} = -u\frac{\partial C}{\partial x} + D\frac{\partial^2 C}{\partial x^2} - \mu C + \gamma \quad \text{Equation 2.55}$$

The relationship between the adsorbed and fluid tracer concentrations is given by the linearized isotherm in Equation 2.56 (Van Genuchten, 1981) and substituting into Equation 2.55 provides the overall continuity equation for a chemical tracer in Equation 2.57.

$$S = K_d C \quad \text{Equation 2.56}$$

$$R\frac{\partial C}{\partial t} = -u\frac{\partial C}{\partial x} + D\frac{\partial^2 C}{\partial x^2} - \mu C + \gamma \quad \text{Equation 2.57}$$

The transport equation in Equation 2.57 includes the chemical retardation factor which is defined in Equation 2.58 (Freeze and Cherry, 1979) and the definition of the Peclet number for CWs provided in Equation 2.59 (Chazarenc *et al.*, 2003). The distribution coefficient, K_d, relates tracer concentration in the liquid and solid phases. The magnitude of K_d depends on the physical properties of the tracer and can also be affected by the porous media through which it travels (Rubin, 2012). In general, tracers which have K_d values close to zero are considered non-sorbing and vice versa (Field and Pinsky, 2000; Vilks and Baik, 2001).

$$R = 1 + \frac{\rho_b K_d}{\varepsilon} \quad \text{Equation 2.58}$$

$$Pe = \frac{uL}{D} \quad \text{Equation 2.59}$$

Chemical retardation has the effect of slowing down the bulk movement of tracer due to adsorption on subsurface media sites (Rezanezhad *et al.*, 2012). First order decay (μ) causes a permanent loss

of tracer and zero order production (γ) generates additional tracer independent of the tracer concentration. For tracers which are considered non-reactive $\mu = \gamma = 0$.

The solution to Equation 2.57 depends on whether an impulse or step change response RTD study is performed. As will be demonstrated in Chapter 5, this methodology will only be applied when modelling response curves from a step change RTD study and hence solutions only applicable to the step change response approach will be discussed. The initial condition for Equation 2.57 is presented in Equation 2.60. Equation 2.61 represents the boundary condition of a step change in chemical tracer in the wetland feed at time zero. Since it is expected that mechanical dispersion will dominate over molecular diffusion downstream conditions should not affect the flow of tracer inside the system (Peters and Smith, 2001) and hence the semi-infinite boundary condition was used as shown in Equation 2.62.

$$C(x, 0) = C_{initial} \qquad \text{Equation 2.60}$$

$$\left(-D\frac{\partial C}{\partial x} + uC\right)\Big|_{x=0} = uC_{inlet} \qquad \text{Equation 2.61}$$

$$\frac{\partial C}{\partial x}(\infty, t) = 0 \qquad \text{Equation 2.62}$$

The analytical solution to Equation 2.57 for the case of a non-reactive chemical tracer ($\mu = \gamma = 0$) was developed by Lindstrom *et al.* (1967) and Gershon and Nir (1969) and is presented in Equation 2.63. It is also recognized that it is possible to solve Equation 2.57 numerically but requires separate treatment which is not included in this text. $A(x, t)$ is a function of the transport properties of the tracer and is defined according to Equation 2.64.

$$C(x, t) = C_{initial} + (C_{inlet} - C_{initial})A(x, t) \qquad \text{Equation 2.63}$$

$$A(x, t) = \frac{1}{2}\operatorname{erfc}\left[\frac{Rx - ut}{2(DRt)^{1/2}}\right] + \left(\frac{u^2 t}{\pi DR}\right)^{\frac{1}{2}} \exp\left[-\frac{(Rx - ut)^2}{4DRt}\right] - \frac{1}{2}\left(1 + \frac{ux}{D} + \frac{u^2 t}{DR}\right)\exp\left(\frac{ux}{D}\right)\operatorname{erfc}\left[\frac{(Rx + ut)}{2(DRt)^{1/2}}\right]$$

Equation 2.64

The solution to Equation 2.57 for the case of a reactive chemical tracer ($\mu, \gamma \neq 0$) was developed by Van Genuchten (1981), with the solution presented in Equation 2.65:

$$C(x, t) = \frac{\gamma}{\mu} + \left(C_{initial} - \frac{\gamma}{\mu}\right)A(x, t) + \left(C_{inlet} - \frac{\gamma}{\mu}\right)B(x, t) \qquad \text{Equation 2.65}$$

Where $A(x,t)$ and $B(x,t)$ are defined in Equation 2.66 and Equation 2.67 respectively.

$$A(x,t) = \exp\left(\frac{-\mu t}{R}\right)\left\{1 - \frac{1}{2}\operatorname{erfc}\left[\frac{Rx-ut}{2(DRt)^{1/2}}\right] - \left(\frac{u^2 t}{\pi DR}\right)^{\frac{1}{2}} \exp\left[-\frac{(Rx-ut)^2}{4DRt}\right] + \frac{1}{2}\left(1 + \frac{ux}{D} + \frac{u^2 t}{DR}\right)\exp\left(\frac{ux}{D}\right)\operatorname{erfc}\left[\frac{(Rx+ut)}{2(DRt)^{1/2}}\right]\right\} \quad \text{Equation 2.66}$$

$$B(x,t) = \frac{u}{(u+v)}\exp\left[\frac{(u-v)x}{2D}\right]\operatorname{erfc}\left[\frac{Rx-ut}{2(DRt)^{1/2}}\right] + \frac{u}{(u-v)}\exp\left[\frac{(u+v)x}{2D}\right]\operatorname{erfc}\left[\frac{Rx+ut}{2(DRt)^{1/2}}\right] + \frac{u^2}{2\mu D}\exp\left(\frac{ux}{D} - \frac{\mu t}{R}\right)\operatorname{erfc}\left[\frac{Rx+ut}{2(DRt)^{1/2}}\right] \quad \text{Equation 2.67}$$

$$v = u\left(1 + \frac{4\mu D}{u^2}\right)^{\frac{1}{2}} \quad \text{Equation 2.68}$$

Alternatively, the mechanical dispersion can be quantified (in the case of both impulse and step change response RTD studies) by using the relation between Pe, $\bar{t}_m$ and σ^2 provided in Equation 2.69 (Fogler, 1999):

$$\frac{\sigma^2}{\bar{t}_m^2} = \frac{2}{Pe} - \frac{2}{Pe^2}(1 - e^{-Pe}) \quad \text{Equation 2.69}$$

2.8 Types of hydraulic tracers

In order for a substance to be considered as an appropriate hydraulic tracer, it is required to meet a certain set of criteria regarding its physical and chemical properties. These criteria are (Headley and Kadlec, 2007):

1. The tracer should be soluble in the feed water;
2. The tracer should not be able to react with the feed water or any of the CW constituents i.e. it should be non-reactive;
3. The tracer should have a low K_d as this would prevent large quantities of tracer from being adsorbed onto the CW matrix;
4. The tracer density should adequately approximate that of the feed water. If the tracer density is too high it would sink to the bottom of the CW and the RTD response would not reflect the actual flow patterns of the water inside the system;
5. The tracer should not be toxic to organisms living inside the CW and to humans;

6. The tracer should have low detection limits and have as little background concentration in the CW as possible; and
7. The detection equipment and the tracer itself should be inexpensive.

The three most common types of tracers used in CW RTD studies are cations and anions, radioactive tracers and chemical dyes (Sabatini, 2000).

2.8.1 Radioactive tracers

Radioactive tracers are attractive since they have low detection limits which results in very little having to be injected into the CW (Zecheru and Goran, 2013). These tracers are not easily influenced by system conditions such as pH and temperature. Radioactive tracers also do not experience interference from other chemical compounds during sample analysis (Choppin *et al.*, 2002). Nevertheless, radioactive tracers pose an inherent health and safety risk and consequently their use has been much more limited when compared to ionic and chemical tracers.

2.8.2 Ionic tracers

Chloride, bromide and lithium ions are commonly used in RTD studies because they do not sorb to the CW matrix and are relatively inexpensive when compared to other types of tracers (Flury and Wai, 2003). Chloride and bromide ions are the most appropriate (Gasser *et al.*, 2014; Rauch-Williams *et al.*, 2010) since they are not subjected to chemical transformations, have low background concentrations inside the CW and are not toxic to humans operating the system and to aquatic organisms.

2.8.3 Chemical dyes

Chemical dyes have been a popular choice for conducting tracer studies in CWs (Knowles *et al.*, 2010; Passeport *et al.*, 2010). Dyes can be directly observed or detected through a sampling analysis (Flury and Wai, 2003). Dyes are large organic molecules which have functional groups attached to the molecular kernel. These functional groups facilitate sorption onto solid surfaces and can lead to immobilization of the dye, rednering it as an ineffective tracer. Flury and Wai (2003) note that the more sulfonic acid functional groups attached to the molecular kernel the less sorption there will be to carbon surfaces such as soil. Fluorescein, Uranine, Sulforhodamine G and Rhodamine WT are the most commonly used tracers as they are not easily sorbed to solid surfaces, have high solubility in water and are physically and chemically stable under a variety of

environmental conditions (Von Möser and Sagl, 1967; Smart and Laidlaw, 1977; Wilson *et al.*, 1986).

The major disadvantage of using ionic species and chemical dyes as tracers *is* their resistance to decay. This may cause an environmental hazard downstream of the RTD study and dedicated disposal infrastructure of the RTD effluent is required to prevent contamination of water bodies with which the RTD effluent comes into contact.

2.9 Biomimicry as a tool for the development of more sustainable HSSF CW designs and hydraulic modelling processes

2.9.1 Definition of Biomimicry

Biomimicry can be classified as an applied science which involves the careful study of biology to derive inspiration for the purposes of solving human problems (El-Zeiny, 2012). Biomimicry can be performed on three levels namely form, process and system (Benyus, 1997). Form entails mimicking the specific physical structure of an organism to develop innovative product designs. An example of this would be the PAX Water Mixer^{TM} which incorporates an impeller in the shape of a *Calla lily* to reduce energy consumption and improve mixing performance. Process entails mimicking physical and chemical processes developed by nature e.g. developing manufacturing processes which use life-friendly chemistry or materials manufacturing at lower temperatures and pressures. System entails mimicking form, physical and chemical processes as well as the interaction of different organisms within a specific network to produce more efficient corporate structures as well as more sustainable power generation systems and water management strategies.

2.9.2 The Biomimicry framework

Biomimicry requires the integration of biology into every aspect of the design process. The framework consists of four categories (Benyus, 1997):

1. Scoping: definition of context and identification of design challenge;
2. Discovering: careful study of forms, processes and systems developed in nature for purposes of inspiration;
3. Creating: execution of design; and
4. Evaluating: quantify the performance of the developed design and measure it against a specified benchmark.

Biomimicry can be applied in two distinctly different scenarios: Biology to Design and Challenge to Biology, as shown in Figure 2.24 and Figure 2.25 respectively.

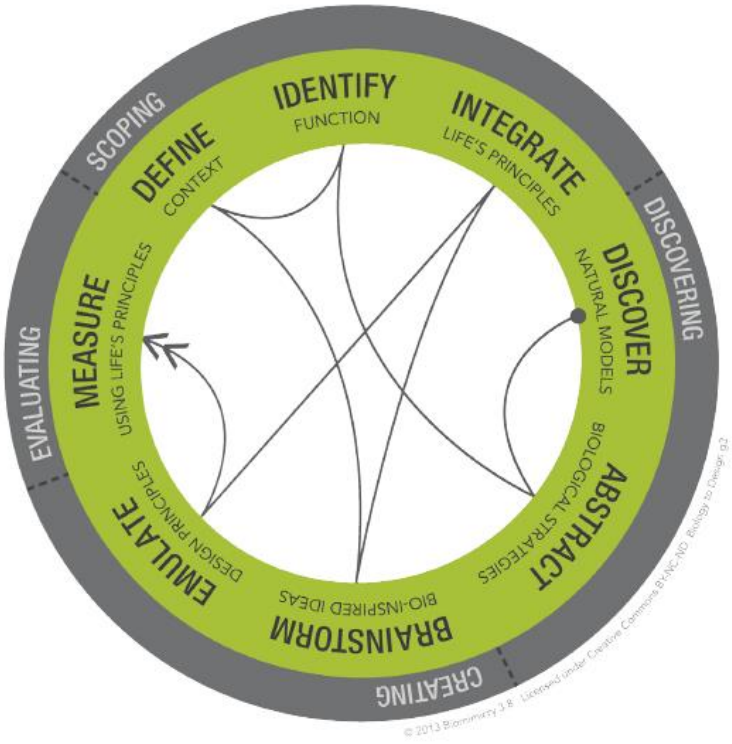

Figure 2.24: Integration of the Biomimicry framework into the Biology to Design scenario. Taken from the Biomimicry Institute

In the Biology to Design scenario an observation of a specific form, process or system in nature inspires the design of an innovative, potentially more sustainable product to solve a specific problem encountered in society. An example would be the study of the keratin fibers on the soles of geckos which allows them to attach to vertical surfaces (Geim *et al.*, 2003). These observations have led to the development of biodegradable tissue adhesives in the medical industry which may be able to seal wounds and possibly replace sutures or staples (Mahdavi *et al.*, 2008).

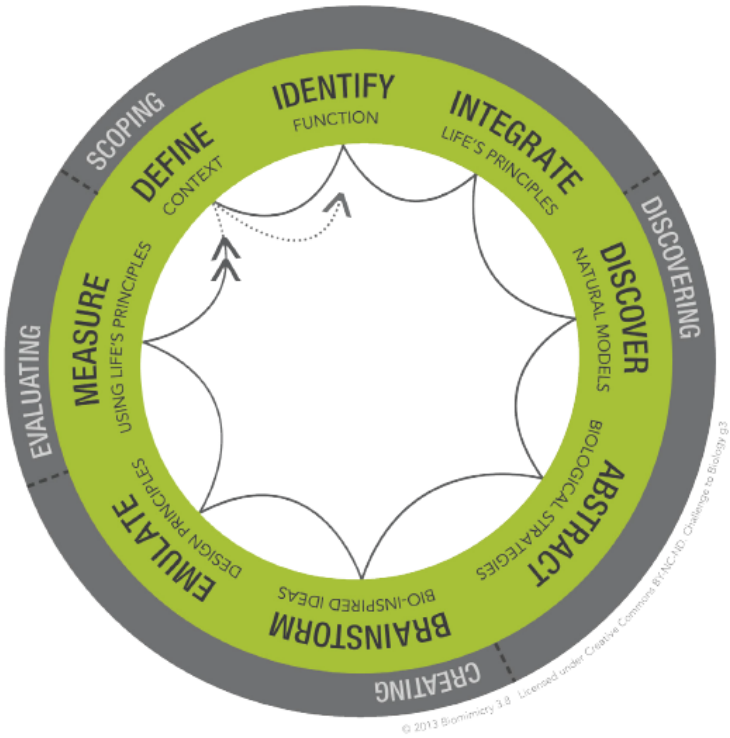

Figure 2.25: Integration of the Biomimicry framework into the Challenge to Biology scenario

In the Challenge to Biology scenario a design team seeks biological insight to solve a specific societal problem. An example of this would be the Eastgate Building in Harare, Zimbabwe and the CH2 Building in Melbourne, Australia. In both cases an interior temperature regulation and ventilation system was required to be designed. The final design included the harnessing of evaporative cooling effects from underground sewage water in the same way as termite mounds are built to take advantage of underground aquifers which are in close proximity (Zari, 2007).

2.9.3 Biomimicry design principles

The successful survival strategies used by species in nature have been summarized into a set of principles which are presented in Figure 2.26.

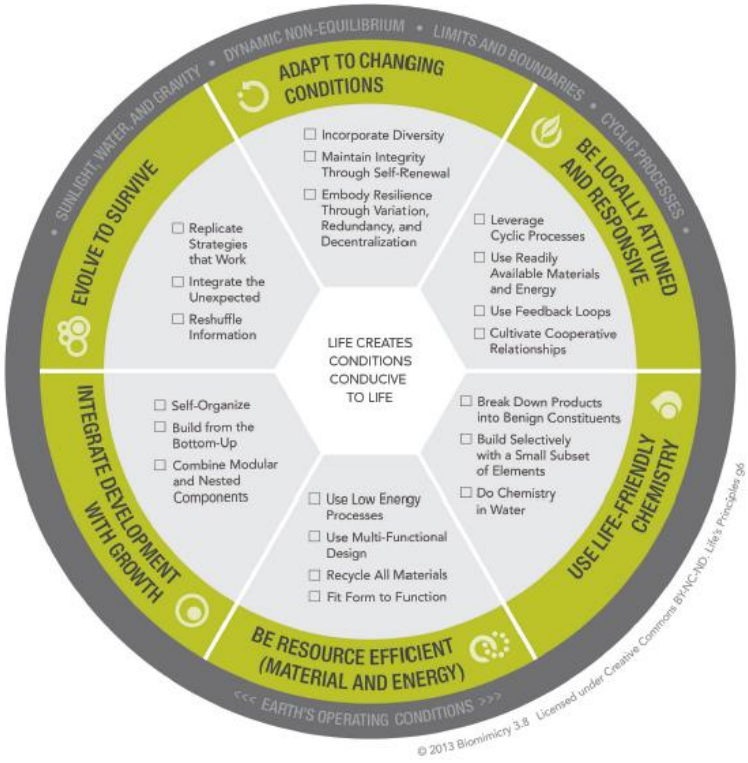

Figure 2.26: Life's Principles. Taken from the Biomimicry Institute

The principles presented in Figure 2.26 are used in one of two stages of the Biomimicry design process. They are used either in the evaluation phase in the product design process as a benchmark against which the product is tested or as a driver for innovative Biomimetic designs at the front end of a project. The latter application is typically found in the Challenge to Biology case and will thus be explored further in this dissertation. In Section 2.9.4 a case study is presented which illustrates how Life's Principles can be used to develop an HSSF CW design which will be able to overcome one of the weaknesses associated with CWs and that is their inability to maintain a high treatment performance when subjected to inconsistent feed conditions.

2.9.4 Case study: HSSF CW poor adaptability to changing feed conditions

Various studies have been performed to understand the effects which certain parameters, such as hydraulic loading as well organic loading have on CW treatment performance (Caselles-Osorio *et al.*, 2007; Vymazal and Kröpfelová, 2009). Galvão and Matos (2012) note that such studies only analyze the response of the wetland system under isolated steady state conditions. These studies do not reveal details of the inherent process stability and buffering capacity of CWs, which

describes the ability of these systems to adapt and maintain treatment efficiency output under sudden and unexpected changes in feed conditions.

The purpose of the study performed by Galvão and Matos (2012) was to determine the buffering capacity of HSSF CWs over a period of five months by analyzing system response to fluctuations in COD mass loading. The experimental set up consisted of three main groups which varied according to the COD mass loading employed. Within each group there existed three subsystems. The first contained no vegetation, the second was colonized with *Phragmites australis* and the third with *Scirpus*. The reason for utilizing different species of vegetation was to determine the relevant buffering capacities of different vegetation types. Each of the wetland subsystems were filled with gravel having a porosity of 30%. In Figure 2.27 a visual of the experimental set up is provided.

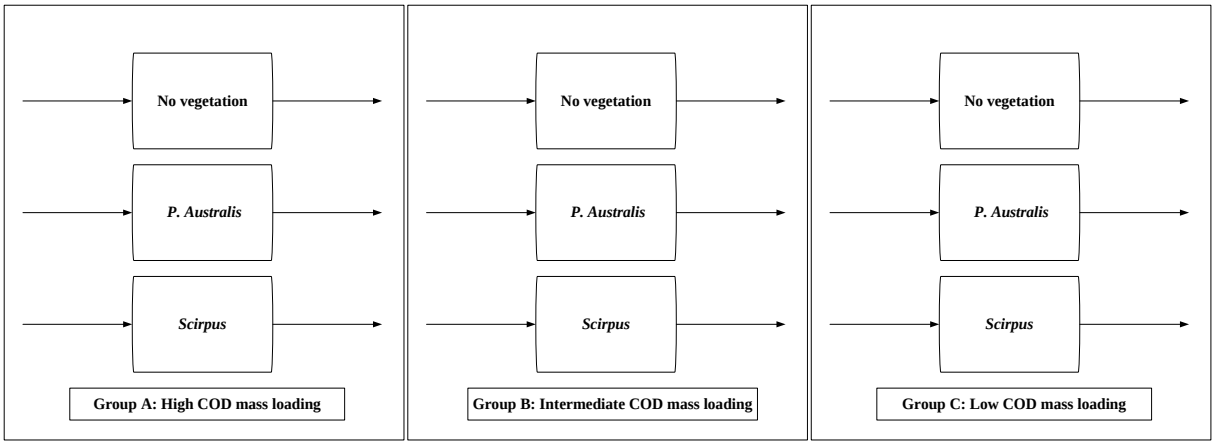

Figure 2.27: Schematic of the experimental set up used by Galvão and Matos (2012)

The research comprised three phases. Phase one lasted three and a half months during which each wetland group accepted a certain COD mass loading to establish a baseline output removal efficiency. Group A was fed with 11.4 g COD/m^2/day, group B with 5.3 g COD/m^2/day and group C with potable tap water to ensure that there was no influent COD. At the start of phase two the COD mass loading was increased by 22% in group A, 7% in group B and the loading in group C was increased to 1.7 g COD/m^2/day. The second phase only lasted two weeks and was used to test the wetland systems' performance in response to a sudden increase in COD loading. During the third phase the initial loading conditions were again implemented to test how the wetlands would

respond to a sudden decrease in COD loading and to determine if the wetlands would eventually output similar removal efficiencies compared to phase one. The final phase lasted four weeks. A summary of the results obtained from phases one and two are provided in Table 2.5.

Table 2.5: Summary of results obtained from study performed by Galvão and Matos (2012)

		Phase 1		**Phase 2**	
Group	**Species**	**Removal rate ($g/m^2/day$)**	**Removal efficiency (%)**	**Removal rate ($g/m^2/day$)**	**Removal efficiency (%)**
A	None	7.85	69	8.83	64
	P	7.64	67	7.68	56
	S	7.94	70	9.65	70
B	None	3.27	62	4.76	84
	P	3.8	72	2.53	45
	S	3.44	65	3.09	55
C	None	N/A	N/A	1.42	84
	P	N/A	N/A	1.27	75
	S	N/A	N/A	1.27	75

The CWs in group A increased their removal rate when exposed to a sudden increase of 22% in the COD loading. This result implies that there was some degree of adaptation of the microbial populations responsible for the removal of COD. However, the majority of the CWs within this group experienced a decrease in removal efficiency during phase two, indicating that they did not adapt fully to the sudden change in feed condition and the buffering capacity of those systems were limited. Wetlands in group B, apart from the unplanted system, experienced a decrease in COD removal rate when exposed to the sudden increase in COD mass loading. This decrease in removal rate indicates that the microbial populations were not able to adapt to the change in feed condition and consequently had no buffering or adaptation capacity to the sudden increase in COD loading.

Using Biomimicry principles to design HSSF CWs with improved apdaptbility to changing feed conditions

According to the Life Principles presented in Figure 2.26, organisms have been able to adapt to changing conditions by using three different strategies:

- Incorporating diversity;

- Embodying resilience through variation, redundancy and decentralization; and
- Maintaining integrity through self-renewal.

These three strategies can be combined to produce a preliminary design such as that presented in Figure 2.28.

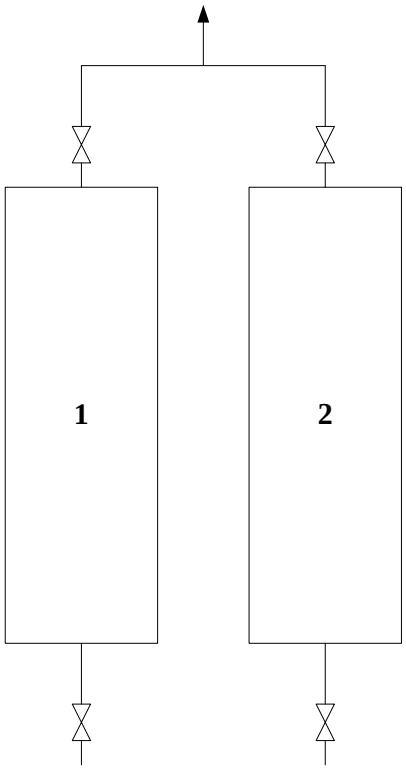

Figure 2.28: Biomimetic HSSF CW design which allows for periodic pulsing through either wetland subsection

In Figure 2.28 the CW is split into two cells to accommodate for periodic pulses of mass loadings. These periodic pulses through the system throughout the operational lifetime would prevent bacteria and vegetation from settling into a state of equilibrium and enhances their capability to respond to dynamic contexts when the need arises. The split system allows for pulses to be sent to one of the cells while the other runs under stable conditions to ensure effluent treatment meets required levels.

2.9.5 Using Biomimicry principles to design HSSF CWs with an integrated clogging management system

As discussed in Section 2.6.2 clogging is a major operational problem for HSSF CWs. Clogging reduces the effective volume utilization of the system and treatment efficiency is decreased as a result. Different management strategies have been developed to remediate the effects of clogging inside HSSF CWs, with two of the most prominent being excavation and washing of the bed media as well as in-situ application of cleaning chemicals such as hydrogen peroxide (Nivala *et al.*, 2012). These strategies are not appropriate especially for HSSF CWs used in rural communities in South Africa where taking the CW offline for extended periods of time for excavation and washing would cut off a primary supply of water for domestic and agricultural use. The other approach of in-situ application of cleaning chemicals may pose health and safety risks to local community members and the long-term effects of these substances on the well-being of the ecosystem inside the CW are unknown (Nivala and Rousseau, 2009).

By examining Biomimicry Life Principles in Figure 2.26 it is possible to develop innovative designs which would incorporate an effective clogging management strategy. Two overarching principles which are applicable to managing wetland clogging are: adapting to changing conditions and integrating development with growth. Within the principle of adapting to changing conditions, the sub-principle of embodying resilience through variation, redundancy and decentralization is appropriate since it advocates maintaining function following a disturbance by incorporating a variety of duplicate forms, processes or systems that are not located exclusively together. This sub-principle can be combined with the sub-principle of combining modular and nested components found within integrating development with growth to produce a set of system designs which limit the effect which wetland clogging has on treatment efficiency. One such CW design would be to modularize the wetland into smaller sub-sections as indicated in Figure 2.29.

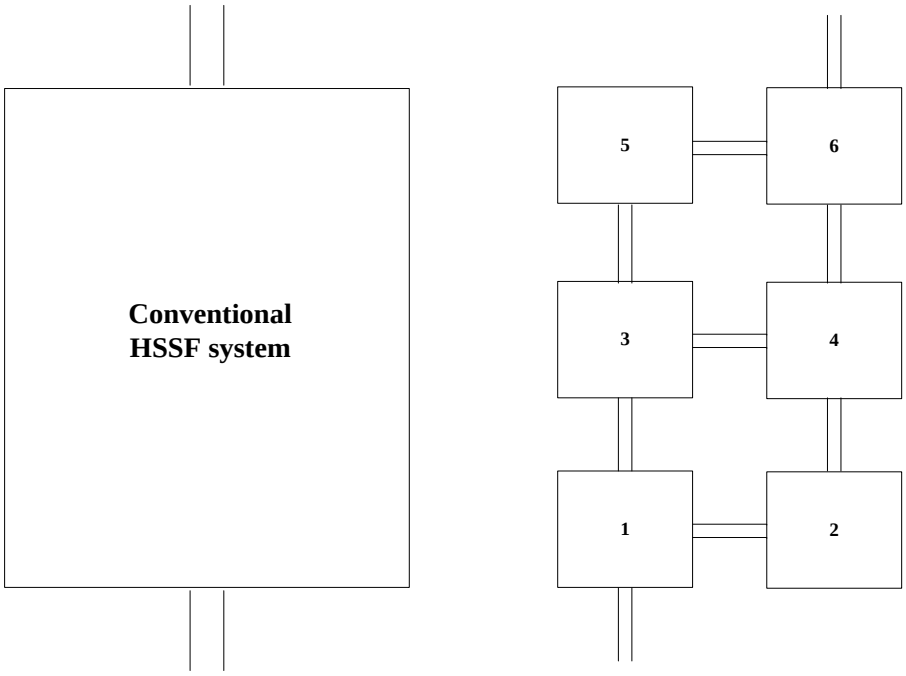

Figure 2.29: Conventional HSSF system (left) and modularized Biomimetic HSSF system (right)

If a section of the CW becomes clogged to the extent that the hydraulic conductivity is dramatically reduced, the section can be removed and the flow paths can be altered to bypass the section undergoing maintenance. This design thus allows for continuous treatment of water which would be a necessity for rural communities that do not have readily available access to water cleaned by other treatment facilities.

2.9.6 Using Biomimicry principles to develop more environmentally friendly hydraulic modelling processes for HSSF CWs

The tracers used in RTD studies for modelling the hydraulic behaviour of HSSF CWs pose a risk to the environment. The RTD effluent containing non-reactive tracer cannot be disposed directly into surrounding water bodies as the tracer concentration may cycle up to a point where the environmental limits are breached. Biomimicry Life Principles dictate that any product design should be locally attuned and responsive and it is a requirement that the design makes use of life-friendly chemistry. Life-friendly chemistry implies utilizing benign components which do not cause permanent damage to the surrounding ecosystem and being locally attuned and responsive means utilizing readily available materials and energy. A tracer which meets these criteria is heat. The energy required to raise the temperature of the feed water above ambient conditions can be

derived from solar water heaters. Heat is also considered a much more benign tracer when compared to conventional chemical tracers as the CW temperature can rapidly equilibrate to ambient conditions after the RTD study and the RTD effluent can be discharged without any additional disposal infrastructure.

2.10 Research objectives

Within the context presented above, there were three main research objectives for this study. These were:

1) To develop a comprehensive comparison between the three available RTD modelling methodologies namely the impulse, step change integral and step change derivative modelling methodologies. This included generating hydraulic data using impulse and step change response experiments from planted and unplanted pilot-scale HSSF CWs at the IMWaRU facility at the University of the Witwatersrand, Johannesburg. To the best of the author's knowledge, little has been published in the form of a direct comparison of the three methodologies and it is intended that the comparison would assist CW designers in selecting the most appropriate modelling methodology in future hydraulic studies.

As shown in Section 2.9 Biomimicry Life Principles are a useful tool for developing innovative HSSF CW designs which produce a much more consistent treatment performance as well as for the development of hydraulic tracers which are more environmentally sustainable. Research objectives 2 and 3 expand on these ideas as follows:

2) To illustrate how hydraulic data obtained from an RTD study can be used to identify regions within an HSSF CW most prone to clogging and couple these results with the Biomimicry Life Principles of adapting to changing conditions and integrating development with growth to produce an HSSF CW design with an inherent clogging management strategy. The outcome of this task may be particularly useful for designers of HSSF CWs for rural communities who wish to build systems which are consistent in their treatment performance and are relatively easy to maintain.
3) To explore the use of heat as a more environmentally friendly alternative to conventional chemicals as a hydraulic tracer for RTD studies on HSSF CWs. To date, little has been published regarding the use of heat as a tracer for RTD studies on HSSF CWs and is most

likely due to its non-conservative behaviour. The movement of heat through the system would be retarded due to absorption by the subsurface media and would also dissipate to the surroundings. These two phenomena distort the heat tracer response curve and would result in an inaccurate description of the hydraulic behaviour of the CW. Thus the task included developing a mathematical model, based on transport phenomena theory, which maps the heat tracer response curve to the response curve which would be obtained if a conservative chemical tracer were to be used. The model would be tested by conducting a dual heat-chemical tracer study on a laboratory-scale unplanted HSSF CW and comparing the hydraulic modelling results obtained from the predicted chemical tracer response curve with the actual experimental chemical tracer response curve.

3. A comparison of three different residence time distribution modelling methodologies for horizontal subsurface flow constructed wetlands

In this chapter the comparison developed between the three available hydraulic modelling methodologies for HSSF CWs is presented. First a discussion highlighting the need for detailed hydraulic modelling of HSSF CWs is presented followed by the methodology used to generate the hydraulic data as well as subsequent modelling results. The experiences gathered generating the hydraulic data as well as the modelling results are then critically assessed and form the basis on which the comparison between the methodologies is built.

This chapter has been submitted for peer review and publication to *Ecological Engineering.* The contribution of the co-authors towards the work is primarily of supervision or collaboration and the experimental work and write-up was conducted by the author of this dissertation. The original data for this chapter is presented in Appendices A to E.

3.1 Abstract

In this paper three different residence time distribution modelling methodologies for horizontal subsurface flow constructed wetlands were compared and these were the impulse response, step change derivative and step change integral modelling methodologies. Impulse response and step change tracer studies were conducted on pilot scale horizontal subsurface flow constructed wetlands to generate the concentration-time data to be fed into the impulse response and step change modelling approaches, respectively. For the unplanted reactor, the two step change modelling methodologies suggested the same fluid flow behaviour reflected by almost identical values for the mean of the residence time distribution ($\bar{t}_m$) and the same value for the number of stirred tanks in series (N) and Peclet number (Pe). The impulse response modelling approach suggested a 7% higher $\bar{t}_m$ and a lower degree of dispersion. For the planted system each modelling methodology suggested different fluid flow behaviour. Practical limitations were attempted to be identified for the two types of tracer experiments. The limitations of the experiments could be considered limitations of the modelling methodologies as they depended on the tracer experiments for data generation. Sufficient data on the peak of the impulse response curve for the unplanted reactor was not able to be collected and may have affected the impulse response modelling methodology results. Sampling down the length of the reactor revealed that tracer dispersion had

an effect of broadening the impulse response curves to the extent that it was almost impossible to identify non-ideal flow behaviour such as short-circuiting. The mathematical techniques employed by each modelling methodology were also critically assessed. It was found that varying the size and hence number of subintervals used in Simpson's 1/3 rule for numerical integration resulted in different values for $\bar{t}_m/\tau$ for each modelling approach. The lower the sensitivity of the modelling methodology the better as choosing a parameter as arbitrary as subinterval size should not have a noticeable effect on reported hydraulic behaviour. For both reactor systems the step change derivative approach was least sensitive to subinterval selection, reporting a 1% and 4% variation in $\bar{t}_m/\tau$ for the planted and unplanted system, respectively whereas $\bar{t}_m/\tau$ determined by the step change integral and impulse response modelling methodologies varied by 10% or more in some cases. The differentiation of F(t) to obtain E(t) was highlighted to be a potential weakness of the step change derivative methodology as it had the capability to amplify background noise which may have affected the calculation of the hydraulic parameters. It was concluded that each modelling methodology had the potential to output a different reactor model for the same reactor and that each approach has its own inherent strengths and weaknesses. The choice of modelling methodology is ultimately dictated by availability of experimental equipment and the designer's confidence in using each of the respective approaches.

Keywords: residence time distribution modelling, waste water treatment, packed bed reactor, horizontal subsurface flow constructed wetland, reactor model

3.2 Introduction

A horizontal subsurface flow constructed wetland (HSSF CW) is an example of a packed bed reactor (Vymazal and Kröpfelová, 2009; Sheridan *et al.*, 2014b), which utilizes a series of interrelated physical, chemical and biological processes to treat various types of waste water (Scholz and Hedmark, 2010; Dordio and Carvalho, 2013; Ligi *et al.*, 2014). These systems are typically packed with a solid matrix such as soil, gravel, clay aggregates or metallurgical slags (Drizo *et al.*, 1999; Dotro *et al.*, 2011b; Sheridan *et al.*, 2013). They may also be planted with different types of macrophytes to enhance the treatment processes (Leto *et al.*, 2013). Some of the benefits of using macrophytes in the system include their ability to transfer oxygen from the

atmosphere to the root zone to facilitate aerobic pollutant degradation processes as well as accumulation of toxic heavy metals in the plant tissue (Stottmeister *et al.*, 2003).

As is the case with other types of packed bed reactors, the hydrodynamic behaviour of CWs has historically been over-simplified as being ideal plug flow (Werner and Kadlec, 2000). The presence of complex plant root structures; the growth of bacterial biofilms within the wetland matrix; the entrapment of suspended solids and the precipitation of heavy metals originating from the feed waste water results in both spatially and temporally-dependent flow resistance (Sheoran and Sheoran, 2006; Suliman *et al.*, 2006a; Knowles *et al.*, 2011). The flow resistance causes non-uniform flow velocity profiles and, hence, different pockets of water reside within the system for different lengths of time, giving rise to a residence time distribution (RTD) and a mean of the residence time distribution which is smaller than or equal to the ideal theoretical residence time (Levenspiel, 1999). Pollutant degradation models built on the ideal plug flow assumption have, thus, proved to be in the large part inaccurate (Marsili-Libelli and Checchi, 2005; Galvão *et al.*, 2010; Sheridan *et al.*, 2014a), since there is no way of incorporating the varying lengths of time spent by different pockets of waste water in contact with elements of the system which can facilitate their degradation. This may lead to the installation of an under-sized CW and an unsatisfactory production performance. Consequently, a pilot scale reactor is built beforehand and an RTD study is conducted to develop a reactor model accounting for the non-ideal flow behaviour which when coupled with kinetic data can facilitate more accurate sizing of the reactor equipment (Lima and Zaiat, 2012; Rüdisüli *et al.*, 2012).

3.3 Background

HSSF CWs use a variety of treatment processes to improve the quality of ground and surface water (Marchand *et al.*, 2010; Galletti *et al.*, 2010), some of which will be discussed in the sections which follow.

3.3.1 Physical treatment processes

Adsorption of phosphates

Soluble inorganic phosphates are transferred from the soil-pore interface to the surface of the soil matrix via adsorption (Huett *et al.*, 2005; Vohla *et al.*, 2011). Adsorption rates are dependent on the granular medium's texture, grain size distribution, iron, calcium, magnesium and aluminium

content (Garcia *et al.*, 2010) as well as environmental factors such as redox potential and pH (Vymazal *et al.*, 1998). The higher the iron, calcium, magnesium and aluminium content the higher the adsorption capacity becomes as a result of more iron, aluminium, magnesium and calcium hydroxide groups on the granular surface (Drizo *et al.*, 1999; Shenker *et al.*, 2005). Adsorbed phosphate can be released back into the water under reduced conditions due to the reductive dissolution of ferric and managenese phosphate minerals (Palmer-Felgate *et al.*, 2010). According to Lüderitz and Gerlach (2002) phosphates can also be adsorbed onto humic substances produced as a result of vegetation breakdown.

Sedimentation and filtration of metals

Sedimentation of metals in HSSF systems is facilitated by the vegetation and substrate present as they decrease water flow velocity and increase hydraulic retention time (Lee and Scholz, 2007). Johnston (1993) noted that the efficiency of settling and sedimentation of metals is proportional to the particle settling velocity and wetland length. Sedimentation of metals is enhanced by flocculant formation as flocs tend to adsorb metals onto their surface (Marchand *et al.*, 2010). Flocculant formation rates are high under alkaline conditions, a strong presence of suspended solids, high ionic strength and high algal density (Matagi *et al.*, 1998).

3.3.2 Biochemical treatment processes

Nitrification

Nitrification is the biological oxidation of ammonium to nitrate, with nitrite as an intermediate (Vymazal, 2007; Burgin and Hamilton, 2007). The process can be described using the following reaction steps:

$$NH_4^+ + 1.5O_2 \rightarrow NO_2^- + 2H^+ + H_2O$$

$$NO_2^- + 0.5O_2 \rightarrow NO_3^-$$

The first reaction step is performed by aerobic bacteria which derive energy from the oxidation of ammonium to nitrite and use carbon dioxide as a carbon source (Tanner *et al.*, 2012). The second step involves the activity of nitrite-oxidising bacteria to convert nitrite to nitrate (Kim *et al.*, 2010). Oxygen is supplied to the nitrifying bacteria via two methods, namely diffusion from the atmosphere to the subsurface layers of the system and translocation from the atmosphere to the

rhizome via plant structure (Van de Moortel *et al.*, 2010; Yalcuk *et al.*, 2010). Since the diffusion of oxygen is approximately $3x10^5$ times smaller than in air (Verberk *et al.*, 2011), translocation of oxygen via vegetation is the primary method for oxygen supply to the nitrifying bacteria. Albuquerque *et al.* (2009) notes, however, that oxygen supply via the rhizomes is consumed rapidly and there is competition for oxygen with other aerobic bacteria. Conseuqently, nitrfication rates are low in HSSF systems with values between 0.01 and 2.15 g N m^{-2} d^{-1} being reported in literature (Reddy and D'angelo, 1997; Tanner *et al.*, 2002). The optimum temperature for the process to occur is between 30-40 ºC and between a pH of 6.6 and 8.0 (Bradley *et al.*, 2002).

Denitrification

Denitrification is the process in which nitrate is converted to dinitrogen gas via a series of intermediates such as nitric oxide and nitrous oxide (Warneke *et al.*, 2011), as shown in the reaction step provided by Vymazal (2007):

$$2NO_3^- \rightarrow 2NO_2^- \rightarrow 2NO \rightarrow N_2O \rightarrow N_2$$

The overall reaction depciting the process is provided by Hauck (1984):

$$6(CH_2O) + 4NO_3^- \rightarrow 6CO_2 + 2N_2 + 6H_2O$$

The process occurs under anaerobic conditions with organic compounds being utilised by bacteria as a carbon source (Wen *et al.*, 2010) and nitrogen being used as an electron acceptor instead of oxygen (Fleming-Singer and Horne, 2002; Noorvee *et al.*, 2007). Jakubaszek and Wojciech (2014) report that for 1 g of nitrate being converted to nitrogen gas, 0.7 g of carbon are required for the bacteria to perform the process. Optimal pH for the process is between 7 and 7.5 whereas optimal temperatures lie between 20 and 25 ºC (Reddy *et al.*, 2014).

Organic transformation and removal

Dissolved organic matter from the influent waste water and that produced from the disintegration of particulate organic matter can then be decomposed via aerobically or anaerobically-facilitated processes (Garcia *et al.*, 2010). Aerobic degradation is performed by aerobic heterotrophic bacteria which use oxygen as a final electron acceptor (Vymazal and Kröpfelová, 2009):

$$C_6H_{12}O_6 + 6O_2 \rightarrow 6CO_2 + 6H_2O + 12e^- + \text{energy}$$

Oxygen transfer rates in HSSF systems are typically low, as noted by Rousseau *et al.* (2007) who estimated it to be approximately 0.7 g O_2 m^{-2} day^{-1}. Consequently, aerobic degradation pathways are not prominent in such systems. Anaerobic degradation is thus the dominant transformation pathway for dissolved organic matter and is a multi-phase process. The first step of the process entails the microbial conversion of complex soluble polymers into simpler monomers such as amino acids (Megonikal *et al.*, 2004). These amino acids then undergo fermentation to produce primarily fatty acids, alcohols as well as hydrogen and carbon dioxide. Sulphate-reducing bacteria then convert the fatty acids into carbon dioxide, water and hydrogen sulphide:

$$CH_3COOH + H_2SO_4 \rightarrow 2CO_2 + 2H_2O + H_2S$$

Methanogenic bacteria also convert fatty acids as well as carbon dioxide and hydrogen into methane as shown in the following two reaction steps:

$$CH_3COOH + 4H_2 \rightarrow 2CH_4 + 2H_2O$$

$$4H_2 + CO_2 \rightarrow 2CH_4 + 2H_2O$$

3.3.3 Modelling treatment processes in HSSF CWs

One of the most popular models used to predict HSSF CW treatment performance is the k-C* model, which was discussed by Rousseau *et al.* (2004):

$$\frac{C_{out} - C^*}{C_{in} - C^*} = e^{-k_{rate}t} \qquad \text{Equation 3.1}$$

This model, like many others found in literature assume ideal plug flow conditions (Sheridan *et al.*, 2014a). Spatial and temporal variation of flow resistance inside the packed media cause the hydraulics to deviate considerably from ideal plug flow, as has been reported in studies on HSSF CWs (Ranieri *et al.*, 2013). Only recently have researchers attempted to include the non-ideal fluid flow behaviour in treatment models (Sheridan *et al.*, 2014b). Such models require the generation of RTD data and subsequent hydraulic modelling using a suitable modelling technique. The impulse response experiment and its associated modelling procedures is the most popular (Headley and Kadlec, 2007). The step change experiment has been used less frequently with an example being the study performed by Suliman *et al.* (2006a).

In this study three different types of RTD modelling methodologies were sought to be compared which could be used for HSSF CWs; one of which required the generation of concentration-time data from an impulse response tracer experiment and the other two from a step change tracer experiment. The tracer studies and subsequent hydraulic modelling was performed on two HSSF CWs; both of which were packed with dolomitic gravel with the one being planted and the other unplanted.

3.4 Research Objectives

In this study, the primary aim was to build a comparison between three available RTD modelling methodologies for HSSF CWs. To accomplish this, the following two research objectives first needed to be met:

1. To conduct impulse and step change tracer studies on HSSF CWs to generate the concentration-time data which could be fed into the three modelling methodologies outlined in Figure 3.1; and
2. To determine hydraulic parameters such as the mean of the RTD, the number of equally sized CSTRs in series, the Peclet number and the hydraulic efficiency using the three different modelling approaches.

The comparison between the methodologies could then be built by attempting to meet the next three objectives:

3. To compare the hydraulic parameters obtained using each of the three approaches against ideal theoretical conditions;
4. To identify practical limitations encountered when conducting the impulse and step change tracer experiments. The limitations of the tracer studies can be considered limitations of the respective methodologies as they depend on the tracer studies for data generation; and
5. To critically assess the mathematical techniques which the modelling methodologies employ.

3.5 Materials and methods

3.5.1 Overview of theoretical framework for modelling methodologies

In Figure 3.1 an overview is provided of the necessary steps involved in each of the three RTD modelling methodologies.

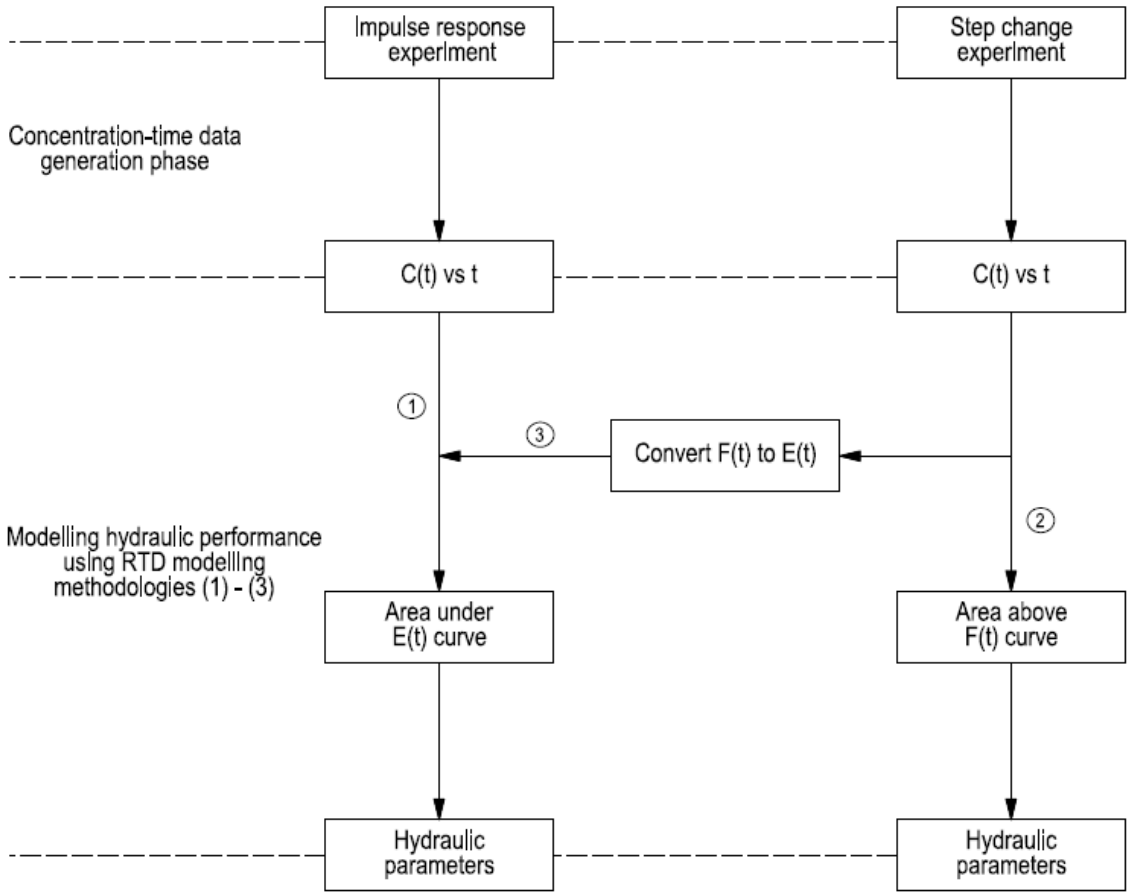

Figure 3.1: Overview of the three different RTD modelling methodologies used in this study

Modelling methodology (1) is referred to as the impulse response modelling methodology and requires concentration-time data generated from an impulse response experiment. Methodologies (2) and (3) are called the step change integral modelling methodology and the step change derivative modelling methodology, respectively. These two approaches require concentration-time data generated from a step change tracer experiment. The sections which follow describe each step in more detail.

3.5.2 Generating concentration-time data using tracer experiments

A flow tracer study is a stimulus-response experiment (Chazarenc *et al.*, 2003), in which an inert soluble tracer is injected either as an impulse or as a step change in concentration into the system inlet pipe and the tracer concentration is measured continuously at the system outlet. The data are then fed into the modelling methodologies to ascertain the flow characteristics of the system. In

Figure 3.2 generic concentration-time curves generated from the impulse and step change tracer experiments are shown.

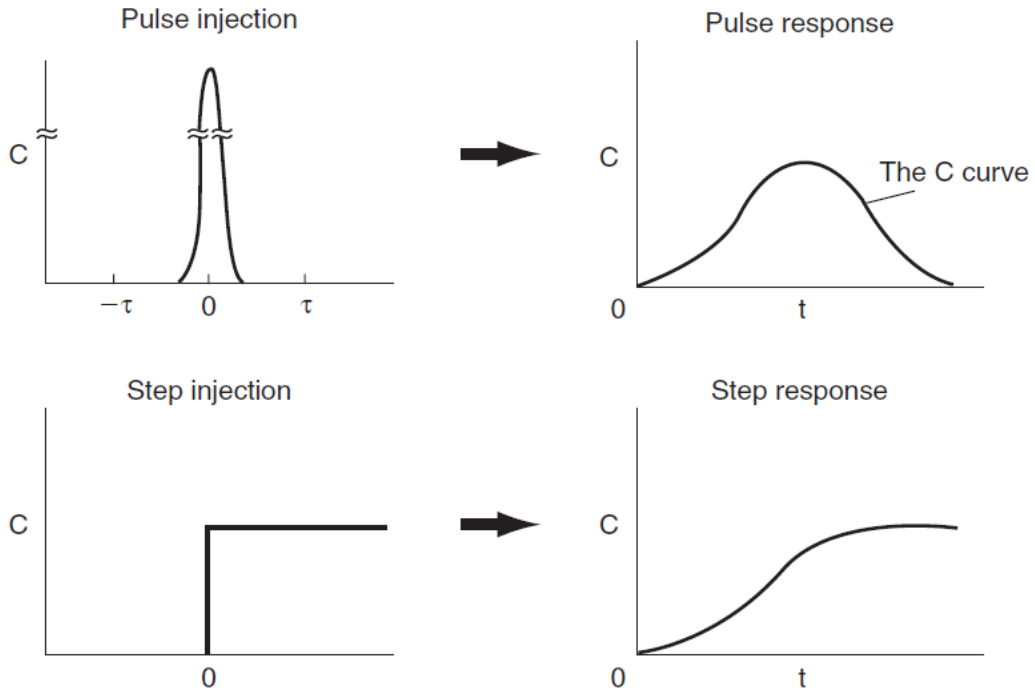

Figure 3.2: Generic concentration-time data generated from the impulse and step change tracer experiments (Fogler, 1999)

The nominal residence time of fluid inside the system is calculated according to Equation 3.2 (Fogler, 1999):

$$\tau = \frac{V}{\dot{v}} \qquad \text{Equation 3.2}$$

The reactor volume must account for the bed porosity, which is determined using Equation 3.3 (Alcocer *et al.*, 2012):

$$V = HLW\varepsilon \qquad \text{Equation 3.3}$$

A successful tracer study requires the flow to be in the laminar range (Sheridan *et al.*, 2014a), which is the case when the Reynolds number is less than 10 (Miller and Clesceri, 2002). The Reynolds number for packed beds is given by Equation 3.4 (Subramanian, 2004):

$$Re_p = \frac{D_p u_s \rho}{(1-\varepsilon)\eta}$$ Equation 3.4

The superficial velocity is determined using Equation 3.5 (Mayo, 2014):

$$u_s = \frac{\dot{v}}{HW}$$ Equation 3.5

3.5.3 Modelling hydraulic performance using RTD modelling methodologies

The RTD modelling methodologies outlined in Figure 3.1 use the concentration-time data generated from the flow tracer study experiments to calculate the mean of the RTD of fluid inside the reactor system as well as the variance, which provides an indication of the flow inhomogeneities around the mean hydraulic residence time. The sections which follow describe the mathematical techniques which each approach uses in the modelling process.

Methodology 1: impulse response modelling methodology

The residence time distribution function, $E(t)$, is determined from the concentration-time curve at the system outlet according to Equation 3.6. A visual description of the mathematical relationship between the two curves is presented in Figure 3.3.

$$E(t) = \frac{C(t)}{\int_0^\infty C(t)dt}$$ Equation 3.6

The mean of RTD is then calculated using $E(t)$ as shown in Equation 3.7:

$$\bar{t}_m = \int_0^\infty tE(t)dt$$ Equation 3.7

The variance is calculated using Equation 3.8:

$$\sigma^2 = \int_0^\infty t^2E(t)dt - \bar{t}_m^2$$ Equation 3.8

The recovery of tracer is determined using Equation 3.9:

$$\%\ \text{recovery} = \frac{\dot{v}\int_0^\infty C(t)dt}{M_0} \times 100$$ Equation 3.9

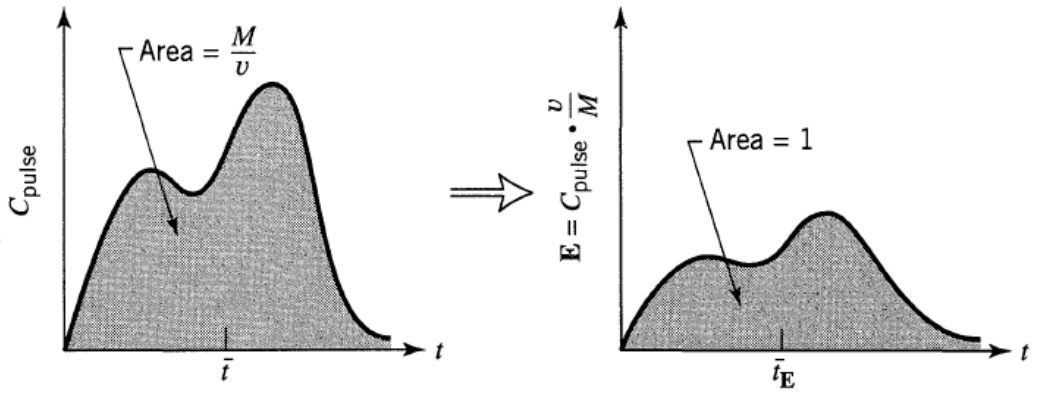

Figure 3.3: Relationship between the concentration-time curve and the RTD function used in the impulse response modelling methodology (Levenspiel, 1999)

Methodology 2: step-change integral modelling methodology

The cumulative distribution curve, $F(t)$, is constructed based on the concentration-time curve using the relation provided in Equation 3.10:

$$F(t) = \frac{C(t)}{C_{max}} \qquad \text{Equation 3.10}$$

The mean of the RTD is determined from the $F(t)$ curve, as shown in Equation 3.11 and in Figure 3.4.

$$\bar{t}_m = \int_0^\infty [1 - F(t)]dt \qquad \text{Equation 3.11}$$

The variance is then determined using Equation 3.12:

$$\sigma^2 = 2\int_0^\infty t[1 - F(t)]dt - \bar{t}_m^2 \qquad \text{Equation 3.12}$$

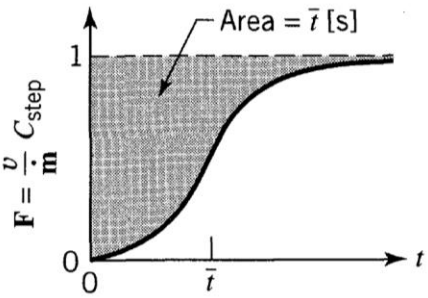

Figure 3.4: Determining the mean of the RTD by computing the area above the F(t) curve (Levenspiel, 1999)

Methodology 3: step-change derivative modelling methodology

The step-change derivative methodology requires differentiating the $F(t)$ curve to obtain the $E(t)$ curve as shown in Equation 3.13 and Figure 3.5.

$$E(t) = \frac{dF(t)}{dt} \qquad \text{Equation 3.13}$$

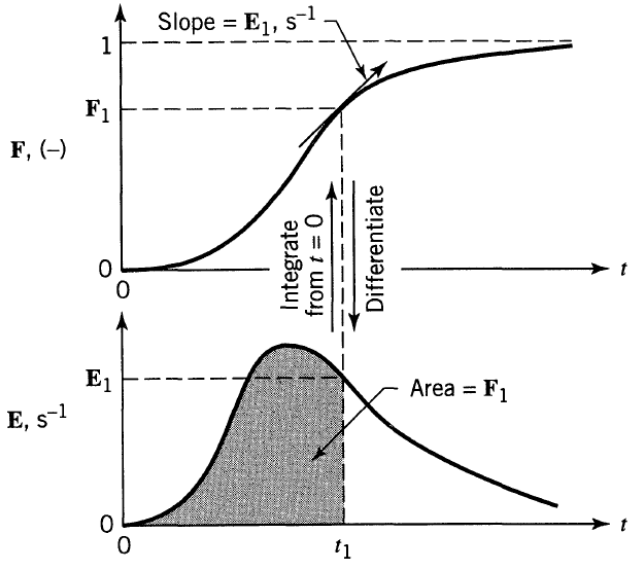

Figure 3.5: The relationship between the RTD function, E(t), and the cumulative distribution function, F(t) (Levenspiel, 1999)

Once the $E(t)$ curve is obtained, Equation 3.7 and Equation 3.8 are then used to determine the mean of the RTD and the variance, respectively.

3.5.4 Using mean and variance of RTD to generate additional hydraulic parameters

Normalizing the E(t) and F(t) curves

The reversible property of flow in the laminar flow region makes it possible to normalize the E(t) and F(t) curves with respect to time. This is useful for comparing hydraulic data generated at different experimental flow rates and comparing hydraulic performance of systems with different volumetric capacities (Wahl *et al.*, 2010; Lange *et al.*, 2011). The data set is normalized by converting it into dimensionless variables as is shown in Equation 3.14 through Equation 3.16 (Fogler, 1999).

$$\theta = \frac{t}{\bar{t}_m} \qquad \text{Equation 3.14}$$

$$E(\theta) = \bar{t}_m E(t) \qquad \text{Equation 3.15}$$

$$F(\theta) = F(t) \qquad \text{Equation 3.16}$$

Where θ effectively represents the number of reactor volumes of fluid which have flowed through the system at a particular point in time.

Developing the tanks in series (TIS) model

The hydraulic data generated from each of the modelling methodologies can be used to determine the number of ideal, equally sized continuously stirred tank reactors (CSTRs) in series that will provide an estimate the same RTD as that of the system under study (Levenspiel, 1999). A demonstration of this rationale is provided in Figure 3.6.

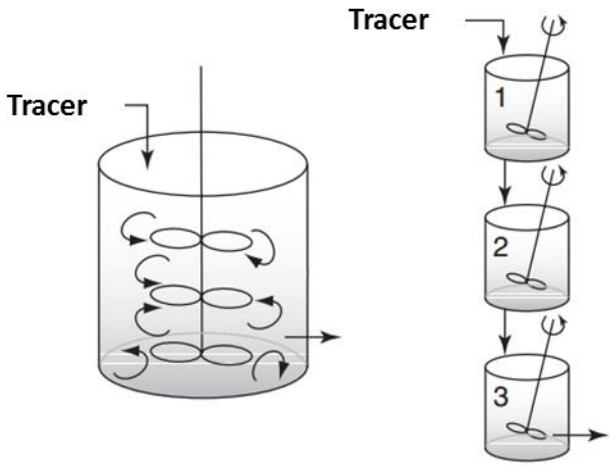

Figure 3.6: TIS model demonstrated for the real reactor (left) using a combination of idealised tanks in series (right). Adapted from Fogler (1999)

The number of tanks in series, N, is determined using Equation 3.17:

$$N = \frac{\bar{t}_m^2}{\sigma^2}$$ Equation 3.17

A graphical interpretation of the model is provided in Figure 3.7.

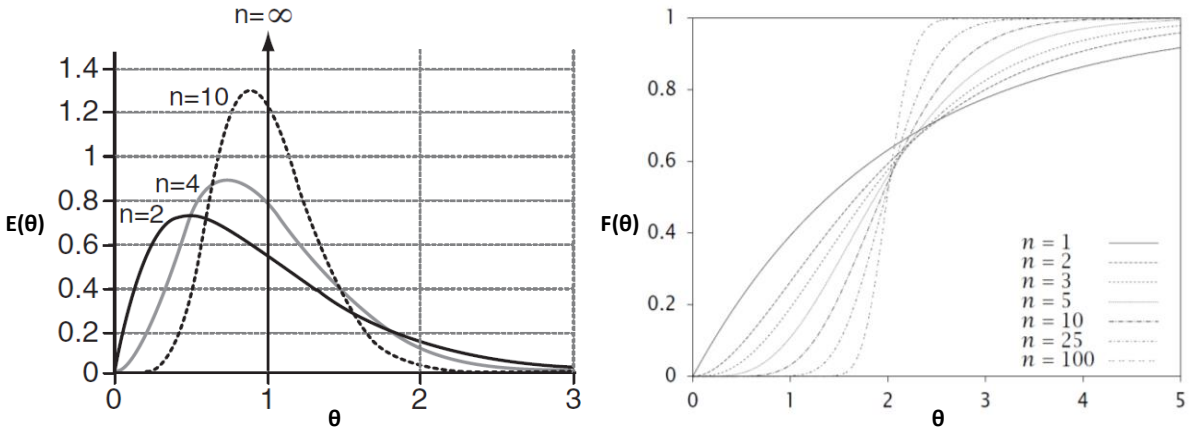

Figure 3.7: Normalized E(t) (left) and F(t) (right) curves for different values of N (Fogler, 1999)

As N → 1, the hydrodynamics approach completely mixed flow. As N → ∞, the hydrodynamics approach ideal plug flow behaviour.

Developing the dispersed plug flow model

The dispersed plug flow model allows for packed bed reactors to be modelled as plug flow reactors (PFRs) with a certain degree of back mixing by adjusting the mass balance to include a dimensionless dispersion number (Levenspiel, 1999). The dispersion number is defined using Equation 3.18 (Fogler, 1999).

$$D_n = \frac{\text{rate of transport by dispersion}}{\text{rate of transport by convection}} = \frac{1}{Pe} \qquad \text{Equation 3.18}$$

Pe can be determined using the correlation provided in Equation 3.19.

$$\frac{\sigma^2}{\bar{t}_m^2} = \frac{2}{Pe} - \frac{2}{Pe^2}(1 - e^{-Pe}) \qquad \text{Equation 3.19}$$

As Pe decreases, the amount of axial dispersion inside the system increases and the hydrodynamics approach completely mixed flow. As Pe increases, the axial dispersion decreases and the system approaches plug flow behaviour.

Effective volume utilization

The effective volume ratio indicates how much of the reactor volume is being utilized to provide the necessary contact between the fluid and bed matrix. The portion of the reactor which is not being used for this purpose is considered dead volume (Albertini *et al.*, 2012). It is calculated using Equation 3.20 (Thackston *et al.*, 1987):

$$e = \frac{\bar{t}_m}{\tau} = \frac{V_{eff}}{V} \qquad \text{Equation 3.20}$$

Hydraulic Efficiency

Hydraulic efficiency is used to evaluate the hydraulic performance of non-ideal reactors, with ideal plug flow systems being 100% efficient (Wahl *et al.*, 2010). The hydraulic efficiency can be described as the capacity of a reactor to utilize its entire volume by uniformly distributing flow to maximize residence time (Holland *et al.*, 2004). One of the most commonly used correlations is that provided by Persson *et al.* (1999) and is shown in Equation 3.21.

$$\Lambda = e\left(1 - \frac{1}{N}\right) \qquad \text{Equation 3.21}$$

3.5.5 Experimental apparatus description

The HSSF CWs used in this study were located at the Industrial and Mining Water Research Unit (IMWaRU) facility at the University of the Witwatersrand, Johannesburg. Both systems were built using HDPE external support troughs and then filled with dolomite gravel (mean particle size 20 mm). The reactors had a length of 4.2 m, width of 0.9 m and depth of 0.7 m.

Thirteen sample ports, constructed from PVC mesh (mesh opening = 20 mm), were installed into both systems in order to accommodate sampling within different regions of the CWs. Three lengths of silicon tubing were cut and attached to each of the sampling wells using cable ties so that samples could be drawn from three different depths, ultimately resolving each system into a three-dimensional grid. The projected surface (normal to the feed) was divided into regions A, B and C. Each system was also divided into Zones 1 to 5 down its length. The spatial distribution of the sampling points, inlet and outlet ports, as well as the designated zones is provided in Figure 3.8.

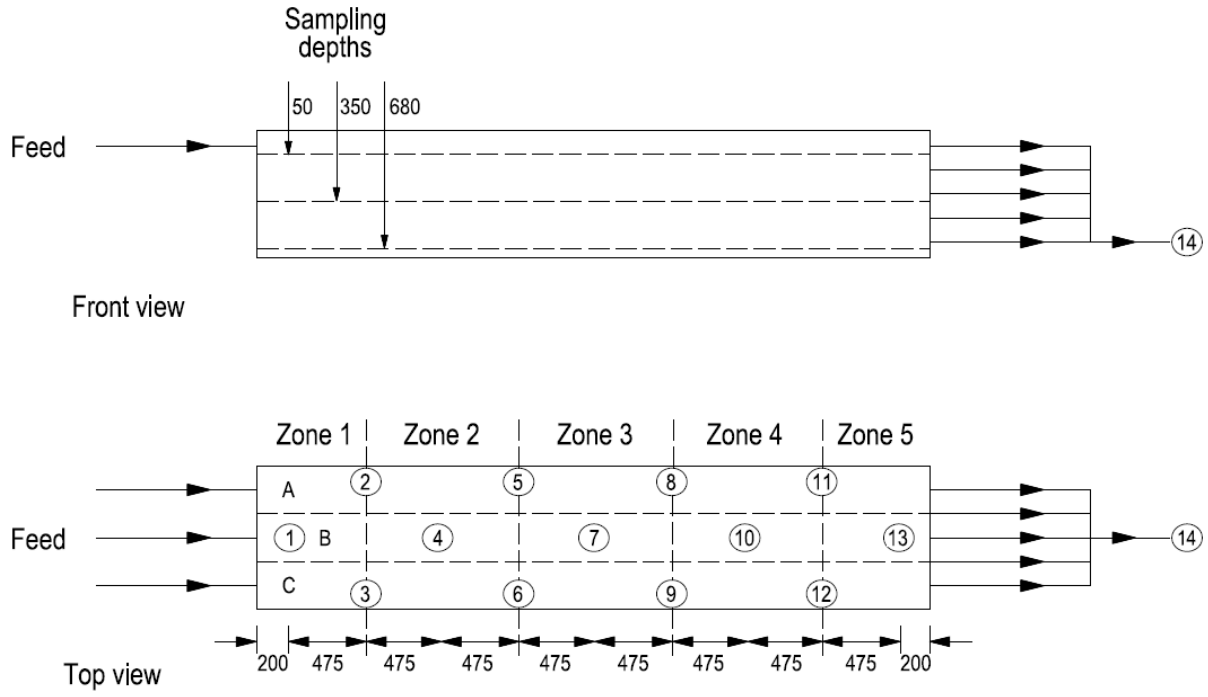

Figure 3.8: Spatial arrangement of inlet, outlet and internal sampling ports as well as the system grid resolution. All dimensions are expressed in mm

Planted wetland vegetation

Each of the five zones within the planted CW contained a different species of vegetation. Polyculture was selected over monoculture due to better treatment performance reported in literature (Karathanasis *et al.*, 2003). Images of the different plant species within the system are provided in Figure 3.9.

Zone 1	Zone 2	Zone 3	Zone 4	Zone 5
Zantedeschia aethiopica	*Cyperus papyrus nana*	*Typha capensis*	*Juncus effusus*	*Chondropetalum tectorum*

Figure 3.9: Zonal distribution of wetland vegetation in planted system

All of the five species are indigenous to South Africa (Coetzee *et al.*, 1999; Kritzinger *et al.*, 1997; Reinten *et al.*, 2011; Rubin *et al.*, 2001; Schiegl *et al.*, 2004). Zone 1 was planted with *Zantedeschia aethiopica* due to their tolerance of various types of high-strength waste waters (Zurita *et al.*, 2006). Each subsequent zone was planted with a species which had a successively lower tolerance for impacted water (Tanner, 1996).

3.5.6 Determining system porosity

The presence of plant root structures decreases the pore volume of subsurface flow systems and has been discussed extensively by Knowles *et al.* (2011). Thus, despite both systems used in this study having the same external physical dimensions their internal effective volumes had the potential to differ. A porosity test was performed on both systems prior to the hydraulic tracer studies. First, both systems were drained completely and the inlet and outlet valves were closed. A hosepipe, fitted with a flow meter (Gardena, Germany), was inserted into sampling port l and each system was filled until the water level coincided with the gravel bed surface. The total volume

measured by the flow meter represented the effective volume of each system. The porosity was determined by dividing this effective volume by the total volume of the system.

3.5.7 Experimental flow rate

The inflow and outflow rates were measured once every 30 min, with the average flow rates for each of the experiments shown in Table 3.1.

Table 3.1: Average flow rates used for hydraulic tracer studies as well as the nominal retention time for each experiment

Experiment	System	Average flow rate (l/min)	τ (min)
Impulse	Unplanted	4.59	268
	Planted	4.30	264
Step change	Unplanted	4.39	281
	Planted	4.13	275

3.5.8 Tracer studies

Both the impulse and the step-change tracer experiments were conducted concurrently throughout the month of June 2015. FWT Red fluorescent dye (Cole-Parmer, USA) was used as the tracer for both sets of tracer studies.

Impulse response tracer studies

Prior to the commencement of each experiment, a 5 m^3 vertical cylindrical feed tank was completely filled with tap water and the tank outlet connected to the CW inlet. The CW inlet and outlet valves were opened to allow the inflow and outflow rates to equalize. A tap continuously supplied water to the feed tank in order to maintain a constant hydrostatic pressure and, hence, constant feed flow rate to the systems. Once the flow rates had equalized, 60 ml of FWT Red were injected into the feed line to the CW. Samples were collected through ports 1 to 14 for the duration of the experiment. A dynamic sampling regime was designed to maximize the resolution of the concentration-time curves (Headley and Kadlec, 2007). A summary of the sampling regime employed is presented in Table 3.2.

Table 3.2: Dynamic sampling regime employed for the impulse tracer studies where X indicates a sample being taken

Time (min)	Ports 1-4	Ports 5-7	Ports 8-13	Port 14
0	X	X	X	X
10	X	X		
20	X	X		X
30	X	X	X	X
60	X	X	X	X
90	X	X	X	X
120	X	X	X	X
150	X	X	X	X
180	X	X	X	X
210	X	X	X	X
240	X	X	X	X
270		X	X	X
300	X	X	X	X
330			X	X
360	X	X	X	X
420			X	X
480	X	X	X	X
600			X	X
720	X	X	X	X

Step change tracer studies

Two 5 m^3 vertical cylindrical tanks were filled with tap water and 300 ml of FWT Red were then added to each tank. In order to ensure solution homogeneity, one of the feed tanks were fitted with a two-blade agitator extending to the bottom of the tank. A pump (ViaAqua VA-300A, USA) was placed inside the second feed tank such that the contents of both tanks were allowed to circulate for 24 hours before commencing the experiments to ensure the tracer was completely mixed. The inlet and outlet flow rates were allowed to equalize, at which time the feed to the CW was switched

over from tap water to the tracer solution. A sampling regime was also designed to maximise the resolution of the cumulative concentration-time curves and is presented in Table 3.3.

Table 3.3: Dynamic sampling regime employed for the step change tracer studies where X indicates a sample being taken

Time (min)	Ports 1-4	Ports 5-6	Port 7	Ports 8-9	Ports 10-13	Port 14
0	X	X	X	X	X	X
15	X	X	X			
30	X	X	X			X
60	X	X	X	X		X
90	X	X	X	X	X	X
120	X	X	X	X	X	X
150	X	X	X	X	X	X
180	X	X	X	X	X	X
210		X	X	X	X	X
240		X	X	X	X	X
270	X	X	X	X	X	X
300	X	X	X	X	X	X
330			X	X	X	X
360	X	X	X	X	X	X
390					X	X
420	X	X	X	X	X	X
480	X	X	X	X	X	X
540				X	X	X
600	X	X	X	X	X	X
720	X	X	X	X	X	X

3.5.9 Sample analysis

Samples were not pre-treated and were analysed within 48 hours of collection. A spectrophotometer (Merck Spectroquant Pharo 300) was used to measure the absorbance of each

sample at 550 nm. Plastic cuvettes with a path length of 10 mm were filled with sample solution and inserted into the spectrophotometer to obtain the absorbance data. Absorbance readings were converted into concentration values by constructing a calibration curve, which had an R^2 of 0.99.

3.6 Results and Discussion

3.6.1 Determining hydraulic performance parameters using modelling methodologies

The RTD functions obtained from the impulse experiments, as well as the cumulative distribution functions obtained from the step-change experiments, are shown in Figure 3.10. These functions were plotted using data obtained from the system outlets.

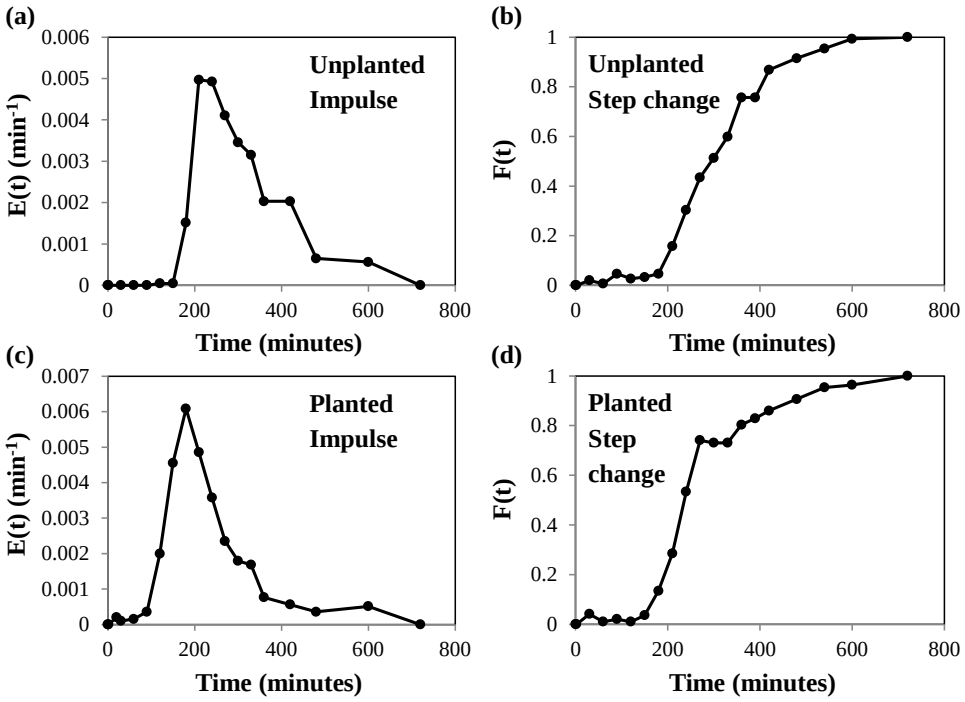

Figure 3.10: E(t) and F(t) curves from the impulse and step change experiments, respectively

Each of the curves in Figure 3.10 displayed a time delay between injection and breakthrough of the tracer at the system outlet. For the impulse response experiments, this was approximately 180 minutes for the unplanted system and 120 minutes for the planted system. The time delay was closer to 210 minutes for the unplanted step-change experiment and 180 minutes for the planted step-change experiment. The well-defined peak and long tail found for both the planted and unplanted impulse response curves is indicative of deviation from plug flow behaviour.

Researchers have found this to be the case in other wetland systems with similar aspect ratios (García *et al.*, 2004; Sheridan *et al.*, 2014a). The E(t) and F(t) curves were used to calculate the hydraulic parameters of the two systems; the results of which are shown in Table 3.4.

Table 3.4: Calculated hydraulic parameters for the planted and unplanted systems using the impulse and step change modelling methodologies

Parameter	**Unplanted**			**Planted**		
	Impulse	**Step change**		**Impulse**	**Step change**	
		Derivative	**Integral**		**Derivative**	**Integral**
ε (%)	47	47	47	43	43	43
V_{eff} (l)	1231	1231	1231	1136	1136	1136
$\dot{v}$ (l/min)	4.59	4.39	4.39	4.3	4.13	4.13
τ (min)	268	281	281	264	275	275
Tracer recovery	100%			100%		
$\bar{t}_m$ (min)	319	311	309	259	265	277
σ^2 (min^2)	11071	11927	11726	17333	13257	14845
N	9	8	8	4	5	5
Pe	17.12	15.38	15.38	6.67	9.52	9.52
e	1.19	1.11	1.10	0.97	0.96	1.01
Λ	1.06	0.97	0.97	0.73	0.78	0.81

The planted system had a 4% lower porosity and this can explain why it was calculated to have a smaller V_{eff} when compared to the unplanted system. The lower porosity could be attributed to the presence of the plant roots in the bed voids and is consistent with results obtained by other researchers (IWA, 2001). The tracer studies were conducted approximately six weeks after planting. Consequently, root zone growth was still in the initial development phase (Tanner, 1996). It is expected that the root zone will develop over the next six months as a result of the correct supply of nitrogen and phosphorus as key nutrients for the wetland plants (Ong *et al.*, 2010) as well as the start of the Southern Hemisphere Spring in the month of September. The growth process should increase the plant root density in the bed voids and hence contribute to further reductions in porosity (Knowles *et al.*, 2011).

A tracer mass recovery of approximately 100% was obtained for both impulse response experiments, indicating that sufficient time was allocated for the tracer studies. There is further evidence of this in Figure 3.10, in which the E(t) curves reached a value of zero and the F(t) curves reached a value of 1 within 720 minutes.

All three modelling methodologies suggested smaller values for N and Pe for the planted system when compared to the unplanted system; implying that the planted system had a higher degree of back mixing. Similar values for N and Pe have been reported for other HSSF CWs having similar bed porosities and compositions (Ríos *et al.*, 2009).

For each of the experiments, $\bar{t}_m$ was comparable with τ, resulting in an effective volume utilisation close to and, in some cases, higher than 100%. The effective volume utilization figures are higher than those reported in literature for other HSSF CWs (El Hamouri *et al.*, 2007; Suliman *et al.*, 2006b; Sheridan *et al.*, 2014a). For instance, the system studied by Sheridan *et al.* (2014a) had outlet ports level with the inlet port and at a single depth; thereby inducing a hull-shaped flow profile and, thus, a larger dead zone volume. In this study, the configuration of the outlet ports allowed the fluid to exit the system at a multitude of depths and, in effect, created an open boundary.

The hydraulic efficiency parameter (Λ) depends on the magnitudes of N and e. The lower degree of back mixing and higher effective volume utilization resulted in a higher hydraulic efficiency for the unplanted system, for all three modelling approaches.

3.6.2 Evaluating modelling results against ideal theoretical conditions

Since the flow rates were slightly different for each experiment, they have been normalized against each other. This was possible because in the laminar flow region the physical properties could be reversed. Both experiments were scaled to a flow rate of 4.5 l/min, with the results shown in Table 3.5 and Table 3.6 for the unplanted and planted systems, respectively. The other hydraulic parameters have not been scaled and remained the same as those presented in Table 3.4.

Unplanted system

Table 3.5: Comparison of hydraulic parameters for the unplanted system, scaled to a flow rate of 4.5 l/min

Parameter	**Impulse**	**Step change**	
		Derivative	**Integral**
$\dot{v}$ (l/min)	4.5	4.5	4.5
τ (min)	274	274	274
$\bar{t}_m$ (min)	325	304	302
N	9	8	8
Pe	17.12	15.38	15.38
e	1.19	1.11	1.10
Λ	1.06	0.97	0.97

$\bar{t}_m$ was greater than τ for each of the modelling methodologies, resulting in an effective volume utilisation greater than 100% in each case. All three methodologies, thus, indicated an absence of dead zones and short circuiting effects within the system, which are phenomena that should be avoided in the design of HSSF CWs and packed bed reactors in general (Chazarenc *et al.*, 2003; Mendoza *et al.*, 2013). Evaporative processes can also reduce subsurface fluid velocities, resulting in experimental retention times being longer than their theoretical equivalents (Headley *et al.*, 2012) and might be a cause of an effective volume utilization greater than 100%. Nevertheless evaporative losses are expected to be relatively minor over the course of a 12 hour experiment. The step-change modelling techniques indicated an almost identical $\bar{t}_m$, which is 11% higher than τ. The impulse response technique indicated a $\bar{t}_m$ which was 19% greater than the τ. Both step-change techniques estimated the same values for N and Pe, whereas the impulse modelling technique suggested a lower degree of dispersion, with an 11.3% higher Pe and an extra CSTR in series.

Planted system

Table 3.6: Comparison of hydraulic parameters for the planted system, scaled to a flow rate of 4.5 l/min

Parameter	**Impulse**	**Step change**	
		Derivative	**Integral**
$\dot{v}$ (l/min)	4.5	4.5	4.5
τ (min)	252	252	252
$\bar{t}_m$ (min)	247	243	254
N	4	5	5
Pe	6.67	9.52	9.52
e	0.98	0.96	1.01
Λ	0.73	0.78	0.81

Each methodology produced a different $\bar{t}_m$ for the planted system. The step change integral technique indicated a $\bar{t}_m$ higher than the τ, resulting in an effective volume utilization slightly higher than 100%. The step-change derivative and impulse techniques both indicated a $\bar{t}_m$ smaller than the theoretical retention time, resulting in a dead volume of 4% and 2% for the two techniques, respectively. Nevertheless, both step change techniques estimated the same degree of back mixing within the system, indicated by the same values for N and Pe. The impulse technique suggested a higher degree of back mixing, reflected by a 30% lower Pe and one less CSTR placed in series. All three techniques reported hydraulic efficiencies lower than 100% and these are attributed to the high degree of dispersion within the system.

3.6.3 Practical limitations of the tracer studies

Capturing sufficient concentration-time data for adequate definition of system response

There were a lack of data points in the region surrounding the peak of the E(t) curve for the unplanted system, as seen in Figure 3.10. This may have affected the shape of the response, as well as the hydraulic parameters calculated for the system. This can be a likely occurrence, even with a well-designed sampling regime put in place (Teefy, 1996). Theoretically the limitation can be overcome by increasing the sampling frequency which would possibly require in-line continuous

analysis. This however would greatly increase the cost associated with performing the study. The step-change experiment has no such drawback. This is shown by the consistent distribution of data points on the F(t) curves, for both planted and unplanted system, in Figure 3.10.

Effect of tracer dispersion on concentration-time curves derived from tracer experiments

In Figure 3.11 and Figure 3.12 the RTD curves and the cumulative distribution curves from sampling ports 1, 4, 7, 10 and 13 from the impulse and step change experiments are presented, respectively. In each of the Figures 3.11 (a)-(f) the peak of the response was largest in magnitude at 0.2 m whereafter it broadened as the tracer travelled through the reactor. In Figures 3.12 (a)-(f) the gradient of the response curve was steepest at 0.2 m and then flattened out with each successive sampling port. These trends observed in Figure 3.11 and Figure 3.12 are indicative of dispersion of tracer as it moved through the system and has been confirmed by other researchers conducting hydraulic studies on HSSF CWs (Sheridan *et al.*, 2014a).

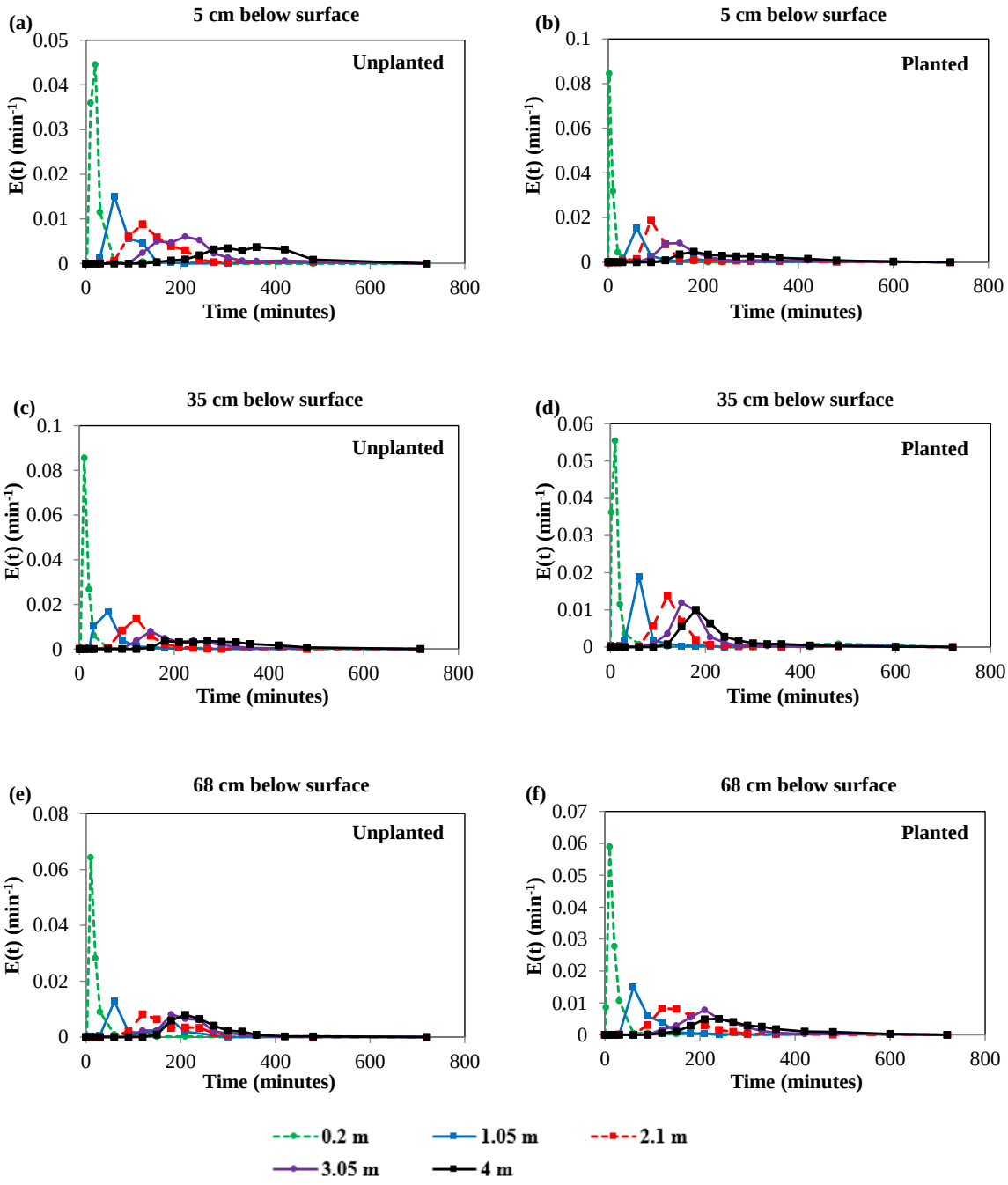

Figure 3.11: RTD curves from the impulse experiments on the planted and unplanted systems

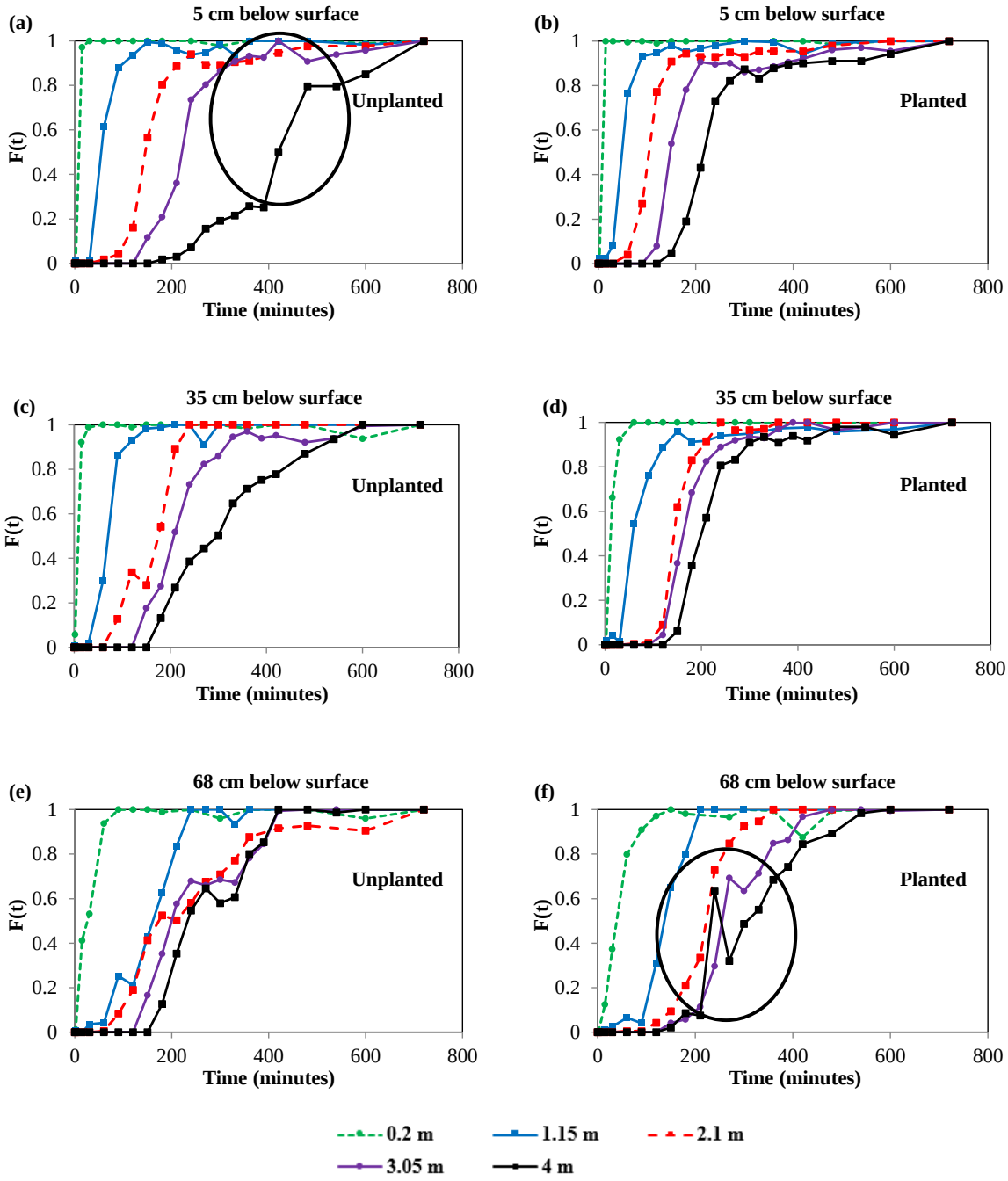

Figure 3.12: Cumulative distribution curves from the step change experiments on the planted and unplanted systems

The cumulative distribution curve obtained from the sampling port at a length of 4 m in Figure 3.12 (f) experienced an unexpected increase in gradient between 210 and 240 min, whereafter it returned to the trend observed before 210 min. This suggests short-circuiting behaviour (Sheridan

et al., 2011). The corresponding impulse response curve had broadened to the extent that it was difficult to identify multi-modal distributions. This was also the case at a length of 4 m in Figure 3.11 (a) and Figure 3.12 (a). Tracer dispersion can thus affect the qualitative description of the reactor hydraulics when using the impulse response experiment and may also have a knock-on effect when quantifying the hydraulic parameters using the impulse response modelling methodology.

3.6.4 Critical assessment of the mathematical techniques used by modelling methodologies

Modelling approach sensitivity to selection of numerical integration procedure

Each modelling approach required numerical integration for the computation of the hydraulic parameters and for this study, Simpson's 1/3 rule was selected. The method works by approximating the curve as a parabola in multiple equally sized subintervals. The areas under the parabolas are then evaluated and summed together to arrive at the approximation provided in Equation 3.22 (Pozrikidis, 1998).

$$I = \frac{z}{3}[f(x_0) + 4f(x_1) + 2f(x_2) + \cdots + 4f(x_{n-1}) + f(x_n)] \qquad \text{Equation 3.22}$$

Where:

$$z = \frac{b-a}{n}$$

With n being the number of equally sized subintervals.

The number of subintervals used is left to the discretion of the user and can range from using one interval in which $z = a - b = x_n - x_0$, to the maximum number of subintervals possible in which a minimum of three data points are required *viz.* $z = \frac{a-b}{2}$. It would thus be desirable for the modelling approach to display the least sensitivity as possible to the number of subintervals employed as it would allow the user to have more confidence in the final answer.

The hydraulic parameter $\bar{t}_m/\tau$ was calculated for different sizes of subintervals to determine how sensitive each modelling approach was to the subinterval selection with the results presented in Figure 3.13.

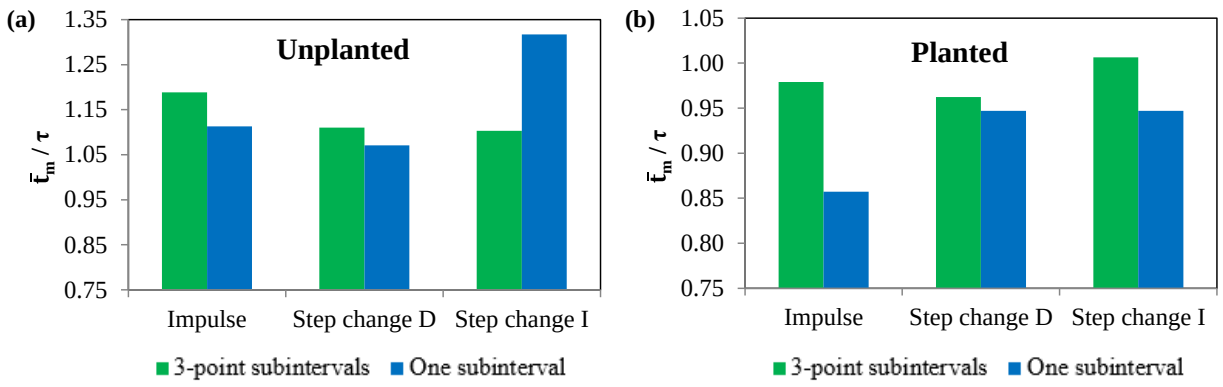

Figure 3.13: Comparison of $\bar{t}_m/\tau$ for when 3-point subintervals and when one subinterval is used for numerical integration using Simpson's 1/3 rule

Each modelling approach displayed a degree of sensitivity to the subinterval selection. For both systems the step change derivative approach was the least sensitive, with a 1% and 4% variation in $\bar{t}_m/\tau$ for the planted and unplanted system, respectively. The other two approaches displayed higher degrees of sensitivity. For example, the impulse response modelling methodology suggested a value of 0.86 for $\bar{t}_m/\tau$ and hence a 14% dead volume for the planted system when one subinterval is used and this changes to a $\bar{t}_m/\tau$ of 0.98 and hence a 2% dead volume when 3-point subintervals are used. A similar variation in $\bar{t}_m/\tau$ was seen for the unplanted system when using the step change integral route.

Modelling approach sensitivity to noisy data generated during data collection phase

Both impulse and step change experiments are capable of generating noisy data, particularly during the sample analysis procedure. At very low concentrations of tracer the relative contribution of background noise to the absorbance measurement is large. Background noise in the system may be caused by slight scratches on the cuvettes or from the presence of fine suspended solids in the sample which deflect the light beam and alter the spectrophotometer reading. It would thus be expected that the F(t) curves used for the step change derivative modelling approaches and the C(t) curve used for the impulse response approach would have contained some degree of noise.

In Figure 3.14 (a) and Figure 3.14 (b), E(t) from the step change derivative and impulse response approaches were compared.

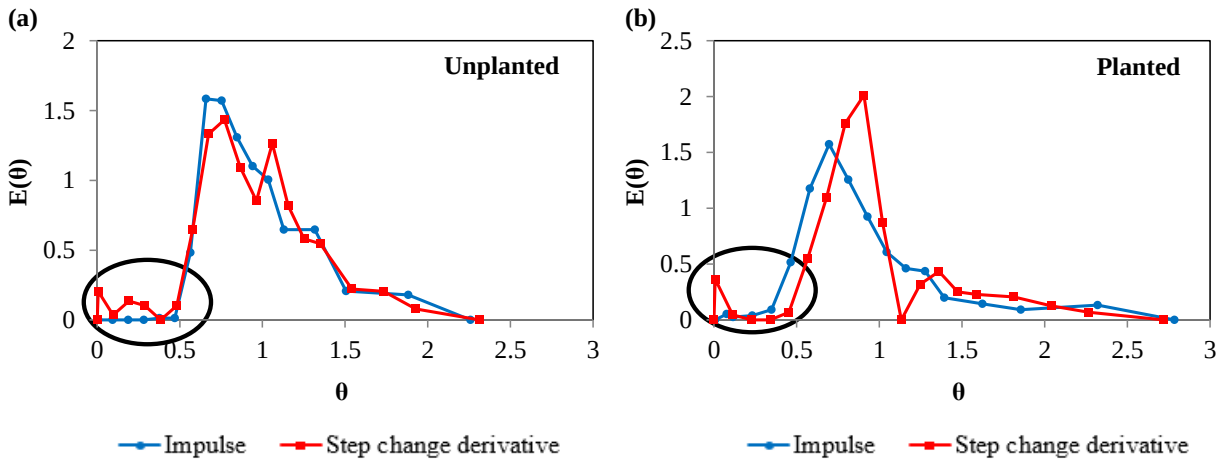

Figure 3.14: Normalized E(t) for planted and unplanted systems with regions of noise highlighted on the E(t) curves from the step change derivative approach

In the region $0 < \theta < 0.5$, E(t) from the step change derivative approach was noisier than E(t) from the impulse experiment and this was the case for both reactor systems. This may be attributed to the differentiation of F(t) to obtain E(t) as differentiating noisy data amplifies the noise (Bequette, 2003) and transfers it to the next stage of the modelling process. The step change derivative approach was thus more sensitive to noisy data compared to the other two approaches, and could potentially contribute to inaccuracies in computing the hydraulic performance parameters.

3.7 Conclusion

Sizing of CWs for waste water treatment requires the integration of treatment kinetics into a reactor model which attempts to reflect the non-ideal flow behaviour through the packed media. One way to build the reactor model is to conduct RTD studies on a pilot scale system. In this paper three different RTD modelling methodologies were compared using two pilot scale HSSF CWs. These were the impulse response, step change integral and step change derivative modelling methodologies. Impulse response and step change tracer experiments were conducted to generate the concentration-time data for the impulse response and step change modelling methodologies, respectively. Hydraulic parameters were then calculated for the two systems using each of the modelling approaches. The comparison between the modelling approaches was then built by attempting to meet the following research objectives:

- To compare the hydraulic parameters obtained using each of the three approaches against each other and ideal theoretical conditions. For the unplanted system, it was found that $\bar{t}_m$ was greater than τ for each of the modelling methodologies. The two step change modelling methodologies suggested the same fluid flow behaviour reflected by almost identical values for $\bar{t}_m$ and the same values for N and Pe. The impulse modelling methodology indicated a 7% higher $\bar{t}_m$ compared to the step change modelling approaches and a lower degree of dispersion. Each modelling methodology suggested different hydraulic behaviour for the planted system. Both step change methodologies quantified the same degree of dispersion for the system; however the step change integral approach determined a $\bar{t}_m$ slightly greater than τ and thus no dead volume in the system whereas the step change derivative approach determined a 4% dead volume caused by $\bar{t}_m$ being slightly less than τ. The impulse response modelling methodology suggested a higher degree of dispersion than both step change modelling approaches and a 2% dead volume for the system.
- To identify practical limitations encountered when conducting the impulse and step change tracer experiments. The limitations of the tracer studies can be considered limitations of the respective methodologies as they depend on the tracer studies for data generation. Despite a well-designed sampling regime put in place for the impulse response tracer experiment, it was not possible to capture sufficient data on the peak of the concentration-time curve for the unplanted system. This affected the shape of the response curve and may have also impacted the modelling results. No such difficulties were encountered with the step change experiments. Sampling down the length of the reactor made it possible to identify another limitation of the impulse response experiment: tracer dispersion had the effect of broadening the impulse response curves to the extent that it was almost impossible to identify non-ideal flow behaviour such as short-circuiting towards the end of the reactor systems. Although tracer dispersion also had an effect on the step change response curves, it was still possible to identify non-ideal flow behaviour which was prevalent in both systems.
- To critically assess the mathematical techniques which the modelling methodologies employ. A sensitivity analysis was performed to determine the effect of changing the size and hence number of subintervals used in Simpson's 1/3 rule for numerical integration on $\bar{t}_m/\tau$ for each modelling methodology. The lower the sensitivity of the modelling methodology the better as choosing a parameter as arbitrary as subinterval size should not have a noticeable effect on

reported hydraulic behaviour. The step change derivative modelling methodology was least sensitive for both reactor systems; displaying a 1% and 4% variation in $\bar{t}_m/\tau$ for the planted and unplanted system, respectively. This was in contrast to the $\bar{t}_m/\tau$ determined by the step change integral and impulse response modelling methodologies which varied by 10% or more in some cases. The differentiation of F(t) to obtain E(t) using the step change derivative methodology was identified as a potential weakness as it had the capability of amplifying background noise which may have affected the calculation of the hydraulic parameters.

The ramifications of this comparison are that each modelling methodology has the potential to output a different reactor model for the same system under study which, when combined with kinetic data may produce a different reactor size for the treatment process. Each modelling methodology also has its own strengths and weaknesses. The absence of an analytical answer to the problem means the choice of modelling methodology is ultimately dictated by other criteria such as experimental equipment availability and the reactor designer's confidence in the respective approaches.

4. Combining hydraulic modelling techniques and Biomimetic design principles to improve horizontal subsurface flow constructed wetland performance

This chapter illustrates how hydraulic modelling of an existing HSSF CW can be used to estimate velocity profiles within the system to identify regions most prone to clogging and the results of which can be combined with Biomimetic design principles to produce a design with an integrated clogging management strategy.

This chapter was presented at the Water Institute of Southern Africa (WISA) 2016 Biennial Conference and Exhibition in Durban, South Africa. The contribution of the co-authors towards the work is primarily of supervision or collaboration and the experimental work and write-up was conducted by the author of this dissertation. The original data for this chapter is presented in Appendices A and E.

4.1 Abstract

South Africa is in the midst of a water supply and quality crisis. The development of necessary water treatment technology is thus of utmost importance to the country, with national government providing funding for the improvement of water quality and supply infrastructure. This is evidenced by the fact that the Department of Science and Technology (DST) is in the process of defining a niche for it to support the Ecological Infrastructure work being performed by the Department of Environmental Affairs (DEA) and the South African National Biodiversity Institute (SANBI). One of the main challenges is developing effective infrastructure for waste water treatment in rural communities. Horizontal subsurface flow constructed wetlands (HSSF CWs) are an attractive solution as they require low capital investment and less human input when compared to conventional treatment technologies. Effective treatment requires the waste water to reside inside the system long enough for the pollutants to be degraded and removed. Plant root development, bacterial biofilm growth, suspended solids accumulation and metal precipitates cause clogging within the packed media and the fluid finds paths of less resistance, creating a short-circuiting effect and potentially, a reduction in treatment performance. Two popular methods for remediating the effects of clogging are excavation and washing as well as in-situ application of cleaning chemicals, with the former being unattractive since the whole system requires to be

taken offline and the latter due to the unknown long-term effects which the cleaning chemicals have on the wetland ecology.

In this study an alternative clogging maintenance strategy is presented with the intended benefit being for rural communities whose sole waste water treatment facility may be a CW and thus cannot afford to have regular system shutdown. Three-dimensional hydraulic modelling was performed by conducting a step change tracer experiment on an existing CW and the mean of the residence time data was used to develop velocity profiles within the system. The modelling identified dead zones and regions with corresponding short-circuiting effects. Biomimetic design principles were then used to improve the existing design by modularizing the regions containing dead zones and hence most prone to clogging. The modified design would thus accommodate easy removal of certain sections while still allowing continuous treatment of the waste water.

Key words: Waste water treatment, rural communities, clogging, hydraulic modelling, Biomimicry

4.2 Introduction

4.2.1 Background

South Africa faces water supply and quality challenges (Hedden and Cilliers, 2014). The development of water treatment technology is thus of utmost importance, with national government providing financial support for the improvement of water quality and supply infrastructure (Tibane and Vermeulen, 2013). This is evidenced by the fact that the DST has defined a niche for it to support the Ecological Infrastructure work being performed by the DEA and SANBI. In 2013, the Department of Water Affairs (DWA) laid out a strategic plan to address the water challenges which the country faces. The plan cites skills development as well as the improvement of infrastructure as one of two main areas to be targeted and views water as a catalyst to the future development of the country (Tibane and Vermeulen, 2013).

One of the main challenges in a South African context is to develop infrastructure that allows for easy and reliable access to clean water for rural communities (Majuru *et al.*, 2012). HSSF CWs are an attractive solution to the problem and their applicability is currently being explored (Ochieng *et al.*, 2010). HSSF CWs are complex ecosystems and are a transition between terrestrial and aquatic environments (Stottmeister *et al.*, 2003). Such systems typically contain a solid matrix,

macrophytes and bacteria which work as a functional unit to improve the quality of water (Marchand *et al.*, 2010; Galletti *et al.*, 2010). Physical, chemical and biological water treatment processes are thus combined into a single unit and require minimal human input for sustenance thus providing a low capital and maintenance cost alternative to traditional treatment technology (Saeed and Sun, 2012). These systems are capable of treating a variety of waste waters to make them suitable for reuse (Vymazal, 2009). These include domestic sewage (Mantovi *et al.*, 2003), storm water runoff (Maillard *et al.*, 2011) and agricultural runoff (Stehle *et al.*, 2011).

4.2.2 Effect of hydraulic behaviour on treatment performance

Effective treatment requires the waste water to reside inside the system for a long enough period of time in order for the pollutants to be degraded and removed (Kantawanichkul *et al.*, 2009). However, researchers have shown that plant root development, bacterial biofilm growth, suspended solids accumulation and metal precipitation cause clogging within the gravel bed (Pedescoll *et al.*, 2011; Knowles *et al.*, 2011). As a result, the fluid finds paths of less resistance through other regions of the wetland. This creates a short-circuiting effect and hence a reduction in treatment efficiency (Min and Wise, 2009). The hydraulic behaviour can be examined by conducting a hydraulic tracer study on the system (Alcocer *et al.*, 2012) in which an inert chemical dye is injected as a step at the inlet and its concentration continuously measured at various points within the system and at the outlet (Sheridan *et al.*, 2014b; Suliman *et al.*, 2006a). Numerical techniques are then used to evaluate the first moment about the cumulative distribution function and hence the mean residence time of the fluid in different regions, which can ultimately assist in drawing up estimates of the velocity profiles inside the system.

4.2.3 Current subsurface clogging management strategies

Different management strategies have been developed to remediate the effects of clogging inside HSSF CWs, with two of the most prominent being excavation and washing of the bed media as well as in-situ application of cleaning chemicals such as hydrogen peroxide (Nivala *et al.*, 2012). Dotro *et al.* (2011a) notes, however, that excavation and washing requires the system to be taken offline for extended periods of time. In-situ application of cleaning chemicals poses health and safety risks to local community members and the long-term effects which the chemicals have on wetland performance are still unknown (Nivala and Rousseau, 2009).

4.2.4 Using Biomimetic design principles to manage clogging effects in HSSF CWs

The application of Biomimicry in the field of CW design is receiving attention by designers and researchers (Van Vuuren, 2014; Kenny *et al.*, 2012). Biomimicry can be classified as an applied science which involves the careful study of nature's systems, designs and processes to derive inspiration for the purposes of solving human problems (El-Zeiny, 2012). One such way to manage clogging in CWs and hence maintain consistent treatment performance is to utilize the Biomimicry design principles which provide a set of guidelines to achieve sustainable system design (Kennedy *et al.*, 2015) and are presented in Figure 4.1.

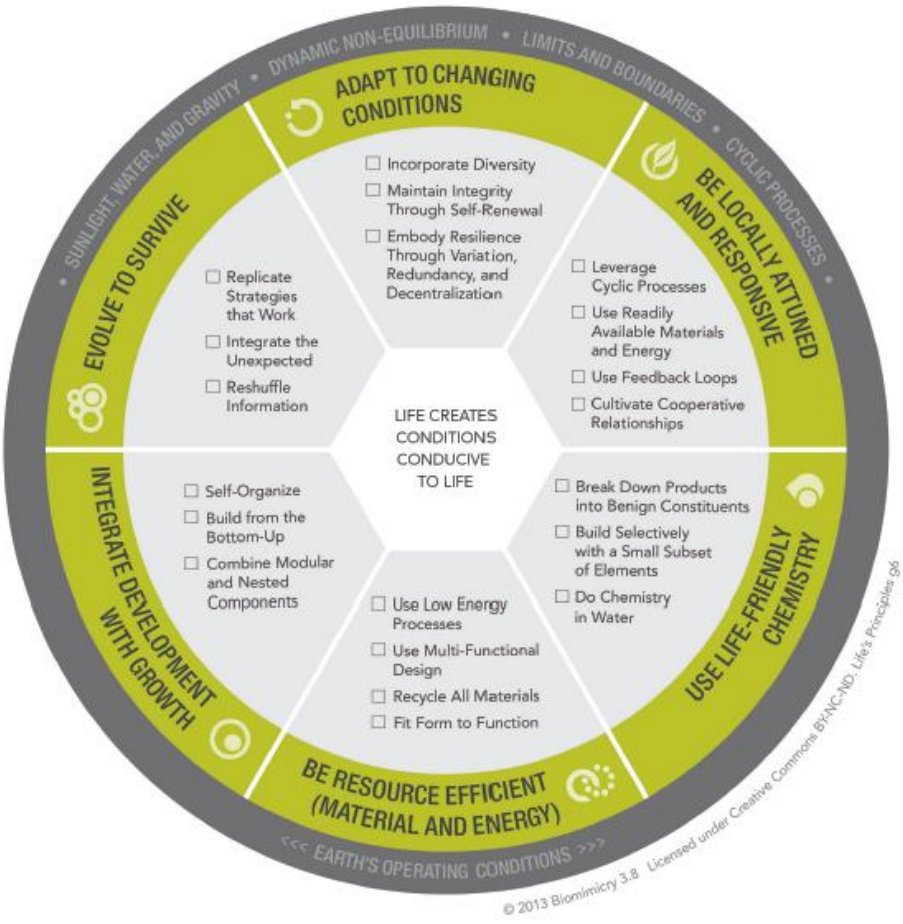

Figure 4.1: Design principles by the Biomimicry Institute

Two overarching principles which are applicable to managing wetland clogging are: adapting to changing conditions and integrating development with growth. Within the principle of adapting to

changing conditions, the sub-principle of embodying resilience through variation, redundancy and decentralization is appropriate since it advocates maintaining function following a disturbance by incorporating a variety of duplicate forms, processes or systems that are not located exclusively together. This sub-principle can be combined with the sub-principle of combining modular and nested components found within integrating development with growth to produce a set of system designs which limit the effect which wetland clogging has on treatment efficiency. One such wetland design would be to modularize the wetland into smaller sub-sections as indicated in Figure 4.2.

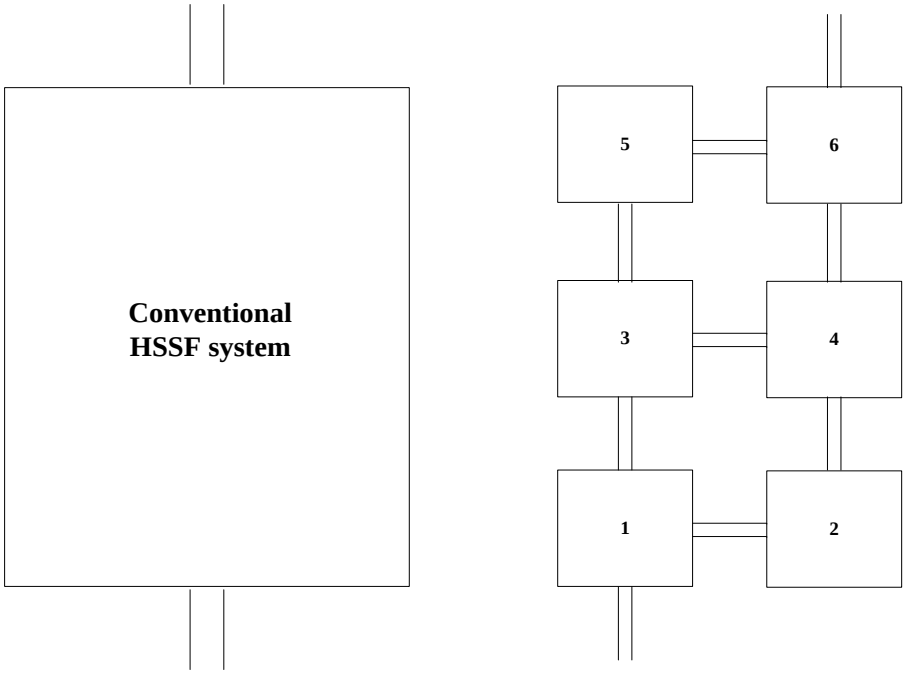

Figure 4.2: Conventional HSSF system (left) and modularized Biomimetic HSSF system (right)

If a section of the wetland becomes clogged to the extent that the hydraulic conductivity is dramatically reduced, the section can be removed and the flow paths can be altered to bypass the section undergoing maintenance. This design thus allows for continuous treatment of water which would be a necessity for rural communities that do not have readily available access to water cleaned by other treatment facilities.

In this paper an illustration is provided of how hydraulic tracer studies can be coupled with Biomimetic design principles to modify the design of an existing HSSF CW for the purpose of better subsurface clogging management and ultimately, a more reliable and improved treatment performance.

4.3 Research objectives

The overall aim of the study can be distilled into the following two objectives:

1. Identify regions most prone to clogging effects in the two systems by conducting hydraulic tracer studies and developing estimates of the velocity profiles; and

2. Use the Biomimetic design principles of modularity and decentralization to modify the design of the two systems so that they can buffer the clogging effects in the zones identified in objective 1.

4.4 Materials and methods

4.4.1 Experimental unit

The CW used in this study was located at the Industrial and Mining Water Research Unit (IMWaRU) facility at the University of the Witwatersrand, Johannesburg. The system was built using an HDPE external support trough and then filled with dolomite gravel. Thirteen sample ports, constructed from PVC mesh (mesh opening = 20 mm), were installed into the system to accommodate sampling within different regions of the CW. Three lengths of silicon tubing were cut and attached to each of the sampling wells using cable ties so that samples could be drawn from three different depths, ultimately resolving the system into a three-dimensional grid. Figure 4.3 provides a visual of the experimental set up.

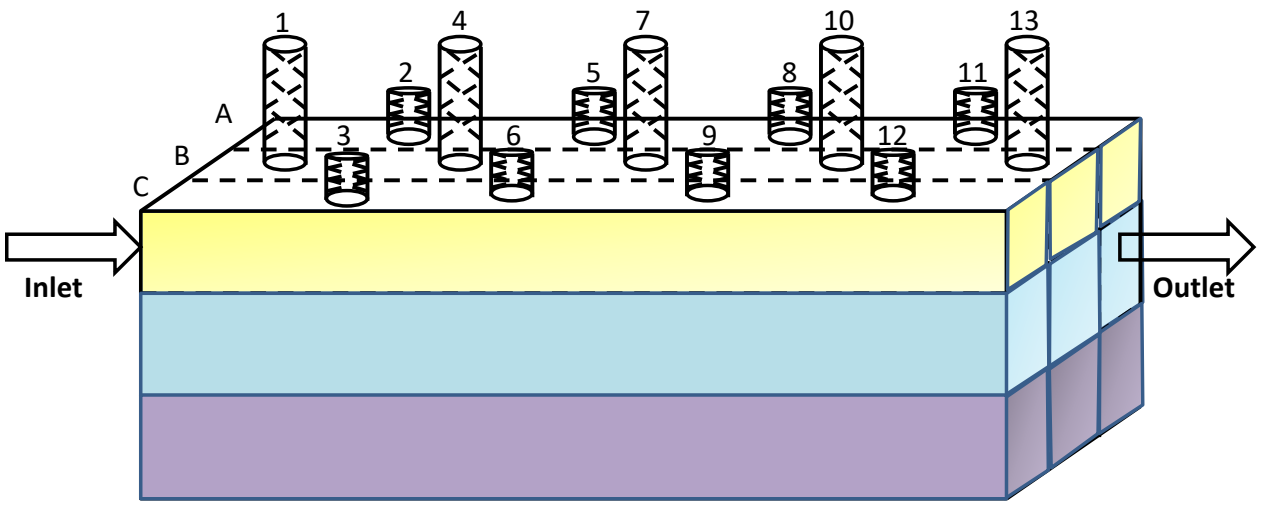

Figure 4.3: Experimental set up indicating the direction of flow of water as well as positioning of sampling wells

In Table 4.1 a summary is provided of the design parameters of the CW.

Table 4.1: Engineering design parameters of the planted CW

Parameter	**Value**
Total length (mm)	4200
Total width (mm)	900
Bed height (mm)	700
Porosity (%)	43
Reactor volume (excluding solids) (m^3)	1.14
Mean particle diameter (mm)	20
Sampling depth 1 (Yellow) (mm)	50
Sampling depth 2 (Blue) (mm)	350
Sampling depth 3 (Purple) (mm)	680

The regions inside the CW as well as the spatial positioning of the different plant species used within the system are shown in Figure 4.4.

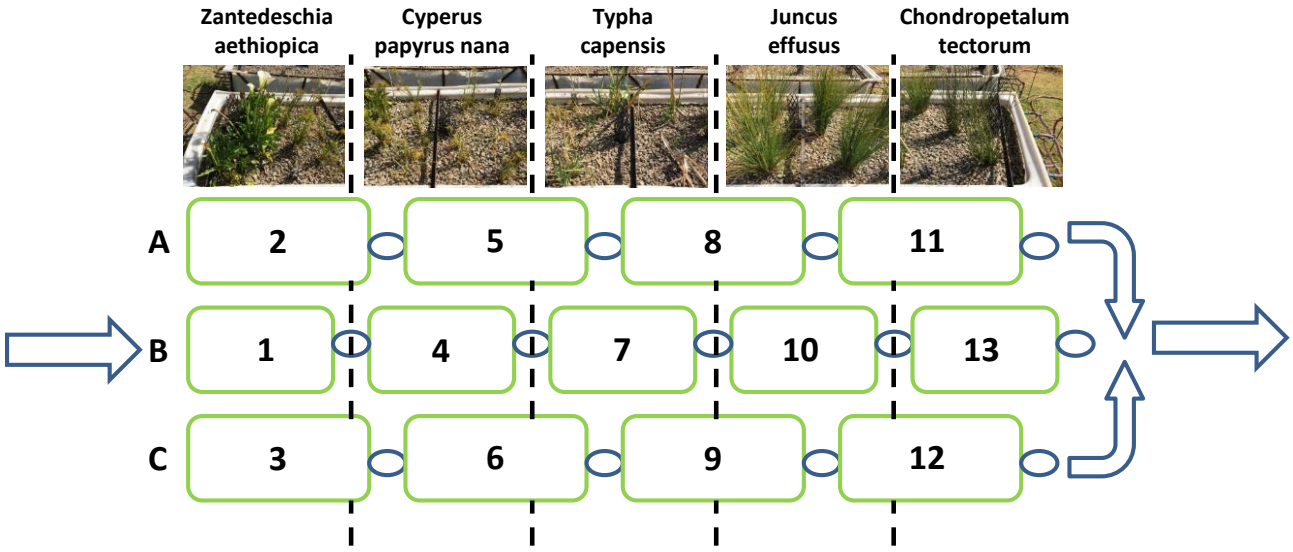

Figure 4.4: Top-view of the regions within the planted CW. Samples were taken from three different depths, resolving the system into a grid of 39 modules. The nomenclature used for each module followed the rule: X,Y where X indicated the region and Y the sampling depth (1,2 or 3).

Table 4.2 provides the physical dimensions of the various regions within the system.

Table 4.2: Physical dimensions of regions within planted CW

Region no.	Length (mm)	Width (mm)
1	200	300
2 and 3	675	300
4-13	950	300

4.4.2 Hydraulic data generation

A step change tracer study was conducted using the fluorescent chemical dye FWT Red (Cole-Parmer, USA). 300 ml of dye was injected into two 5 m^3 vertical cylindrical tanks filled with tap water. The contents of the two tanks were circulated continuously for 24 hours by means of a submersible pump to ensure 10 m^3 of homogeneous tracer solution was available for the study. The inlet and outlet flow rates were allowed to equalise, at which time the feed to the CW was switched over from tap water to the tracer solution. Samples were taken every 30 min from each sampling well for a period of 12 hours. Inlet and outlet flow rates were monitored continuously

using a flow meter (Gardena, Germany) and the average experimental flow rate ($\dot{v}$) was calculated to be 4.13 l/min. Absorbance measurements of the samples were taken using the Merck Spectroquant Pharo 300 at a wavelength of 550 nm. Absorbance readings were converted to tracer concentration by constructing a calibration curve which had an R^2 of 0.99.

4.4.3 Hydraulic modelling

The concentration-time curve obtained for each sampling port was converted to the cumulative distribution curve using Equation 4.1:

$$F(t) = \frac{C(t)}{C_{max}} \qquad \text{Equation 4.1}$$

Where C_{max} is the concentration of tracer as $t \to \infty$ and $F(t)$ being the cumulative distribution curve. The mean residence time of the fluid was then determined using Equation 4.2.

$$\bar{t}_m = \int_0^{\infty}[1 - F(t)]dt \qquad \text{Equation 4.2}$$

Equation 4.2 requires numerical integration of the area below $1 - F(t)$. For this work, Simpson's 1/3 rule was chosen. The method works by approximating the curve as a parabola in multiple equally sized subintervals and summing their areas together to produce the formula shown in Equation 4.3.

$$I = \frac{z}{3}[f(x_0) + 4f(x_1) + 2f(x_2) + \cdots + 4f(x_{n-1}) + f(x_n)] \qquad \text{Equation 4.3}$$

Where:

$$z = \frac{b-a}{n} \qquad \text{Equation 4.4}$$

With z being the number of equally sized subintervals.

The nominal hydraulic retention time indicates the residence time of the water inside the CW under ideal conditions that is, without any short-circuiting effects (Sheridan *et al.*, 2011), and is provided by Equation 4.5.

$$\tau = \frac{V}{\dot{v}} \qquad \text{Equation 4.5}$$

The ideal theoretical velocity profile was determined by plotting the nominal retention time at a sampling port against its length from the inlet. The gradient of the curve was thus determined using Equation 4.6:

$$m_{theoretical} = \frac{\tau_{i+1} - \tau_i}{x_{i+1} - x_i} \quad \text{Equation 4.6}$$

Where the gradient represented the inverse of the magnitude of the velocity (u) under ideal conditions in module i+1 in a specific zone and at a specific depth in the system. Similarly, the experimentally determined mean residence time at a specific sampling port was plotted against its corresponding length and the gradient determined using Equation 4.7.

$$m_{experimental} = \frac{\bar{t}_{m,i+1} - \bar{t}_{m,i}}{x_{i+1} - x_i} \quad \text{Equation 4.7}$$

Where the gradient represented the inverse of the magnitude of the estimated experimental velocity in module i+1 in a specific zone and at a specific depth in the system.

The rules laid out in Table 4.3 were then used to identify non-ideal flow behaviour within specific modules of the wetland.

Table 4.3: Mathematical rules used to characterize hydraulics in modules inside CW

$m_{experimental} = m_{theoretical}$	$u_{experimental} = u_{theoretical}$	Plug (ideal) flow
$m_{experimental} < m_{theoretical}$	$u_{experimental} > u_{theoretical}$	Channeling/short-circuiting
$m_{experimental} > m_{theoretical}$	$u_{experimental} < u_{theoretical}$	Dead zone/clogging

4.5 Results and discussion

In Figure 4.5 (a) - Figure 4.5 (c) the mean residence time at each sampling well is plotted against its corresponding length down the system. The black dotted line in each figure represents the curve which would be obtained under ideal conditions that is, with no dead zones and short-circuiting effects.

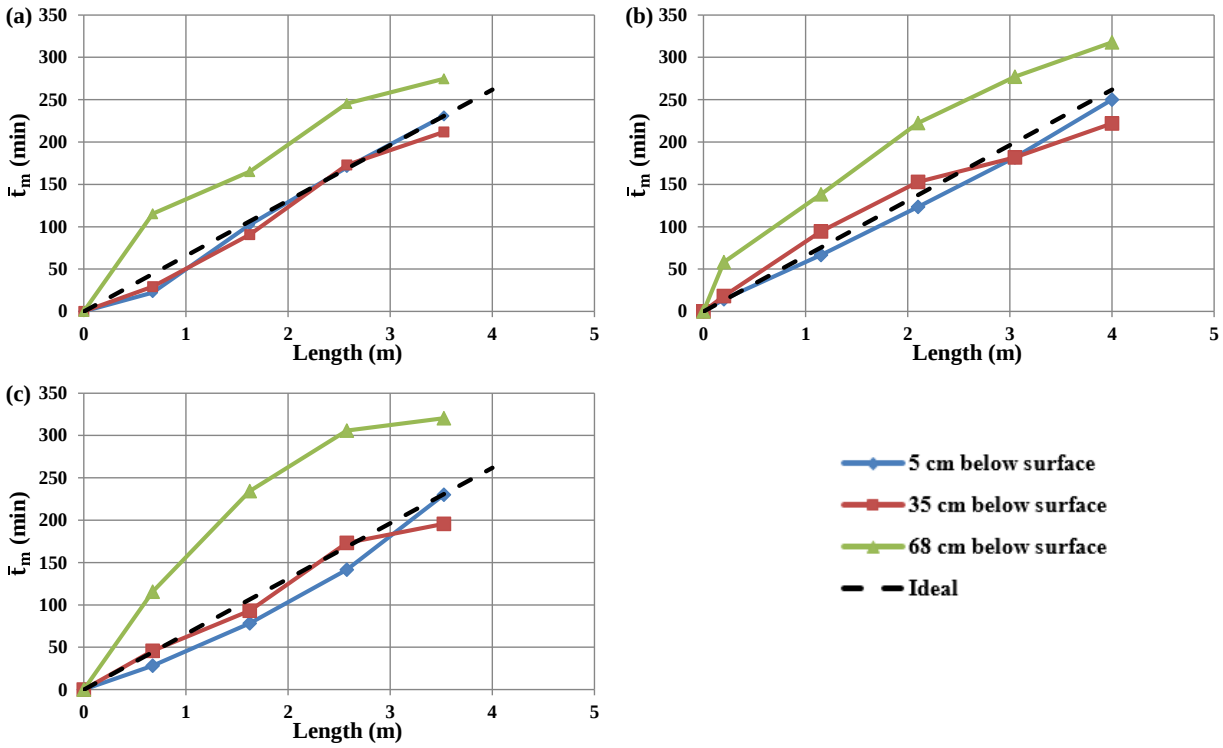

Figure 4.5: Mean residence time versus length down CW. (a) represents data collected from zone A, (b) from zone B and (c) from Zone C

In each of zones A – C the experimental curves deviate from the ideal curve, indicating non-ideal flow behaviour. The data presented in Figure 4.5 were then used with the mathematical rules in Table 4.3 to construct Figure 4.6, which provides a three-dimensional visualization of the dead zones and short-circuiting within the system under study.

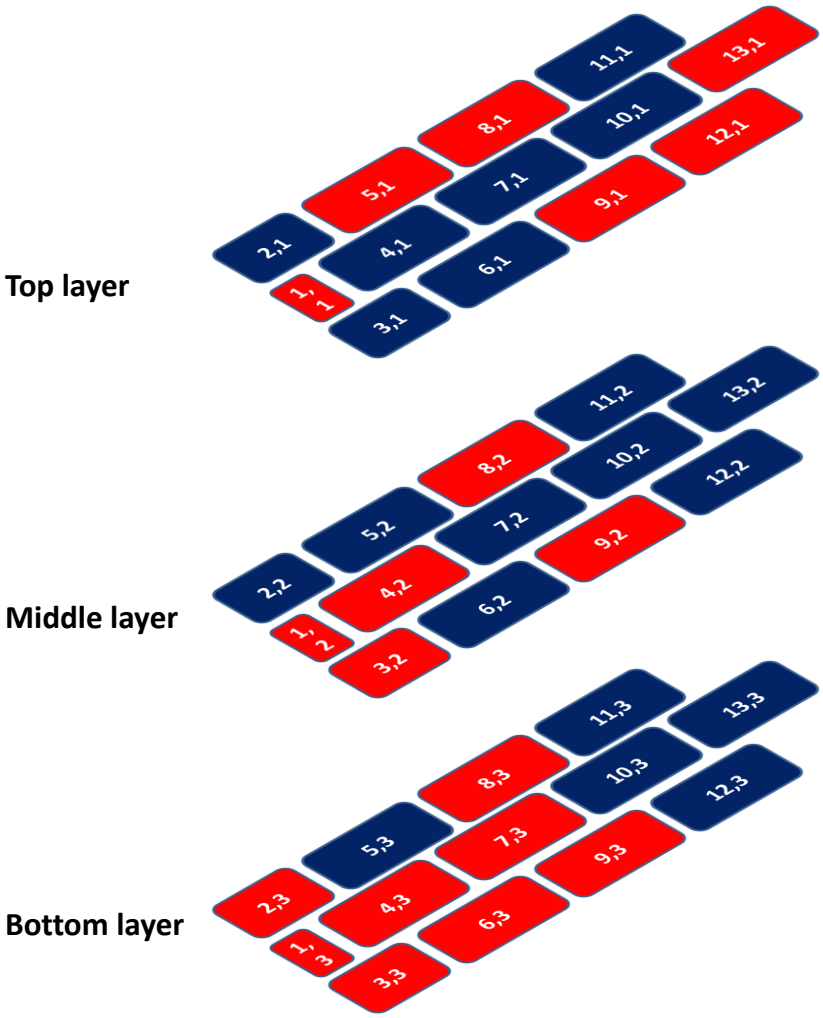

Figure 4.6: Three-dimensional view indicating estimates of the fluid flow behaviour within each of the three layers of the CW. Blue modules indicate modules in which channeling/short-circuiting occurred and red modules indicate modules in which dead zones existed.

Vegetative contributions to CW clogging has been discussed extensively by researchers (Knowles *et al.*, 2011). The effects which the vegetation has on the hydraulics in this system may be caused by dense live root penetration (Tanner, 1994) as well as the stems which are physically and chemically stable due to the presence of esters in the plant tissue (Tanner *et al.*, 1998). These two types of plant material block the pore spaces and present physical barriers to the fluid flow. In addition, plants transfer oxygen from the atmosphere to their root zones, inducing aerobic conditions in the upper layers of the CW (Stottmeister *et al.*, 2003). The oxidizing conditions facilitate ferric hydroxide precipitation which creates a thick sludge in and around the plant roots

and hence further contributes to the clogging (Nivala *et al.*, 2007). Figure 4.4 may be used in conjunction with Figure 4.6 to explain some of the non-ideal flow behaviour in the upper two layers. Upon examination of the distribution of the *Zantedeschia aethiopica* at the front end of the system shown in Figure 4.4, it is seen that the vegetation is highly concentrated in zone B with comparatively less planting along the sides in zones A and C. This may explain the dead zone found in module 1,1 and the channeling of fluid down the sides in modules 2,1 and 3,1 where the hydraulic conductivity is higher. A similar scenario is observed in modules 8,1 and 8,2 as well as in 9,1 and 9,2 in which there is a relatively dense distribution of *Typha capensis* and *Juncus effusus* down the sides of the system, possibly causing dead zones and a more sparsely populated zone B resulting in higher subsurface fluid velocities in modules 7,1 and 7,2 as well as in 10,1 and 10,2.

The presence of dead zones in the bottom layer of the system in modules 1,3; 2,3 and 3,3 may be explained by three interdependent reasons. Firstly, inlet ports to the system are only situated level with the surface of the gravel inducing a hull-shaped flow profile and a large dead zone at the bottom of the system near the inlet. A similar effect was observed by other CW researchers with the same inlet manifold structure (Sheridan *et al.*, 2014a). Low subsurface fluid velocities enhance the likelihood of sedimentation of larger suspended solids within these modules, contributing to the clogging process (Kadlec *et al.*, 2009). Bacteria then feed off the organic matter depositions thereby assisting with proliferation and biofilm formation (Dupin *et al.*, 2001). The biofilms are capable of secreting a polymeric slime which block pore spaces hence preventing the passage of fluid (Knowles *et al.*, 2011; Madigan *et al.*, 2009). The other dead zones found in the bottom layer of the system may be due to a combination of various clogging processes, such as straining and trapping, adsorption and chemical precipitation (Knowles *et al.*, 2011).

4.5.1 Modification of CW design using Biomimetic design principles

According to the hydraulic modelling performed on the system, almost every region (comprising the modules in all three topographical layers) had a dead zone and hence some clogging effects. Consequently, each region was modularized using a combination of isolation valves and bypass streams so that any region within the CW could be taken offline for gravel cleaning while still ensuring the rest of the reactor treats water. It should be noted that regions themselves were not modularized topographically due to the practical construction difficulties of such a task. The suggested biomimetic design is presented in Figure 4.7.

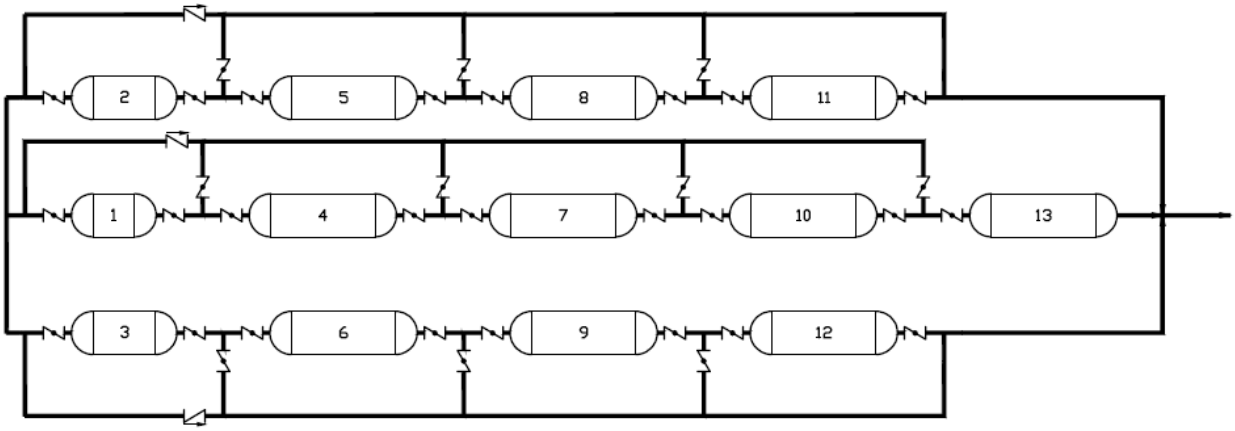

Figure 4.7: Plan-view of suggested biomimetic design of CW based on hydraulic modelling results. Streams showing interactions between adjacent regions have not been included in the diagram due to spatial constraints.

In order for the above design to work as best as possible in a rural community, a step-by-step manual detailing the protocols of clogging management for the system should be written up. It should include the following information:

- Which valves must be opened/closed and the order in which they must be opened/closed in order to isolate and remove the clogged region;
- How to clean the solid matrix in the clogged region; and
- How to re-install the cleaned region and return the system to standard operating conditions.

4.6 Conclusions and recommendations

Three-dimensional hydraulic modelling was performed on an existing HSSF CW by conducting a step change tracer study and using the mean residence time data to estimate the velocity profiles within the system. The modelling identified dead zones and regions in which short-circuiting occurred. Biomimetic design principles were then applied to improve the design of the system by modularizing the regions prone to clogging. The suggested design allows for different sections of the wetland to be removed for de-clogging while still enabling the rest of the system to continue treating water. The clogging management solution presented in this study is intended to benefit rural communities in South Africa, whose waste water treatment facility may be a CW and shutdown of the whole facility for clogging maintenance is not a viable option. By writing an easy

to follow clogging maintenance protocol, members of the community may be able to implement the clogging management strategy for the suggested system design while still allowing continuous treatment of the waste water.

5. Heat as a hydraulic tracer for horizontal subsurface flow constructed wetlands

This chapter explores heat as a hydraulic tracer for HSSF CWs with the intention being to develop more environmentally sustainable hydraulic modelling processes.

This chapter has been submitted for peer review and publication to *Water Research.* The contribution of the co-authors towards the work is primarily of supervision or collaboration and the experimental work and write-up was conducted by the author of this dissertation. The original data for this chapter is presented in Appendix F.

5.1 Abstract

Hydraulic tracer studies for horizontal subsurface flow constructed wetlands (HSSF CWs) require the addition of a conservative chemical tracer to track the flow path of the waste water inside the subsurface media. However since one would wish to use fully conservative tracers (i.e. they do not degrade) disposal problems of the wetland effluent can be created. In this study the use of heat as a hydraulic tracer was explored. Heat is considered a more environmentally friendly alternative to chemical tracers as the post-study wetland and effluent temperature can rapidly equilibrate to ambient conditions. Nevertheless the non-conservative behaviour of heat creates a distorted response curve at the outlet from which the hydraulic performance indices cannot be easily computed. In this study a mapping methodology was developed which accepts a heat tracer response curve as an input and is converted to a conservative chemical tracer response curve by establishing a mathematical relationship between heat and conservative solute hydrodynamic dispersion. The methodology was tested by conducting a dual heat-chemical tracer study on a laboratory scale unplanted HSSF CW and the predicted chemical tracer response was compared with the actual experimental chemical tracer response data. The predicted response curve adequately matched the experimental response curve supported by the fact that there was a 5% and 6% relative difference in Peclet number and mean of the residence time distribution (RTD) respectively. The outcome of this study is that it is possible to use the proposed mapping methodology in conjunction with a heat tracer to quantify hydraulic behaviour of HSSF CWs without having to use a conservative chemical tracer.

Keywords: Hydraulics, constructed wetlands, heat tracer, mapping methodology

5.2 Introduction

Residence time distribution (RTD) studies are used to assess the hydraulic performance of horizontal subsurface flow constructed wetlands (HSSF CWs) (Mateus *et al.*, 2012). These studies entail addition of a tracer into the CW feed and continuous monitoring of the concentration at the outlet, after which suitable numerical methods are applied to the response curve to quantify a set of performance indices (Asraf-Snir and Gitis, 2011; Lappalainen *et al.*, 2011). Accurate characterization of hydraulic behaviour requires the tracer to be conservative (Cucco and Umgiesser, 2006). In essence the tracer should be highly soluble in the feed water to prevent sorption onto the wetland sediments (Matamoros and Bayona, 2006) as well as being resistant to biological, chemical and photochemical decay (Gutowski *et al.*, 2015; Keefe *et al.*, 2004). Examples of conservative tracers include fluorescent dyes such as fluorescein (Lemke *et al.*, 2013) and Rhodamine WT (Hensley and Cohen, 2012), the chloride ion (Gasser *et al.*, 2014) and the bromide ion (Rauch-Williams *et al.*, 2010). These tracers potentially pose downstream environmental risks since they show a high persistence. Dedicated disposal infrastructure for the reactor effluent is required as a result and this ultimately increases the cost of performing the study.

Heat has frequently been used in hydrogeology as a tracer for groundwater movement (Rau *et al.*, 2014; Wagner *et al.*, 2014). Applications include quantifying hydrodynamic exchanges at the streambed-aquifer interface in the hyporheic zone (Jensen and Engesgaard, 2011) as well as for the identification and characterization of fractures in aquifers (Banks *et al.*, 2014; Hausner *et al.*, 2015; Leaf *et al.*, 2012). The drawback of using heat is its non-conservative behaviour (Westhoff *et al.*, 2010). A temperature gradient across the fluid-solid interface causes heat to be easily absorbed by the packed media (Engelhardt *et al.*, 2013), effectively retarding the velocity of the tracer with the consequence being an altered response curve and distorted description of the hydraulic behaviour of the system. Nevertheless, it is preferred over conventional chemical tracers due to the availability of cheap and simple to operate temperature measurement devices (Anibas *et al.*, 2011) and the effluent from the study need not be disposed; rather it can be temporarily stored allowing it to equilibrate with ambient conditions and then be re-used.

5.2.1 Aim

To date, little has been published regarding the use of heat as a tracer for RTD studies on HSSF CWs and is most likely due to its non-conservative behaviour. In this study a mathematical model

was sought to be developed, based on transport phenomena theory, which maps an input of response data obtained from a non-invasive tracer in the form of heat to the response curve which would be obtained from a conservative chemical tracer. This approach would allow for accurate hydraulic behaviour of the wetland to be ascertained without having to tackle the environmental hazards posed by conservative chemical tracers. The model was then tested by conducting a combined conservative solute and heat tracer RTD study on a laboratory-scale unplanted HSSF CW. The shape of the predicted conservative tracer response curve was compared with the actual experimental response curve as well as their corresponding hydraulic performance indices.

5.3 Background

5.3.1 Hydraulic modelling using an RTD study

An RTD study is used to quantify the extent of mixing inside an HSSF CW (Maltais-Landry *et al.*, 2009). In the step change response experiment, a tracer is introduced as a step in concentration in the feed pipe and its concentration monitored at the outlet (Vonortas *et al.*, 2011) so that the cumulative distribution curve can be determined according to Equation 5.1. The response curve can then be used to quantify hydraulic behaviour using the method of moments as well as a variety of reactor models including the tanks in series (TIS) and advective-dispersive transport models (Langergraber *et al.*, 2009).

$$F(t) = \frac{C(t)}{C_{max}} \qquad \text{Equation 5.1}$$

5.3.2 Method of moments analysis

Hydraulic behaviour is described by determining the first and second temporal moments of the response curve in Equation 5.1 (Schuetz *et al.*, 2012). The first moment is the centroid of the response curve (Holland *et al.*, 2004), representing the mean of the RTD of fluid inside the system and is calculated using Equation 5.2. $\bar{t}_m$ is compared to the nominal residence time τ, shown in Equation 5.3, to provide the effective volume utilization in Equation 5.4 (Bodin *et al.*, 2012). Effective volume utilization can vary considerably between different HSSF CWs and is a function of the aspect ratio (Molle *et al.*, 2008), positioning of inlet and outlet ports (Sheridan *et al.*, 2014a), plant root density (Pedescoll *et al.*, 2013) as well as the extent of subsurface media clogging due to biofilm growth (Knowles *et al.*, 2011) and hydroxide precipitate accumulation (Riefler *et al.*, 2008).

$$\bar{t}_m = \int_0^\infty [1 - F(t)]dt \quad \text{Equation 5.2}$$

$$\tau = \frac{V_{total}\varepsilon}{\dot{v}} \quad \text{Equation 5.3}$$

$$e = \frac{\bar{t}_m}{\tau} \quad \text{Equation 5.4}$$

The second temporal moment is the variance of the response curve, which provides an indication of the spread of tracer as it flows through the system (Drummond *et al.*, 2012) and is calculated using Equation 5.5 (Jackson *et al.*, 2012).

$$\sigma^2 = 2\int_0^\infty t[1 - F(t)]dt - \bar{t}_m{}^2 \quad \text{Equation 5.5}$$

σ^2 and $\bar{t}_m$ obtained from the RTD study are used to derive reactor models describing the hydraulic behaviour of the wetland, some of which are presented in Section 5.3.3.

5.3.3 Deriving reactor model characteristics from the RTD

Tanks in series (TIS) model

In this approach the response curve is analysed to determine the number of equally sized continuously stirred tanks reactors (CSTRs) placed in series that will provide the same $F(t)$ curve as the HSSF CW under study and is determined using Equation 5.6 (Bodin *et al.*, 2013). When $n = 1$, the degree of back mixing is high and the HSSF CW can be modelled as a single CSTR. As $n \rightarrow \infty$, the degree of back mixing tends to zero and the CW can be modelled as a plug flow reactor (PFR).

$$N = \frac{\bar{t}_m{}^2}{\sigma^2} \quad \text{Equation 5.6}$$

Advective-dispersive transport with retardation and decay

Hydrodynamic dispersion can be quantified by fitting the response curve to the solution of the partial differential equation describing movement of a chemical tracer inside the subsurface media, as provided in Equation 5.7 (Šimůnek *et al.*, 2003). μ and γ are first order decay and zero order production coefficients respectively which are applicable to reactive chemical tracers (Malaguerra *et al.*, 2013; Van Genuchten, 1981). The transport equation in Equation 5.7 includes the chemical retardation factor which is defined in Equation 5.8 (Freeze and Cherry, 1979) and the definition of

the Peclet number for CWs provided in Equation 5.9 (Chazarenc *et al.*, 2003). The distribution coefficient, K_d, relates tracer concentration in the liquid and solid phases. The magnitude of K_d depends on the physical properties of the tracer and can also be affected by the porous media through which it travels (Rubin, 2012). In general, tracers which have K_d values close to zero are considered non-sorbing and vice versa (Field and Pinsky, 2000; Vilks and Baik, 2001).

$$R\frac{\partial C}{\partial t} = D\frac{\partial^2 C}{\partial x^2} - u\frac{\partial C}{\partial x} - \mu C + \gamma \qquad \text{Equation 5.7}$$

$$R = 1 + \frac{\rho_b K_d}{\varepsilon} \qquad \text{Equation 5.8}$$

$$Pe = \frac{uL}{D} \qquad \text{Equation 5.9}$$

Equation 5.7 has been solved at a series of time values to demonstrate the effect which retardation, first order decay and zero order production have on the response curve and the solutions are presented in Figure 5.1. Chemical retardation (R) has the effect of slowing down the bulk movement of tracer due to adsorption on subsurface media sites (Rezanezhad *et al.*, 2012). First order decay (μ) causes a permanent loss of tracer as a result of reaction with the wetland sediment or leakage to the environs and hence an attenuation of the response signal while zero order production (γ) generates additional tracer and a steady state signal greater than one.

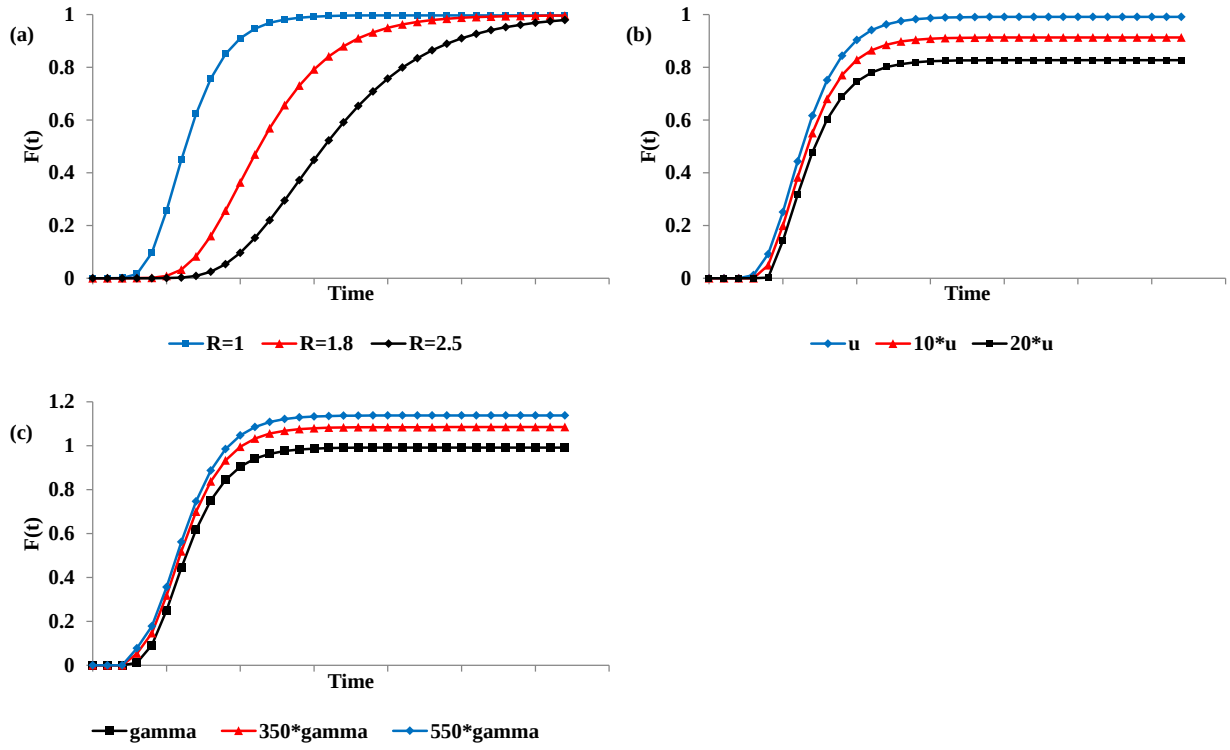

Figure 5.1: Effect of retardation (a), first order decay (b) and zero order production (c) on the response curve from an RTD study

The convolution integral

In this method the RTD function, E(t), is combined with data pertaining to CW inlet concentration to predict corresponding outlet concentrations. This is a particularly useful approach for determining the conversion of chemical species inside the CW assuming a first order reaction rate is applicable (Sheridan *et al.*, 2014b). The logic is depicted in Figure 5.2.

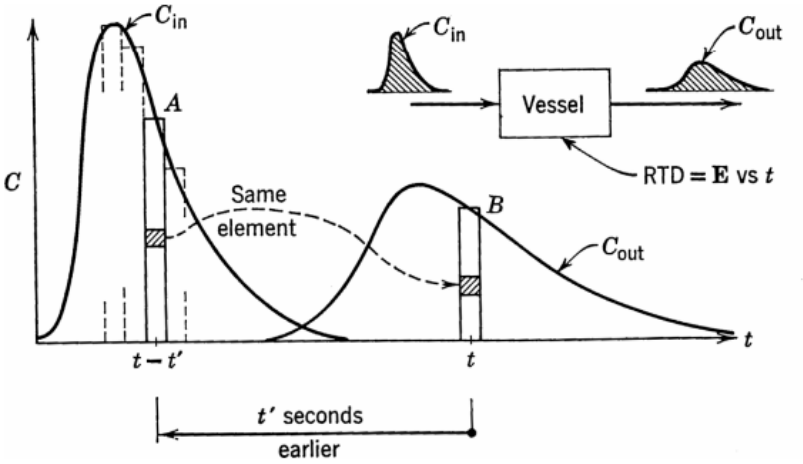

Figure 5.2: The convolution integral. Taken from Levenspiel (1999)

By performing a mass balance on tracer about to leave at time t Equation 5.10 is obtained:

$$C_{out} = \int_0^t C_{in}(t')E(t - t')dt' \qquad \text{Equation 5.10}$$

Equation 5.10 can be written using the convolution integral as shown in Equation 5.11.

$$C_{out} = C_{inlet} * E(t) \qquad \text{Equation 5.11}$$

The conceptual thinking behind the methodology was developed for the impulse response experiment from which the $E(t)$ curve is directly determined. The method holds for the case of the step change response experiment by converting $F(t)$ to $E(t)$ using Equation 5.12 (Levenspiel, 1999):

$$E(t) = \frac{dF(t)}{dt} \qquad \text{Equation 5.12}$$

5.4 Research objectives

The overall aim of developing a methodology to obtain accurate hydraulic information of an HSSF CW using a heat tracer could be achieved by fulfilling the following research objectives:

1. To develop the heat tracer transport equation with a similar form or functionality to the chemical tracer transport equation presented in Equation 5.7;
2. To solve the chemical and heat tracer transport equations subject to initial and boundary conditions applicable to a step change RTD study;

3. To establish a mathematical relationship between the heat and chemical tracer hence allowing transferral of data from the heat space to chemical space; and
4. To test the methodology by conducting a dual heat and chemical tracer study on a laboratory scale unplanted HSSF CW.

5.5 Materials and methods

The development of the methodology as well as subsequent testing is summarized in the flowchart presented in Figure 5.3 and discussed in detail in the sections which follow.

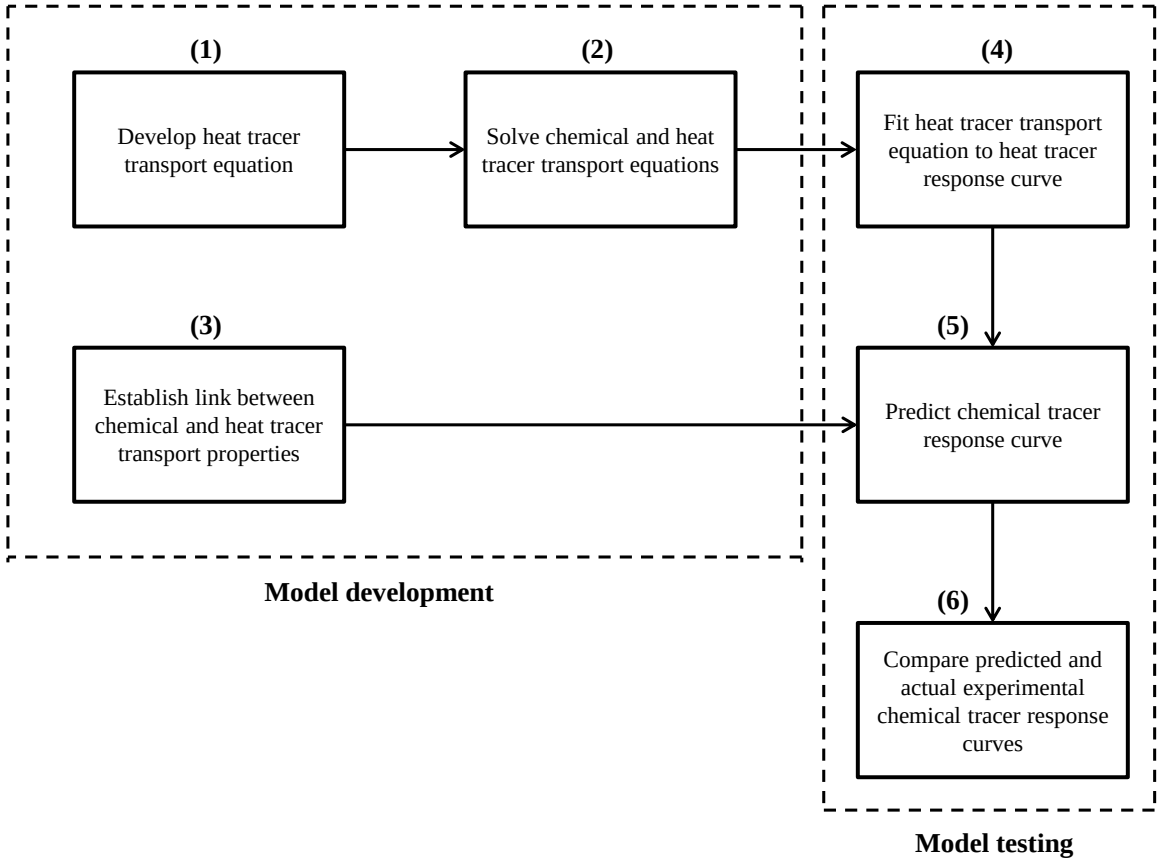

Figure 5.3: Flow diagram of proposed methodology to obtain hydraulic information of an HSSF CW from a heat tracer study and subsequent testing

5.5.1 Development of heat tracer transport equation

The heat tracer transport equation was developed by drawing analogies with the chemical tracer transport equation presented in Equation 5.7. A representative shell of cross sectional area HW and thickness Δx was constructed and is shown in Figure 5.4. Heat and chemical transport

processes in porous media can be compared directly by considering temperature to be analogous to concentration of solute associated with a parcel of fluid being transported inside the system (Bons *et al.*, 2013). Mathematical descriptions of possible transport processes are presented in Table 5.1. Both types of tracers are subjected to convective and dispersive transport (Hecht-Méndez *et al.*, 2010). The magnitude of convective transport is affected by the capability of the porous media to capture pockets of heat as they move with the bulk fluid through the subsurface system (Giambastiani *et al.*, 2013). Heat is dissipated through the physical boundaries of the wetland and is dependent on the extent of insulation and the temperature driving force between the system and ambient conditions (Economopoulou and Tsihrintzis, 2003).

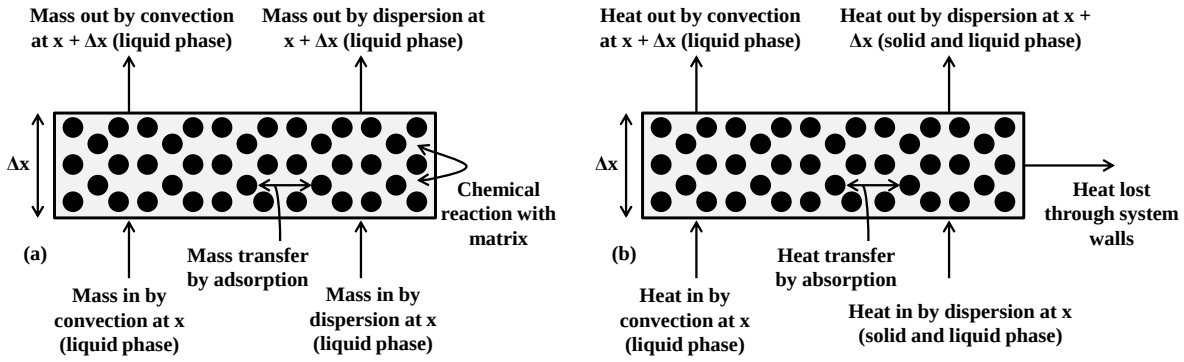

Figure 5.4: Comparison of transport processes occurring inside shell for (a) chemical tracer and (b) heat tracer

Table 5.1: Comparison of analogous transport processes of a chemical and heat tracer applied in an HSSF CW

Liquid phase	**Chemical tracer**	**Heat tracer**
Accumulation	$\varepsilon \frac{\partial C}{\partial t}$	$\varepsilon \rho_f C_{pf} \frac{\partial T_f}{\partial t}$
Convective transport	$u\varepsilon \frac{\partial C}{\partial x}$	$u\varepsilon \rho_f C_{pf} \frac{\partial T_f}{\partial x}$
Dispersive transport	$D\varepsilon \frac{\partial^2 C}{\partial x^2}$	$\varepsilon D_{heat,f} \frac{\partial^2 T_f}{\partial x^2}$
Interactions with wetland matrix	$\alpha_{f/s} a_v (C - \rho_b S)$	$h_{f/_s} a_v [T_f - T_s]$
Sink term	$\varepsilon \mu C - \varepsilon \gamma$	$\frac{2U_{wall}[H + W]}{HW} [T_f - T_a]$

Solid phase	Chemical tracer	Heat tracer
Accumulation	$\rho_b \frac{\partial S}{\partial t}$	$\rho_b C_{ps} \frac{\partial T_s}{\partial t}$
Dispersive transport		$k_s \frac{\partial T_s}{\partial x}$
Interactions with liquid phase	$\alpha_{f/s} a_v (C - \rho_b S)$	$h_{f/_s} a_v [T_f - T_s]$

It was assumed that fluid and solid temperatures at the solid-pore interface equilibrate rapidly (De Marsily, 1986), hence the relation $T_f = T_s$. The energy equation describing heat tracer transport is shown in Equation 5.13 with the definition for the thermal retardation factor R_T (Shook, 2001) presented in Equation 5.14.

$$R_T \frac{\partial T}{\partial t} = -u \frac{\partial T}{\partial x} + \lambda_T \frac{\partial^2 T}{\partial x^2} - \frac{2U_{wall}[H+W]}{\varepsilon \rho_f C_{pf} HW} T + \frac{2U_{wall}[H+W]}{\varepsilon \rho_f C_{pf} HW} T_a \quad \text{Equation 5.13}$$

$$R_T = 1 + \frac{\rho_b C_{ps}}{\varepsilon \rho_f C_{pf}} \quad \text{Equation 5.14}$$

5.5.2 Solving transport equations for chemical and heat tracers

Transport equation for chemical tracer

Since the purpose of this study is to map heat tracer data to a non-reactive chemical tracer $\mu = \gamma = 0$. The initial condition for Equation 5.7 is presented in Equation 5.15. The two applicable boundary conditions are a step change in chemical tracer in the wetland feed at time zero, expressed in Equation 5.16 and the semi-infinite assumption as provided in Equation 5.17.

$$C(x, 0) = C_{initial} \quad \text{Equation 5.15}$$

$$\left(-D \frac{\partial C}{\partial x} + uC\right)\Big|_{x=0} = uC_{inlet} \quad \text{Equation 5.16}$$

$$\frac{\partial C}{\partial x}(\infty, t) = 0 \quad \text{Equation 5.17}$$

Equation 5.7 was solved analytically using the methodology developed by Lindstrom *et al.* (1967) and Gershon and Nir (1969), with the solution presented in Equation 5.18. $A(x, t)$ is a function of the transport properties of the tracer and is defined according to Equation 5.19.

$$C(x, t) = C_{initial} + (C_{inlet} - C_{initial}) A(x, t) \quad \text{Equation 5.18}$$

$$A(x,t) = \frac{1}{2}\operatorname{erfc}\left[\frac{Rx-ut}{2(DRt)^{1/2}}\right] + \left(\frac{u^2t}{\pi DR}\right)^{\frac{1}{2}} \exp\left[-\frac{(Rx-ut)^2}{4DRt}\right] - \frac{1}{2}\left(1 + \frac{ux}{D} + \frac{u^2t}{DR}\right)\exp\left(\frac{ux}{D}\right)\operatorname{erfc}\left[\frac{(Rx+ut)}{2(DRt)^{1/2}}\right]$$

Equation 5.19

Transport equation for heat tracer

The initial condition for Equation 5.13 is provided in Equation 5.20:

$$T(x,0) = T_{initial}$$

Equation 5.20

Similar to the chemical tracer, the appropriate boundary conditions were a step change in temperature in the wetland feed at time zero and the semi-infinite assumption, expressed in Equation 5.21 and Equation 5.22 respectively:

$$\left(-\lambda_T \frac{\partial T}{\partial x} + u\rho_f C_{pf} T\right)\Big|_{x=0} = u\rho_f C_{pf} T_{inlet}$$

Equation 5.21

$$\frac{\partial T}{\partial x}(\infty, t) = 0$$

Equation 5.22

Equation 5.13 was solved analytically using the methodology developed by Van Genuchten (1981), with the solution presented in Equation 5.23:

$$T(x,t) = \frac{\gamma}{\mu} + \left(T_{initial} - \frac{\gamma}{\mu}\right)A(x,t) + \left(T_{inlet} - \frac{\gamma}{\mu}\right)B(x,t)$$

Equation 5.23

Where $A(x,t)$ and $B(x,t)$ are defined in Equation 5.24 and Equation 5.25 respectively.

$$A(x,t) = \exp\left(\frac{-\mu t}{R_T}\right)\left\{1 - \frac{1}{2}\operatorname{erfc}\left[\frac{R_T x-ut}{2(\lambda_T R_T t)^{1/2}}\right] - \left(\frac{u^2t}{\pi\lambda_T R_T}\right)^{\frac{1}{2}} \exp\left[-\frac{(R_T x-ut)^2}{4\lambda_T R_T t}\right] + \frac{1}{2}\left(1 + \frac{ux}{\lambda_T} + \frac{u^2t}{\lambda_T R_T}\right)\exp\left(\frac{ux}{\lambda_T}\right)\operatorname{erfc}\left[\frac{(R_T x+ut)}{2(\lambda_T R_T t)^{1/2}}\right]\right\}$$

Equation 5.24

$$B(x,t) = \frac{u}{(u+v)}\exp\left[\frac{(u-v)x}{2\lambda_T}\right]\operatorname{erfc}\left[\frac{R_T x-ut}{2(\lambda_T R_T t)^{1/2}}\right] + \frac{u}{(u-v)}\exp\left[\frac{(u+v)x}{2\lambda_T}\right]\operatorname{erfc}\left[\frac{R_T x+ut}{2(\lambda_T R_T t)^{1/2}}\right] + \frac{u^2}{2\mu\lambda_T}\exp\left(\frac{ux}{\lambda_T} - \frac{\mu t}{R_T}\right)\operatorname{erfc}\left[\frac{R_T x+ut}{2(\lambda_T R_T t)^{1/2}}\right]$$

Equation 5.25

$$v = u\left(1 + \frac{4\mu\lambda_T}{u^2}\right)^{\frac{1}{2}}$$

Equation 5.26

$$\mu = \frac{2U_{wall}[H+W]}{\varepsilon\rho_f C_{pf} HW}$$ Equation 5.27

$$\gamma = \frac{2U_{wall}[H+W]}{\varepsilon\rho_f C_{pf} HW} T_a$$ Equation 5.28

5.5.3 Development of link between heat and chemical tracer transport

The proposed mapping methodology requires fitting the solution to the heat tracer transport equation, as shown in Equation 5.23, to the heat tracer response curve to determine the thermal dispersion coefficient λ_T. Hence a relationship was developed between λ_T and the chemical dispersion coefficient D in order for the hydraulic data to be transferred to the chemical tracer space. Total thermal and chemical dispersion are functions of molecular diffusion as well as mechanical dispersion, which occurs as a result of the fluid flowing through channels of different geometries and hydraulic conductivity (Bons *et al.*, 2013). Mechanical dispersion of fluid in the subsurface media can occur in both the longitudinal and transverse directions (Delgado, 2007). This leads to the formulation of the chemical dispersion coefficient in Equation 5.29 and the thermal dispersion coefficient in Equation 5.30 (Rau *et al.*, 2012; Van Genuchten, 1981).

$$D = \varepsilon D_m + u[\alpha_l + \alpha_t]$$ Equation 5.29

Where α_l and α_t are defined as the longitudinal and transverse solute dispersivity, respectively.

$$\lambda_T = \frac{k_0}{\varepsilon\rho_f C_{pf} + \rho_b C_{ps}} + u[\beta_l + \beta_t]$$ Equation 5.30

Where k_0 is the system thermal conductivity defined in Equation 5.31 and β_l and β_t the longitudinal and transverse thermal dispersivity, respectively.

$$k_0 = {k_f}^{\varepsilon} + {k_s}^{(1-\varepsilon)}$$ Equation 5.31

Hydrodynamic dispersivity is a function of the subsurface media heterogeneity and is, in essence, the physical property which an RTD study attempts to evaluate. Based on this premise the total thermal dispersivity should be equal to the total chemical dispersivity of the system (De Marsily, 1986) and thus:

$$[\beta_l + \beta_t] = [\alpha_l + \alpha_t]$$ Equation 5.32

Therefore re-arranging Equation 5.30 and using the relation provided in Equation 5.32 yields the function linking the chemical and thermal dispersion coefficients in Equation 5.33:

$$D = \varepsilon D_m + \left[\lambda_T - \frac{k_0}{\varepsilon \rho_f C_{pf}}\right] \quad \text{Equation 5.33}$$

5.5.4 Testing of mapping methodology: experimental set up

The methodology developed herein was tested by conducting a combined chemical and heat hydraulic tracer study on a laboratory-scale unplanted HSSF CW with the experimental set up presented in Figure 5.5.

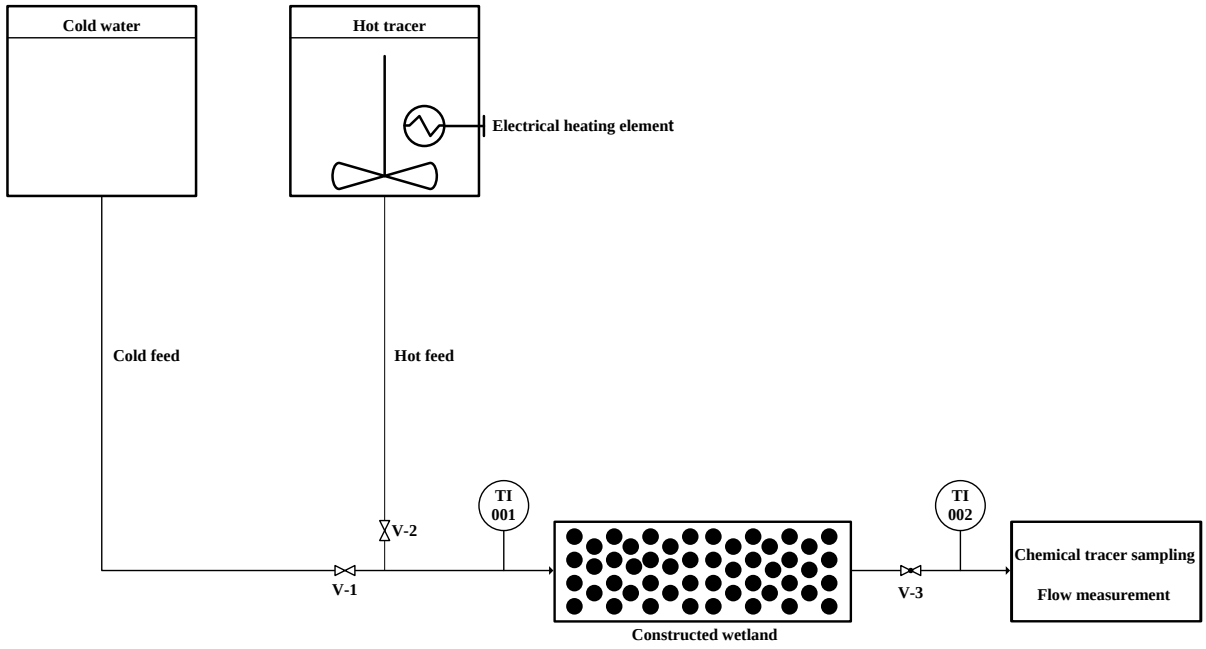

Figure 5.5: Experimental set up for conducting hydraulic tracer study on laboratory-scale unplanted HSSF CW

Physical and thermal properties of wetland

The external support trough of the wetland consisted of 20 mm thick pinewood to provide structural integrity inside which 43 mm of polystyrene was inserted for thermal insulation and plastic pond liner as a hydraulic seal. The subsurface bed had dimensions of 1.03 x 0.19 x 0.16 m (L x W x H) and contained dolomite gravel with a mean particle size of 20 mm as the packing

material. A summary of the thermal and physical properties of the system are provided in Table 5.2. The overall heat transfer coefficient U_{wall} was determined using Equation 5.34 (Fogler, 1999).

$$\frac{1}{U_{wall}} = \frac{1}{h_{air}} + \frac{1}{h_{water}} + \frac{\delta_{pond\ liner}}{k_{pond\ liner}} + \frac{\delta_{polystyrene}}{k_{polystyrene}} + \frac{\delta_{pinewood}}{k_{pinewood}} \quad \text{Equation 5.34}$$

Table 5.2: Thermal properties of laboratory-scale HSSF CW

Transport property	**Unit**	**Value**	**Reference**
h_{air}	$W/m^2.K$	25	Heldman and Moraru (2003)
h_{water}	$W/m^2.K$	1000	Heldman and Moraru (2003)
$k_{pond\ liner}$	W/m.K	0.38	Gaal *et al.* (2004)
$k_{polystyrene}$	W/m.K	0.18	Van Krevelen and Te Nijenhuis (2009)
$k_{pinewood}$	W/m.K	0.15	Mohapatra *et al.* (2014)
U_{wall}	$W/m^2.K$	0.67	Calculated value
k_{gravel}	W/m.K	4.44	Hamdhan and Clarke (2010)
k_{water}	W/m.K	0.62	Ramires *et al.* (1995)
$C_{p,gravel}$	kJ/kg.K	1.18	Hamdhan and Clarke (2010)
$C_{p,water}$	kJ/kg.K	4.18	Rosiek and Batlles (2009)
ρ_{gravel}	kg/m^3	2526	Experimentally determined
ρ_{water}	kg/m^3	994	Costa *et al.* (1986)
ε	-	0.48	Experimentally determined

Hydraulic design of experimental set up

The feed tank used for the hydraulic study was placed 4 m above the wetland to ensure adequate hydrostatic feed pressure. 15 mm polypropylene piping was used for the hot and cold feed lines as well as for the wetland discharge. The hot feed line was insulated using polyethylene (PE) foam. The wetland consisted of three inlet ports and one outlet port all of which were situated 50 mm from the base of the bed. A syphon breaker was used at the wetland outlet for level control.

5.5.5 Testing of mapping methodology: hydraulic tracer study

The chemical tracer used in the hydraulic study was FWT Red (Cole-Parmer, USA) which is a variant of Rhodamine WT applicable to water tracing. The dye was assumed to be conservative and non-sorbing (Hensley and Cohen, 2012) hence the transport properties μ, γ and K_d were set to zero. 120 L of a 200 ppm tracer solution was made by dissolving 2 mL of tracer in 10 L batches of water and then thoroughly mixed. The tracer solution was then heated to 55 °C and was regulated throughout the experiment using the feed tank thermostat. Once the target feed temperature had been reached, the cold water feed was switched over to the hot tracer feed using the valve configuration shown in Figure 5.5.

Temperature was logged at the wetland inlet and outlet using type K thermocouples and tracer samples were collected at the outlet in 2 minute intervals. This was done until a steady temperature was reached at the system outlet. In Table 5.3 a summary is provided of the experimental conditions as well as relevant transport properties of the two tracers used.

Table 5.3: Summary of experimental conditions and transport properties of heat and chemical tracers used in the hydraulic study

Property	**Unit**	**Value**	**Reference**
$\dot{v}$	L/min	1.68	-
τ	min	8.93	-
Target feed temperature	°C	55	-
Target feed tracer concentration	ppm	200	-
R_T	-	1.78	-
R	-	1	-
D_m	m^2/s	$2.9x10^{-10}$	Gell *et al.* (2001) and Chandler (2012)

Chemical tracer samples were analysed immediately after sample aliquot collection. A spectrophotometer (Merck Spectroquant Pharo 300) was used to measure the absorbance at a wavelength of 550 nm. Absorbance readings were related to tracer concentration using a calibration curve which had an R^2 of 0.99.

Testing of mapping methodology: optimization techniques

Curve fitting was used during two phases of the modelling exercise; to determine λ_T from the heat tracer response curve and also for removing noise from the experimental chemical tracer response curve against which the predicted response curve would be compared. In both cases the evolutionary curve fitting technique in Microsoft Excel was used which draws on a genetic algorithm (GA) to determine the unknown coefficients in the model function. A GA mimics the process of natural selection to arrive at an optimal solution to the curve fitting problem (Kuo and Lin, 2010; Roush and Branton, 2005). In this method an initial population of chromosomes representing potential solutions to the problem are generated. Processes of crossover and mutation may then be used to generate new chromosomes whose fitnesses are evaluated against the performance function given as:

$$SS_{min} = \sum_{i=1}^{n}[F(t_i) - F_{model}(t_i)]^2 \qquad \text{Equation 5.35}$$

Where F_{model} is the model function provided as Equation 5.23 when determining λ_T and Equation 5.36 for removing noise from the experimental chemical response curve:

$$F_{model} = c_4 + \frac{[c_1 - c_4]}{\left[1+\left(\frac{t_i}{c_3}\right)^{c_2}\right]} \qquad \text{Equation 5.36}$$

The least fit chromosomes are discarded and hence each successive generation contains fitter solutions to the problem. The algorithm is said to be converged when the relative difference of at least 99% of the candidate solutions is less than the specified tolerance. In Table 5.4 a summary is provided of the specified GA parameters for the two optimization problems in the study.

Table 5.4: GA parameters specified for curve fitting problems in modelling phase of hydraulic study

Parameter	**Value**
Initial population size	100
Mutation rate	0.075
Convergence	0.0001

5.6 Results and discussion

5.6.1 Non-conservative behaviour of heat tracer

In Figure 5.6 the mean feed temperature is presented together with the temperature breakthrough curve at the wetland outlet from the tracer study. There is a lag time of 8 minutes until the temperature at the outlet rises from ambient conditions. The breakthrough curve is at its steepest between 8 and 10 minutes after which the gradient decays with time and the response tends asymptotically towards the inlet temperature. The study was completed after 64 minutes due to there being no change in outlet temperature in the preceding sampling interval. The steady state outlet temperature was measured to be 53.1 °C and hence a steady state heat loss of 0.15 W was calculated. The heat lost through the side walls represents a small fraction of the amount of heat leaving the system at steady state (< 4%) and hence distortion of the heat tracer response curve is primarily dependent on retardation.

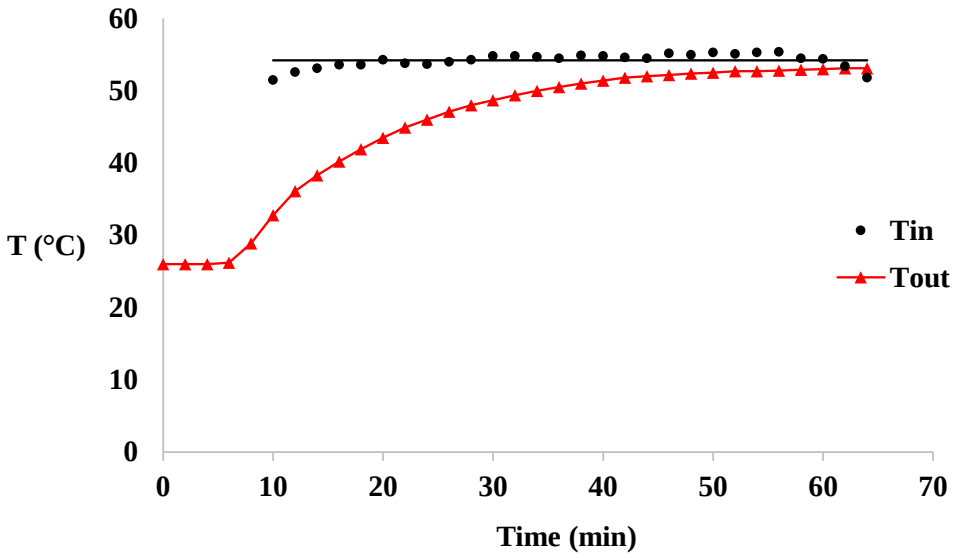

Figure 5.6: Wetland inlet and outlet temperatures as a function of time during the hydraulic tracer study

In Figure 5.7 the response curves of both the heat and chemical tracer are presented. The heat tracer response curve lags the chemical tracer response curve. This is an expected result due to the ease with which heat can be transferred from the fluid to the subsurface media when compared to

the FWT Red whose analogous transport mechanism can be considered negligible. The same result was observed by Taniguchi and Sharma (1990) who compared heat and bromide as tracers by simulating groundwater recharge in columns containing Bassendean sand and Collie loam. The temperature front velocity was shown to be consistently slower than the bromide front velocity thus highlighting the sorbing nature of heat. Constantz *et al.* (2003) note that the impact of the non-conservative behaviour of heat becomes significant in systems which are prone to developing preferential flow paths. In such systems heat absorbed into the wetland matrix and side walls skew the response curve to the right in effect hiding the early tracer breakthrough resulting from channeling effects. In Table 5.5 a comparison is made between hydraulic performance indices determined from the experimental chemical and heat response curves. The most significant difference between the hydraulic performance indices is $\bar{t}_m$ which is 1.6 times larger for the heat tracer and is attributed to its larger retardation factor when compared to the chemical tracer. From Figure 5.6, Figure 5.7 as well as from the comparison presented in Table 5.5 it is thus evident that applying Equation 5.2 – Equation 5.6 to the heat tracer response curve would result in a noticeably different hydraulic performance characterization when applied to the conservative chemical tracer response curve and hence motivates the need for a mapping methodology, such as the one described in the preceding section, if heat is to be considered as a practicable hydraulic tracer for HSSF CWs.

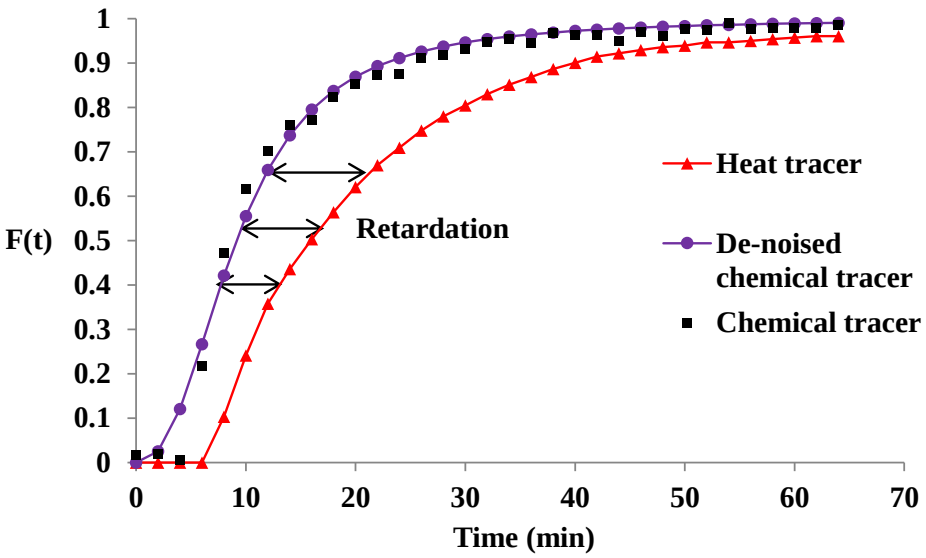

Figure 5.7: Heat and chemical tracer breakthrough curves from hydraulic tracer study

5.6.2 Predicted vs experimental chemical tracer response curves

The experimental and predicted chemical tracer response curves are presented in Figure 5.8 and the comparison of the calculated hydraulic performance indices are shown in Table 5.5. The experimental chemical response curve suggests N < 1. A value of N and Pe close to 1 indicates a high degree of back mixing (Renou *et al.*, 2003) and this was expected as a result of the convergence of flow paths at the single outlet port of the system. Effective volume utilization figures slightly higher than 100% could also be explained by the outlet port configuration employed. The back mixing experienced at the outlet would likely have caused pockets of tracer to be trapped along the edges of the system and these pockets would have a flow velocity much lower than the bulk hence skewing the first temporal moment to the right.

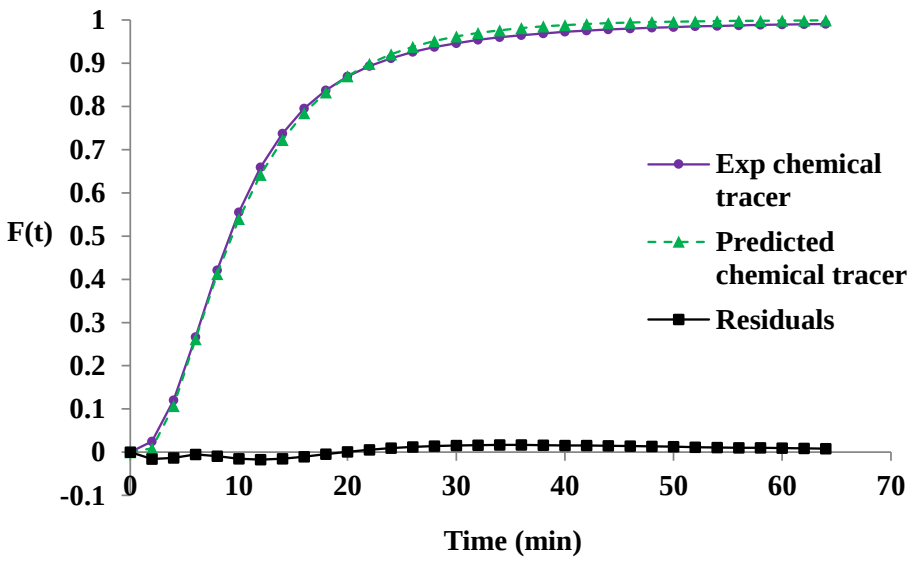

Figure 5.8: Comparison of experimental and predicted chemical tracer response curves

Table 5.5: Comparison of calculated hydraulic performance indices using experimental and predicted chemical tracer response curves

Performance index	**Unit**	**Experimental heat**	**Experimental chemical**	**Predicted chemical**
$\bar{t}_m$	min	17.50	10.64	9.99
e	-	1.96	1.19	1.12
N	-	1.42	0.96	1.45
λ_T (heat) or D (chemical)		0.035	0.037	0.035
Pe	-	3.36	3.21	3.37

There appears to be no lag between the two curves hence validating the assumption made in the development of the mapping methodology that $K_d = 0$ and hence $R = 1$. There appears to be no discernible difference in the shape of the response curves as well as a 5% and 6% relative difference in the Peclet number and calculated mean of the RTD respectively hence confirming that the magnitude of the predicted chemical dispersion coefficient from the mapping methodology was computed with a high degree of accuracy. The predicted chemical response curve reflects a

slightly higher concentration than the experimental curve from 26 minutes onwards at which point $C(t)$ has surpassed $0.9C_{inlet}$. The experimental chemical response curve does not reach a steady state value of 1 hence amplifying the difference in σ^2 between predicted and experimental responses and a smaller number of tanks in series for the experimental response. The deviation may be attributed to a possible chemical tracer sink for which the developed methodology does not account by setting $\mu = \gamma = 0$. Elevated temperature as a result of the application of the heat tracer may have enhanced the chemical tracer degradation kinetics and hence a lower steady state $F(t)$ value than under conditions between 20 and 30 °C.

5.7 Conclusion

A methodology was developed which is capable of transforming heat tracer data to conservative chemical tracer data with the intention of quantifying HSSF CW hydraulic performance using a more environmentally friendly hydraulic tracer. This was achieved by developing the heat tracer transport equation and establishing a link between the heat and chemical dispersion coefficients through the hydrodynamic dispersivity inherent to the subsurface media. The model was tested on a laboratory-scale unplanted HSSF CW by conducting a dual heat-chemical hydraulic tracer study and comparing the predicted chemical response curve, using the heat response curve as an input, against the actual experimental chemical response curve. The methodology adequately transferred the heat tracer data into the conservative chemical tracer space reflected by minimal difference in shape between predicted and actual experimental chemical response curves as well as a 5% and 6% relative difference in the Peclet number and mean of the RTD, respectively. Model validation can be extended by conducting dual tracer studies on wetlands containing different subsurface media, inlet-outlet port configurations, aspect ratios as well as on planted systems. The transport analogies developed between the heat and chemical tracer may also be applied when using other types of non-conservative hydraulic tracers which are readily available such as metal and microbial constituents found in the waste water fed to the CW so long as the retardation, degradation and production coefficients in the non-conservative transport equation can be satisfactorily determined.

6. Discussion and concluding remarks

6.1 Discussion

This chapter presents a summary of the findings in this dissertation and relates these findings to the research objectives laid out in Section 2.10.

The first primary objective of this study was to build a comprehensive comparison of the three available RTD modelling methodologies for HSSF CWs with the intent being to produce a practical guide assisting CW designers in selecting the most appropriate RTD modelling methodology for future HSSF CWs. This was achieved by generating hydraulic data using the impulse and step change response experiments from a planted and an unplanted pilot-scale HSSF CW. The comparison comprised three main discussion points:

- A comparison of the hydraulic parameters obtained using each of the three modelling approaches against each other and ideal theoretical conditions;
- Identification of the practical limitations encountered when conducting the impulse and step change tracer experiments. The limitations of the tracer studies can be considered limitations of the respective methodologies as they depend on the tracer studies for data generation; and
- A critical assessment of the mathematical techniques which the modelling methodologies employ.

It was found that each of the three modelling methodologies were capable of suggesting different hydraulic behaviour for the same system under study. For instance with the planted CW, the step change integral modelling methodology suggested a $\bar{t}_m$ 1% higher than the theoretical retention time whereas the step change derivative and impulse modelling approaches suggested a $\bar{t}_m$ smaller than the theoretical retention time with a 4% and 2% dead zone volume estimation respectively. The deviation in suggested hydraulic behaviour is significant, especially if one considers the scale of the CWs which were studied. By contrasting the result obtained from the step change integral approach with the step change derivative approach, there is a variation of 210 L of effective volume utilization and this difference is solely attributed to the mathematical techniques which each approach employs since both accept hydraulic data from the same tracer experiment (step change response experiment). The degree of dispersion also differed, with the impulse modelling approach suggesting a 30% higher Pe when compared to the step change modelling approaches. Since one

relies on RTD studies for non-ideal hydraulic behaviour characterization of HSSF CWs, there is no way of determining the true hydraulic behaviour of the system independently and evaluating the results obtained from each modelling approach against this benchmark. These results are a key finding of this study and must be borne in mind by CW designers when selecting a modelling approach. The designer should then look at the practical limitations of the tracer experiments themselves on which the modelling approaches depend as well as the mathematical techniques which each employs and these discussion points constituted the second and third elements of the comparison which was built.

Despite a well-designed sampling regime put in place for the impulse response tracer experiment, it was not possible to capture sufficient data on the peak of the concentration-time curve for the unplanted system. This affected the shape of the response curve and may have also impacted the modelling results. No such difficulties were encountered with the step change experiments. Sampling down the length of the reactor made it possible to identify another limitation of the impulse response experiment: tracer dispersion had the effect of broadening the impulse response curves to the extent that it was almost impossible to identify non-ideal hydraulic behaviour towards the end of the CWs. Although tracer dispersion also had an effect on the step change response curves, it was still possible to identify non-ideal flow behaviour which was actually prevalent in both systems. It is thought that these two findings would be particularly useful to other CW designers as the observations have been made on real-life systems as opposed to surmising this information from generic response curves which has been done in literature in the past.

A sensitivity analysis was performed to determine the effect of changing the size and hence number of subintervals used in Simpson's 1/3 rule for numerical integration on $\bar{t}_m/\tau$ for each modelling methodology. The step change derivative modelling methodology was least sensitive for both reactor systems; displaying a 1% and 4% variation in $\bar{t}_m/\tau$ for the planted and unplanted system, respectively. This was in contrast to the $\bar{t}_m/\tau$ determined by the step change integral and impulse response modelling methodologies which varied by 10% or more in some cases. It is not possible based solely on these results to develop a general rule as to which modelling methodology is least/most sensitive to subinterval size selection when performing numerical integration in the modelling process. In order to take this discussion further, the sensitivity analysis should be performed using different versions of Simpson's numerical integration techniques and also be

performed on hydraulic data sets obtained from a variety of HSSF CWs. These are considered essential tasks by the author as there does not appear to be an analytical approach explaining why a specific modelling methodology is more/less sensitive to subinterval size and selection for numerical integration. Other CW designers would thus be much more comfortable using this portion of the guide if it were based on a much more expansive data set. To add to this discussion, it was shown in this study that the step change derivative approach has a major weak point: the differentiation of F(t) to obtain E(t) amplified background noise which may have affected the calculation of the hydraulic parameters. Depending on the shape of the F(t) curve and the quantity of noise introduced during the sampling analysis procedure, the author speculates that in some instances estimated hydraulic parameters using the step change derivative approach may differ by as much as 10% when compared to the results obtained using the step change integral approach.

In addition to these findings, it is noted that the choice of modelling methodology is also dictated by other factors such as economics, logistics and environmental footprint. Despite the advantages of the step change tracer experiment discussed in part 2 of the comparison, the experiment typically requires more tracer when compared to the impulse response experiment as well as additional infrastructure such as an agitator and recirculation pump to ensure homogeneous composition of the feed hence possibly making the step change experiment more expensive and time-consuming to set up. The step change experiment exposes a higher quantity of tracer to the wetland constituents over a longer period of time when compared to the impulse response experiment. This also results in a more concentrated RTD effluent (assuming a chemical tracer is used) when compared to the impulse response experiment which would require a more stringent disposal protocol.

The second and third primary objectives of this dissertation required investigation into the use of Biomimicry as a tool in developing more sustainable hydraulic designs as well as hydraulic modelling processes of HSSF CWs.

Wetland clogging is an operational problem especially in systems servicing remote communities which do not have readily available access to other types of water treatment facilities. Once the system has become clogged to the extent that it cannot meet discharge requirements of downstream users it requires to be taken offline for an extended period of time for extensive cleaning of the

subsurface media and this could lead to an accumulation of untreated sewage and a shortage of water for revenue-generating activities such as agriculture. The second objective thus focused on how hydraulic modelling techniques, such as those used in the first primary task of this study, could be combined with Biomimicry design principles to develop an HSSF CW design which has an integrated clogging management strategy. The overall objective comprised the following two tasks:

- Identification of regions inside the CW which are most prone to clogging effects by conducting an RTD study and using the hydraulic data to develop estimates of the velocity profiles of the system; and
- Use the Biomimetic design principles of modularity and decentralization to modify the design of the CW so that it can buffer the clogging effects in the zones identified using the velocity profile estimates.

Dead zones were identified in the upper two layers along the entire length of the CW. Dead zones were also identified close to the inlet ports of the system. Low subsurface fluid velocities in these regions enhance the likelihood of sedimentation of organic constituents in the waste water which contributes towards clogging of the subsurface media pores. Almost every region contained a module which was subjected to some extent of clogging. Consequently, each region was modularized using a combination of isolation valves and bypass streams so that any region within the CW could be taken offline for gravel cleaning while still ensuring the rest of the system treats water. It is thought that such a design may be able to circumvent the operational effects caused by clogging. However it requires local community members to be trained in how to isolate a particular clogged region, how to clean it as well as how to re-install the clogged region and return the system to standard operating conditions. There is limited information available on the implementation of such modular HSSF CWs in a South African context and thus is currently an unproven technology. Further long-term testing of these designs first needs to be performed before they can be implemented on a wider scale.

The third and final objective of this dissertation focused on how improvements can be made to the hydraulic modelling process itself from an environmental perspective. In order for a tracer to represent the flow path of the fluid through the CW as accurately as possible, it is required to be non-reactive and non-sorbing to the subsurface media. However, it is these same properties of the

chemical tracer which make the RTD study effluent an environmental hazard hence requiring dedicated disposal infrastructure. Deriving inspiration from the Biomimicry design principles, it was decided to explore the use of heat as a hydraulic tracer. In this case, the CW would be able to equilibrate with ambient temperature within a short space of time after the RTD study and the effluent would thus not require specialized disposal infrastructure. The main challenge of using heat, however, is its non-conservative behaviour which causes a distortion of the response curve and an inaccurate representation of the hydraulic behaviour of the system. The task was thus split into attempting to achieve the following two objectives:

- Development of a mathematical model which maps a heat tracer response curve as an input to a response curve which would be obtained if a conservative chemical tracer were used. Hydraulic characterization would then be made possible without having to use chemicals in a tracer study; and
- Testing of the mathematical model using data obtained from a dual heat-chemical tracer study on a laboratory-scale unplanted HSSF CW.

First the differential equation describing heat tracer transport in an HSSF CW was developed and it was found to be similar in structure to the reactive chemical tracer transport equation as a result of there being a sink term in the form of heat loss to the surroundings. The methodology which was developed in this study requires fitting the solution of the heat tracer transport equation to the heat tracer response curve to determine the heat dispersion coefficient. Heat and chemical dispersion are both a function of the hydrodynamic dispersivity which is a function of the CW subsurface media and this formed the basis of the link between heat and chemical tracer transport. The chemical dispersion coefficient can then be found and used in the solution for the chemical tracer transport equation to predict the chemical tracer response curve.

Testing of the developed model and methodology consisted of comparing the predicted and actual experimental chemical tracer response curves from the tracer study performed on a laboratory-scale unplanted HSSF CW. Minimal difference in shape between the predicted and experimental response curves was observed and it was found that there was a 5% and 6% relative difference in the Peclet number and mean of the RTD, respectively. These results indicate that the methodology mapped the heat tracer response to conservative chemical tracer response with adequate accuracy. Nevertheless, the developed methodology does have its weaknesses. The developed heat tracer transport equation is one-dimensional. Further accuracy may be introduced by developing two or

three-dimensional transport equations. However based on the results obtained in this study it is believed that the development of higher order transport equations would be of diminishing benefit to the user. The model requires input of heat transport properties pertaining to the fluid, gravel matrix and layers of insulation. The user should go to great lengths in obtaining heat transport data which adequately describes the system being studied as inaccurate properties would eventually lead to an inaccurate prediction of the chemical tracer response curve and hence an inaccurate characterization of the hydraulic behaviour of the system.

6.2 Concluding remarks

It has been demonstrated in tasks two and three of this dissertation that any form of hydraulic modelling and design of HSSF CWs requires an RTD experiment which is cost-effective and easy to set up as well as an RTD modelling methodology which is reliable no matter the nature of the raw hydraulic data generated. It is thus considered imperative that the comparison built between the three available RTD modelling methodologies in task one of this thesis be developed further by generating data from more HSSF CWs.

Research task two illustrated that Biomimicry can add significant value to the research and development phase for innovative HSSF CW designs which counteract traditional operational problems such as clogging. It is recommended that the modular, decentralized design developed in this study be tested by treating various types of waste water over extended periods of time and compare the total volumetric throughput as well as effluent quality with a traditional HSSF CW design. As highlighted in Section 2.9.4, poor adaptability to changing feed conditions is another operational problem associated with HSSF CWs. It is also recommended in further work that Biomimicry be utilized to develop an HSSF CW design which improves adaptability and test this design by introducing random step changes in COD, nutrient content as well as metals content in the feed and comparing dynamic response with that obtained using traditional CW designs.

The main outcome of research task 3 was the development of a model and methodology which allow for a more environmentally friendly hydraulic tracer in the form of heat to be used in RTD studies for HSSF CWs while still being able to characterize hydraulic behaviour of the system with a similar degree of accuracy if a non-biodegradable chemical tracer were to be used. Practically speaking the experiments which were conducted could be improved by installing in-line

temperature sensors connected to data loggers placed in multiple sampling ports throughout the system as it would have made it possible to build a three-dimensional model of the heat flow inside the system. Flow rate to the system could also have been better regulated by installing a feed pump as opposed to utilizing a head tank and gate valve on the feed line. It is recommended that the model and methodology be tested further on planted as well as pilot-scale systems in order to test the effects of retention time scale up. It is also recommended that the model and methodology be tested on systems with little or no insulation as it is thought that eventually there will be a point at which heat loss to surroundings will be too rapid and important hydraulic characteristics will not be able to be transferred from the heat tracer space to the chemical tracer space. It is also realized that the methodology developed herein is applicable to non-conservative substances in general and potentially opens the opportunity to use hydraulic tracers which are readily available in the waste water feed such as metals and microbial constituents. This would represent a significant step towards achieving zero additional material and energy input for hydraulic modelling processes of HSSF CWs.

7. References

Abou-Elela, S. I., Golinielli, G., Abou-Taleb, E. M. & Hellal, M. S. 2013. Municipal wastewater treatment in horizontal and vertical flows constructed wetlands. *Ecological Engineering,* 61**,** 460-468.

Adam, K., Krogstad, T., Suliman, F. R. & Jenssen, P. D. 2005. Phosphorous sorption by Filtralite P—small scale box experiment. *Journal of Environmental Science and Health,* 40**,** 1239-1250.

Albertini, A., Reis, A., Teles, F., Souza, J., Rolim Filho, J., Freire, V., Santos, R., Martins, J., Cavada, B. & Martins, D. 2012. The new flow system approach in packed bed reactor applicable for immobilized enzyme. *Journal of Molecular Catalysis B: Enzymatic,* 79**,** 1-7.

Albuquerque, A., Oliveira, J., Semitela, S. & Amaral, L. 2009. Influence of bed media characteristics on ammonia and nitrate removal in shallow horizontal subsurface flow constructed wetlands. *Bioresource technology,* 100**,** 6269-6277.

Alcocer, D. J. R., Vallejos, G. G. & Champagne, P. 2012. Assessment of the plug flow and dead volume ratios in a sub-surface horizontal-flow packed-bed reactor as a representative model of a sub-surface horizontal constructed wetland. *Ecological Engineering,* 40**,** 18-26.

Ali, I., Asim, M. & Khan, T. A. 2012. Low cost adsorbents for the removal of organic pollutants from wastewater. *Journal of environmental management,* 113**,** 170-183.

Allende, K. L., Fletcher, T. & Sun, G. 2012. The effect of substrate media on the removal of arsenic, boron and iron from an acidic wastewater in planted column reactors. *Chemical Engineering Journal,* 179**,** 119-130.

Anibas, C., Buis, K., Verhoeven, R., Meire, P. & Batelaan, O. 2011. A simple thermal mapping method for seasonal spatial patterns of groundwater–surface water interaction. *Journal of Hydrology,* 397**,** 93-104.

Ann, Y., Reddy, K. & Delfino, J. 1999. Influence of chemical amendments on phosphorus immobilization in soils from a constructed wetland. *Ecological Engineering,* 14**,** 157-167.

Arias, C., Del Bubba, M. & Brix, H. 2001. Phosphorus removal by sands for use as media in subsurface flow constructed reed beds. *Water research,* 35**,** 1159-1168.

Asraf-Snir, M. & Gitis, V. 2011. Tracer studies with fluorescent-dyed microorganisms—A new method for determination of residence time in chlorination reactors. *Chemical engineering journal,* 166**,** 579-585.

Ávila, C., Pedescoll, A., Matamoros, V., Bayona, J. M. & García, J. 2010. Capacity of a horizontal subsurface flow constructed wetland system for the removal of emerging pollutants: an injection experiment. *Chemosphere,* 81**,** 1137-1142.

Ávila, C., Reyes, C., Bayona, J. M. & García, J. 2013. Emerging organic contaminant removal depending on primary treatment and operational strategy in horizontal subsurface flow constructed wetlands: influence of redox. *Water research,* 47**,** 315-325.

Baird, A. J., Surridge, B. W. & Money, R. P. 2004. An assessment of the piezometer method for measuring the hydraulic conductivity of a Cladium mariscus—Phragmites australis root mat in a Norfolk (UK) fen. *Hydrological Processes,* 18**,** 275-291.

Bakker, E. S., Sarneel, J. M., Gulati, R. D., Liu, Z. & van Donk, E. 2013. Restoring macrophyte diversity in shallow temperate lakes: biotic versus abiotic constraints. *Hydrobiologia,* 710**,** 23-37.

Baldantoni, D., Alfani, A., Di Tommasi, P., Bartoli, G. & De Santo, A. V. 2004. Assessment of macro and microelement accumulation capability of two aquatic plants. *Environmental Pollution,* 130**,** 149-156.

Banks, E. W., Shanafield, M. A. & Cook, P. G. 2014. Induced temperature gradients to examine groundwater flowpaths in open boreholes. *Groundwater,* 52**,** 943-951.

Bar-Cohen, Y. 2006. Biomimetics? using nature to inspire human innovation. *Bioinspiration & biomimetics,* 1**,** P1.

Barlow, S. & Schlatter, J. 2010. Risk assessment of carcinogens in food. *Toxicology and applied pharmacology,* 243**,** 180-190.

Beckwith, C. W. & Baird, A. J. 2001. Effect of biogenic gas bubbles on water flow through poorly decomposed blanket peat. *Water Resources Research,* 37**,** 551-558.

Behrends, L., Bailey, E., Jansen, P., Houke, L. & Smith, S. 2007. Integrated constructed wetland systems: design, operation, and performance of low-cost decentralized wastewater treatment systems. *Water science and technology,* 55**,** 155-162.

Benyus, J. M. 1997. *Biomimicry*, William Morrow New York.

Bequette, B. W. 2003. *Process control: modeling, design, and simulation*, Prentice Hall Professional.

Bezbaruah, A. N. & Zhang, T. C. 2005. Quantification of oxygen release by bulrush (Scirpus validus) roots in a constructed treatment wetland. *Biotechnology and bioengineering,* 89**,** 308-318.

Bodin, H., Mietto, A., Ehde, P. M., Persson, J. & Weisner, S. E. 2012. Tracer behaviour and analysis of hydraulics in experimental free water surface wetlands. *Ecological Engineering,* 49**,** 201-211.

Bodin, H., Persson, J., Englund, J.-E. & Milberg, P. 2013. Influence of residence time analyses on estimates of wetland hydraulics and pollutant removal. *Journal of Hydrology,* 501**,** 1-12.

Bonanno, G. & Giudice, R. L. 2010. Heavy metal bioaccumulation by the organs of Phragmites australis (common reed) and their potential use as contamination indicators. *Ecological indicators,* 10**,** 639-645.

Bondurant, P. C. 2010. Design standards within constructed wetlands for the reduction of mosquito populations in Clark County, Nevada.

Bons, P. D., van Milligen, B. P. & Blum, P. 2013. A general unified expression for solute and heat dispersion in homogeneous porous media. *Water Resources Research,* 49**,** 6166-6178.

Bradley, B. R., Daigger, G. T., Rubin, R. & Tchobanoglous, G. 2002. Evaluation of onsite wastewater treatment technologies using sustainable development criteria. *Clean Technologies and Environmental Policy,* 4**,** 87-99.

Brix, H. 1987. Treatment of wastewater in the rhizosphere of wetland plants-the root-zone method. *Water Science & Technology,* 19**,** 107-118.

Brix, H. 1994. Use of constructed wetlands in water pollution control: historical development, present status, and future perspectives. *Water science and technology,* 30**,** 209-224.

Brix, H. 1997. Do macrophytes play a role in constructed treatment wetlands? *Water science and technology,* 35**,** 11-17.

Brix, H. & Arias, C. A. 2005. The use of vertical flow constructed wetlands for on-site treatment of domestic wastewater: New Danish guidelines. *Ecological engineering,* 25**,** 491-500.

Brovelli, A., Carranza-Diaz, O., Rossi, L. & Barry, D. A. 2011. Design methodology accounting for the effects of porous medium heterogeneity on hydraulic residence time and

biodegradation in horizontal subsurface flow constructed wetlands. *Ecological Engineering,* 37**,** 758–770.
Burgin, A. J. & Hamilton, S. K. 2007. Have we overemphasized the role of denitrification in aquatic ecosystems? A review of nitrate removal pathways. *Frontiers in Ecology and the Environment,* 5**,** 89-96.
Cade-Menun, B. J. & Paytan, A. 2010. Nutrient temperature and light stress alter phosphorus and carbon forms in culture-grown algae. *Marine Chemistry,* 121**,** 27-36.
Camacho, J. V., Martínez, A. D. L., Gómez, R. G. & Sanz, J. M. 2007. A comparative study of five horizontal subsurface flow constructed wetlands using different plant species for domestic wastewater treatment. *Environmental technology,* 28**,** 1333-1343.
Caselles-Osorio, A., Puigagut, J., Segú, E., Vaello, N., Granés, F., García, D. & García, J. 2007. Solids accumulation in six full-scale subsurface flow constructed wetlands. *Water Research,* 41**,** 1388-1398.
Chandler, I. 2012. *Vertical variation in diffusion coefficient within sediments.* University of Warwick.
Chatterjee, S. 2014. Assessment of Nelumbo nucifera and Hydrilla verticillata in the treatment of pharmaceutical industry effluent from 24 Parganas, West Bengal. *International Journal of Science and Engineering,* 7**,** 100-105.
Chazarenc, F., Merlin, G. & Gonthier, Y. 2003. Hydrodynamics of horizontal subsurface flow constructed wetlands. *Ecological Engineering,* 21**,** 165-173.
Chen, H. 2011. Surface-flow constructed treatment wetlands for pollutant removal: applications and perspectives. *Wetlands,* 31**,** 805-814.
Choppin, G. R., Liljenzin, J.-O. & Rydberg, J. 2002. *Radiochemistry and nuclear chemistry*, Butterworth-Heinemann.
Coban, O., Kuschk, P., Kappelmeyer, U., Spott, O., Martienssen, M., Jetten, M. S. & Knoeller, K. 2015. Nitrogen transforming community in a horizontal subsurface-flow constructed wetland. *Water research,* 74**,** 203-212.
Coetzee, C., Jefthas, E. & Reinten, E. 1999. Indigenous plant genetic resources of South Africa.
Conn, R. M. & Fiedler, F. R. 2006. Increasing hydraulic residence time in constructed stormwater treatment wetlands with designed bottom topography. *Water environment research,* 78**,** 2514-2523.
Constantz, J., Cox, M. H. & Su, G. W. 2003. Comparison of heat and bromide as ground water tracers near streams. *Ground Water,* 41**,** 647-656.
Costa, E., De Lucas, A. & Garcia, P. 1986. Fluid dynamics of gas-liquid-solid fluidized beds. *Industrial & Engineering Chemistry Process Design and Development,* 25**,** 849-854.
Coulson, J. M. & Richardson, J. F. 1991. *Chemical engineering. Vol 2, Particle technology and Separation processes*, Oxford, Pergamon.
Crites, R. W. 1994. Design criteria and practice for constructed wetlands. *Water Science and Technology,* 29**,** 1-6.
Cucco, A. & Umgiesser, G. 2006. Modeling the Venice Lagoon residence time. *Ecological Modelling,* 193**,** 34-51.
Dama-Fakir, P., Toerien, A. & Janisch, C. 2012. Looking to nature for solutions on water treatment.
Davies, T. & Cottingham, P. 1993. Phosphorus removal from wastewater in a constructed wetland. *Constructed wetlands for water quality improvement,* 315**,** 320.
De Marsily, G. 1986. Quantitative hydrogeology. Paris School of Mines, Fontainebleau.

Deblonde, T., Cossu-Leguille, C. & Hartemann, P. 2011. Emerging pollutants in wastewater: a review of the literature. *International journal of hygiene and environmental health,* 214**,** 442-448.

Del Bubba, M., Arias, C. & Brix, H. 2003. Phosphorus adsorption maximum of sands for use as media in subsurface flow constructed reed beds as measured by the Langmuir isotherm. *Water Research,* 37**,** 3390-3400.

Delgado, J. 2007. Longitudinal and transverse dispersion in porous media. *Chemical Engineering Research and Design,* 85**,** 1245-1252.

Delzer, G. C. & McKenzie, S. W. 2003. Five-Day Biochemical Oxygen Demand. *USGS TWRI Book 9–A7.*

Deng, H., Ye, Z. & Wong, M. 2004. Accumulation of lead, zinc, copper and cadmium by 12 wetland plant species thriving in metal-contaminated sites in China. *Environmental Pollution,* 132**,** 29-40.

Dhote, S. & Dixit, S. 2009. Water quality improvement through macrophytes—a review. *Environmental Monitoring and Assessment,* 152**,** 149-153.

Divan, A. M., de Oliveira, P. L., Perry, C. T., Atz, V. L., Azzarini-Rostirola, L. N. & Raya-Rodriguez, M. T. 2009. Using wild plant species as indicators for the accumulation of emissions from a thermal power plant, Candiota, South Brazil. *Ecological Indicators,* 9**,** 1156-1162.

Dordio, A. V. & Carvalho, A. J. P. 2013. Organic xenobiotics removal in constructed wetlands, with emphasis on the importance of the support matrix. *Journal of Hazardous materials,* 252**,** 272-292.

Dotro, G., Griffin, P., Jefferson, B. & Butterworth, E. 2011a. Managing clogging in Severn Trent wetlands. *Constructed Wetland: Domestic, Commercial & Industrial, 14e15 July*.

Dotro, G., Larsen, D. & Palazolo, P. 2011b. Preliminary evaluation of biological and physical–chemical chromium removal mechanisms in gravel media used in constructed wetlands. *Water, Air, & Soil Pollution,* 215**,** 507-515.

Drizo, A., Frost, C., Grace, J. & Smith, K. 1999. Physico-chemical screening of phosphate-removing substrates for use in constructed wetland systems. *Water Research,* 33**,** 3595-3602.

Drizo, A., Frost, C., Smith, K. & Grace, J. 1997. Phosphate and ammonium removal by constructed wetlands with horizontal subsurface flow, using shale as a substrate. *Water Science and Technology,* 35**,** 95-102.

Drummond, J., Covino, T., Aubeneau, A., Leong, D., Patil, S., Schumer, R. & Packman, A. 2012. Effects of solute breakthrough curve tail truncation on residence time estimates: A synthesis of solute tracer injection studies. *Journal of Geophysical Research: Biogeosciences (2005–2012),* 117.

Dunne, E. J. & Reddy, K. R. 2005. Phosphorus biogeochemistry of wetlands in agricultural watersheds. *In:* Dunne, E. J., Reddy, R. & Carton, O. T. (eds.) *Nutrient management in agricultural watersheds: a wetland solution.* Wageningen, The Netherlands: Wageningen Academic Publishers.

Dupin, H. J., Kitanidis, P. K. & McCarty, P. L. 2001. Simulations of two-dimensional modeling of biomass aggregate growth in network models. *Water resources research,* 37**,** 2981-2994.

Dupin, H. J. & McCarty, P. L. 2000. Impact of colony morphologies and disinfection on biological clogging in porous media. *Environmental science & technology,* 34**,** 1513-1520.

Economopoulou, M. A. & Tsihrintzis, V. A. 2003. Design methodology and area sensitivity analysis of horizontal subsurface flow constructed wetlands. *Water resources management,* 17**,** 147-174.

Edwards, K. R., Čižková, H., Zemanová, K. & Šantrůčková, H. 2006. Plant growth and microbial processes in a constructed wetland planted with Phalaris arundinacea. *Ecological Engineering,* 27**,** 153-165.

El-Sheikh, M. A., Saleh, H. I., El-Quosy, D. E. & Mahmoud, A. A. 2010. Improving water quality in polluated drains with free water surface constructed wetlands. *Ecological Engineering,* 36**,** 1478-1484.

El-Zeiny, R. M. A. 2012. Biomimicry as a problem solving methodology in interior architecture. *Procedia-Social and Behavioral Sciences,* 50**,** 502-512.

El Hamouri, B., Nazih, J. & Lahjouj, J. 2007. Subsurface-horizontal flow constructed wetland for sewage treatment under Moroccan climate conditions. *Desalination,* 215**,** 153-158.

Engelhardt, I., Prommer, H., Moore, C., Schulz, M., Schüth, C. & Ternes, T. A. 2013. Suitability of temperature, hydraulic heads, and acesulfame to quantify wastewater-related fluxes in the hyporheic and riparian zone. *Water Resources Research,* 49**,** 426-440.

Ergun, S. 1952. Fluid flow through packed columns. *Chem. Eng. Prog.,* 48**,** 89-94.

Esser, D., Ricard, B., Fernandès, N. & Merlin, G. Physical-chemical phosphorus removal in vertical flow reed bed treatment systems. Proc. 9th IWA International Conference on Wetland Systems for Water Pollution Control, 2004. 26-30.

Fan, J., Zhang, B., Zhang, J., Ngo, H. H., Guo, W., Liu, F., Guo, Y. & Wu, H. 2013. Intermittent aeration strategy to enhance organics and nitrogen removal in subsurface flow constructed wetlands. *Bioresource technology,* 141**,** 117-122.

Faulwetter, J. L., Gagnon, V., Sundberg, C., Chazarenc, F., Burr, M. D., Brisson, J., Camper, A. K. & Stein, O. R. 2009. Microbial processes influencing performance of treatment wetlands: a review. *Ecological engineering,* 35**,** 987-1004.

Field, M. S. & Pinsky, P. F. 2000. A two-region nonequilibrium model for solute transport in solution conduits in karstic aquifers. *Journal of Contaminant Hydrology,* 44**,** 329-351.

Fleming-Singer, M. S. & Horne, A. J. 2002. Enhanced nitrate removal efficiency in wetland microcosms using an episediment layer for denitrification. *Environmental science & technology,* 36**,** 1231-1237.

Flury, M. & Wai, N. N. 2003. Dyes as tracers for vadose zone hydrology. *Reviews of Geophysics,* 41.

Fogler, H. S. 1999. *Elements of Chemical Reaction Engineering,* London, UK, Prentice Hall Inc.

Foyer, C. H., Lelandais, M. & Kunert, K. J. 1994. Photooxidative stress in plants. *Physiologia Plantarum,* 92**,** 696-717.

Freeze, R. A. & Cherry, J. 1979. Groundwater, 604 pp. Prentice-Hall, Englewood Cliffs, NJ.

Gaal, P., Thermitus, M.-A. & Stroe, D. E. 2004. Thermal conductivity measurements using the flash method. *Journal of thermal analysis and calorimetry,* 78**,** 185-189.

Galletti, A., Verlicchi, P. & Ranieri, E. 2010. Removal and accumulation of Cu, Ni and Zn in horizontal subsurface flow constructed wetlands: Contribution of vegetation and filling medium. *Science of the Total Environment,* 408**,** 5097-5105.

Galvão, A. & Matos, J. 2012. Response of horizontal sub-surface flow constructed wetlands to sudden organic load changes. *Ecological Engineering,* 49**,** 123-129.

Galvão, A. F., Matos, J. S., Ferreira, F. S. & Correia, F. N. 2010. Simulating flows in horizontal subsurface flow constructed wetlands operating in Portugal. *Ecological Engineering,* 36**,** 596-600.

García, J., Chiva, J., Aguirre, P., Alvarez, E., Sierra, J. P. & Mujeriego, R. 2004. Hydraulic behaviour of horizontal subsurface flow constructed wetlands with different aspect ratio and granular medium size. *Ecological Engineering,* 23**,** 177-187.

Garcia, J., Rousseau, D. P., Morato, J., Lesage, E., Matamoros, V. & Bayona, J. M. 2010. Contaminant removal processes in subsurface-flow constructed wetlands: a review. *Critical Reviews in Environmental Science and Technology,* 40**,** 561-661.

Gasser, G., Pankratov, I., Elhanany, S., Glazman, H. & Lev, O. 2014. Calculation of wastewater effluent leakage to pristine water sources by the weighted average of multiple tracer approach. *Water Resources Research,* 50**,** 4269-4282.

Geim, A. K., Dubonos, S., Grigorieva, I., Novoselov, K., Zhukov, A. & Shapoval, S. Y. 2003. Microfabricated adhesive mimicking gecko foot-hair. *Nature materials,* 2**,** 461-463.

Gell, C., Brockwell, D. J., Beddard, G. S., Radford, S. E., Kalverda, A. P. & Smith, D. A. 2001. Accurate use of single molecule fluorescence correlation spectroscopy to determine molecular diffusion times. *Single Molecules,* 2**,** 177-181.

Gersberg, R., Elkins, B. & Goldman, C. 1983. Nitrogen removal in artificial wetlands. *Water Research,* 17**,** 1009-1014.

Gersberg, R., Elkins, B. & Goldman, C. 1984. Use of artificial wetlands to remove nitrogen from wastewater. *Journal (Water Pollution Control Federation)***,** 152-156.

Gersberg, R., Elkins, B., Lyon, S. & Goldman, C. 1986. Role of aquatic plants in wastewater treatment by artificial wetlands. *Water Research,* 20**,** 363-368.

Gershon, N. & Nir, A. 1969. Effects of boundary conditions of models on tracer distribution in flow through porous mediums. *Water Resources Research,* 5**,** 830-839.

Ghermandi, A., Bixio, D. & Thoeye, C. 2007. The role of free water surface constructed wetlands as polishing step in municipal wastewater reclamation and reuse. *Science of the Total Environment,* 380**,** 247-258.

Giambastiani, B., Colombani, N. & Mastrocicco, M. 2013. Limitation of using heat as a groundwater tracer to define aquifer properties: experiment in a large tank model. *Environmental earth sciences,* 70**,** 719-728.

Giraldi, D., de Michieli Vitturi, M. & Iannelli, R. 2010. FITOVERT: a dynamic numerical model of subsurface vertical flow constructed wetlands. *Environmental Modelling & Software,* 25**,** 633-640.

Giraldi, D., Vitturi, M. d. M., Zaramella, M., Marion, A. & Iannelli, R. 2009. Hydrodynamics of vertical subsurface flow constructed wetlands: tracer tests with rhodamine WT and numerical modelling. *ecological engineering,* 35**,** 265-273.

Glaser, P., Chanton, J., Morin, P., Rosenberry, D., Siegel, D., Ruud, O., Chasar, L. & Reeve, A. S. 2004. Surface deformations as indicators of deep ebullition fluxes in a large northern peatland. *Global Biogeochemical Cycles,* 18.

Gopal, B. 1999. Natural and constructed wetlands for wastewater treatement: Potentials and problems. *Water Science and Technology,* 40**,** 27-35.

Gottschall, N., Boutin, C., Crolla, A., Kinsley, C. & Champagne, P. 2007. The role of plants in the removal of nutrients at a constructed wetland treating agricultural (dairy) wastewater, Ontario, Canada. *Ecological Engineering,* 29**,** 154-163.

Goulet, R. & Pick, F. 2001. Diel changes in iron concentrations in surface-flow constructed wetlands. *Water science and technology,* 44**,** 421-426.
Gschlößl, T. & Stuible, H. 2000. Reed bed systems: design, performance and maintainability. *Water science and technology,* 41**,** 73-76.
Gutowski, L., Olsson, O., Lange, J. & Kümmerer, K. 2015. Photolytic transformation products and biological stability of the hydrological tracer Uranine. *Science of The Total Environment,* 533**,** 446-453.
Haberl, R., Grego, S., Langergraber, G., Kadlec, R. H., Cicalini, A.-R., Dias, S. M., Novais, J. M., Aubert, S., Gerth, A. & Thomas, H. 2003. Constructed wetlands for the treatment of organic pollutants. *Journal of soils and sediments,* 3**,** 109-124.
Hafeznezami, S., Kim, J.-L. & Redman, J. 2012. Evaluating removal efficiency of heavy metals in constructed wetlands. *Journal of Environmental Engineering,* 138**,** 475-482.
Hamdhan, I. N. & Clarke, B. G. Determination of thermal conductivity of coarse and fine sand soils. Proceedings of World Geothermal Congress, 2010.
Hassard, F., Biddle, J., Cartmell, E., Jefferson, B., Tyrrel, S. & Stephenson, T. 2015. Rotating biological contactors for wastewater treatment–A review. *Process Safety and Environmental Protection,* 94**,** 285-306.
Hauck, R. 1984. Atmospheric Nitrogen. Chemistry, Nitrification, Denitrification, and their Interrelationships. *The Natural Environment and the Biogeochemical Cycles.* Springer.
Hausner, M. B., Kryder, L., Klenke, J., Reinke, R. & Tyler, S. W. 2015. Interpreting Variations in Groundwater Flows from Repeated Distributed Thermal Perturbation Tests. *Groundwater*.
Headley, T. & Tanner, C. 2012. Constructed wetlands with floating emergent macrophytes: an innovative stormwater treatment technology. *Critical reviews in environmental science and technology,* 42**,** 2261-2310.
Headley, T. R., Davison, L., Huett, D. O. & Müller, R. 2012. Evapotranspiration from subsurface horizontal flow wetlands planted with Phragmites australis in sub-tropical Australia. *Water research,* 46**,** 345-354.
Headley, T. R. & Kadlec, R. H. 2007. Conducting hydraulic tracer studies of constructed wetlands: a practical guide. *Ecohydrology & hydrobiology,* 7**,** 269-282.
Hecht-Méndez, J., Molina-Giraldo, N., Blum, P. & Bayer, P. 2010. Evaluating MT3DMS for heat transport simulation of closed geothermal systems. *Groundwater,* 48**,** 741-756.
Hedden, S. & Cilliers, J. 2014. Parched prospects-the emerging water crisis in South Africa.
Hedström, A. 2006. Wollastonite as reactive filter medium for sorption of wastewater ammonium and phosphorus. *Environmental technology,* 27**,** 801-809.
Heldman, D. R. & Moraru, C. I. 2003. *Encyclopedia of agricultural, food, and biological engineering,* Taylor & Francis.
Hensley, R. T. & Cohen, M. J. 2012. Controls on solute transport in large spring-fed karst rivers. *Limnology and Oceanography,* 57**,** 912-924.
Holland, J. F., Martin, J. F., Granata, T., Bouchard, V., Quigley, M. & Brown, L. 2004. Effects of wetland depth and flow rate on residence time distribution characteristics. *Ecological Engineering,* 23**,** 189-203.
Huett, D., Morris, S., Smith, G. & Hunt, N. 2005. Nitrogen and phosphorus removal from plant nursery runoff in vegetated and unvegetated subsurface flow wetlands. *Water research,* 39**,** 3259-3272.
IWA 2001. *Constructed wetlands for pollution control: processes, performance, design and operation,* Iwa Publishing.

Jackson, T. R., Haggerty, R., Apte, S. V., Coleman, A. & Drost, K. J. 2012. Defining and measuring the mean residence time of lateral surface transient storage zones in small streams. *Water Resources Research,* 48.

Jacob, D. L. & Otte, M. L. 2003. Conflicting processes in the wetland plant rhizosphere: metal retention or mobilization? *Water, Air and Soil Pollution: Focus,* 3**,** 91-104.

Jakubaszek, A. & Wojciech, M. 2014. Statistical analysis of nitrogen in the soil of constructed wetland with horizontal sub-surface flow. *Civil and Environmental Engineering Reports,* 12**,** 33-43.

Jensen, J. K. & Engesgaard, P. 2011. Nonuniform groundwater discharge across a streambed: Heat as a tracer. *Vadose Zone Journal,* 10**,** 98-109.

Jetten, M. S., Logemann, S., Muyzer, G., Robertson, L. A., de Vries, S., van Loosdrecht, M. C. & Kuenen, J. G. 1997. Novel principles in the microbial conversion of nitrogen compounds. *Antonie van Leeuwenhoek,* 71**,** 75-93.

Johansen, N., Brix, H. & Arias, C. Design and characterization of a compact constructed wetland system removing BOD, nitrogen and phosphorus from single household sewage. Arusha, Tanzania, 16-19 September 2002, 2002.

Johnson, M. 2010. A numerical scheme to calculate temperature and salinity dependent air-water transfer velocities for any gas. *Ocean Science,* 6**,** 913-932.

Johnston, C. 1993. Mechanisms of wetland-water quality interaction. *Constructed Wetlands for Water Quality Improvement. Lewis Publishers, MI***,** 293-299.

Jong, J. d. 1976. Purification of wastewater with the aid of rush or reed ponds. *Biological Control of Water Pollution. J. Tourbier & Rw Pierson, Jr., eds*.

Kadlec, R. 2009. Comparison of free water and horizontal subsurface treatment wetlands. *Ecological engineering,* 35**,** 159-174.

Kadlec, R. H., Knight, R. L., Vymazal, J., Brix, H., Cooper, P. & Haberl, R. 2000. *Constructed Wetlands for Pollution Control. Processes, Performance, Design and Operation,* Cornwall, UK, IWA Publishing.

Kadlec, R. H., Wallace, S. & Knight, R. L. 2009. *Treatment Wetlands,* Boca Raton, FL, CRC Press.

Kantawanichkul, S., Kladprasert, S. & Brix, H. 2009. Treatment of high-strength wastewater in tropical vertical flow constructed wetlands planted with Typha angustifolia and Cyperus involucratus. *Ecological engineering,* 35**,** 238-247.

Kantawanichkul, S., Pilaila, S., Tanapiyawanich, W., Tikampornpittaya, W. & Kamkrua, S. 1999. Wastewater treatment by tropical plants in vertical-flow constructed wetlands. *Water science and technology,* 40**,** 173-178.

Karathanasis, A., Potter, C. & Coyne, M. S. 2003. Vegetation effects on fecal bacteria, BOD, and suspended solid removal in constructed wetlands treating domestic wastewater. *Ecological engineering,* 20**,** 157-169.

Keefe, S. H., Barber, L. B., Runkel, R. L., Ryan, J. N., McKnight, D. M. & Wass, R. D. 2004. Conservative and reactive solute transport in constructed wetlands. *Water Resources Research,* 40.

Kellner, E., Waddington, J. & Price, J. 2005. Dynamics of biogenic gas bubbles in peat: Potential effects on water storage and peat deformation. *Water Resources Research,* 41.

Kennedy, B., Buikema, A. & James, J. K. Integrating biology, design, and engineering for sustainable innovation. Integrated STEM Education Conference (ISEC), 2015 IEEE, 2015. IEEE, 88-93.

Kenny, J., Desha, C., Kumar, A. & Hargroves, C. Using biomimicry to inform urban infrastructure design that addresses 21st Century needs. 1st International Conference on Urban Sustainability and Resilience: Conference Proceedings, 2012. UCL London.

Kim, S.-W., Miyahara, M., Fushinobu, S., Wakagi, T. & Shoun, H. 2010. Nitrous oxide emission from nitrifying activated sludge dependent on denitrification by ammonia-oxidizing bacteria. *Bioresource technology,* 101**,** 3958-3963.

Kivaisi, A. K. 2001. The potential for constructed wetlands for wastewater treatment and reuse in developing countries: a review. *Ecological engineering,* 16**,** 545-560.

Klute, A. 1986. *Methods of soil analysis. Part 1. Physical and mineralogical methods,* American Society of Agronomy, Inc.

Knowles, P., Dotro, G., Nivala, J. & García, J. 2011. Clogging in subsurface-flow treatment wetlands: occurrence and contributing factors. *Ecological Engineering,* 37**,** 99-112.

Knowles, P., Griffin, P. & Davies, P. A. 2010. Complementary methods to investigate the development of clogging within a horizontal sub-surface flow tertiary treatment wetland. *Water research,* 44**,** 320-330.

Konnerup, D., Koottatep, T. & Brix, H. 2009. Treatment of domestic wastewater in tropical, subsurface flow constructed wetlands planted with Canna and Heliconia. *Ecological engineering,* 35**,** 248-257.

Koskiaho, J. 2003. Flow velocity retardation and sediment retention in two constructed wetland–ponds. *Ecological Engineering,* 19**,** 325-337.

Kritzinger, E., Van Vuuren, R. J., Woodward, B., Rong, I., Spreeth, M. & Slabbert, M. 1997. Elimination of external and internal contaminants in rhizomes of Zantedeschia aethiopica with commercial fungicides and antibiotics. *Pathogen and Microbial Contamination Management in Micropropagation.* Springer.

Kuo, R. & Lin, L. 2010. Application of a hybrid of genetic algorithm and particle swarm optimization algorithm for order clustering. *Decision Support Systems,* 49**,** 451-462.

Lange, J., Schuetz, T., Gregoire, C., Elsässer, D., Schulz, R., Passeport, E. & Tournebize, J. 2011. Multi-tracer experiments to characterise contaminant mitigation capacities for different types of artificial wetlands. *International Journal of Environmental and Analytical Chemistry,* 91**,** 768-785.

Langergraber, G., Giraldi, D., Mena, J., Meyer, D., Peña, M., Toscano, A., Brovelli, A. & Korkusuz, E. A. 2009. Recent developments in numerical modelling of subsurface flow constructed wetlands. *Science of the total environment,* 407**,** 3931-3943.

Lappalainen, K., Gorshkova, E., Manninen, M. & Alopaeus, V. 2011. Characteristics of liquid and tracer dispersion in trickle-bed reactors: Effect on CFD modeling and experimental analyses. *Computers & chemical engineering,* 35**,** 41-49.

Lavrova, S. & Koumanova, B. 2010. Influence of recirculation in a lab-scale vertical flow constructed wetland on the treatment efficiency of landfill leachate. *Bioresource technology,* 101**,** 1756-1761.

Leaf, A. T., Hart, D. J. & Bahr, J. M. 2012. Active thermal tracer tests for improved hydrostratigraphic characterization. *Groundwater,* 50**,** 726-735.

Lee, B.-H. & Scholz, M. 2007. What is the role of Phragmites australis in experimental constructed wetland filters treating urban runoff? *Ecological Engineering,* 29**,** 87-95.

Lee, C. g., Fletcher, T. D. & Sun, G. 2009. Nitrogen removal in constructed wetland systems. *Engineering in Life Sciences,* 9**,** 11-22.

Lemke, D., Liao, Z., Wöhling, T., Osenbrück, K. & Cirpka, O. A. 2013. Concurrent conservative and reactive tracer tests in a stream undergoing hyporheic exchange. *Water Resources Research,* 49**,** 3024-3037.

Lesage, E., Rousseau, D., Meers, E., Tack, F. & De Pauw, N. 2007. Accumulation of metals in a horizontal subsurface flow constructed wetland treating domestic wastewater in Flanders, Belgium. *Science of the Total Environment,* 380**,** 102-115.

Lesley, B., Daniel, H. & Paul, Y. 2008. Iron and manganese removal in wetland treatment systems: rates, processes and implications for management. *Science of the Total Environment,* 394**,** 1-8.

Leto, C., Tuttolomondo, T., La Bella, S., Leone, R. & Licata, M. 2013. Effects of plant species in a horizontal subsurface flow constructed wetland–phytoremediation of treated urban wastewater with Cyperus alternifolius L. and Typha latifolia L. in the West of Sicily (Italy). *Ecological engineering,* 61**,** 282-291.

Levenspiel, O. 1999. Chemical reaction engineering. *Industrial & engineering chemistry research,* 38**,** 4140-4143.

Leverenz, H. L., Haunschild, K., Hopes, G., Tchobanoglous, G. & Darby, J. L. 2010. Anoxic treatment wetlands for denitrification. *Ecological Engineering,* 36**,** 1544-1551.

Li, Y., Zhu, G., Ng, W. J. & Tan, S. K. 2014. A review on removing pharmaceutical contaminants from wastewater by constructed wetlands: design, performance and mechanism. *Science of the Total Environment,* 468**,** 908-932.

Li, Y. H., Zhu, J. N., Liu, Q. F., Liu, Y., Liu, M., Liu, L. & Zhang, Q. 2013. Comparison of the diversity of root-associated bacteria in Phragmites australis and Typha angustifolia L. in artificial wetlands. *World Journal of Microbiology and Biotechnology,* 29**,** 1499-1508.

Ligi, T., Oopkaup, K., Truu, M., Preem, J.-K., Nõlvak, H., Mitsch, W. J., Mander, Ü. & Truu, J. 2014. Characterization of bacterial communities in soil and sediment of a created riverine wetland complex using high-throughput 16S rRNA amplicon sequencing. *Ecological Engineering,* 72**,** 56-66.

Lim, P., Tay, M., Mak, K. & Mohamed, N. 2003. The effect of heavy metals on nitrogen and oxygen demand removal in constructed wetlands. *Science of the total environment,* 301**,** 13-21.

Lim, P., Wong, T. & Lim, D. 2001. Oxygen demand, nitrogen and copper removal by free-water-surface and subsurface-flow constructed wetlands under tropical conditions. *Environment International,* 26**,** 425-431.

Lima, D. M. F. & Zaiat, M. 2012. The influence of the degree of back-mixing on hydrogen production in an anaerobic fixed-bed reactor. *International journal of hydrogen energy,* 37**,** 9630-9635.

Lindstrom, F. T., Haque, R., Freed, V. H. & Boersma, L. 1967. The movement of some herbicides in soils. Linear diffusion and convection of chemicals in soils. *Environmental science & technology,* 1**,** 561-565.

Liolios, K. A., Moutsopoulos, K. N. & Tsihrintzis, V. A. 2012. Modeling of flow and BOD fate in horizontal subsurface flow constructed wetlands. *Chemical engineering journal,* 200**,** 681-693.

Lockhart, A. M. 1999. *A comparison of constructed wetlands used to treat domestic wastes: Conventional, drawdown, and aerated systems*, University of Iowa.

Lüderitz, V. & Gerlach, F. 2002. Phosphorus removal in different constructed wetlands. *Acta biotechnologica,* 22**,** 91-99.

Machemer, S. D. & Wildeman, T. R. 1992. Adsorption compared with sulfide precipitation as metal removal processes from acid mine drainage in a constructed wetland. *Journal of contaminant Hydrology,* 9**,** 115-131.

Madigan, M. T., Martinko, J. M. & Brock, T. D. 2009. *Brock Mikrobiologie,* Pearson Deutschland GmbH.

Mahdavi, A., Ferreira, L., Sundback, C., Nichol, J. W., Chan, E. P., Carter, D. J., Bettinger, C. J., Patanavanich, S., Chignozha, L. & Ben-Joseph, E. 2008. A biodegradable and biocompatible gecko-inspired tissue adhesive. *Proceedings of the National Academy of Sciences,* 105**,** 2307-2312.

Maillard, E., Payraudeau, S., Faivre, E., Grégoire, C., Gangloff, S. & Imfeld, G. 2011. Removal of pesticide mixtures in a stormwater wetland collecting runoff from a vineyard catchment. *Science of the Total Environment,* 409**,** 2317-2324.

Majuru, B., Jagals, P. & Hunter, P. R. 2012. Assessing rural small community water supply in Limpopo, South Africa: water service benchmarks and reliability. *Science of the Total Environment,* 435**,** 479-486.

Malaguerra, F., Albrechtsen, H.-J. & Binning, P. J. 2013. Assessment of the contamination of drinking water supply wells by pesticides from surface water resources using a finite element reactive transport model and global sensitivity analysis techniques. *Journal of hydrology,* 476**,** 321-331.

Maltais-Landry, G., Maranger, R., Brisson, J. & Chazarenc, F. 2009. Nitrogen transformations and retention in planted and artificially aerated constructed wetlands. *Water Research,* 43**,** 535-545.

Mander, Ü., Maddison, M., Soosaar, K. & Karabelnik, K. 2011. The impact of pulsing hydrology and fluctuating water table on greenhouse gas emissions from constructed wetlands. *Wetlands,* 31**,** 1023-1032.

Mander, Ü., Teiter, S., Kuusemets, V., Lohmus, K., Öövel, M., Nurk, K. & Augustin, J. 2003. Nitrogen and phosphorus budgets in a subsurface flow wastewater treatment wetland. *Computational Mechanics Inc, 2003.***,** 135-148.

Mantovi, P., Marmiroli, M., Maestri, E., Tagliavini, S., Piccinini, S. & Marmiroli, N. 2003. Application of a horizontal subsurface flow constructed wetland on treatment of dairy parlor wastewater. *Bioresource Technology,* 88**,** 85-94.

Marchand, L., Mench, M., Jacob, D. & Otte, M. 2010. Metal and metalloid removal in constructed wetlands, with emphasis on the importance of plants and standardized measurements: a review. *Environmental pollution,* 158**,** 3447-3461.

Marsili-Libelli, S. & Checchi, N. 2005. Identification of dynamic models for horizontal subsurface constructed wetlands. *Ecological Modelling,* 187**,** 201-218.

Masi, F., Conte, G., Martinuzzi, N. & Pucci, B. Winery high organic content wastewaters treated by constructed wetlands in Mediterranean climate. Proceedings of the 8th International Conference on Wetland Systems for Water Pollution Control, 2002. 274-282.

Masters, G. M. & Ela, W. P. 2008. *Introduction to Environmental Engineering and Science,* Upper Saddle River, NJ, Pearson Education.

Matagi, S., Swai, D. & Mugabe, R. 1998. A review of heavy metal removal mechanisms in wetlands. *Afr. J. Trop. Hydrobiol. Fish.,* 8**,** 13-25.

Matamoros, V., Arias, C., Brix, H. & Bayona, J. M. 2007. Removal of pharmaceuticals and personal care products (PPCPs) from urban wastewater in a pilot vertical flow constructed wetland and a sand filter. *Environmental science & technology,* 41**,** 8171-8177.

Matamoros, V. & Bayona, J. M. 2006. Elimination of pharmaceuticals and personal care products in subsurface flow constructed wetlands. *Environmental science & technology,* 40**,** 5811-5816.

Mateus, D. M., Vaz, M. M. & Pinho, H. J. 2012. Fragmented limestone wastes as a constructed wetland substrate for phosphorus removal. *Ecological Engineering,* 41**,** 65-69.

Mayo, A. W. 2014. Modelling dynamics of organic carbon in water hyacinth Eichhornia Crassipes (Mart.) Solms artificial wetlands. *International Journal of Water Resources and Environmental Engineering,* 6**,** 121-130.

McIntyre, B. D. & Riha, S. J. 1991. Hydraulic conductivity and nitrogen removal in an artificial wetland system. *Journal of environmental quality,* 20**,** 259-263.

Megonikal, J. P., Hines, M. E. & Visscher, P. T. 2004. Anaerobic metabolism: linkage to trace gases and aerobic processes. *In:* Schlesinger, W. H. (ed.) *Biogeochemistry*. Oxford, U.K: Elsevier-Pergamon.

Mendoza, J., Granados, M., De Godos, I., Acién, F., Molina, E., Banks, C. & Heaven, S. 2013. Fluid-dynamic characterization of real-scale raceway reactors for microalgae production. *Biomass and Bioenergy,* 54**,** 267-275.

Miller, P. A. & Clesceri, N. L. 2002. *Waste sites as biological reactors: characterization and modeling*, CRC Press.

Min, J. H. & Wise, W. R. 2009. Simulating short-circuiting flow in a constructed wetland: the implications of bathymetry and vegetation effects. *Hydrological Processes,* 23**,** 830-841.

Mitsch, W. J. & Gosselink, J. G. 1993. *Wetlands,* New York, Van Nostrand Reinhold.

Mohanty, M. & Patra, H. K. 2011. Attenuation of chromium toxicity by bioremediation technology. *Reviews of Environmental Contamination and Toxicology Volume 210.* Springer.

Mohapatra, R. C., Mishra, A. & Choudhury, B. B. 2014. Measurement on Thermal Conductivity of Pine Wood Dust Filled Epoxy Composites. *American Journal of Mechanical Engineering,* 2**,** 114-119.

Molle, P., Prost-Boucle, S. & Lienard, A. 2008. Potential for total nitrogen removal by combining vertical flow and horizontal flow constructed wetlands: a full-scale experiment study. *Ecological engineering,* 34**,** 23-29.

Mufarrege, M., Hadad, H. & Maine, M. 2010. Response of Pistia stratiotes to heavy metals (Cr, Ni, and Zn) and phosphorous. *Archives of environmental contamination and toxicology,* 58**,** 53-61.

Mulder, A., Graaf, A., Robertson, L. & Kuenen, J. 1995. Anaerobic ammonium oxidation discovered in a denitrifying fluidized bed reactor. *FEMS microbiology ecology,* 16**,** 177-184.

Nahlik, A. M. & Mitsch, W. J. 2006. Tropical treatment wetlands dominated by free-floating macrophytes for water quality improvement in Costa Rica. *Ecological Engineering,* 28**,** 246-257.

Nelson, P. O., Chung, A. K. & Hudson, M. C. 1981. Factors affecting the fate of heavy metals in the activated sludge process. *Journal (Water Pollution Control Federation)***,** 1323-1333.

Nguyen, C. 2003. Rhizodeposition of organic C by plants: mechanisms and controls. *Agronomie,* 23**,** 375-396.

Nguyen, L. M. 2000. Organic matter composition, microbial biomass and microbial activity in gravel-bed constructed wetlands treating farm dairy wastewaters. *Ecological Engineering,* 16**,** 199-221.

Nivala, J., Hoos, M., Cross, C., Wallace, S. & Parkin, G. 2007. Treatment of landfill leachate using an aerated, horizontal subsurface-flow constructed wetland. *Science of the Total Environment,* 380**,** 19-27.

Nivala, J., Knowles, P., Dotro, G., García, J. & Wallace, S. 2012. Clogging in subsurface-flow treatment wetlands: measurement, modeling and management. *Water research,* 46**,** 1625-1640.

Nivala, J. & Rousseau, D. P. 2009. Reversing clogging in subsurface-flow constructed wetlands by hydrogen peroxide treatment: two case studies. *Water Science & Technology,* 59.

Noorvee, A., Põldvere, E. & Mander, Ü. 2007. The effect of pre-aeration on the purification processes in the long-term performance of a horizontal subsurface flow constructed wetland. *Science of the Total Environment,* 380**,** 229-236.

Ochieng, G. M., Seanego, E. S. & Nkwonta, O. I. 2010. Impacts of mining on water resources in South Africa: A review. *Scientific Research and Essays,* 5**,** 3351-3357.

Ochoa-Hueso, R., Allen, E. B., Branquinho, C., Cruz, C., Dias, T., Fenn, M. E., Manrique, E., Pérez-Corona, M. E., Sheppard, L. J. & Stock, W. D. 2011. Nitrogen deposition effects on Mediterranean-type ecosystems: an ecological assessment. *Environmental Pollution,* 159**,** 2265-2279.

Ong, S.-A., Uchiyama, K., Inadama, D., Ishida, Y. & Yamagiwa, K. 2010. Performance evaluation of laboratory scale up-flow constructed wetlands with different designs and emergent plants. *Bioresource technology,* 101**,** 7239-7244.

Paing, J. & Voisin, J. 2005. Vertical flow constructed wetlands for municipal wastewater and septage treatment in French rural area. *Water Science & Technology,* 51**,** 145-155.

Palmer-Felgate, E. J., Mortimer, R. J., Krom, M. D. & Jarvie, H. P. 2010. Impact of point-source pollution on phosphorus and nitrogen cycling in stream-bed sediments. *Environmental science & technology,* 44**,** 908-914.

Park, W. 2009. Integrated constructed wetland systems employing alum sludge and oyster shells as filter media for P removal. *Ecological Engineering,* 35**,** 1275-1282.

Passeport, E., Tournebize, J., Jankowfsky, S., Prömse, B., Chaumont, C., Coquet, Y. & Lange, J. 2010. Artificial wetland and forest buffer zone: hydraulic and tracer characterization. *Vadose Zone Journal,* 9**,** 73-84.

Patten, B. C. 1990. *Wetlands and shallow continental waterbodies: Volume I. Natural and human relationships,* SPB Academic Publishing.

Paul, E. & Clark, F. 1996. Ammonification and nitrification. *Soil microbiology and biochemistry. Academic, San Diego***,** 182-183.

Pedescoll, A., Corzo, A., Alvarez, E., García, J. & Puigagut, J. 2011. The effect of primary treatment and flow regime on clogging development in horizontal subsurface flow constructed wetlands: an experimental evaluation. *Water research,* 45**,** 3579-3589.

Pedescoll, A., Sidrach-Cardona, R., Hijosa-Valsero, M. & Bécares, E. 2015. Design parameters affecting metals removal in horizontal constructed wetlands for domestic wastewater treatment. *Ecological Engineering,* 80**,** 92-99.

Pedescoll, A., Sidrach-Cardona, R., Sánchez, J., Carretero, J., Garfi, M. & Bécares, E. 2013. Design configurations affecting flow pattern and solids accumulation in horizontal free water and subsurface flow constructed wetlands. *Water research,* 47**,** 1448-1458.

Persson, J. 2000. The hydraulic performance of ponds of various layouts. *Urban Water,* 2**,** 243-250.

Persson, J., Somes, N. & Wong, T. 1999. Hydraulics efficiency of constructed wetlands and ponds. *Water science and technology,* 40**,** 291-300.

Peters, G. P. & Smith, D. W. 2001. Numerical study of boundary conditions for solute transport through a porous medium. *International journal for numerical and analytical methods in geomechanics,* 25**,** 629-650.

Poach, M., Hunt, P., Sadler, E., Matheny, T., Johnson, M., Stone, K., Humenik, F. & Rice, J. 2002. Ammonia volatilization from constructed wetlands that treat swine wastewater. *Transactions of the ASAE,* 45**,** 619.

Pozrikidis, C. 1998. *Numerical computation in science and engineering*, Oxford university press New York.

Prochaska, C. & Zouboulis, A. 2006. Removal of phosphates by pilot vertical-flow constructed wetlands using a mixture of sand and dolomite as substrate. *Ecological Engineering,* 26**,** 293-303.

Ramires, M. L., de Castro, C. A. N., Nagasaka, Y., Nagashima, A., Assael, M. J. & Wakeham, W. A. 1995. Standard reference data for the thermal conductivity of water. *Journal of Physical and Chemical Reference Data,* 24**,** 1377-1381.

Ranieri, E., Gorgoglione, A. & Solimeno, A. 2013. A comparison between model and experimental hydraulic performances in a pilot-scale horizontal subsurface flow constructed wetland. *Ecological Engineering,* 60**,** 45-49.

Rau, G. C., Andersen, M. S. & Acworth, R. I. 2012. Experimental investigation of the thermal dispersivity term and its significance in the heat transport equation for flow in sediments. *Water Resources Research,* 48.

Rau, G. C., Andersen, M. S., McCallum, A. M., Roshan, H. & Acworth, R. I. 2014. Heat as a tracer to quantify water flow in near-surface sediments. *Earth-Science Reviews,* 129**,** 40-58.

Rauch-Williams, T., Hoppe-Jones, C. & Drewes, J. 2010. The role of organic matter in the removal of emerging trace organic chemicals during managed aquifer recharge. *Water research,* 44**,** 449-460.

Reddy, K. & D'angelo, E. 1997. Biogeochemical indicators to evaluate pollutant removal efficiency in constructed wetlands. *Water Science and Technology,* 35**,** 1-10.

Reddy, K., Kadlec, R., Flaig, E. & Gale, P. 1999. Phosphorus retention in streams and wetlands: a review. *Critical reviews in environmental science and technology,* 29**,** 83-146.

Reddy, K., Patrick, W. & Broadbent, F. 1984. Nitrogen transformations and loss in flooded soils and sediments. *Critical Reviews in Environmental Science and Technology,* 13**,** 273-309.

Reddy, L. D., Kumar, D. & Asolekar, S. R. 2014. Typologies for Successful Operation and Maintenance of Horizontal Sub-Surface Flow Constructed Wetlands. *International Journal of Engineering Research***,** 2347-5013.

Reed, S. C., Crites, R. W. & Middlebrooks, E. J. 1995. *Natural systems for waste management and treatment,* McGraw-Hill, Inc.

Reinten, E., Coetzee, J. & Van Wyk, B.-E. 2011. The potential of South African indigenous plants for the international cut flower trade. *South African Journal of Botany,* 77**,** 934-946.

Renou, S., Perrier, M., Dochain, D. & Gendron, S. 2003. Solution of the convection–dispersion–reaction equation by a sequencing method. *Computers & chemical engineering,* 27**,** 615-629.

Rezanezhad, F., Price, J. S. & Craig, J. R. 2012. The effects of dual porosity on transport and retardation in peat: A laboratory experiment. *Canadian Journal of Soil Science,* 92**,** 723-732.

Riefler, R. G., Krohn, J., Stuart, B. & Socotch, C. 2008. Role of sulfur-reducing bacteria in a wetland system treating acid mine drainage. *Science of the total environment,* 394**,** 222-229.

Ríos, D. A., Vélez, A. T., Peña, M. & Parra, C. M. 2009. Changes of flow patterns in a horizontal subsurface flow constructed wetland treating domestic wastewater in tropical regions. *Ecological Engineering,* 35**,** 274-280.

Rosal, R., Rodríguez, A., Perdigón-Melón, J. A., Petre, A., García-Calvo, E., Gómez, M. J., Agüera, A. & Fernández-Alba, A. R. 2010. Occurrence of emerging pollutants in urban wastewater and their removal through biological treatment followed by ozonation. *Water Research,* 44**,** 578-588.

Rose, A. H. 1976. *Chemical microbiology,* New York, Plenum Press.

Rosiek, S. & Batlles, F. 2009. Integration of the solar thermal energy in the construction: Analysis of the solar-assisted air-conditioning system installed in CIESOL building. *Renewable Energy,* 34**,** 1423-1431.

Roush, W. & Branton, S. 2005. A comparison of fitting growth models with a genetic algorithm and nonlinear regression. *Poultry science,* 84**,** 494-502.

Rousseau, D., Santa, S., Mander, Ü., Koiv, M. & Vohla, C. Quantification of oxygene transfer pathways in horizontal subsurface-flow constructed wetlands. Proceedings of the Second International Symposium on Wetland Pollutant Dynamic and Control, 2007. 260-262.

Rousseau, D. P., Vanrolleghem, P. A. & De Pauw, N. 2004. Model-based design of horizontal subsurface flow constructed treatment wetlands: a review. *Water Research,* 38**,** 1484-1493.

Rubin, F., Palmer, A. & Tyson, C. 2001. Patterns of endemism within the Karoo National Park, South Africa. *Bothalia,* 31**,** 117-133.

Rubin, S. 2012. *Anomalous, non-conservative chemical transport in saturated porous media.* Weizmann Institute of Science.

Rüdisüli, M., Schildhauer, T. J., Biollaz, S. M. & van Ommen, J. R. 2012. Scale-up of bubbling fluidized bed reactors—a review. *Powder Technology,* 217**,** 21-38.

Sabatini, D. A. 2000. Sorption and intraparticle diffusion of fluorescent dyes with consolidated aquifer media. *Ground Water,* 38**,** 651-656.

Saeed, T., Afrin, R., Al Muyeed, A. & Sun, G. 2012. Treatment of tannery wastewater in a pilot-scale hybrid constructed wetland system in Bangladesh. *Chemosphere,* 88**,** 1065-1073.

Saeed, T. & Sun, G. 2012. A review on nitrogen and organics removal mechanisms in subsurface flow constructed wetlands: Dependency on environmental parameters, operating conditions and supporting media. *Journal of environmental management,* 112**,** 429-448.

Salt, D. E., Blaylock, M., Kumar, N. P., Dushenkov, V., Ensley, B. D., Chet, I. & Raskin, I. 1995. Phytoremediation: a novel strategy for the removal of toxic metals from the environment using plants. *Nature biotechnology,* 13**,** 468-474.

Savant, N. & De Datta, S. 1982. Nitrogen transformations in wetland rice soils [Includes fertilizer aspects]. *Advances in Agronomy*.

Schiegl, S., Stockhammer, P., Scott, C. & Wadley, L. 2004. A mineralogical and phytolith study of the Middle Stone Age hearths in Sibudu Cave, KwaZulu-Natal, South Africa: Sibudu Cave. *South African Journal of Science,* 100**,** p. 185-194.

Scholz, M. 2011. Wetland Systems. Springer-Verlag, London.

Scholz, M. & Hedmark, Å. 2010. Constructed wetlands treating runoff contaminated with nutrients. *Water, Air, and Soil Pollution,* 205**,** 323-332.

Scholz, M. & Lee, B. h. 2005. Constructed wetlands: a review. *International journal of environmental studies,* 62**,** 421-447.

Schuetz, T., Weiler, M., Lange, J. & Stoelzle, M. 2012. Two-dimensional assessment of solute transport in shallow waters with thermal imaging and heated water. *Advances in Water Resources,* 43**,** 67-75.

Seeger, E. M., Maier, U., Grathwohl, P., Kuschk, P. & Kaestner, M. 2013. Performance evaluation of different horizontal subsurface flow wetland types by characterization of flow behavior, mass removal and depth-dependent contaminant load. *Water research,* 47**,** 769-780.

Seidel, K. 1964. Abbau von bacterium coli durch hohere wasserpflanzen. *Naturwissenschaften,* 51**,** 395.

Seidel, K. 1966. Reinigung von Gewassern durch hohere Pflanzen. *Naturwissenschaften,* 53**,** 289-297.

Seo, D. C., Yu, K. & DeLaune, R. D. 2008. Comparison of monometal and multimetal adsorption in Mississippi River alluvial wetland sediment: batch and column experiments. *Chemosphere,* 73**,** 1757-1764.

Shenker, M., Seitelbach, S., Brand, S., Haim, A. & Litaor, M. 2005. Redox reactions and phosphorus release in re-flooded soils of an altered wetland. *European Journal of Soil Science,* 56**,** 515-525.

Sheoran, A. & Sheoran, V. 2006. Heavy metal removal mechanism of acid mine drainage in wetlands: a critical review. *Minerals engineering,* 19**,** 105-116.

Sheridan, C., Glasser, D. & Hildebrandt, D. A calculation of the hydraulic properties of a vegetated gravel bed filter using an impulse-response tracer experiment to quantify non-ideal behaviour. Proceedings of the 12th International Conference on Environmental Science and Technology. Global Network on Environmental Science and Technology, Rhodes, Greece, 2011. 1711-1716.

Sheridan, C., Harding, K., Koller, E. & De Pretto, A. 2013. A comparison of charcoal-and slag-based constructed wetlands for acid mine drainage remediation. *Water SA,* 39**,** 369-374.

Sheridan, C., Hildebrand, D. & Glasser, D. 2014a. Turning wine (waste) into water: Toward technological advances in the use of constructed wetlands for winery effluent treatment. *AIChE Journal,* 60**,** 420-431.

Sheridan, C. M., Glasser, D. & Hildebrandt, D. 2014b. Estimating rate constants of contaminant removal in constructed wetlands treating winery effluent: A comparison of three different methods. *Process Safety and Environmental Protection,* 92**,** 903-916.

Shook, G. M. 2001. Predicting thermal breakthrough in heterogeneous media from tracer tests. *Geothermics,* 30**,** 573-589.

Siedlecka, A., Tukendorf, A., Skórzynska-Polit, E., Maksymiec, W., Wójcik, M., Baszynski, T. & Krupa, Z. 2001. Angiosperms (Asteraceae, Convolvulaceae, Fabaceae and Poaceae; other than Brassicaceae). *Metals in the Environment. Analysis by Biodiversity. Marcel Dekker, Inc., New York***,** 171-217.

Šimůnek, J., Jarvis, N. J., Van Genuchten, M. T. & Gärdenäs, A. 2003. Review and comparison of models for describing non-equilibrium and preferential flow and transport in the vadose zone. *Journal of Hydrology,* 272**,** 14-35.

Sliekers, A. O., Derwort, N., Gomez, J. C., Strous, M., Kuenen, J. & Jetten, M. 2002. Completely autotrophic nitrogen removal over nitrite in one single reactor. *Water Research,* 36**,** 2475-2482.

Smart, P. & Laidlaw, I. 1977. An evaluation of some fluorescent dyes for water tracing. *Water Resources Research,* 13**,** 15-33.

Soda, S., Hamada, T., Yamaoka, Y., Ike, M., Nakazato, H., Saeki, Y., Kasamatsu, T. & Sakurai, Y. 2012. Constructed wetlands for advanced treatment of wastewater with a complex matrix from a metal-processing plant: bioconcentration and translocation factors of various metals in Acorus gramineus and Cyperus alternifolius. *Ecological Engineering,* 39**,** 63-70.

Stehle, S., Elsaesser, D., Gregoire, C., Imfeld, G., Niehaus, E., Passeport, E., Payraudeau, S., Schäfer, R. B., Tournebize, J. & Schulz, R. 2011. Pesticide risk mitigation by vegetated treatment systems: a meta-analysis. *Journal of Environmental Quality,* 40**,** 1068-1080.

Stein, O. R., Borden-Stewart, D. J., Hook, P. B. & Jones, W. L. 2007. Seasonal influence on sulfate reduction and zinc sequestration in subsurface treatment wetlands. *Water research,* 41**,** 3440-3448.

Stottmeister, U., Wießner, A., Kuschk, P., Kappelmeyer, U., Kästner, M., Bederski, O., Müller, R. & Moormann, H. 2003. Effects of plants and microorganisms in constructed wetlands for wastewater treatment. *Biotechnology advances,* 22**,** 93-117.

Stumm, W. & Morgan, J. J. 1981. *Aquatic chemistry: an introduction emphasizing chemical equilibria in natural waters*, John Wiley.

Su, T.-M., Yang, S.-C., Shih, S.-S. & Lee, H.-Y. 2009. Optimal design for hydraulic efficiency performance of free-water-surface constructed wetlands. *Ecological Engineering,* 35**,** 1200-1207.

Subramanian, R. S. 2004. Flow through packed beds and fluidized beds. *Clarkson University*.

Suliman, F., French, H., Haugen, L. & Søvik, A. 2006a. Change in flow and transport patterns in horizontal subsurface flow constructed wetlands as a result of biological growth. *Ecological Engineering,* 27**,** 124-133.

Suliman, F., Futsaether, C. & Oxaal, U. 2007. Hydraulic performance of horizontal subsurface flow constructed wetlands for different strategies of filling the filter medium into the filter basin. *ecological engineering,* 29**,** 45-55.

Suliman, F., Futsaether, C., Oxaal, U., Haugen, L. & Jenssen, P. 2006b. Effect of the inlet–outlet positions on the hydraulic performance of horizontal subsurface-flow wetlands constructed with heterogeneous porous media. *Journal of contaminant hydrology,* 87**,** 22-36.

Sundareshwar, P., Morris, J., Koepfler, E. & Fornwalt, B. 2003. Phosphorus limitation of coastal ecosystem processes. *Science,* 299**,** 563-565.

Taniguchi, M. & Sharma, M. 1990. Solute and heat transport experiments for estimating recharge rate. *Journal of Hydrology,* 119**,** 57-69.

Tanner, C. 2001. Plants as ecosystem engineers in subsurface-flow treatment wetlands. *Water Science and Technology,* 44**,** 9-17.

Tanner, C. C. 1994. Growth and nutrition of Schoenoplectus validus in agricultural wastewaters. *Aquatic botany,* 47**,** 131-153.

Tanner, C. C. 1996. Plants for constructed wetland treatment systems—a comparison of the growth and nutrient uptake of eight emergent species. *Ecological engineering,* 7**,** 59-83.

Tanner, C. C., Kadlec, R. H., Gibbs, M. M., Sukias, J. P. & Nguyen, M. L. 2002. Nitrogen processing gradients in subsurface-flow treatment wetlands—influence of wastewater characteristics. *Ecological Engineering,* 18**,** 499-520.

Tanner, C. C., Sukias, J. P., Headley, T. R., Yates, C. R. & Stott, R. 2012. Constructed wetlands and denitrifying bioreactors for on-site and decentralised wastewater treatment: comparison of five alternative configurations. *Ecological Engineering,* 42**,** 112-123.

Tanner, C. C., Sukias, J. P. & Upsdell, M. P. 1998. Organic matter accumulation during maturation of gravel-bed constructed wetlands treating farm dairy wastewaters. *Water Research,* 32**,** 3046-3054.

Taylor, G. D., Fletcher, T. D., Wong, T. H., Breen, P. F. & Duncan, H. P. 2005. Nitrogen composition in urban runoff—implications for stormwater management. *Water Research,* 39**,** 1982-1989.

Tchobanoglous, G. & Burton, F. L. 1991. Wastewater engineering. *Management,* 7**,** 1-4.

Teefy, S. 1996. *Tracer studies in water treatment facilities: a protocol and case studies*, American Water Works Association.

Thackston, E. L., Shields Jr, F. D. & Schroeder, P. R. 1987. Residence time distributions of shallow basins. *Journal of Environmental Engineering,* 113**,** 1319-1332.

Tibane, E. & Vermeulen, A. 2013. Water Affairs. *South Africa Yearbook 2013/2014.* Department of Government Communication and Information System.

Trang, N. T. D., Konnerup, D., Schierup, H.-H., Chiem, N. H. & Brix, H. 2010. Kinetics of pollutant removal from domestic wastewater in a tropical horizontal subsurface flow constructed wetland system: effects of hydraulic loading rate. *Ecological engineering,* 36**,** 527-535.

Van de Graaf, A. A., Mulder, A., de Bruijn, P., Jetten, M., Robertson, L. A. & Kuenen, J. G. 1995. Anaerobic oxidation of ammonium is a biologically mediated process. *Applied and environmental microbiology,* 61**,** 1246-1251.

Van de Moortel, A. M., Meers, E., De Pauw, N. & Tack, F. M. 2010. Effects of vegetation, season and temperature on the removal of pollutants in experimental floating treatment wetlands. *Water, Air, & Soil Pollution,* 212**,** 281-297.

Van Genuchten, M. T. 1981. Analytical solutions for chemical transport with simultaneous adsorption, zero-order production and first-order decay. *Journal of Hydrology,* 49**,** 213-233.

Van Krevelen, D. W. & Te Nijenhuis, K. 2009. *Properties of polymers: their correlation with chemical structure; their numerical estimation and prediction from additive group contributions*, Elsevier.

Van Vuuren, L. 2014. Biomimicry: exploring nature's genius for a better tomorrow. *Water Wheel,* 13**,** 12-15.

Verberk, W. C., Bilton, D. T., Calosi, P. & Spicer, J. I. 2011. Oxygen supply in aquatic ectotherms: partial pressure and solubility together explain biodiversity and size patterns. *Ecology,* 92**,** 1565-1572.

Vilks, P. & Baik, M.-H. 2001. Laboratory migration experiments with radionuclides and natural colloids in a granite fracture. *Journal of contaminant hydrology,* 47**,** 197-210.

Vitousek, P. M., Aber, J. D., Howarth, R. W., Likens, G. E., Matson, P. A., Schindler, D. W., Schlesinger, W. H. & Tilman, D. G. 1997. Human alteration of the global nitrogen cycle: sources and consequences. *Ecological applications,* 7**,** 737-750.

Vohla, C., Alas, R., Nurk, K., Baatz, S. & Mander, Ü. 2007. Dynamics of phosphorus, nitrogen and carbon removal in a horizontal subsurface flow constructed wetland. *Science of the Total Environment,* 380**,** 66-74.

Vohla, C., Kõiv, M., Bavor, H. J., Chazarenc, F. & Mander, Ü. 2011. Filter materials for phosphorus removal from wastewater in treatment wetlands—A review. *Ecological Engineering,* 37**,** 70-89.

Von Möser, H. & Sagl, H. 1967. Die Direktmessung hydrologischer Farbtracer im Gelande. *Steirische Beitr. Hydrogeol,* 18**,** 179-183.
Vonortas, A., Hipolito, A., Rolland, M., Boyer, C. & Papayannakos, N. 2011. Fluid flow characteristics of string reactors packed with spherical particles. *Chemical engineering & technology,* 34**,** 208-216.
Vymazal, J. 1995. *Algae and element cycling in wetlands,* Lewis Publishers Inc.
Vymazal, J. 2002. The use of sub-surface constructed wetlands for wastewater treatment in the Czech Republic: 10 years experience. *Ecological Engineering,* 18**,** 633-646.
Vymazal, J. 2005. Constructed wetlands for wastewater treatment in Europe. *Nutrient management in agricultural watersheds: a wetland solution. Wageningen, The Netherlands: Wageningen Academic Publishers***,** 230-244.
Vymazal, J. 2007. Removal of nutrients in various types of constructed wetlands. *Science of the total environment,* 380**,** 48-65.
Vymazal, J. 2009. The use constructed wetlands with horizontal sub-surface flow for various types of wastewater. *Ecological Engineering,* 35**,** 1-17.
Vymazal, J. 2010. Constructed wetlands for wastewater treatment. *Water,* 2**,** 530-549.
Vymazal, J. 2011. Long-term performance of constructed wetlands with horizontal sub-surface flow: Ten case studies from the Czech Republic. *Ecological Engineering,* 37**,** 54-63.
Vymazal, J., Brix, H., Cooper, P. F., Green, M. B. & Haberl, R. 1998. *Constructed wetlands for wastewater treatment in Europe,* Leiden, The Netherlands, Backhuys Publishers.
Vymazal, J. & Krása, P. 2003. Distribution of Mn, Al, Cu and Zn in a constructed wetland receiving municipal sewage. *Water Science and Technology,* 48**,** 299-305.
Vymazal, J. & Kröpfelová, L. 2009. Removal of organics in constructed wetlands with horizontal sub-surface flow: a review of the field experience. *Science of the total environment,* 407**,** 3911-3922.
Wagner, V., Li, T., Bayer, P., Leven, C., Dietrich, P. & Blum, P. 2014. Thermal tracer testing in a sedimentary aquifer: field experiment (Lauswiesen, Germany) and numerical simulation. *Hydrogeology Journal,* 22**,** 175-187.
Wahl, M. D., Brown, L. C., Soboyejo, A. O., Martin, J. & Dong, B. 2010. Quantifying the hydraulic performance of treatment wetlands using the moment index. *Ecological Engineering,* 36**,** 1691-1699.
Wallace, S. 2004. Engineered Wetlands Lead the Way. *Land and Water.*
Wallace, S. D. & Knight, R. L. 2006. *Small-scale constructed wetland treatment systems: feasibility, design criteria and O & M requirements,* IWA Publishing.
Warneke, S., Schipper, L. A., Matiasek, M. G., Scow, K. M., Cameron, S., Bruesewitz, D. A. & McDonald, I. R. 2011. Nitrate removal, communities of denitrifiers and adverse effects in different carbon substrates for use in denitrification beds. *Water research,* 45**,** 5463-5475.
Weis, J. S. & Weis, P. 2004. Metal uptake, transport and release by wetland plants: implications for phytoremediation and restoration. *Environment international,* 30**,** 685-700.
Wen, Y., Chen, Y., Zheng, N., Yang, D. & Zhou, Q. 2010. Effects of plant biomass on nitrate removal and transformation of carbon sources in subsurface-flow constructed wetlands. *Bioresource technology,* 101**,** 7286-7292.
Werner, T. M. & Kadlec, R. H. 2000. Wetland residence time distribution modeling. *Ecological Engineering,* 15**,** 77-90.
Westhoff, M., Bogaard, T. & Savenije, H. 2010. Quantifying the effect of in-stream rock clasts on the retardation of heat along a stream. *Advances in water resources,* 33**,** 1417-1425.

Wilson, J. T., Leach, L. E., Henson, M. & Jones, J. N. 1986. In situ biorestoration as a ground water remediation technique. *Groundwater Monitoring & Remediation,* 6**,** 56-64.

Wolverton, B. C., Barlow, R. M., McDonald, R. C. & Pierson, R. W. 1976. Application of vascular aquatic plants for pollution removal, energy and food production in a biological system. *In:* Tourbier, J. & Pierson, R. W. (eds.) *Biological control of water pollution.* Philadelphia: Univ. Pennsylvania Press.

Wörman, A. & Kronnäs, V. 2005. Effect of pond shape and vegetation heterogeneity on flow and treatment performance of constructed wetlands. *Journal of Hydrology,* 301**,** 123-138.

Woulds, C. & Ngwenya, B. T. 2004. Geochemical processes governing the performance of a constructed wetland treating acid mine drainage, Central Scotland. *Applied Geochemistry,* 19**,** 1773-1783.

Wu, H., Zhang, J., Li, P., Zhang, J., Xie, H. & Zhang, B. 2011. Nutrient removal in constructed microcosm wetlands for treating polluted river water in northern China. *Ecological Engineering,* 37**,** 560-568.

Yadav, A. K., Abbassi, R., Kumar, N., Satya, S., Sreekrishnan, T. & Mishra, B. 2012. The removal of heavy metals in wetland microcosms: Effects of bed depth, plant species, and metal mobility. *Chemical Engineering Journal,* 211**,** 501-507.

Yalcuk, A., Pakdil, N. B. & Turan, S. Y. 2010. Performance evaluation on the treatment of olive mill waste water in vertical subsurface flow constructed wetlands. *Desalination,* 262**,** 209-214.

Yao, K.-M., Habibian, M. T. & O'Melia, C. R. 1971. Water and waste water filtration. Concepts and applications. *Environmental science & technology,* 5**,** 1105-1112.

Young, E. O. & Ross, D. S. 2001. Phosphate release from seasonally flooded soils. *Journal of Environmental Quality,* 30**,** 91-101.

Zari, M. P. 2007. Biomimetic approaches to architectural design for increased sustainability. *Auckland, New Zealand*.

Zarro, E. 2014. Bio-inspired Product Design: The Study of Pinicola Shelves.

Zecheru, M. & Goran, N. The use of chemical tracers to water injection processes applied on Romanian reservoirs. EPJ Web of Conferences, 2013. EDP Sciences, 02005.

Zhang, L., Xia, X., Zhao, Y., Xi, B., Yan, Y., Guo, X., Xiong, Y. & Zhan, J. 2011. The ammonium nitrogen oxidation process in horizontal subsurface flow constructed wetlands. *Ecological Engineering,* 37**,** 1614-1619.

Zhao, D.-y., Luo, J., Zeng, J., Wang, M., Yan, W.-m., Huang, R. & Wu, Q. L. 2014. Effects of submerged macrophytes on the abundance and community composition of ammonia-oxidizing prokaryotes in a eutrophic lake. *Environmental Science and Pollution Research,* 21**,** 389-398.

Zhu, T., Jenssen, P., Maehlum, T. & Krogstad, T. 1997. Phosphorus sorption and chemical characteristics of lightweight aggregates (LWA)-potential filter media in treatment wetlands. *Water Science and Technology,* 35**,** 103-108.

Zurita, F., De Anda, J. & Belmont, M. 2009. Treatment of domestic wastewater and production of commercial flowers in vertical and horizontal subsurface-flow constructed wetlands. *Ecological Engineering,* 35**,** 861-869.

Zurita, F., de Anda, J. & Belmont, M. A. 2006. Performance of laboratory-scale wetlands planted with tropical ornamental plants to treat domestic wastewater. *Water quality research journal of Canada,* 41**,** 410-417.

8. Appendices

Appendix A: Calibration curve for FWT Red relating tracer concentration and absorbance measured and spectrophotometer at a wavelength of 550 nm.

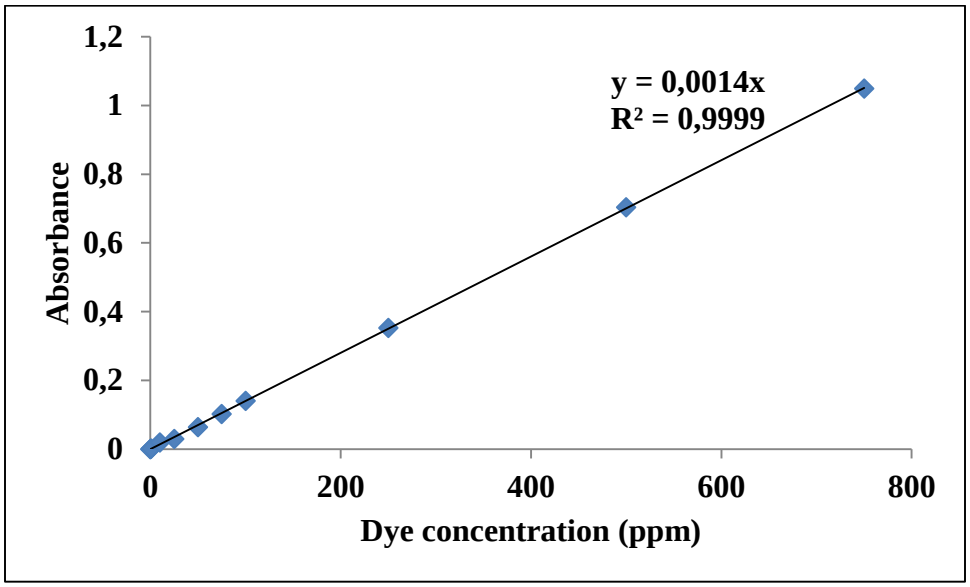

Appendix B: Hydraulic data from impulse response experiment on unplanted HSSF CW.

Appendix B.1: Hydraulic data from port 1,1.

Sample no.	Time (min)	Absorbance	C(t)	E(t)
1	0	0.000	0.000	0.000
2	2	0.000	0.000	0.000
3	10	0.319	227.857	0.036
4	20	0.396	282.857	0.045
5	30	0.102	72.857	0.011
6	60	0.003	2.143	0.000
7	90	0.001	0.714	0.000
8	120	0.004	2.857	0.000
9	150	0.004	2.857	0.000
10	210	0.002	1.429	0.000
11	300	0.000	0.000	0.000
12	480	0.000	0.000	0.000
13	720	0.000	0.000	0.000

Appendix B.2: Hydraulic data from port 1,2.

Sample no.	Time (min)	Absorbance	C(t) (ppm)	E(t)
1	0	0.000	0.000	0.000
2	2	0.000	0.000	0.000
3	10	0.829	592.143	0.086
4	20	0.259	185.000	0.027
5	30	0.059	42.143	0.006
6	60	0.003	2.143	0.000
7	90	0.003	2.143	0.000
8	120	0.004	2.857	0.000
9	150	0.005	3.571	0.001
10	210	0.006	4.286	0.001
11	300	0.002	1.429	0.000
12	480	0.000	0.000	0.000
13	720	0.000	0.000	0.000

Appendix B.3: Hydraulic data from port 1,3.

Sample no.	Time (min)	Absorbance	C(t) (ppm)	E(t)
1	0	0.000	0.000	0.000
2	2	0.003	2.143	0.000
3	10	0.896	640.000	0.064
4	20	0.393	280.714	0.028
5	30	0.125	89.286	0.009
6	60	0.013	9.286	0.001
7	90	0.013	9.286	0.001
8	120	0.006	4.286	0.000
9	150	0.002	1.429	0.000
10	210	0.003	2.143	0.000
11	300	0.000	0.000	0.000
12	480	0.004	2.857	0.000
13	720	0.000	0.000	0.000

Appendix B.4: Hydraulic data from port 2,1.

Sample no.	Time (min)	Absorbance	C(t) (ppm)	E(t)
1	0	0.000	0.000	0.000
2	2	0.000	0.000	0.000
3	10	0.002	1.429	0.000
4	20	0.010	7.143	0.001
5	30	0.084	60.000	0.005
6	60	0.343	245.000	0.019
7	90	0.063	45.000	0.004
8	120	0.004	2.857	0.000
9	150	0.003	2.143	0.000
10	210	0.005	3.571	0.000
11	300	0.000	0.000	0.000
12	480	0.003	2.143	0.000
13	720	0.000	0.000	0.000

Appendix B.5: Hydraulic data from port 2,2.

Sample no.	Time (min)	Absorbance	C(t) (ppm)	E(t)
1	0	0.000	0.000	0.000
2	2	0.001	0.714	0.000
3	10	0.000	0.000	0.000
4	20	0.036	25.714	0.001
5	30	0.305	217.857	0.010
6	60	0.527	376.429	0.018
7	90	0.098	70.000	0.003
8	120	0.014	10.000	0.000
9	150	0.010	7.143	0.000
10	210	0.006	4.286	0.000
11	300	0.008	5.714	0.000
12	480	0.000	0.000	0.000
13	720	0.000	0.000	0.000

Appendix B.6: Hydraulic data from port 2,3.

Sample no.	Time (min)	Absorbance	C(t) (ppm)	E(t)
1	0	0.000	0.000	0.000
2	2	0.000	0.000	0.000
3	10	0.001	0.714	0.000
4	20	0.004	2.857	0.000
5	30	0.094	67.143	0.002
6	60	0.745	532.143	0.018
7	90	0.295	210.714	0.007
8	120	0.053	37.857	0.001
9	150	0.029	20.714	0.001
10	210	0.017	12.143	0.000
11	300	0.006	4.286	0.000
12	480	0.000	0.000	0.000
13	720	0.000	0.000	0.000

Appendix B.7: Hydraulic data from port 3,1.

Sample no.	Time (min)	Absorbance	C(t) (ppm)	E(t)
1	0	0.000	0.000	0.000
2	2	0.004	2.857	0.000
3	10	0.002	1.429	0.000
4	20	0.021	15.000	0.001
5	30	0.629	449.286	0.036
6	60	0.161	115.000	0.009
7	90	0.017	12.143	0.001
8	120	0.006	4.286	0.000
9	150	0.006	4.286	0.000
10	210	0.005	3.571	0.000
11	300	0.000	0.000	0.000
12	480	0.004	2.857	0.000
13	720	0.000	0.000	0.000

Appendix B.8: Hydraulic data from port 3,2.

Sample no.	Time (min)	Absorbance	C(t) (ppm)	E(t)
1	0	0.000	0.000	0.000
2	2	0.000	0.000	0.000
3	10	0.007	5.000	0.000
4	20	0.016	11.429	0.001
5	30	0.807	576.429	0.045
6	60	0.103	73.571	0.006
7	90	0.014	10.000	0.001
8	120	0.012	8.571	0.001
9	150	0.008	5.714	0.000
10	210	0.000	0.000	0.000
11	300	0.003	0.000	0.000
12	480	0.006	4.286	0.000
13	720	0.000	0.000	0.000

Appendix B.9: Hydraulic data from port 3,3.

Sample no.	Time (min)	Absorbance	C(t) (ppm)	E(t)
1	0	0.000	0.000	0.000
2	2	0.004	2.857	0.000
3	10	0.003	2.143	0.000
4	20	0.134	95.714	0.003
5	30	1.276	911.429	0.029
6	60	0.439	313.571	0.010
7	90	0.095	67.857	0.002
8	120	0.050	35.714	0.001
9	150	0.036	25.714	0.001
10	210	0.016	11.429	0.000
11	300	0.006	4.286	0.000
12	480	0.000	0.000	0.000
13	720	0.000	0.000	0.000

Appendix B.10: Hydraulic data from port 4,1.

Sample no.	Time (min)	Absorbance	C(t) (ppm)	E(t)
1	0	0.000	0.000	0.000
2	2	0.000	0.000	0.000
3	10	0.000	0.000	0.000
4	20	0.000	0.000	0.000
5	30	0.023	16.429	0.001
6	60	0.255	182.143	0.015
7	90	0.094	67.143	0.006
8	120	0.079	56.429	0.005
9	150	0.005	3.571	0.000
10	180	0.005	3.571	0.000
11	210	0.000	0.000	0.000
12	300	0.002	1.429	0.000
13	480	0.004	2.857	0.000
14	720	0.000	0.000	0.000

Appendix B.11: Hydraulic data from port 4,2.

Sample no.	Time (min)	Absorbance	C(t) (ppm)	E(t)
1	0	0.000	0.000	0.000
2	2	0.000	0.000	0.000
3	10	0.002	1.429	0.000
4	20	0.003	2.143	0.000
5	30	0.136	97.143	0.010
6	60	0.225	160.714	0.017
7	90	0.053	37.857	0.004
8	120	0.014	10.000	0.001
9	150	0.011	7.857	0.001
10	180	0.003	2.143	0.000
11	210	0.004	2.857	0.000
12	300	0.000	0.000	0.000
13	480	0.002	1.429	0.000
14	720	0.000	0.000	0.000

Appendix B.12: Hydraulic data from port 4,3.

Sample no.	Time (min)	Absorbance	C(t) (ppm)	E(t)
1	0	0.000	0.000	0.000
2	2	0.001	0.714	0.000
3	10	0.004	2.857	0.000
4	20	0.000	0.000	0.000
5	30	0.013	9.286	0.001
6	60	0.240	171.429	0.013
7	90	0.034	24.286	0.002
8	120	0.027	19.286	0.001
9	150	0.036	25.714	0.002
10	180	0.114	81.429	0.006
11	210	0.036	25.714	0.002
12	300	0.000	0.000	0.000
13	480	0.000	0.000	0.000
14	720	0.000	0.000	0.000

Appendix B.13: Hydraulic data from port 5,1.

Sample no.	Time (min)	Absorbance	C(t) (ppm)	E(t)
1	0	0.000	0.000	0.000
2	2	0.000	0.000	0.000
3	10	0.000	0.000	0.000
4	20	0.000	0.000	0.000
5	30	0.006	4.286	0.000
6	60	0.056	40.000	0.002
7	90	0.247	176.429	0.008
8	120	0.232	165.714	0.007
9	150	0.188	134.286	0.006
10	180	0.169	120.714	0.005
11	210	0.039	27.857	0.001
12	240	0.019	13.571	0.001
13	270	0.009	6.429	0.000
14	300	0.011	7.857	0.000
15	480	0.008	5.714	0.000
16	720	0.000	0.000	0.000

Appendix B.14: Hydraulic data from port 5,2.

Sample no.	Time (min)	Absorbance	C(t) (ppm)	E(t)
1	0	0.000	0.000	0.000
2	2	0.000	0.000	0.000
3	10	0.000	0.000	0.000
4	20	0.000	0.000	0.000
5	30	0.003	2.143	0.000
6	60	0.244	174.286	0.008
7	90	0.337	240.714	0.011
8	120	0.217	155.000	0.007
9	150	0.075	53.571	0.003
10	180	0.029	20.714	0.001
11	210	0.027	19.286	0.001
12	240	0.014	10.000	0.000
13	270	0.007	5.000	0.000
14	300	0.002	1.429	0.000
15	480	0.000	0.000	0.000
16	720	0.000	0.000	0.000

Appendix B.15: Hydraulic data from port 5,3.

Sample no.	Time (min)	Absorbance	C(t) (ppm)	E(t)
1	0	0.000	0.000	0.000
2	2	0.000	0.000	0.000
3	10	0.000	0.000	0.000
4	20	0.000	0.000	0.000
5	30	0.004	2.857	0.000
6	60	0.025	17.857	0.001
7	90	0.322	230.000	0.012
8	120	0.204	145.714	0.007
9	150	0.114	81.429	0.004
10	180	0.057	40.714	0.002
11	210	0.025	17.857	0.001
12	240	0.024	17.143	0.001
13	270	0.021	15.000	0.001
14	300	0.033	23.571	0.001
15	480	0.003	2.143	0.000
16	720	0.000	0.000	0.000

Appendix B.16: Hydraulic data from port 6,1.

Sample no.	Time (min)	Absorbance	C(t) (ppm)	E(t)
1	0	0.000	0.000	0.000
2	2	0.000	0.000	0.000
3	10	0.000	0.000	0.000
4	20	0.000	0.000	0.000
5	30	0.001	0.714	0.000
6	60	0.032	22.857	0.002
7	90	0.159	113.571	0.010
8	120	0.139	99.286	0.009
9	150	0.099	70.714	0.006
10	180	0.014	10.000	0.001
11	210	0.003	2.143	0.000
12	240	0.009	6.429	0.001
13	270	0.008	5.714	0.001
14	300	0.008	5.714	0.001
15	480	0.005	3.571	0.000
16	720	0.000	0.000	0.000

Appendix B.17: Hydraulic data from port 6,2.

Sample no.	Time (min)	Absorbance	C(t) (ppm)	E(t)
1	0	0.000	0.000	0.000
2	2	0.000	0.000	0.000
3	10	0.000	0.000	0.000
4	20	0.000	0.000	0.000
5	30	0.000	0.000	0.000
6	60	0.221	157.857	0.008
7	90	0.436	311.429	0.016
8	120	0.128	91.429	0.005
9	150	0.082	58.571	0.003
10	180	0.028	20.000	0.001
11	210	0.009	6.429	0.000
12	240	0.002	1.429	0.000
13	270	0.002	1.429	0.000
14	300	0.000	0.000	0.000
15	480	0.005	3.571	0.000
16	720	0.000	0.000	0.000

Appendix B.18: Hydraulic data from port 6,3.

Sample no.	Time (min)	Absorbance	C(t) (ppm)	E(t)
1	0	0.000	0.000	0.000
2	2	0.000	0.000	0.000
3	10	0.000	0.000	0.000
4	20	0.000	0.000	0.000
5	30	0.003	2.143	0.000
6	60	0.225	160.714	0.010
7	90	0.158	112.857	0.007
8	120	0.056	40.000	0.003
9	150	0.032	22.857	0.001
10	180	0.024	17.143	0.001
11	210	0.032	22.857	0.001
12	240	0.026	18.571	0.001
13	270	0.020	14.286	0.001
14	300	0.017	12.143	0.001
15	480	0.005	3.571	0.000
16	720	0.000	0.000	0.000

Appendix B.19: Hydraulic data from port 7,1.

Sample no.	Time (min)	Absorbance	C(t) (ppm)	E(t)
1	0	0.000	0.000	0.000
2	2	0.000	0.000	0.000
3	10	0.000	0.000	0.000
4	20	0.000	0.000	0.000
5	30	0.002	1.429	0.000
6	60	0.015	10.714	0.001
7	90	0.144	102.857	0.006
8	120	0.208	148.571	0.009
9	150	0.139	99.286	0.006
10	180	0.093	66.429	0.004
11	210	0.071	50.714	0.003
12	240	0.021	15.000	0.001
13	270	0.008	5.714	0.000
14	300	0.007	5.000	0.000
15	480	0.011	7.857	0.000
16	720	0.000	0.000	0.000

Appendix B.20: Hydraulic data from port 7,2.

Sample no.	Time (min)	Absorbance	C(t) (ppm)	E(t)
1	0	0.000	0.000	0.000
2	2	0.000	0.000	0.000
3	10	0.000	0.000	0.000
4	20	0.000	0.000	0.000
5	30	0.000	0.000	0.000
6	60	0.011	7.857	0.001
7	90	0.145	103.571	0.008
8	120	0.242	172.857	0.014
9	150	0.103	73.571	0.006
10	180	0.037	26.429	0.002
11	210	0.018	12.857	0.001
12	240	0.008	5.714	0.000
13	270	0.003	2.143	0.000
14	300	0.001	0.714	0.000
15	480	0.000	0.000	0.000
16	720	0.000	0.000	0.000

Appendix B.21: Hydraulic data from port 7,3.

Sample no.	Time (min)	Absorbance	C(t) (ppm)	E(t)
1	0	0.000	0.000	0.000
2	2	0.000	0.000	0.000
3	10	0.000	0.000	0.000
4	20	0.000	0.000	0.000
5	30	0.001	0.714	0.000
6	60	0.004	2.857	0.000
7	90	0.059	42.143	0.002
8	120	0.226	161.429	0.008
9	150	0.176	125.714	0.006
10	180	0.090	64.286	0.003
11	210	0.096	68.571	0.003
12	240	0.092	65.714	0.003
13	270	0.038	27.143	0.001
14	300	0.020	14.286	0.001
15	480	0.000	0.000	0.000
16	720	0.000	0.000	0.000

Appendix B.22: Hydraulic data from port 8,1.

Sample no.	Time (min)	Absorbance	C(t) (ppm)	E(t)
1	0	0.000	0.000	0.000
2	2	0.000	0.000	0.000
3	10	0.000	0.000	0.000
4	20	0.000	0.000	0.000
5	30	0.000	0.000	0.000
6	60	0.003	2.143	0.000
7	90	0.002	1.429	0.000
8	120	0.075	53.571	0.002
9	150	0.129	92.143	0.004
10	180	0.186	132.857	0.005
11	210	0.216	154.286	0.006
12	240	0.168	120.000	0.005
13	270	0.085	60.714	0.003
14	300	0.041	29.286	0.001
15	420	0.017	12.143	0.001
16	480	0.007	5.000	0.000
17	720	0.000	0.000	0.000

Appendix B.23: Hydraulic data from port 8,2.

Sample no.	Time (min)	Absorbance	C(t) (ppm)	E(t)
1	0	0.000	0.000	0.000
2	2	0.000	0.000	0.000
3	10	0.000	0.000	0.000
4	20	0.000	0.000	0.000
5	30	0.000	0.000	0.000
6	60	0.001	0.714	0.000
7	90	0.021	15.000	0.001
8	120	0.158	112.857	0.006
9	150	0.192	137.143	0.007
10	180	0.155	110.714	0.005
11	210	0.140	100.000	0.005
12	240	0.082	58.571	0.003
13	270	0.046	32.857	0.002
14	300	0.023	16.429	0.001
15	420	0.007	5.000	0.000
16	480	0.005	3.571	0.000
17	720	0.000	0.000	0.000

Appendix B.24: Hydraulic data from port 8,3.

Sample no.	Time (min)	Absorbance	C(t) (ppm)	E(t)
1	0	0.000	0.000	0.000
2	2	0.000	0.000	0.000
3	10	0.000	0.000	0.000
4	20	0.000	0.000	0.000
5	30	0.000	0.000	0.000
6	60	0.001	0.714	0.000
7	90	0.003	2.143	0.000
8	120	0.108	77.143	0.004
9	150	0.214	152.857	0.009
10	180	0.188	134.286	0.008
11	210	0.107	76.429	0.004
12	240	0.040	28.571	0.002
13	270	0.027	19.286	0.001
14	300	0.017	12.143	0.001
15	420	0.020	14.286	0.001
16	480	0.003	2.143	0.000
17	720	0.000	0.000	0.000

Appendix B.25: Hydraulic data from port 9,1.

Sample no.	Time (min)	Absorbance	C(t) (ppm)	E(t)
1	0	0.000	0.000	0.000
2	2	0.000	0.000	0.000
3	10	0.000	0.000	0.000
4	20	0.000	0.000	0.000
5	30	0.000	0.000	0.000
6	60	0.000	0.000	0.000
7	90	0.003	2.143	0.000
8	120	0.148	105.714	0.006
9	150	0.175	125.000	0.007
10	180	0.187	133.571	0.008
11	210	0.092	65.714	0.004
12	240	0.032	22.857	0.001
13	270	0.019	13.571	0.001
14	300	0.025	17.857	0.001
15	420	0.004	2.857	0.000
16	480	0.003	2.143	0.000
17	720	0.000	0.000	0.000

Appendix B.26: Hydraulic data from port 9,2.

Sample no.	Time (min)	Absorbance	C(t) (ppm)	E(t)
1	0	0.000	0.000	0.000
2	2	0.000	0.000	0.000
3	10	0.000	0.000	0.000
4	20	0.000	0.000	0.000
5	30	0.000	0.000	0.000
6	60	0.005	3.571	0.000
7	90	0.028	20.000	0.001
8	120	0.255	182.143	0.007
9	150	0.274	195.714	0.007
10	180	0.173	123.571	0.004
11	210	0.157	112.143	0.004
12	240	0.087	62.143	0.002
13	270	0.175	125.000	0.004
14	300	0.018	12.857	0.000
15	420	0.009	6.429	0.000
16	480	0.002	1.429	0.000
17	720	0.000	0.000	0.000

Appendix B.27: Hydraulic data from port 9,3.

Sample no.	Time (min)	Absorbance	C(t) (ppm)	E(t)
1	0	0.000	0.000	0.000
2	2	0.000	0.000	0.000
3	10	0.000	0.000	0.000
4	20	0.000	0.000	0.000
5	30	0.000	0.000	0.000
6	60	0.008	5.714	0.000
7	90	0.007	5.000	0.000
8	120	0.195	139.286	0.008
9	150	0.245	175.000	0.010
10	180	0.144	102.857	0.006
11	210	0.087	62.143	0.003
12	240	0.023	16.429	0.001
13	270	0.019	13.571	0.001
14	300	0.019	13.571	0.001
15	420	0.011	7.857	0.000
16	480	0.000	0.000	0.000
17	720	0.000	0.000	0.000

Appendix B.28: Hydraulic data from port 10,1.

Sample no.	Time (min)	Absorbance	C(t) (ppm)	E(t)
1	0	0.000	0.000	0.000
2	2	0.000	0.000	0.000
3	10	0.000	0.000	0.000
4	20	0.000	0.000	0.000
5	30	0.000	0.000	0.000
6	60	0.000	0.000	0.000
7	90	0.000	0.000	0.000
8	120	0.061	43.571	0.002
9	150	0.125	89.286	0.005
10	180	0.119	85.000	0.005
11	210	0.152	108.571	0.006
12	240	0.132	94.286	0.005
13	270	0.058	41.429	0.002
14	300	0.033	23.571	0.001
15	330	0.016	11.429	0.001
16	360	0.014	10.000	0.001
17	420	0.016	11.429	0.001
18	480	0.012	8.571	0.000
19	720	0.000	0.000	0.000

Appendix B.29: Hydraulic data from port 10,2.

Sample no.	Time (min)	Absorbance	C(t) (ppm)	E(t)
1	0	0.000	0.000	0.000
2	2	0.000	0.000	0.000
3	10	0.000	0.000	0.000
4	20	0.000	0.000	0.000
5	30	0.000	0.000	0.000
6	60	0.000	0.000	0.000
7	90	0.003	2.143	0.000
8	120	0.093	66.429	0.004
9	150	0.197	140.714	0.008
10	180	0.120	85.714	0.005
11	210	0.082	58.571	0.003
12	240	0.092	65.714	0.004
13	270	0.075	53.571	0.003
14	300	0.045	32.143	0.002
15	330	0.027	19.286	0.001
16	360	0.012	8.571	0.000
17	420	0.009	6.429	0.000
18	480	0.008	5.714	0.000
19	720	0.000	0.000	0.000

Appendix B.30: Hydraulic data from port 10,3.

Sample no.	Time (min)	Absorbance	C(t) (ppm)	E(t)
1	0	0.000	0.000	0.000
2	2	0.000	0.000	0.000
3	10	0.000	0.000	0.000
4	20	0.000	0.000	0.000
5	30	0.000	0.000	0.000
6	60	0.000	0.000	0.000
7	90	0.000	0.000	0.000
8	120	0.048	34.286	0.002
9	150	0.047	33.571	0.002
10	180	0.165	117.857	0.008
11	210	0.133	95.000	0.007
12	240	0.123	87.857	0.006
13	270	0.040	28.571	0.002
14	300	0.027	19.286	0.001
15	330	0.020	14.286	0.001
16	360	0.009	6.429	0.000
17	420	0.002	1.429	0.000
18	480	0.001	0.714	0.000
19	720	0.000	0.000	0.000

Appendix B.31: Hydraulic data from port 11,1.

Sample no.	Time (min)	Absorbance	C(t) (ppm)	E(t)
1	0	0.000	0.000	0.000
2	2	0.000	0.000	0.000
3	10	0.000	0.000	0.000
4	20	0.000	0.000	0.000
5	30	0.000	0.000	0.000
6	60	0.000	0.000	0.000
7	90	0.000	0.000	0.000
8	120	0.004	2.857	0.000
9	150	0.021	15.000	0.001
10	180	0.055	39.286	0.002
11	210	0.110	78.571	0.003
12	240	0.136	97.143	0.004
13	270	0.275	196.429	0.009
14	300	0.144	102.857	0.005
15	330	0.098	70.000	0.003
16	360	0.058	41.429	0.002
17	420	0.030	21.429	0.001
18	480	0.010	7.143	0.000
19	720	0.000	0.000	0.000

Appendix B.32: Hydraulic data from port 11,2.

Sample no.	Time (min)	Absorbance	C(t) (ppm)	E(t)
1	0	0.000	0.000	0.000
2	2	0.000	0.000	0.000
3	10	0.000	0.000	0.000
4	20	0.000	0.000	0.000
5	30	0.000	0.000	0.000
6	60	0.000	0.000	0.000
7	90	0.000	0.000	0.000
8	120	0.015	10.714	0.000
9	150	0.054	38.571	0.002
10	180	0.150	107.143	0.005
11	210	0.158	112.857	0.005
12	240	0.139	99.286	0.004
13	270	0.123	87.857	0.004
14	300	0.108	77.143	0.003
15	330	0.095	67.857	0.003
16	360	0.053	37.857	0.002
17	420	0.019	13.571	0.001
18	480	0.010	7.143	0.000
19	720	0.000	0.000	0.000

Appendix B.33: Hydraulic data from port 11,3.

Sample no.	Time (min)	Absorbance	C(t) (ppm)	E(t)
1	0	0.000	0.000	0.000
2	2	0.000	0.000	0.000
3	10	0.000	0.000	0.000
4	20	0.000	0.000	0.000
5	30	0.000	0.000	0.000
6	60	0.000	0.000	0.000
7	90	0.000	0.000	0.000
8	120	0.006	4.286	0.000
9	150	0.021	15.000	0.001
10	180	0.114	81.429	0.006
11	210	0.172	122.857	0.008
12	240	0.129	92.143	0.006
13	270	0.072	51.429	0.004
14	300	0.038	27.143	0.002
15	330	0.033	23.571	0.002
16	360	0.019	13.571	0.001
17	420	0.010	7.143	0.000
18	480	0.005	3.571	0.000
19	720	0.000	0.000	0.000

Appendix B.34: Hydraulic data from port 12,1.

Sample no.	Time (min)	Absorbance	C(t) (ppm)	E(t)
1	0	0.000	0.000	0.000
2	2	0.000	0.000	0.000
3	10	0.000	0.000	0.000
4	20	0.000	0.000	0.000
5	30	0.000	0.000	0.000
6	60	0.000	0.000	0.000
7	90	0.000	0.000	0.000
8	120	0.002	1.429	0.000
9	150	0.037	26.429	0.002
10	180	0.110	78.571	0.005
11	210	0.155	110.714	0.007
12	240	0.154	110.000	0.007
13	270	0.094	67.143	0.004
14	300	0.055	39.286	0.002
15	330	0.048	34.286	0.002
16	360	0.023	16.429	0.001
17	420	0.011	7.857	0.000
18	480	0.007	5.000	0.000
19	720	0.000	0.000	0.000

Appendix B.35: Hydraulic data from port 12,2.

Sample no.	Time (min)	Absorbance	C(t) (ppm)	E(t)
1	0	0.000	0.000	0.000
2	2	0.000	0.000	0.000
3	10	0.000	0.000	0.000
4	20	0.000	0.000	0.000
5	30	0.000	0.000	0.000
6	60	0.000	0.000	0.000
7	90	0.000	0.000	0.000
8	120	0.009	6.429	0.000
9	150	0.089	63.571	0.002
10	180	0.250	178.571	0.006
11	210	0.225	160.714	0.005
12	240	0.202	144.286	0.005
13	270	0.154	110.000	0.003
14	300	0.115	82.143	0.003
15	330	0.094	67.143	0.002
16	360	0.048	34.286	0.001
17	420	0.024	17.143	0.001
18	480	0.025	17.857	0.001
19	720	0.000	0.000	0.000

Appendix B.36: Hydraulic data from port 12,3.

Sample no.	Time (min)	Absorbance	C(t) (ppm)	E(t)
1	0	0.000	0.000	0.000
2	2	0.000	0.000	0.000
3	10	0.000	0.000	0.000
4	20	0.000	0.000	0.000
5	30	0.000	0.000	0.000
6	60	0.000	0.000	0.000
7	90	0.000	0.000	0.000
8	120	0.010	7.143	0.000
9	150	0.067	47.857	0.003
10	180	0.182	130.000	0.008
11	210	0.141	100.714	0.006
12	240	0.105	75.000	0.005
13	270	0.074	52.857	0.003
14	300	0.045	32.143	0.002
15	330	0.032	22.857	0.001
16	360	0.012	8.571	0.001
17	420	0.006	4.286	0.000
18	480	0.008	5.714	0.000
19	720	0.000	0.000	0.000

Appendix B.37: Hydraulic data from port 13,1.

Sample no.	Time (min)	Absorbance	C(t) (ppm)	E(t)
1	0	0.000	0.000	0.000
2	2	0.000	0.000	0.000
3	10	0.000	0.000	0.000
4	20	0.000	0.000	0.000
5	30	0.000	0.000	0.000
6	60	0.000	0.000	0.000
7	90	0.000	0.000	0.000
8	120	0.000	0.000	0.000
9	150	0.008	5.714	0.000
10	180	0.017	12.143	0.001
11	210	0.023	16.429	0.001
12	240	0.046	32.857	0.002
13	270	0.079	56.429	0.003
14	300	0.084	60.000	0.003
15	330	0.072	51.429	0.003
16	360	0.091	65.000	0.004
17	420	0.078	55.714	0.003
18	480	0.021	15.000	0.001
19	720	0.000	0.000	0.000

Appendix B.38: Hydraulic data from port 13,2.

Sample no.	Time (min)	Absorbance	C(t) (ppm)	E(t)
1	0	0.000	0.000	0.000
2	2	0.000	0.000	0.000
3	10	0.000	0.000	0.000
4	20	0.000	0.000	0.000
5	30	0.000	0.000	0.000
6	60	0.000	0.000	0.000
7	90	0.000	0.000	0.000
8	120	0.000	0.000	0.000
9	150	0.020	14.286	0.001
10	180	0.107	76.429	0.004
11	210	0.090	64.286	0.003
12	240	0.089	63.571	0.003
13	270	0.107	76.429	0.004
14	300	0.096	68.571	0.003
15	330	0.091	65.000	0.003
16	360	0.067	47.857	0.002
17	420	0.047	33.571	0.002
18	480	0.020	14.286	0.001
19	720	0.000	0.000	0.000

Appendix B.39: Hydraulic data from port 13,3.

Sample no.	Time (min)	Absorbance	C(t) (ppm)	E(t)
1	0	0.000	0.000	0.000
2	2	0.000	0.000	0.000
3	10	0.000	0.000	0.000
4	20	0.000	0.000	0.000
5	30	0.000	0.000	0.000
6	60	0.000	0.000	0.000
7	90	0.000	0.000	0.000
8	120	0.000	0.000	0.000
9	150	0.013	9.286	0.001
10	180	0.090	64.286	0.006
11	210	0.120	85.714	0.008
12	240	0.098	70.000	0.006
13	270	0.062	44.286	0.004
14	300	0.034	24.286	0.002
15	330	0.030	21.429	0.002
16	360	0.012	8.571	0.001
17	420	0.004	2.857	0.000
18	480	0.003	2.143	0.000
19	720	0.000	0.000	0.000

Appendix B.40: Hydraulic data from port 14.

Sample no.	Time (min)	Absorbance	C(t) (ppm)	E(t)
1	0	0.000	0.000	0.000
2	2	0.000	0.000	0.000
3	30	0.000	0.000	0.000
4	60	0.000	0.000	0.000
5	90	0.000	0.000	0.000
6	120	0.001	0.714	0.000
7	150	0.001	0.714	0.000
8	180	0.035	25.000	0.002
9	210	0.115	82.143	0.005
10	240	0.114	81.429	0.005
11	270	0.095	67.857	0.004
12	300	0.080	57.143	0.003
13	330	0.073	52.143	0.003
14	360	0.047	33.571	0.002
15	420	0.047	33.571	0.002
16	480	0.015	10.714	0.001
17	600	0.013	9.286	0.001
18	720	0.000	0.000	0.000

Appendix C: Hydraulic data from impulse response experiment on planted HSSF CW.

Appendix C.1: Hydraulic data from port 1,1.

Sample no.	Time (min)	Absorbance	C(t) (ppm)	E(t)
1	0	0.000	0.000	0.000
2	2	0.886	632.857	0.085
3	10	0.334	238.571	0.032
4	20	0.047	33.571	0.004
5	30	0.023	16.429	0.002
6	60	0.003	2.143	0.000
7	90	0.004	2.857	0.000
8	120	0.007	5.000	0.001
9	150	0.006	4.286	0.001
10	180	0.004	2.857	0.000
11	210	0.000	0.000	0.000
12	240	0.000	0.000	0.000
13	300	0.005	3.571	0.000
14	360	0.002	1.429	0.000
15	480	0.005	3.571	0.000
16	720	0.000	0.000	0.000

Appendix C.2: Hydraulic data from port 1,2.

Sample no.	Time (min)	Absorbance	C(t) (ppm)	E(t)
1	0	0.000	0.000	0.000
2	2	0.456	325.714	0.036
3	10	0.698	498.571	0.055
4	20	0.145	103.571	0.012
5	30	0.046	32.857	0.004
6	60	0.010	7.143	0.001
7	90	0.004	2.857	0.000
8	120	0.003	2.143	0.000
9	150	0.002	1.429	0.000
10	180	0.008	5.714	0.001
11	210	0.002	1.429	0.000
12	240	0.000	0.000	0.000
13	300	0.000	0.000	0.000
14	360	0.007	5.000	0.001
15	480	0.011	7.857	0.001
16	720	0.000	0.000	0.000

Appendix C.3: Hydraulic data from port 1,3.

Sample no.	Time (min)	Absorbance	C(t) (ppm)	E(t)
1	0	0.000	0.000	0.000
2	2	0.108	77.143	0.009
3	10	0.740	528.571	0.059
4	20	0.349	249.286	0.028
5	30	0.134	95.714	0.011
6	60	0.006	4.286	0.000
7	90	0.007	5.000	0.001
8	120	0.004	2.857	0.000
9	150	0.003	2.143	0.000
10	180	0.006	4.286	0.000
11	210	0.005	3.571	0.000
12	240	0.000	0.000	0.000
13	300	0.000	0.000	0.000
14	360	0.001	0.714	0.000
15	480	0.004	2.857	0.000
16	720	0.000	0.000	0.000

Appendix C.4: Hydraulic data from port 2,1.

Sample no.	Time (min)	Absorbance	C(t) (ppm)	E(t)
1	0	0.000	0.000	0.000
2	2	0.008	5.714	0.001
3	10	0.439	313.571	0.039
4	20	0.363	259.286	0.033
5	30	0.129	92.143	0.012
6	60	0.013	9.286	0.001
7	90	0.013	9.286	0.001
8	120	0.004	2.857	0.000
9	150	0.000	0.000	0.000
10	180	0.004	2.857	0.000
11	210	0.006	4.286	0.001
12	240	0.001	0.714	0.000
13	300	0.003	2.143	0.000
14	360	0.001	0.714	0.000
15	480	0.005	3.571	0.000
16	720	0.000	0.000	0.000

Appendix C.5: Hydraulic data from port 2,2.

Sample no.	Time (min)	Absorbance	C(t) (ppm)	E(t)
1	0	0.000	0.000	0.000
2	2	0.000	0.000	0.000
3	10	1.153	823.571	0.045
4	20	0.786	561.429	0.030
5	30	0.350	250.000	0.014
6	60	0.069	49.286	0.003
7	90	0.019	13.571	0.001
8	120	0.007	5.000	0.000
9	150	0.009	6.429	0.000
10	180	0.000	0.000	0.000
11	210	0.003	2.143	0.000
12	240	0.000	0.000	0.000
13	300	0.008	5.714	0.000
14	360	0.002	1.429	0.000
15	480	0.004	2.857	0.000
16	720	0.000	0.000	0.000

Appendix C.6: Hydraulic data from port 2,3.

Sample no.	Time (min)	Absorbance	C(t) (ppm)	E(t)
1	0	0.000	0.000	0.000
2	2	0.002	1.429	0.000
3	10	0.238	170.000	0.006
4	20	0.453	323.571	0.012
5	30	0.301	215.000	0.008
6	60	0.403	287.857	0.010
7	90	0.240	171.429	0.006
8	120	0.091	65.000	0.002
9	150	0.038	27.143	0.001
10	180	0.014	10.000	0.000
11	210	0.007	5.000	0.000
12	240	0.005	3.571	0.000
13	300	0.004	2.857	0.000
14	360	0.005	3.571	0.000
15	480	0.003	2.143	0.000
16	720	0.000	0.000	0.000

Appendix C.7: Hydraulic data from port 3,1.

Sample no.	Time (min)	Absorbance	C(t) (ppm)	E(t)
1	0	0.000	0.000	0.000
2	2	0.001	0.714	0.000
3	10	0.140	100.000	0.013
4	20	0.489	349.286	0.046
5	30	0.089	63.571	0.008
6	60	0.019	13.571	0.002
7	90	0.006	4.286	0.001
8	120	0.005	3.571	0.000
9	150	0.000	0.000	0.000
10	180	0.003	2.143	0.000
11	210	0.001	0.714	0.000
12	240	0.012	8.571	0.001
13	300	0.003	2.143	0.000
14	360	0.000	0.000	0.000
15	480	0.001	0.714	0.000
16	720	0.000	0.000	0.000

Appendix C.8: Hydraulic data from port 3,2.

Sample no.	Time (min)	Absorbance	C(t) (ppm)	E(t)
1	0	0.000	0.000	0.000
2	2	0.006	4.286	0.000
3	10	0.171	122.143	0.008
4	20	0.805	575.000	0.039
5	30	0.293	209.286	0.014
6	60	0.060	42.857	0.003
7	90	0.020	14.286	0.001
8	120	0.013	9.286	0.001
9	150	0.001	0.714	0.000
10	180	0.009	6.429	0.000
11	210	0.003	2.143	0.000
12	240	0.003	2.143	0.000
13	300	0.007	5.000	0.000
14	360	0.000	0.000	0.000
15	480	0.007	5.000	0.000
16	720	0.000	0.000	0.000

Appendix C.9: Hydraulic data from port 3,3.

Sample no.	Time (min)	Absorbance	C(t) (ppm)	E(t)
1	0	0.000	0.000	0.000
2	2	0.007	5.000	0.000
3	10	0.020	14.286	0.000
4	20	0.866	618.571	0.014
5	30	0.819	585.000	0.013
6	60	0.512	365.714	0.008
7	90	0.255	182.143	0.004
8	120	0.128	91.429	0.002
9	150	0.046	32.857	0.001
10	180	0.026	18.571	0.000
11	210	0.037	26.429	0.001
12	240	0.017	12.143	0.000
13	300	0.030	21.429	0.000
14	360	0.018	12.857	0.000
15	480	0.015	10.714	0.000
16	720	0.000	0.000	0.000

Appendix C.10: Hydraulic data from port 4,1.

Sample no.	Time (min)	Absorbance	C(t) (ppm)	E(t)
1	0	0.000	0.000	0.000
2	2	0.001	0.714	0.000
3	10	0.004	2.857	0.000
4	20	0.002	1.429	0.000
5	30	0.008	5.714	0.001
6	60	0.138	98.571	0.015
7	90	0.025	17.857	0.003
8	120	0.010	7.143	0.001
9	150	0.002	1.429	0.000
10	180	0.014	10.000	0.002
11	210	0.006	4.286	0.001
12	240	0.007	5.000	0.001
13	300	0.004	2.857	0.000
14	360	0.001	0.714	0.000
15	480	0.006	4.286	0.001
16	720	0.000	0.000	0.000

Appendix C.11: Hydraulic data from port 4,2.

Sample no.	Time (min)	Absorbance	C(t) (ppm)	E(t)
1	0	0.000	0.000	0.000
2	2	0.007	5.000	0.000
3	10	0.004	2.857	0.000
4	20	0.006	4.286	0.000
5	30	0.025	17.857	0.002
6	60	0.278	198.571	0.019
7	90	0.025	17.857	0.002
8	120	0.014	10.000	0.001
9	150	0.004	2.857	0.000
10	180	0.004	2.857	0.000
11	210	0.005	3.571	0.000
12	240	0.000	0.000	0.000
13	300	0.003	2.143	0.000
14	360	0.002	1.429	0.000
15	480	0.008	5.714	0.001
16	720	0.000	0.000	0.000

Appendix C.12: Hydraulic data from port 4,3.

Sample no.	Time (min)	Absorbance	C(t) (ppm)	E(t)
1	0	0.000	0.000	0.000
2	2	0.002	1.429	0.000
3	10	0.004	2.857	0.000
4	20	0.005	3.571	0.000
5	30	0.002	1.429	0.000
6	60	0.545	389.286	0.015
7	90	0.214	152.857	0.006
8	120	0.139	99.286	0.004
9	150	0.034	24.286	0.001
10	180	0.014	10.000	0.000
11	210	0.017	12.143	0.000
12	240	0.008	5.714	0.000
13	300	0.006	4.286	0.000
14	360	0.002	1.429	0.000
15	480	0.013	9.286	0.000
16	720	0.000	0.000	0.000

Appendix C.13: Hydraulic data from port 5,1.

Sample no.	Time (min)	Absorbance	C(t) (ppm)	E(t)
1	0	0.000	0.000	0.000
2	2	0.000	0.000	0.000
3	10	0.000	0.000	0.000
4	20	0.000	0.000	0.000
5	30	0.003	2.143	0.000
6	60	0.214	152.857	0.013
7	90	0.070	50.000	0.004
8	120	0.030	21.429	0.002
9	150	0.008	5.714	0.000
10	180	0.005	3.571	0.000
11	210	0.003	2.143	0.000
12	240	0.010	7.143	0.001
13	270	0.002	1.429	0.000
14	300	0.014	10.000	0.001
15	360	0.013	9.286	0.001
16	480	0.011	7.857	0.001
17	720	0.000	0.000	0.000

Appendix C.14: Hydraulic data from port 5,2.

Sample no.	Time (min)	Absorbance	C(t) (ppm)	E(t)
1	0	0.000	0.000	0.000
2	2	0.000	0.000	0.000
3	10	0.000	0.000	0.000
4	20	0.000	0.000	0.000
5	30	0.009	6.429	0.001
6	60	0.249	177.857	0.015
7	90	0.104	74.286	0.006
8	120	0.044	31.429	0.003
9	150	0.010	7.143	0.001
10	180	0.004	2.857	0.000
11	210	0.014	10.000	0.001
12	240	0.002	1.429	0.000
13	270	0.001	0.714	0.000
14	300	0.008	5.714	0.000
15	360	0.004	2.857	0.000
16	480	0.003	2.143	0.000
17	720	0.000	0.000	0.000

Appendix C.15: Hydraulic data from port 5,3.

Sample no.	Time (min)	Absorbance	C(t) (ppm)	E(t)
1	0	0.000	0.000	0.000
2	2	0.000	0.000	0.000
3	10	0.000	0.000	0.000
4	20	0.000	0.000	0.000
5	30	0.009	6.429	0.000
6	60	0.119	85.000	0.006
7	90	0.118	84.286	0.006
8	120	0.080	57.143	0.004
9	150	0.046	32.857	0.002
10	180	0.032	22.857	0.002
11	210	0.031	22.143	0.002
12	240	0.022	15.714	0.001
13	270	0.017	12.143	0.001
14	300	0.014	10.000	0.001
15	360	0.013	9.286	0.001
16	480	0.010	7.143	0.001
17	720	0.000	0.000	0.000

Appendix C.16: Hydraulic data from port 6,1.

Sample no.	Time (min)	Absorbance	C(t) (ppm)	E(t)
1	0	0.000	0.000	0.000
2	2	0.000	0.000	0.000
3	10	0.000	0.000	0.000
4	20	0.000	0.000	0.000
5	30	0.005	3.571	0.001
6	60	0.097	69.286	0.011
7	90	0.038	27.143	0.004
8	120	0.017	12.143	0.002
9	150	0.005	3.571	0.001
10	180	0.012	8.571	0.001
11	210	0.008	5.714	0.001
12	240	0.010	7.143	0.001
13	270	0.007	5.000	0.001
14	300	0.012	8.571	0.001
15	360	0.001	0.714	0.000
16	480	0.007	5.000	0.001
17	720	0.000	0.000	0.000

Appendix C.17: Hydraulic data from port 6,2.

Sample no.	Time (min)	Absorbance	C(t) (ppm)	E(t)
1	0	0.000	0.000	0.000
2	2	0.000	0.000	0.000
3	10	0.000	0.000	0.000
4	20	0.000	0.000	0.000
5	30	0.008	5.714	0.000
6	60	0.214	152.857	0.011
7	90	0.164	117.143	0.009
8	120	0.074	52.857	0.004
9	150	0.026	18.571	0.001
10	180	0.012	8.571	0.001
11	210	0.014	10.000	0.001
12	240	0.008	5.714	0.000
13	270	0.006	4.286	0.000
14	300	0.014	10.000	0.001
15	360	0.006	4.286	0.000
16	480	0.003	2.143	0.000
17	720	0.000	0.000	0.000

Appendix C.18: Hydraulic data from port 6,3.

Sample no.	Time (min)	Absorbance	C(t) (ppm)	E(t)
1	0	0.000	0.000	0.000
2	2	0.000	0.000	0.000
3	10	0.000	0.000	0.000
4	20	0.000	0.000	0.000
5	30	0.008	5.714	0.000
6	60	0.223	159.286	0.006
7	90	0.150	107.143	0.004
8	120	0.182	130.000	0.005
9	150	0.165	117.857	0.004
10	180	0.132	94.286	0.003
11	210	0.090	64.286	0.002
12	240	0.060	42.857	0.002
13	270	0.046	32.857	0.001
14	300	0.020	14.286	0.001
15	360	0.014	10.000	0.000
16	480	0.013	9.286	0.000
17	720	0.000	0.000	0.000

Appendix C.19: Hydraulic data from port 7,1.

Sample no.	Time (min)	Absorbance	C(t) (ppm)	E(t)
1	0	0.000	0.000	0.000
2	2	0.000	0.000	0.000
3	10	0.000	0.000	0.000
4	20	0.000	0.000	0.000
5	30	0.004	2.857	0.000
6	60	0.012	8.571	0.001
7	90	0.163	116.429	0.019
8	120	0.069	49.286	0.008
9	150	0.012	8.571	0.001
10	180	0.008	5.714	0.001
11	210	0.011	7.857	0.001
12	240	0.005	3.571	0.001
13	270	0.006	4.286	0.001
14	300	0.005	3.571	0.001
15	360	0.005	3.571	0.001
16	480	0.001	0.714	0.000
17	720	0.000	0.000	0.000

Appendix C.20: Hydraulic data from port 7,2.

Sample no.	Time (min)	Absorbance	C(t) (ppm)	E(t)
1	0	0.000	0.000	0.000
2	2	0.000	0.000	0.000
3	10	0.000	0.000	0.000
4	20	0.000	0.000	0.000
5	30	0.001	0.714	0.000
6	60	0.004	2.857	0.000
7	90	0.161	115.000	0.006
8	120	0.394	281.429	0.014
9	150	0.197	140.714	0.007
10	180	0.057	40.714	0.002
11	210	0.020	14.286	0.001
12	240	0.010	7.143	0.000
13	270	0.007	5.000	0.000
14	300	0.007	5.000	0.000
15	360	0.000	0.000	0.000
16	480	0.007	5.000	0.000
17	720	0.000	0.000	0.000

Appendix C.21: Hydraulic data from port 7,3.

Sample no.	Time (min)	Absorbance	C(t) (ppm)	E(t)
1	0	0.000	0.000	0.000
2	2	0.000	0.000	0.000
3	10	0.000	0.000	0.000
4	20	0.000	0.000	0.000
5	30	0.004	2.857	0.000
6	60	0.001	0.714	0.000
7	90	0.103	73.571	0.003
8	120	0.275	196.429	0.008
9	150	0.270	192.857	0.008
10	180	0.202	144.286	0.006
11	210	0.100	71.429	0.003
12	240	0.051	36.429	0.002
13	270	0.032	22.857	0.001
14	300	0.010	7.143	0.000
15	360	0.010	7.143	0.000
16	480	0.002	1.429	0.000
17	720	0.000	0.000	0.000

Appendix C.22: Hydraulic data from port 8,1.

Sample no.	Time (min)	Absorbance	C(t) (ppm)	E(t)
1	0	0.000	0.000	0.000
2	2	0.000	0.000	0.000
3	10	0.000	0.000	0.000
4	20	0.000	0.000	0.000
5	30	0.000	0.000	0.000
6	60	0.000	0.000	0.000
7	90	0.107	76.429	0.006
8	120	0.191	136.429	0.011
9	150	0.095	67.857	0.006
10	180	0.047	33.571	0.003
11	210	0.020	14.286	0.001
12	240	0.014	10.000	0.001
13	270	0.012	8.571	0.001
14	300	0.005	3.571	0.000
15	330	0.009	6.429	0.001
16	360	0.011	7.857	0.001
17	420	0.005	3.571	0.000
18	480	0.004	2.857	0.000
19	600	0.002	1.429	0.000
20	720	0.000	0.000	0.000

Appendix C.23: Hydraulic data from port 8,2.

Sample no.	Time (min)	Absorbance	C(t) (ppm)	E(t)
1	0	0.000	0.000	0.000
2	2	0.000	0.000	0.000
3	10	0.000	0.000	0.000
4	20	0.000	0.000	0.000
5	30	0.000	0.000	0.000
6	60	0.000	0.000	0.000
7	90	0.049	35.000	0.003
8	120	0.137	97.857	0.009
9	150	0.105	75.000	0.007
10	180	0.056	40.000	0.004
11	210	0.026	18.571	0.002
12	240	0.025	17.857	0.002
13	270	0.014	10.000	0.001
14	300	0.007	5.000	0.000
15	330	0.004	2.857	0.000
16	360	0.008	5.714	0.001
17	420	0.010	7.143	0.001
18	480	0.001	0.714	0.000
19	600	0.005	3.571	0.000
20	720	0.000	0.000	0.000

Appendix C.24: Hydraulic data from port 8,3.

Sample no.	Time (min)	Absorbance	C(t) (ppm)	E(t)
1	0	0.000	0.000	0.000
2	2	0.000	0.000	0.000
3	10	0.000	0.000	0.000
4	20	0.000	0.000	0.000
5	30	0.000	0.000	0.000
6	60	0.000	0.000	0.000
7	90	0.019	13.571	0.002
8	120	0.055	39.286	0.005
9	150	0.059	42.143	0.005
10	180	0.042	30.000	0.004
11	210	0.025	17.857	0.002
12	240	0.022	15.714	0.002
13	270	0.016	11.429	0.001
14	300	0.013	9.286	0.001
15	330	0.012	8.571	0.001
16	360	0.011	7.857	0.001
17	420	0.014	10.000	0.001
18	480	0.007	5.000	0.001
19	600	0.009	6.429	0.001
20	720	0.000	0.000	0.000

Appendix C.25: Hydraulic data from port 9,1.

Sample no.	Time (min)	Absorbance	C(t) (ppm)	E(t)
1	0	0.000	0.000	0.000
2	2	0.000	0.000	0.000
3	10	0.000	0.000	0.000
4	20	0.000	0.000	0.000
5	30	0.000	0.000	0.000
6	60	0.000	0.000	0.000
7	90	0.062	44.286	0.005
8	120	0.123	87.857	0.010
9	150	0.036	25.714	0.003
10	180	0.032	22.857	0.002
11	210	0.019	13.571	0.001
12	240	0.017	12.143	0.001
13	270	0.013	9.286	0.001
14	300	0.015	10.714	0.001
15	330	0.013	9.286	0.001
16	360	0.005	3.571	0.000
17	420	0.004	2.857	0.000
18	480	0.010	7.143	0.001
19	600	0.009	6.429	0.001
20	720	0.000	0.000	0.000

Appendix C.26: Hydraulic data from port 9,2.

Sample no.	Time (min)	Absorbance	C(t) (ppm)	E(t)
1	0	0.000	0.000	0.000
2	2	0.000	0.000	0.000
3	10	0.000	0.000	0.000
4	20	0.000	0.000	0.000
5	30	0.000	0.000	0.000
6	60	0.000	0.000	0.000
7	90	0.059	42.143	0.004
8	120	0.118	84.286	0.009
9	150	0.067	47.857	0.005
10	180	0.041	29.286	0.003
11	210	0.030	21.429	0.002
12	240	0.030	21.429	0.002
13	270	0.016	11.429	0.001
14	300	0.015	10.714	0.001
15	330	0.014	10.000	0.001
16	360	0.005	3.571	0.000
17	420	0.008	5.714	0.001
18	480	0.005	3.571	0.000
19	600	0.006	4.286	0.000
20	720	0.000	0.000	0.000

Appendix C.27: Hydraulic data from port 9,3.

Sample no.	Time (min)	Absorbance	C(t) (ppm)	E(t)
1	0	0.000	0.000	0.000
2	2	0.000	0.000	0.000
3	10	0.000	0.000	0.000
4	20	0.000	0.000	0.000
5	30	0.000	0.000	0.000
6	60	0.000	0.000	0.000
7	90	0.063	45.000	0.002
8	120	0.081	57.857	0.002
9	150	0.079	56.429	0.002
10	180	0.116	82.857	0.003
11	210	0.176	125.714	0.005
12	240	0.194	138.571	0.006
13	270	0.137	97.857	0.004
14	300	0.088	62.857	0.003
15	330	0.049	35.000	0.001
16	360	0.026	18.571	0.001
17	420	0.012	8.571	0.000
18	480	0.012	8.571	0.000
19	600	0.010	7.143	0.000
20	720	0.000	0.000	0.000

Appendix C.28: Hydraulic data from port 10,1.

Sample no.	Time (min)	Absorbance	C(t) (ppm)	E(t)
1	0	0.000	0.000	0.000
2	2	0.000	0.000	0.000
3	10	0.000	0.000	0.000
4	20	0.000	0.000	0.000
5	30	0.000	0.000	0.000
6	60	0.000	0.000	0.000
7	90	0.041	29.286	0.002
8	120	0.163	116.429	0.008
9	150	0.168	120.000	0.009
10	180	0.088	62.857	0.004
11	210	0.047	33.571	0.002
12	240	0.023	16.429	0.001
13	270	0.012	8.571	0.001
14	300	0.015	10.714	0.001
15	330	0.017	12.143	0.001
16	360	0.012	8.571	0.001
17	420	0.015	10.714	0.001
18	480	0.004	2.857	0.000
19	600	0.004	2.857	0.000
20	720	0.000	0.000	0.000

Appendix C.29: Hydraulic data from port 10,2.

Sample no.	Time (min)	Absorbance	C(t) (ppm)	E(t)
1	0	0.000	0.000	0.000
2	2	0.000	0.000	0.000
3	10	0.000	0.000	0.000
4	20	0.000	0.000	0.000
5	30	0.000	0.000	0.000
6	60	0.000	0.000	0.000
7	90	0.015	10.714	0.001
8	120	0.065	46.429	0.004
9	150	0.213	152.143	0.012
10	180	0.173	123.571	0.010
11	210	0.048	34.286	0.003
12	240	0.022	15.714	0.001
13	270	0.006	4.286	0.000
14	300	0.010	7.143	0.001
15	330	0.006	4.286	0.000
16	360	0.005	3.571	0.000
17	420	0.001	0.714	0.000
18	480	0.005	3.571	0.000
19	600	0.003	2.143	0.000
20	720	0.000	0.000	0.000

Appendix C.30: Hydraulic data from port 10,3.

Sample no.	Time (min)	Absorbance	C(t) (ppm)	E(t)
1	0	0.000	0.000	0.000
2	2	0.000	0.000	0.000
3	10	0.000	0.000	0.000
4	20	0.000	0.000	0.000
5	30	0.000	0.000	0.000
6	60	0.000	0.000	0.000
7	90	0.001	0.714	0.000
8	120	0.041	29.286	0.002
9	150	0.073	52.143	0.003
10	180	0.139	99.286	0.005
11	210	0.198	141.429	0.008
12	240	0.127	90.714	0.005
13	270	0.097	69.286	0.004
14	300	0.058	41.429	0.002
15	330	0.031	22.143	0.001
16	360	0.016	11.429	0.001
17	420	0.007	5.000	0.000
18	480	0.009	6.429	0.000
19	600	0.003	2.143	0.000
20	720	0.000	0.000	0.000

Appendix C.31: Hydraulic data from port 11,1.

Sample no.	Time (min)	Absorbance	C(t) (ppm)	E(t)
1	0	0.000	0.000	0.000
2	2	0.000	0.000	0.000
3	10	0.000	0.000	0.000
4	20	0.000	0.000	0.000
5	30	0.000	0.000	0.000
6	60	0.000	0.000	0.000
7	90	0.000	0.000	0.000
8	120	0.023	16.429	0.001
9	150	0.127	90.714	0.007
10	180	0.125	89.286	0.007
11	210	0.174	124.286	0.009
12	240	0.046	32.857	0.002
13	270	0.027	19.286	0.001
14	300	0.018	12.857	0.001
15	330	0.016	11.429	0.001
16	360	0.014	10.000	0.001
17	420	0.006	4.286	0.000
18	480	0.007	5.000	0.000
19	600	0.014	10.000	0.001
20	720	0.000	0.000	0.000

Appendix C.32: Hydraulic data from port 11,2.

Sample no.	Time (min)	Absorbance	C(t) (ppm)	E(t)
1	0	0.000	0.000	0.000
2	2	0.000	0.000	0.000
3	10	0.000	0.000	0.000
4	20	0.000	0.000	0.000
5	30	0.000	0.000	0.000
6	60	0.000	0.000	0.000
7	90	0.000	0.000	0.000
8	120	0.024	17.143	0.001
9	150	0.125	89.286	0.007
10	180	0.128	91.429	0.008
11	210	0.076	54.286	0.005
12	240	0.043	30.714	0.003
13	270	0.027	19.286	0.002
14	300	0.017	12.143	0.001
15	330	0.013	9.286	0.001
16	360	0.017	12.143	0.001
17	420	0.017	12.143	0.001
18	480	0.006	4.286	0.000
19	600	0.011	7.857	0.001
20	720	0.000	0.000	0.000

Appendix C.33: Hydraulic data from port 11,3.

Sample no.	Time (min)	Absorbance	C(t) (ppm)	E(t)
1	0	0.000	0.000	0.000
2	2	0.000	0.000	0.000
3	10	0.000	0.000	0.000
4	20	0.000	0.000	0.000
5	30	0.000	0.000	0.000
6	60	0.000	0.000	0.000
7	90	0.000	0.000	0.000
8	120	0.011	7.857	0.001
9	150	0.041	29.286	0.003
10	180	0.065	46.429	0.005
11	210	0.064	45.714	0.005
12	240	0.042	30.000	0.003
13	270	0.038	27.143	0.003
14	300	0.021	15.000	0.002
15	330	0.024	17.143	0.002
16	360	0.013	9.286	0.001
17	420	0.022	15.714	0.002
18	480	0.010	7.143	0.001
19	600	0.017	12.143	0.001
20	720	0.000	0.000	0.000

Appendix C.34: Hydraulic data from port 12,1.

Sample no.	Time (min)	Absorbance	C(t) (ppm)	E(t)
1	0	0.000	0.000	0.000
2	2	0.000	0.000	0.000
3	10	0.000	0.000	0.000
4	20	0.000	0.000	0.000
5	30	0.000	0.000	0.000
6	60	0.000	0.000	0.000
7	90	0.000	0.000	0.000
8	120	0.009	6.429	0.001
9	150	0.061	43.571	0.003
10	180	0.069	49.286	0.004
11	210	0.052	37.143	0.003
12	240	0.066	47.143	0.004
13	270	0.059	42.143	0.003
14	300	0.058	41.429	0.003
15	330	0.045	32.143	0.003
16	360	0.030	21.429	0.002
17	420	0.019	13.571	0.001
18	480	0.011	7.857	0.001
19	600	0.009	6.429	0.001
20	720	0.000	0.000	0.000

Appendix C.35: Hydraulic data from port 12,2.

Sample no.	Time (min)	Absorbance	C(t) (ppm)	E(t)
1	0	0.000	0.000	0.000
2	2	0.000	0.000	0.000
3	10	0.000	0.000	0.000
4	20	0.000	0.000	0.000
5	30	0.000	0.000	0.000
6	60	0.000	0.000	0.000
7	90	0.000	0.000	0.000
8	120	0.023	16.429	0.002
9	150	0.095	67.857	0.008
10	180	0.090	64.286	0.007
11	210	0.054	38.571	0.004
12	240	0.029	20.714	0.002
13	270	0.020	14.286	0.002
14	300	0.020	14.286	0.002
15	330	0.016	11.429	0.001
16	360	0.008	5.714	0.001
17	420	0.006	4.286	0.000
18	480	0.006	4.286	0.000
19	600	0.010	7.143	0.001
20	720	0.000	0.000	0.000

Appendix C.36: Hydraulic data from port 12,3.

Sample no.	Time (min)	Absorbance	C(t) (ppm)	E(t)
1	0	0.000	0.000	0.000
2	2	0.000	0.000	0.000
3	10	0.000	0.000	0.000
4	20	0.000	0.000	0.000
5	30	0.000	0.000	0.000
6	60	0.000	0.000	0.000
7	90	0.000	0.000	0.000
8	120	0.018	12.857	0.000
9	150	0.060	42.857	0.001
10	180	0.096	68.571	0.002
11	210	0.230	164.286	0.006
12	240	0.257	183.571	0.006
13	270	0.207	147.857	0.005
14	300	0.139	99.286	0.003
15	330	0.106	75.714	0.003
16	360	0.065	46.429	0.002
17	420	0.025	17.857	0.001
18	480	0.012	8.571	0.000
19	600	0.013	9.286	0.000
20	720	0.000	0.000	0.000

Appendix C.37: Hydraulic data from port 13,1.

Sample no.	Time (min)	Absorbance	C(t) (ppm)	E(t)
1	0	0.000	0.000	0.000
2	2	0.000	0.000	0.000
3	10	0.000	0.000	0.000
4	20	0.000	0.000	0.000
5	30	0.000	0.000	0.000
6	60	0.000	0.000	0.000
7	90	0.000	0.000	0.000
8	120	0.014	10.000	0.001
9	150	0.065	46.429	0.004
10	180	0.088	62.857	0.005
11	210	0.063	45.000	0.003
12	240	0.053	37.857	0.003
13	270	0.049	35.000	0.003
14	300	0.049	35.000	0.003
15	330	0.045	32.143	0.002
16	360	0.037	26.429	0.002
17	420	0.028	20.000	0.002
18	480	0.015	10.714	0.001
19	600	0.005	3.571	0.000
20	720	0.000	0.000	0.000

Appendix C.38: Hydraulic data from port 13,2.

Sample no.	Time (min)	Absorbance	C(t) (ppm)	E(t)
1	0	0.000	0.000	0.000
2	2	0.000	0.000	0.000
3	10	0.000	0.000	0.000
4	20	0.000	0.000	0.000
5	30	0.000	0.000	0.000
6	60	0.000	0.000	0.000
7	90	0.000	0.000	0.000
8	120	0.011	7.857	0.001
9	150	0.087	62.143	0.006
10	180	0.158	112.857	0.010
11	210	0.100	71.429	0.006
12	240	0.044	31.429	0.003
13	270	0.028	20.000	0.002
14	300	0.017	12.143	0.001
15	330	0.013	9.286	0.001
16	360	0.013	9.286	0.001
17	420	0.007	5.000	0.000
18	480	0.005	3.571	0.000
19	600	0.002	1.429	0.000
20	720	0.000	0.000	0.000

Appendix C.39: Hydraulic data from port 13,3.

Sample no.	Time (min)	Absorbance	C(t) (ppm)	E(t)
1	0	0.000	0.000	0.000
2	2	0.000	0.000	0.000
3	10	0.000	0.000	0.000
4	20	0.000	0.000	0.000
5	30	0.000	0.000	0.000
6	60	0.000	0.000	0.000
7	90	0.000	0.000	0.000
8	120	0.008	5.714	0.001
9	150	0.014	10.000	0.001
10	180	0.039	27.857	0.003
11	210	0.068	48.571	0.005
12	240	0.070	50.000	0.005
13	270	0.056	40.000	0.004
14	300	0.040	28.571	0.003
15	330	0.036	25.714	0.003
16	360	0.025	17.857	0.002
17	420	0.014	10.000	0.001
18	480	0.013	9.286	0.001
19	600	0.004	2.857	0.000
20	720	0.000	0.000	0.000

Appendix C.40: Hydraulic data from port 14.

Sample no.	Time (min)	Absorbance	C(t) (ppm)	E(t)
1	0	0.000	0.000	0.000
2	2	0.000	0.000	0.000
3	20	0.004	2.857	0.000
4	30	0.002	1.429	0.000
5	60	0.003	2.143	0.000
6	90	0.007	5.000	0.000
7	120	0.039	27.857	0.002
8	150	0.089	63.571	0.005
9	180	0.119	85.000	0.006
10	210	0.095	67.857	0.005
11	240	0.070	50.000	0.004
12	270	0.046	32.857	0.002
13	300	0.035	25.000	0.002
14	330	0.033	23.571	0.002
15	360	0.015	10.714	0.001
16	420	0.011	7.857	0.001
17	480	0.007	5.000	0.000
18	600	0.010	7.143	0.001
19	720	0.000	0.000	0.000

Appendix D: Hydraulic data from step change response experiment on unplanted HSSF CW.

Appendix D.1: Hydraulic data from port 1,1.

Sample no.	Time (min)	Absorbance	C(t) (ppm)	F(t)
1	0	0.000	0.000	0.000
2	2	0.001	0.714	0.006
3	15	0.170	121.429	0.971
4	30	0.175	125.000	1.000
5	60	0.175	125.000	1.000
6	90	0.175	125.000	1.000
7	120	0.175	125.000	1.000
8	150	0.175	125.000	1.000
9	180	0.175	125.000	1.000
10	240	0.175	125.000	1.000
11	300	0.171	122.143	0.977
12	360	0.175	125.000	1.000
13	420	0.175	125.000	1.000
14	480	0.175	125.000	1.000
15	600	0.173	123.571	0.989
16	720	0.175	125.000	1.000

Appendix D.2: Hydraulic data from port 1,2.

Sample no.	Time (min)	Absorbance	C(t) (ppm)	F(t)
1	0	0.000	0.000	0.000
2	2	0.010	7.143	0.057
3	15	0.161	115.000	0.920
4	30	0.173	123.571	0.989
5	60	0.175	125.000	1.000
6	90	0.175	125.000	1.000
7	120	0.173	123.571	0.989
8	150	0.175	125.000	1.000
9	180	0.175	125.000	1.000
10	240	0.175	125.000	1.000
11	300	0.175	125.000	1.000
12	360	0.172	122.857	0.983
13	420	0.175	125.000	1.000
14	480	0.175	125.000	1.000
15	600	0.164	117.143	0.937
16	720	0.175	125.000	1.000

Appendix D.3: Hydraulic data from port 1,3.

Sample no.	Time (min)	Absorbance	C(t) (ppm)	F(t)
1	0	0.000	0.000	0.000
2	2	0.002	1.429	0.011
3	15	0.072	51.429	0.411
4	30	0.093	66.429	0.531
5	60	0.164	117.143	0.937
6	90	0.175	125.000	1.000
7	120	0.175	125.000	1.000
8	150	0.175	125.000	1.000
9	180	0.173	123.571	0.989
10	240	0.175	125.000	1.000
11	300	0.168	120.000	0.960
12	360	0.175	125.000	1.000
13	420	0.175	125.000	1.000
14	480	0.175	125.000	1.000
15	600	0.168	120.000	0.960
16	720	0.175	125.000	1.000

Appendix D.4: Hydraulic data from port 2,1.

Sample no.	Time (min)	Absorbance	C(t) (ppm)	F(t)
1	0	0.000	0.000	0.000
2	2	0.001	0.714	0.006
3	15	0.000	0.000	0.000
4	30	0.086	61.429	0.491
5	60	0.163	116.429	0.931
6	90	0.167	119.286	0.954
7	120	0.156	111.429	0.891
8	150	0.165	117.857	0.943
9	180	0.169	120.714	0.966
10	240	0.171	122.143	0.977
11	300	0.160	114.286	0.914
12	360	0.172	122.857	0.983
13	420	0.175	125.000	1.000
14	480	0.170	121.429	0.971
15	600	0.172	122.857	0.983
16	720	0.175	125.000	1.000

Appendix D.5: Hydraulic data from port 2,2.

Sample no.	Time (min)	Absorbance	C(t) (ppm)	F(t)
1	0	0.000	0.000	0.000
2	2	0.001	0.714	0.006
3	15	0.000	0.000	0.000
4	30	0.036	25.714	0.216
5	60	0.142	101.429	0.850
6	90	0.156	111.429	0.934
7	120	0.154	110.000	0.922
8	150	0.161	115.000	0.964
9	180	0.167	119.286	1.000
10	240	0.167	119.286	1.000
11	300	0.166	118.571	0.994
12	360	0.166	118.571	0.994
13	420	0.167	119.286	1.000
14	480	0.167	119.286	1.000
15	600	0.167	119.286	1.000
16	720	0.167	119.286	1.000

Appendix D.6: Hydraulic data from port 2,3.

Sample no.	Time (min)	Absorbance	C(t) (ppm)	F(t)
1	0	0.000	0.000	0.000
2	2	0.001	0.714	0.006
3	15	0.000	0.000	0.000
4	30	0.049	35.000	0.295
5	60	0.076	54.286	0.458
6	90	0.134	95.714	0.807
7	120	0.143	102.143	0.861
8	150	0.156	111.429	0.940
9	180	0.161	115.000	0.970
10	240	0.166	118.571	1.000
11	300	0.164	117.143	0.988
12	360	0.165	117.857	0.994
13	420	0.166	118.571	1.000
14	480	0.166	118.571	1.000
15	600	0.166	118.571	1.000
16	720	0.166	118.571	1.000

Appendix D.7: Hydraulic data from port 3,1.

Sample no.	Time (min)	Absorbance	C(t) (ppm)	F(t)
1	0	0.000	0.000	0.000
2	2	0.002	1.429	0.012
3	15	0.000	0.000	0.000
4	30	0.020	14.286	0.117
5	60	0.171	122.143	1.000
6	90	0.165	117.857	0.965
7	120	0.164	117.143	0.959
8	150	0.170	121.429	0.994
9	180	0.171	122.143	1.000
10	240	0.171	122.143	1.000
11	300	0.171	122.143	1.000
12	360	0.171	122.143	1.000
13	420	0.171	122.143	1.000
14	480	0.171	122.143	1.000
15	600	0.169	120.714	0.988
16	720	0.171	122.143	1.000

Appendix D.8: Hydraulic data from port 3,2.

Sample no.	Time (min)	Absorbance	C(t) (ppm)	F(t)
1	0	0.000	0.000	0.000
2	2	0.003	2.143	0.018
3	15	0.000	0.000	0.000
4	30	0.045	32.143	0.269
5	60	0.151	107.857	0.904
6	90	0.167	119.286	1.000
7	120	0.161	115.000	0.964
8	150	0.166	118.571	0.994
9	180	0.167	119.286	1.000
10	240	0.167	119.286	1.000
11	300	0.167	119.286	1.000
12	360	0.167	119.286	1.000
13	420	0.167	119.286	1.000
14	480	0.167	119.286	1.000
15	600	0.166	118.571	0.994
16	720	0.167	119.286	1.000

Appendix D.9: Hydraulic data from port 3,3.

Sample no.	Time (min)	Absorbance	C(t) (ppm)	F(t)
1	0	0.000	0.000	0.000
2	2	0.005	3.571	0.029
3	15	0.000	0.000	0.000
4	30	0.014	10.000	0.080
5	60	0.070	50.000	0.402
6	90	0.117	83.571	0.672
7	120	0.142	101.429	0.816
8	150	0.160	114.286	0.920
9	180	0.172	122.857	0.989
10	240	0.169	120.714	0.971
11	300	0.166	118.571	0.954
12	360	0.164	117.143	0.943
13	420	0.172	122.857	0.989
14	480	0.174	124.286	1.000
15	600	0.173	123.571	0.994
16	720	0.174	124.286	1.000

Appendix D.10: Hydraulic data from port 4,1.

Sample no.	Time (min)	Absorbance	C(t) (ppm)	F(t)
1	0	0.000	0.000	0.000
2	2	0.002	1.429	0.011
3	15	0.000	0.000	0.000
4	30	0.002	1.429	0.011
5	60	0.107	76.429	0.615
6	90	0.153	109.286	0.879
7	120	0.163	116.429	0.937
8	150	0.173	123.571	0.994
9	180	0.172	122.857	0.989
10	210	0.167	119.286	0.960
11	240	0.163	116.429	0.937
12	270	0.165	117.857	0.948
13	300	0.171	122.143	0.983
14	330	0.163	116.429	0.937
15	360	0.174	124.286	1.000
16	420	0.174	124.286	1.000
17	480	0.174	124.286	1.000
18	600	0.171	122.143	0.983
19	720	0.174	124.286	1.000

Appendix D.11: Hydraulic data from port 4,2.

Sample no.	Time (min)	Absorbance	C(t) (ppm)	F(t)
1	0	0.000	0.000	0.000
2	2	0.001	0.714	0.006
3	15	0.000	0.000	0.000
4	30	0.003	2.143	0.018
5	60	0.050	35.714	0.298
6	90	0.145	103.571	0.863
7	120	0.156	111.429	0.929
8	150	0.165	117.857	0.982
9	180	0.166	118.571	0.988
10	210	0.168	120.000	1.000
11	240	0.168	120.000	1.000
12	270	0.153	109.286	0.911
13	300	0.168	120.000	1.000
14	330	0.168	120.000	1.000
15	360	0.168	120.000	1.000
16	420	0.168	120.000	1.000
17	480	0.168	120.000	1.000
18	600	0.168	120.000	1.000
19	720	0.168	120.000	1.000

Appendix D.12: Hydraulic data from port 4,3.

Sample no.	Time (min)	Absorbance	C(t) (ppm)	F(t)
1	0	0.000	0.000	0.000
2	2	0.001	0.714	0.006
3	15	0.000	0.000	0.000
4	30	0.006	4.286	0.036
5	60	0.007	5.000	0.042
6	90	0.042	30.000	0.253
7	120	0.035	25.000	0.211
8	150	0.071	50.714	0.428
9	180	0.104	74.286	0.627
10	210	0.139	99.286	0.837
11	240	0.166	118.571	1.000
12	270	0.166	118.571	1.000
13	300	0.166	118.571	1.000
14	330	0.155	110.714	0.934
15	360	0.166	118.571	1.000
16	420	0.166	118.571	1.000
17	480	0.166	118.571	1.000
18	600	0.166	118.571	1.000
19	720	0.166	118.571	1.000

Appendix D.13: Hydraulic data from port 5,1.

Sample no.	Time (min)	Absorbance	C(t) (ppm)	F(t)
1	0	0.000	0.000	0.000
2	2	0.000	0.000	0.000
3	15	0.000	0.000	0.000
4	30	0.000	0.000	0.000
5	60	0.000	0.000	0.000
6	90	0.042	30.000	0.250
7	120	0.124	88.571	0.738
8	150	0.148	105.714	0.881
9	180	0.153	109.286	0.911
10	210	0.160	114.286	0.952
11	240	0.159	113.571	0.946
12	270	0.156	111.429	0.929
13	300	0.152	108.571	0.905
14	330	0.150	107.143	0.893
15	360	0.168	120.000	1.000
16	420	0.168	120.000	1.000
17	480	0.163	116.429	0.970
18	600	0.162	115.714	0.964
19	720	0.168	120.000	1.000

Appendix D.14: Hydraulic data from port 5,2.

Sample no.	Time (min)	Absorbance	C(t) (ppm)	F(t)
1	0	0.000	0.000	0.000
2	2	0.000	0.000	0.000
3	15	0.000	0.000	0.000
4	30	0.000	0.000	0.000
5	60	0.001	0.714	0.006
6	90	0.055	39.286	0.320
7	120	0.124	88.571	0.721
8	150	0.150	107.143	0.872
9	180	0.153	109.286	0.890
10	210	0.158	112.857	0.919
11	240	0.163	116.429	0.948
12	270	0.158	112.857	0.919
13	300	0.154	110.000	0.895
14	330	0.164	117.143	0.953
15	360	0.159	113.571	0.924
16	420	0.171	122.143	0.994
17	480	0.171	122.143	0.994
18	600	0.171	122.143	0.994
19	720	0.172	122.857	1.000

Appendix D.15: Hydraulic data from port 5,3.

Sample no.	Time (min)	Absorbance	C(t) (ppm)	F(t)
1	0	0.000	0.000	0.000
2	2	0.000	0.000	0.000
3	15	0.000	0.000	0.000
4	30	0.000	0.000	0.000
5	60	0.004	2.857	0.025
6	90	0.067	47.857	0.416
7	120	0.136	97.143	0.845
8	150	0.124	88.571	0.770
9	180	0.160	114.286	0.994
10	210	0.151	107.857	0.938
11	240	0.156	111.429	0.969
12	270	0.153	109.286	0.950
13	300	0.158	112.857	0.981
14	330	0.161	115.000	1.000
15	360	0.161	115.000	1.000
16	420	0.161	115.000	1.000
17	480	0.161	115.000	1.000
18	600	0.161	115.000	1.000
19	720	0.161	115.000	1.000

Appendix D.16: Hydraulic data from port 6,1.

Sample no.	Time (min)	Absorbance	C(t) (ppm)	F(t)
1	0	0.000	0.000	0.000
2	2	0.000	0.000	0.000
3	15	0.000	0.000	0.000
4	30	0.000	0.000	0.000
5	60	0.004	2.857	0.023
6	90	0.054	38.571	0.316
7	120	0.102	72.857	0.596
8	150	0.150	107.143	0.877
9	180	0.166	118.571	0.971
10	210	0.171	122.143	1.000
11	240	0.169	120.714	0.988
12	270	0.165	117.857	0.965
13	300	0.158	112.857	0.924
14	330	0.155	110.714	0.906
15	360	0.166	118.571	0.971
16	420	0.165	117.857	0.965
17	480	0.171	122.143	1.000
18	600	0.166	118.571	0.971
19	720	0.171	122.143	1.000

Appendix D.17: Hydraulic data from port 6,2.

Sample no.	Time (min)	Absorbance	C(t) (ppm)	F(t)
1	0	0.000	0.000	0.000
2	2	0.000	0.000	0.000
3	15	0.000	0.000	0.000
4	30	0.000	0.000	0.000
5	60	0.008	5.714	0.048
6	90	0.103	73.571	0.613
7	120	0.122	87.143	0.726
8	150	0.148	105.714	0.881
9	180	0.158	112.857	0.940
10	210	0.168	120.000	1.000
11	240	0.167	119.286	0.994
12	270	0.164	117.143	0.976
13	300	0.162	115.714	0.964
14	330	0.167	119.286	0.994
15	360	0.168	120.000	1.000
16	420	0.168	120.000	1.000
17	480	0.168	120.000	1.000
18	600	0.168	120.000	1.000
19	720	0.168	120.000	1.000

Appendix D.18: Hydraulic data from port 6,3.

Sample no.	Time (min)	Absorbance	C(t) (ppm)	F(t)
1	0	0.000	0.000	0.000
2	2	0.000	0.000	0.000
3	15	0.000	0.000	0.000
4	30	0.000	0.000	0.000
5	60	0.023	16.429	0.133
6	90	0.105	75.000	0.607
7	120	0.134	95.714	0.775
8	150	0.145	103.571	0.838
9	180	0.149	106.429	0.861
10	210	0.154	110.000	0.890
11	240	0.149	106.429	0.861
12	270	0.149	106.429	0.861
13	300	0.147	105.000	0.850
14	330	0.141	100.714	0.815
15	360	0.158	112.857	0.913
16	420	0.162	115.714	0.936
17	480	0.168	120.000	0.971
18	600	0.170	121.429	0.983
19	720	0.173	123.571	1.000

Appendix D.19: Hydraulic data from port 7,1.

Sample no.	Time (min)	Absorbance	C(t) (ppm)	F(t)
1	0	0.000	0.000	0.000
2	2	0.000	0.000	0.000
3	15	0.000	0.000	0.000
4	30	0.000	0.000	0.000
5	60	0.003	2.143	0.018
6	90	0.007	5.000	0.042
7	120	0.027	19.286	0.161
8	150	0.095	67.857	0.565
9	180	0.135	96.429	0.804
10	210	0.149	106.429	0.887
11	240	0.158	112.857	0.940
12	270	0.150	107.143	0.893
13	300	0.150	107.143	0.893
14	330	0.152	108.571	0.905
15	360	0.153	109.286	0.911
16	420	0.159	113.571	0.946
17	480	0.164	117.143	0.976
18	600	0.164	117.143	0.976
19	720	0.168	120.000	1.000

Appendix D.20: Hydraulic data from port 7,2.

Sample no.	Time (min)	Absorbance	C(t) (ppm)	F(t)
1	0	0.000	0.000	0.000
2	2	0.000	0.000	0.000
3	15	0.000	0.000	0.000
4	30	0.000	0.000	0.000
5	60	0.000	0.000	0.000
6	90	0.020	14.286	0.127
7	120	0.053	37.857	0.338
8	150	0.044	31.429	0.280
9	180	0.085	60.714	0.541
10	210	0.140	100.000	0.892
11	240	0.157	112.143	1.000
12	270	0.157	112.143	1.000
13	300	0.157	112.143	1.000
14	330	0.157	112.143	1.000
15	360	0.157	112.143	1.000
16	420	0.157	112.143	1.000
17	480	0.157	112.143	1.000
18	600	0.157	112.143	1.000
19	720	0.157	112.143	1.000

Appendix D.21: Hydraulic data from port 7,3.

Sample no.	Time (min)	Absorbance	C(t) (ppm)	F(t)
1	0	0.000	0.000	0.000
2	2	0.000	0.000	0.000
3	15	0.000	0.000	0.000
4	30	0.000	0.000	0.000
5	60	0.001	0.714	0.006
6	90	0.015	10.714	0.084
7	120	0.034	24.286	0.190
8	150	0.074	52.857	0.413
9	180	0.094	67.143	0.525
10	210	0.090	64.286	0.503
11	240	0.104	74.286	0.581
12	270	0.121	86.429	0.676
13	300	0.127	90.714	0.709
14	330	0.138	98.571	0.771
15	360	0.157	112.143	0.877
16	420	0.164	117.143	0.916
17	480	0.166	118.571	0.927
18	600	0.162	115.714	0.905
19	720	0.179	127.857	1.000

Appendix D.22: Hydraulic data from port 8,1.

Sample no.	Time (min)	Absorbance	C(t) (ppm)	F(t)
1	0	0.000	0.000	0.000
2	2	0.000	0.000	0.000
3	15	0.000	0.000	0.000
4	30	0.000	0.000	0.000
5	60	0.000	0.000	0.000
6	90	0.000	0.000	0.000
7	120	0.014	10.000	0.085
8	150	0.034	24.286	0.207
9	180	0.076	54.286	0.463
10	210	0.112	80.000	0.683
11	240	0.129	92.143	0.787
12	270	0.142	101.429	0.866
13	300	0.135	96.429	0.823
14	330	0.138	98.571	0.841
15	360	0.149	106.429	0.909
16	420	0.156	111.429	0.951
17	480	0.154	110.000	0.939
18	540	0.157	112.143	0.957
19	600	0.163	116.429	0.994
20	720	0.164	117.143	1.000

Appendix D.23: Hydraulic data from port 8,2.

Sample no.	Time (min)	Absorbance	C(t) (ppm)	F(t)
1	0	0.000	0.000	0.000
2	2	0.000	0.000	0.000
3	15	0.000	0.000	0.000
4	30	0.000	0.000	0.000
5	60	0.000	0.000	0.000
6	90	0.000	0.000	0.000
7	120	0.013	9.286	0.082
8	150	0.067	47.857	0.424
9	180	0.090	64.286	0.570
10	210	0.138	98.571	0.873
11	240	0.148	105.714	0.937
12	270	0.154	110.000	0.975
13	300	0.151	107.857	0.956
14	330	0.141	100.714	0.892
15	360	0.152	108.571	0.962
16	420	0.158	112.857	1.000
17	480	0.158	112.857	1.000
18	540	0.158	112.857	1.000
19	600	0.158	112.857	1.000
20	720	0.158	112.857	1.000

Appendix D.24: Hydraulic data from port 8,3.

Sample no.	Time (min)	Absorbance	C(t) (ppm)	F(t)
1	0	0.000	0.000	0.000
2	2	0.000	0.000	0.000
3	15	0.000	0.000	0.000
4	30	0.000	0.000	0.000
5	60	0.000	0.000	0.000
6	90	0.000	0.000	0.000
7	120	0.033	23.571	0.201
8	150	0.074	52.857	0.451
9	180	0.095	67.857	0.579
10	210	0.137	97.857	0.835
11	240	0.146	104.286	0.890
12	270	0.150	107.143	0.915
13	300	0.153	109.286	0.933
14	330	0.145	103.571	0.884
15	360	0.162	115.714	0.988
16	420	0.161	115.000	0.982
17	480	0.160	114.286	0.976
18	540	0.164	117.143	1.000
19	600	0.161	115.000	0.982
20	720	0.164	117.143	1.000

Appendix D.25: Hydraulic data from port 9,1.

Sample no.	Time (min)	Absorbance	C(t) (ppm)	F(t)
1	0	0.000	0.000	0.000
2	2	0.000	0.000	0.000
3	15	0.000	0.000	0.000
4	30	0.000	0.000	0.000
5	60	0.000	0.000	0.000
6	90	0.000	0.000	0.000
7	120	0.012	8.571	0.071
8	150	0.076	54.286	0.452
9	180	0.115	82.143	0.685
10	210	0.141	100.714	0.839
11	240	0.154	110.000	0.917
12	270	0.150	107.143	0.893
13	300	0.147	105.000	0.875
14	330	0.144	102.857	0.857
15	360	0.160	114.286	0.952
16	420	0.160	114.286	0.952
17	480	0.168	120.000	1.000
18	540	0.159	113.571	0.946
19	600	0.162	115.714	0.964
20	720	0.168	120.000	1.000

Appendix D.26: Hydraulic data from port 9,2.

Sample no.	Time (min)	Absorbance	C(t) (ppm)	F(t)
1	0	0.000	0.000	0.000
2	2	0.000	0.000	0.000
3	15	0.000	0.000	0.000
4	30	0.000	0.000	0.000
5	60	0.000	0.000	0.000
6	90	0.000	0.000	0.000
7	120	0.020	14.286	0.122
8	150	0.065	46.429	0.396
9	180	0.097	69.286	0.591
10	210	0.130	92.857	0.793
11	240	0.145	103.571	0.884
12	270	0.141	100.714	0.860
13	300	0.141	100.714	0.860
14	330	0.142	101.429	0.866
15	360	0.158	112.857	0.963
16	420	0.164	117.143	1.000
17	480	0.164	117.143	1.000
18	540	0.161	115.000	0.982
19	600	0.159	113.571	0.970
20	720	0.164	117.143	1.000

Appendix D.27: Hydraulic data from port 9,3.

Sample no.	Time (min)	Absorbance	C(t) (ppm)	F(t)
1	0	0.000	0.000	0.000
2	2	0.000	0.000	0.000
3	15	0.000	0.000	0.000
4	30	0.000	0.000	0.000
5	60	0.000	0.000	0.000
6	90	0.000	0.000	0.000
7	120	0.027	19.286	0.162
8	150	0.089	63.571	0.533
9	180	0.111	79.286	0.665
10	210	0.141	100.714	0.844
11	240	0.147	105.000	0.880
12	270	0.147	105.000	0.880
13	300	0.144	102.857	0.862
14	330	0.129	92.143	0.772
15	360	0.167	119.286	1.000
16	420	0.156	111.429	0.934
17	480	0.162	115.714	0.970
18	540	0.158	112.857	0.946
19	600	0.163	116.429	0.976
20	720	0.167	119.286	1.000

Appendix D.28: Hydraulic data from port 10,1.

Sample no.	Time (min)	Absorbance	C(t) (ppm)	F(t)
1	0	0.000	0.000	0.000
2	2	0.000	0.000	0.000
3	15	0.000	0.000	0.000
4	30	0.000	0.000	0.000
5	60	0.000	0.000	0.000
6	90	0.000	0.000	0.000
7	120	0.000	0.000	0.000
8	150	0.019	13.571	0.117
9	180	0.034	24.286	0.209
10	210	0.059	42.143	0.362
11	240	0.120	85.714	0.736
12	270	0.131	93.571	0.804
13	300	0.141	100.714	0.865
14	330	0.148	105.714	0.908
15	360	0.152	108.571	0.933
16	390	0.151	107.857	0.926
17	420	0.163	116.429	1.000
18	480	0.148	105.714	0.908
19	540	0.153	109.286	0.939
20	600	0.156	111.429	0.957
21	720	0.163	116.429	1.000

Appendix D.29: Hydraulic data from port 10,2.

Sample no.	Time (min)	Absorbance	C(t) (ppm)	F(t)
1	0	0.000	0.000	0.000
2	2	0.000	0.000	0.000
3	15	0.000	0.000	0.000
4	30	0.000	0.000	0.000
5	60	0.000	0.000	0.000
6	90	0.000	0.000	0.000
7	120	0.000	0.000	0.000
8	150	0.029	20.714	0.177
9	180	0.045	32.143	0.274
10	210	0.085	60.714	0.518
11	240	0.120	85.714	0.732
12	270	0.135	96.429	0.823
13	300	0.141	100.714	0.860
14	330	0.155	110.714	0.945
15	360	0.159	113.571	0.970
16	390	0.154	110.000	0.939
17	420	0.156	111.429	0.951
18	480	0.151	107.857	0.921
19	540	0.154	110.000	0.939
20	600	0.163	116.429	0.994
21	720	0.164	117.143	1.000

Appendix D.30: Hydraulic data from port 10,3.

Sample no.	Time (min)	Absorbance	C(t) (ppm)	F(t)
1	0	0.000	0.000	0.000
2	2	0.000	0.000	0.000
3	15	0.000	0.000	0.000
4	30	0.000	0.000	0.000
5	60	0.000	0.000	0.000
6	90	0.000	0.000	0.000
7	120	0.000	0.000	0.000
8	150	0.026	18.571	0.167
9	180	0.055	39.286	0.353
10	210	0.090	64.286	0.577
11	240	0.106	75.714	0.679
12	270	0.103	73.571	0.660
13	300	0.107	76.429	0.686
14	330	0.105	75.000	0.673
15	360	0.122	87.143	0.782
16	390	0.132	94.286	0.846
17	420	0.155	110.714	0.994
18	480	0.156	111.429	1.000
19	540	0.156	111.429	1.000
20	600	0.156	111.429	1.000
21	720	0.156	111.429	1.000

Appendix D.31: Hydraulic data from port 11,1.

Sample no.	Time (min)	Absorbance	C(t) (ppm)	F(t)
1	0	0.000	0.000	0.000
2	2	0.000	0.000	0.000
3	15	0.000	0.000	0.000
4	30	0.000	0.000	0.000
5	60	0.000	0.000	0.000
6	90	0.000	0.000	0.000
7	120	0.000	0.000	0.000
8	150	0.000	0.000	0.000
9	180	0.006	4.286	0.038
10	210	0.022	15.714	0.141
11	240	0.043	30.714	0.276
12	270	0.068	48.571	0.436
13	300	0.083	59.286	0.532
14	330	0.108	77.143	0.692
15	360	0.136	97.143	0.872
16	390	0.137	97.857	0.878
17	420	0.130	92.857	0.833
18	480	0.138	98.571	0.885
19	540	0.146	104.286	0.936
20	600	0.150	107.143	0.962
21	720	0.156	111.429	1.000

Appendix D.32: Hydraulic data from port 11,2.

Sample no.	Time (min)	Absorbance	C(t) (ppm)	F(t)
1	0	0.000	0.000	0.000
2	2	0.000	0.000	0.000
3	15	0.000	0.000	0.000
4	30	0.000	0.000	0.000
5	60	0.000	0.000	0.000
6	90	0.000	0.000	0.000
7	120	0.000	0.000	0.000
8	150	0.000	0.000	0.000
9	180	0.039	27.857	0.248
10	210	0.074	52.857	0.471
11	240	0.099	70.714	0.631
12	270	0.113	80.714	0.720
13	300	0.133	95.000	0.847
14	330	0.133	95.000	0.847
15	360	0.145	103.571	0.924
16	390	0.145	103.571	0.924
17	420	0.147	105.000	0.936
18	480	0.150	107.143	0.955
19	540	0.157	112.143	1.000
20	600	0.157	112.143	1.000
21	720	0.157	112.143	1.000

Appendix D.33: Hydraulic data from port 11,3.

Sample no.	Time (min)	Absorbance	C(t) (ppm)	F(t)
1	0	0.000	0.000	0.000
2	2	0.000	0.000	0.000
3	15	0.000	0.000	0.000
4	30	0.000	0.000	0.000
5	60	0.000	0.000	0.000
6	90	0.000	0.000	0.000
7	120	0.000	0.000	0.000
8	150	0.000	0.000	0.000
9	180	0.019	13.571	0.115
10	210	0.059	42.143	0.358
11	240	0.095	67.857	0.576
12	270	0.110	78.571	0.667
13	300	0.122	87.143	0.739
14	330	0.129	92.143	0.782
15	360	0.144	102.857	0.873
16	390	0.146	104.286	0.885
17	420	0.158	112.857	0.958
18	480	0.152	108.571	0.921
19	540	0.157	112.143	0.952
20	600	0.152	108.571	0.921
21	720	0.165	117.857	1.000

Appendix D.34: Hydraulic data from port 12,1.

Sample no.	Time (min)	Absorbance	C(t) (ppm)	F(t)
1	0	0.000	0.000	0.000
2	2	0.000	0.000	0.000
3	15	0.000	0.000	0.000
4	30	0.000	0.000	0.000
5	60	0.000	0.000	0.000
6	90	0.000	0.000	0.000
7	120	0.000	0.000	0.000
8	150	0.000	0.000	0.000
9	180	0.011	7.857	0.069
10	210	0.068	48.571	0.425
11	240	0.088	62.857	0.550
12	270	0.106	75.714	0.663
13	300	0.112	80.000	0.700
14	330	0.119	85.000	0.744
15	360	0.133	95.000	0.831
16	390	0.132	94.286	0.825
17	420	0.139	99.286	0.869
18	480	0.154	110.000	0.963
19	540	0.148	105.714	0.925
20	600	0.156	111.429	0.975
21	720	0.160	114.286	1.000

Appendix D.35: Hydraulic data from port 12,2.

Sample no.	Time (min)	Absorbance	C(t) (ppm)	F(t)
1	0	0.000	0.000	0.000
2	2	0.000	0.000	0.000
3	15	0.000	0.000	0.000
4	30	0.000	0.000	0.000
5	60	0.000	0.000	0.000
6	90	0.000	0.000	0.000
7	120	0.000	0.000	0.000
8	150	0.000	0.000	0.000
9	180	0.015	10.714	0.093
10	210	0.040	28.571	0.248
11	240	0.070	50.000	0.435
12	270	0.086	61.429	0.534
13	300	0.097	69.286	0.602
14	330	0.095	67.857	0.590
15	360	0.125	89.286	0.776
16	390	0.129	92.143	0.801
17	420	0.149	106.429	0.925
18	480	0.155	110.714	0.963
19	540	0.157	112.143	0.975
20	600	0.156	111.429	0.969
21	720	0.161	115.000	1.000

Appendix D.36: Hydraulic data from port 12,3.

Sample no.	Time (min)	Absorbance	C(t) (ppm)	F(t)
1	0	0.000	0.000	0.000
2	2	0.000	0.000	0.000
3	15	0.000	0.000	0.000
4	30	0.000	0.000	0.000
5	60	0.000	0.000	0.000
6	90	0.000	0.000	0.000
7	120	0.000	0.000	0.000
8	150	0.000	0.000	0.000
9	180	0.066	47.143	0.407
10	210	0.071	50.714	0.438
11	240	0.098	70.000	0.605
12	270	0.109	77.857	0.673
13	300	0.125	89.286	0.772
14	330	0.132	94.286	0.815
15	360	0.149	106.429	0.920
16	390	0.141	100.714	0.870
17	420	0.147	105.000	0.907
18	480	0.153	109.286	0.944
19	540	0.148	105.714	0.914
20	600	0.162	115.714	1.000
21	720	0.162	115.714	1.000

Appendix D.37: Hydraulic data from port 13,1.

Sample no.	Time (min)	Absorbance	C(t) (ppm)	F(t)
1	0	0.000	0.000	0.000
2	2	0.000	0.000	0.000
3	15	0.000	0.000	0.000
4	30	0.000	0.000	0.000
5	60	0.000	0.000	0.000
6	90	0.000	0.000	0.000
7	120	0.000	0.000	0.000
8	150	0.000	0.000	0.000
9	180	0.003	2.143	0.018
10	210	0.005	3.571	0.030
11	240	0.012	8.571	0.072
12	270	0.026	18.571	0.156
13	300	0.032	22.857	0.192
14	330	0.036	25.714	0.216
15	360	0.043	30.714	0.257
16	390	0.042	30.000	0.251
17	420	0.084	60.000	0.503
18	480	0.133	95.000	0.796
19	540	0.133	95.000	0.796
20	600	0.142	101.429	0.850
21	720	0.167	119.286	1.000

Appendix D.38: Hydraulic data from port 13,2.

Sample no.	Time (min)	Absorbance	C(t) (ppm)	F(t)
1	0	0.000	0.000	0.000
2	2	0.000	0.000	0.000
3	15	0.000	0.000	0.000
4	30	0.000	0.000	0.000
5	60	0.000	0.000	0.000
6	90	0.000	0.000	0.000
7	120	0.000	0.000	0.000
8	150	0.000	0.000	0.000
9	180	0.020	14.286	0.131
10	210	0.041	29.286	0.268
11	240	0.059	42.143	0.386
12	270	0.068	48.571	0.444
13	300	0.077	55.000	0.503
14	330	0.099	70.714	0.647
15	360	0.109	77.857	0.712
16	390	0.115	82.143	0.752
17	420	0.119	85.000	0.778
18	480	0.133	95.000	0.869
19	540	0.143	102.143	0.935
20	600	0.153	109.286	1.000
21	720	0.153	109.286	1.000

Appendix D.39: Hydraulic data from port 13,3.

Sample no.	Time (min)	Absorbance	C(t) (ppm)	F(t)
1	0	0.000	0.000	0.000
2	2	0.000	0.000	0.000
3	15	0.000	0.000	0.000
4	30	0.000	0.000	0.000
5	60	0.000	0.000	0.000
6	90	0.000	0.000	0.000
7	120	0.000	0.000	0.000
8	150	0.000	0.000	0.000
9	180	0.019	13.571	0.127
10	210	0.053	37.857	0.353
11	240	0.082	58.571	0.547
12	270	0.097	69.286	0.647
13	300	0.087	62.143	0.580
14	330	0.091	65.000	0.607
15	360	0.120	85.714	0.800
16	390	0.128	91.429	0.853
17	420	0.150	107.143	1.000
18	480	0.150	107.143	1.000
19	540	0.148	105.714	0.987
20	600	0.150	107.143	1.000
21	720	0.150	107.143	1.000

Appendix D.40: Hydraulic data from port 14.

Sample no.	Time (min)	Absorbance	C(t) (ppm)	F(t)
1	0	0.000	0.000	0.000
2	2	0.000	0.000	0.000
3	30	0.003	2.143	0.020
4	60	0.001	0.714	0.007
5	90	0.007	5.000	0.046
6	120	0.004	2.857	0.026
7	150	0.005	3.571	0.033
8	180	0.007	5.000	0.046
9	210	0.024	17.143	0.158
10	240	0.046	32.857	0.303
11	270	0.066	47.143	0.434
12	300	0.078	55.714	0.513
13	330	0.091	65.000	0.599
14	360	0.115	82.143	0.757
15	390	0.115	82.143	0.757
16	420	0.132	94.286	0.868
17	480	0.139	99.286	0.914
18	540	0.145	103.571	0.954
19	600	0.151	107.857	0.993
20	720	0.152	108.571	1.000

Appendix E: Hydraulic data from step change response experiment on planted HSSF CW.

Appendix E.1: Hydraulic data from port 1,1.

Sample no.	Time (min)	Absorbance	C(t) (ppm)	F(t)
1	0	0.000	0.000	0.000
2	2	0.000	0.000	0.000
3	15	0.205	146.429	1.000
4	30	0.205	146.429	1.000
5	60	0.204	145.714	0.995
6	90	0.205	146.429	1.000
7	120	0.203	145.000	0.990
8	150	0.205	146.429	1.000
9	180	0.205	146.429	1.000
10	270	0.205	146.429	1.000
11	300	0.205	146.429	1.000
12	360	0.205	146.429	1.000
13	420	0.205	146.429	1.000
14	480	0.202	144.286	0.985
15	600	0.205	146.429	1.000
16	720	0.205	146.429	1.000

Appendix E.2: Hydraulic data from port 1,2.

Sample no.	Time (min)	Absorbance	C(t) (ppm)	F(t)
1	0	0.000	0.000	0.000
2	2	0.002	1.429	0.010
3	15	0.137	97.857	0.662
4	30	0.191	136.429	0.923
5	60	0.207	147.857	1.000
6	90	0.207	147.857	1.000
7	120	0.207	147.857	1.000
8	150	0.207	147.857	1.000
9	180	0.207	147.857	1.000
10	270	0.207	147.857	1.000
11	300	0.207	147.857	1.000
12	360	0.207	147.857	1.000
13	420	0.198	141.429	0.957
14	480	0.207	147.857	1.000
15	600	0.207	147.857	1.000
16	720	0.207	147.857	1.000

Appendix E.3: Hydraulic data from port 1,3.

Sample no.	Time (min)	Absorbance	C(t) (ppm)	F(t)
1	0	0.000	0.000	0.000
2	2	0.001	0.714	0.005
3	15	0.026	18.571	0.124
4	30	0.078	55.714	0.373
5	60	0.167	119.286	0.799
6	90	0.190	135.714	0.909
7	120	0.203	145.000	0.971
8	150	0.209	149.286	1.000
9	180	0.205	146.429	0.981
10	270	0.202	144.286	0.967
11	300	0.209	149.286	1.000
12	360	0.208	148.571	0.995
13	420	0.183	130.714	0.876
14	480	0.208	148.571	0.995
15	600	0.209	149.286	1.000
16	720	0.209	149.286	1.000

Appendix E.4: Hydraulic data from port 2,1.

Sample no.	Time (min)	Absorbance	C(t) (ppm)	F(t)
1	0	0.000	0.000	0.000
2	2	0.005	3.571	0.024
3	15	0.121	86.429	0.585
4	30	0.187	133.571	0.903
5	60	0.201	143.571	0.971
6	90	0.207	147.857	1.000
7	120	0.205	146.429	0.990
8	150	0.207	147.857	1.000
9	180	0.198	141.429	0.957
10	270	0.207	147.857	1.000
11	300	0.207	147.857	1.000
12	360	0.207	147.857	1.000
13	420	0.207	147.857	1.000
14	480	0.206	147.143	0.995
15	600	0.206	147.143	0.995
16	720	0.207	147.857	1.000

Appendix E.5: Hydraulic data from port 2,2.

Sample no.	Time (min)	Absorbance	C(t) (ppm)	F(t)
1	0	0.000	0.000	0.000
2	2	0.000	0.000	0.000
3	15	0.052	37.143	0.255
4	30	0.167	119.286	0.819
5	60	0.187	133.571	0.917
6	90	0.196	140.000	0.961
7	120	0.204	145.714	1.000
8	150	0.204	145.714	1.000
9	180	0.204	145.714	1.000
10	270	0.204	145.714	1.000
11	300	0.204	145.714	1.000
12	360	0.203	145.000	0.995
13	420	0.204	145.714	1.000
14	480	0.203	145.000	0.995
15	600	0.204	145.714	1.000
16	720	0.204	145.714	1.000

Appendix E.6: Hydraulic data from port 2,3.

Sample no.	Time (min)	Absorbance	C(t) (ppm)	F(t)
1	0	0.000	0.000	0.000
2	2	0.001	0.714	0.005
3	15	0.006	4.286	0.030
4	30	0.004	2.857	0.020
5	60	0.021	15.000	0.105
6	90	0.068	48.571	0.340
7	120	0.118	84.286	0.590
8	150	0.155	110.714	0.775
9	180	0.172	122.857	0.860
10	270	0.200	142.857	1.000
11	300	0.200	142.857	1.000
12	360	0.200	142.857	1.000
13	420	0.199	142.143	0.995
14	480	0.200	142.857	1.000
15	600	0.200	142.857	1.000
16	720	0.200	142.857	1.000

Appendix E.7: Hydraulic data from port 3,1.

Sample no.	Time (min)	Absorbance	C(t) (ppm)	F(t)
1	0	0.000	0.000	0.000
2	2	0.003	2.143	0.014
3	15	0.024	17.143	0.116
4	30	0.183	130.714	0.884
5	60	0.203	145.000	0.981
6	90	0.206	147.143	0.995
7	120	0.202	144.286	0.976
8	150	0.207	147.857	1.000
9	180	0.205	146.429	0.990
10	270	0.201	143.571	0.971
11	300	0.207	147.857	1.000
12	360	0.207	147.857	1.000
13	420	0.207	147.857	1.000
14	480	0.207	147.857	1.000
15	600	0.207	147.857	1.000
16	720	0.207	147.857	1.000

Appendix E.8: Hydraulic data from port 3,2.

Sample no.	Time (min)	Absorbance	C(t) (ppm)	F(t)
1	0	0.000	0.000	0.000
2	2	0.003	2.143	0.014
3	15	0.009	6.429	0.043
4	30	0.105	75.000	0.505
5	60	0.188	134.286	0.904
6	90	0.199	142.143	0.957
7	120	0.204	145.714	0.981
8	150	0.206	147.143	0.990
9	180	0.202	144.286	0.971
10	270	0.208	148.571	1.000
11	300	0.208	148.571	1.000
12	360	0.207	147.857	0.995
13	420	0.206	147.143	0.990
14	480	0.204	145.714	0.981
15	600	0.206	147.143	0.990
16	720	0.208	148.571	1.000

Appendix E.9: Hydraulic data from port 3,3.

Sample no.	Time (min)	Absorbance	C(t) (ppm)	F(t)
1	0	0.000	0.000	0.000
2	2	0.008	5.714	0.040
3	15	0.002	1.429	0.010
4	30	0.005	3.571	0.025
5	60	0.053	37.857	0.264
6	90	0.077	55.000	0.383
7	120	0.109	77.857	0.542
8	150	0.151	107.857	0.751
9	180	0.177	126.429	0.881
10	270	0.197	140.714	0.980
11	300	0.201	143.571	1.000
12	360	0.201	143.571	1.000
13	420	0.201	143.571	1.000
14	480	0.197	140.714	0.980
15	600	0.201	143.571	1.000
16	720	0.201	143.571	1.000

Appendix E.10: Hydraulic data from port 4,1.

Sample no.	Time (min)	Absorbance	C(t) (ppm)	F(t)
1	0	0.000	0.000	0.000
2	2	0.005	3.571	0.025
3	15	0.005	3.571	0.025
4	30	0.017	12.143	0.083
5	60	0.156	111.429	0.765
6	90	0.190	135.714	0.931
7	120	0.193	137.857	0.946
8	150	0.200	142.857	0.980
9	180	0.194	138.571	0.951
10	210	0.197	140.714	0.966
11	240	0.200	142.857	0.980
12	300	0.204	145.714	1.000
13	360	0.203	145.000	0.995
14	420	0.192	137.143	0.941
15	480	0.202	144.286	0.990
16	600	0.204	145.714	1.000
17	720	0.204	145.714	1.000

Appendix E.11: Hydraulic data from port 4,2.

Sample no.	Time (min)	Absorbance	C(t) (ppm)	F(t)
1	0	0.000	0.000	0.000
2	2	0.004	2.857	0.019
3	15	0.009	6.429	0.042
4	30	0.003	2.143	0.014
5	60	0.117	83.571	0.544
6	90	0.164	117.143	0.763
7	120	0.191	136.429	0.888
8	150	0.206	147.143	0.958
9	180	0.196	140.000	0.912
10	210	0.197	140.714	0.916
11	240	0.202	144.286	0.940
12	300	0.204	145.714	0.949
13	360	0.209	149.286	0.972
14	420	0.210	150.000	0.977
15	480	0.206	147.143	0.958
16	600	0.208	148.571	0.967
17	720	0.215	153.571	1.000

Appendix E.12: Hydraulic data from port 4,3.

Sample no.	Time (min)	Absorbance	C(t) (ppm)	F(t)
1	0	0.000	0.000	0.000
2	2	0.000	0.000	0.000
3	15	0.002	1.429	0.010
4	30	0.005	3.571	0.025
5	60	0.013	9.286	0.065
6	90	0.008	5.714	0.040
7	120	0.062	44.286	0.312
8	150	0.129	92.143	0.648
9	180	0.159	113.571	0.799
10	210	0.199	142.143	1.000
11	240	0.199	142.143	1.000
12	300	0.199	142.143	1.000
13	360	0.199	142.143	1.000
14	420	0.199	142.143	1.000
15	480	0.199	142.143	1.000
16	600	0.199	142.143	1.000
17	720	0.199	142.143	1.000

Appendix E.13: Hydraulic data from port 5,1.

Sample no.	Time (min)	Absorbance	C(t) (ppm)	F(t)
1	0	0.000	0.000	0.000
2	2	0.000	0.000	0.000
3	15	0.000	0.000	0.000
4	30	0.000	0.000	0.000
5	60	0.052	37.143	0.251
6	90	0.122	87.143	0.589
7	120	0.182	130.000	0.879
8	150	0.191	136.429	0.923
9	180	0.187	133.571	0.903
10	210	0.188	134.286	0.908
11	240	0.199	142.143	0.961
12	270	0.198	141.429	0.957
13	300	0.203	145.000	0.981
14	360	0.204	145.714	0.986
15	420	0.198	141.429	0.957
16	480	0.202	144.286	0.976
17	600	0.207	147.857	1.000
18	720	0.207	147.857	1.000

Appendix E.14: Hydraulic data from port 5,2.

Sample no.	Time (min)	Absorbance	C(t) (ppm)	F(t)
1	0	0.000	0.000	0.000
2	2	0.000	0.000	0.000
3	15	0.000	0.000	0.000
4	30	0.000	0.000	0.000
5	60	0.066	47.143	0.325
6	90	0.143	102.143	0.704
7	120	0.176	125.714	0.867
8	150	0.190	135.714	0.936
9	180	0.196	140.000	0.966
10	210	0.196	140.000	0.966
11	240	0.194	138.571	0.956
12	270	0.196	140.000	0.966
13	300	0.203	145.000	1.000
14	360	0.203	145.000	1.000
15	420	0.199	142.143	0.980
16	480	0.196	140.000	0.966
17	600	0.203	145.000	1.000
18	720	0.203	145.000	1.000

Appendix E.15: Hydraulic data from port 5,3.

Sample no.	Time (min)	Absorbance	C(t) (ppm)	F(t)
1	0	0.000	0.000	0.000
2	2	0.000	0.000	0.000
3	15	0.000	0.000	0.000
4	30	0.000	0.000	0.000
5	60	0.014	10.000	0.070
6	90	0.048	34.286	0.241
7	120	0.078	55.714	0.392
8	150	0.111	79.286	0.558
9	180	0.127	90.714	0.638
10	210	0.132	94.286	0.663
11	240	0.168	120.000	0.844
12	270	0.171	122.143	0.859
13	300	0.187	133.571	0.940
14	360	0.197	140.714	0.990
15	420	0.192	137.143	0.965
16	480	0.195	139.286	0.980
17	600	0.199	142.143	1.000
18	720	0.199	142.143	1.000

Appendix E.16: Hydraulic data from port 6,1.

Sample no.	Time (min)	Absorbance	C(t) (ppm)	F(t)
1	0	0.000	0.000	0.000
2	2	0.000	0.000	0.000
3	15	0.000	0.000	0.000
4	30	0.000	0.000	0.000
5	60	0.082	58.571	0.404
6	90	0.144	102.857	0.709
7	120	0.190	135.714	0.936
8	150	0.197	140.714	0.970
9	180	0.203	145.000	1.000
10	210	0.198	141.429	0.975
11	240	0.203	145.000	1.000
12	270	0.201	143.571	0.990
13	300	0.203	145.000	1.000
14	360	0.203	145.000	1.000
15	420	0.203	145.000	1.000
16	480	0.203	145.000	1.000
17	600	0.203	145.000	1.000
18	720	0.203	145.000	1.000

Appendix E.17: Hydraulic data from port 6,2.

Sample no.	Time (min)	Absorbance	C(t) (ppm)	F(t)
1	0	0.000	0.000	0.000
2	2	0.000	0.000	0.000
3	15	0.000	0.000	0.000
4	30	0.000	0.000	0.000
5	60	0.075	53.571	0.369
6	90	0.127	90.714	0.626
7	120	0.170	121.429	0.837
8	150	0.185	132.143	0.911
9	180	0.195	139.286	0.961
10	210	0.187	133.571	0.921
11	240	0.193	137.857	0.951
12	270	0.203	145.000	1.000
13	300	0.200	142.857	0.985
14	360	0.203	145.000	1.000
15	420	0.195	139.286	0.961
16	480	0.202	144.286	0.995
17	600	0.203	145.000	1.000
18	720	0.203	145.000	1.000

Appendix E.18: Hydraulic data from port 6,3.

Sample no.	Time (min)	Absorbance	C(t) (ppm)	F(t)
1	0	0.000	0.000	0.000
2	2	0.000	0.000	0.000
3	15	0.000	0.000	0.000
4	30	0.000	0.000	0.000
5	60	0.007	5.000	0.038
6	90	0.022	15.714	0.119
7	120	0.031	22.143	0.168
8	150	0.046	32.857	0.249
9	180	0.071	50.714	0.384
10	210	0.068	48.571	0.368
11	240	0.085	60.714	0.459
12	270	0.104	74.286	0.562
13	300	0.129	92.143	0.697
14	360	0.167	119.286	0.903
15	420	0.184	131.429	0.995
16	480	0.185	132.143	1.000
17	600	0.185	132.143	1.000
18	720	0.185	132.143	1.000

Appendix E.19: Hydraulic data from port 7,1.

Sample no.	Time (min)	Absorbance	C(t) (ppm)	F(t)
1	0	0.000	0.000	0.000
2	2	0.000	0.000	0.000
3	15	0.000	0.000	0.000
4	30	0.000	0.000	0.000
5	60	0.008	5.714	0.040
6	90	0.053	37.857	0.268
7	120	0.153	109.286	0.773
8	150	0.180	128.571	0.909
9	180	0.187	133.571	0.944
10	210	0.184	131.429	0.929
11	240	0.184	131.429	0.929
12	270	0.188	134.286	0.949
13	300	0.184	131.429	0.929
14	330	0.189	135.000	0.955
15	360	0.189	135.000	0.955
16	420	0.189	135.000	0.955
17	480	0.194	138.571	0.980
18	600	0.198	141.429	1.000
19	720	0.198	141.429	1.000

Appendix E.20: Hydraulic data from port 7,2.

Sample no.	Time (min)	Absorbance	C(t) (ppm)	F(t)
1	0	0.000	0.000	0.000
2	2	0.000	0.000	0.000
3	15	0.000	0.000	0.000
4	30	0.000	0.000	0.000
5	60	0.001	0.714	0.005
6	90	0.002	1.429	0.010
7	120	0.018	12.857	0.090
8	150	0.124	88.571	0.620
9	180	0.166	118.571	0.830
10	210	0.183	130.714	0.915
11	240	0.200	142.857	1.000
12	270	0.193	137.857	0.965
13	300	0.193	137.857	0.965
14	330	0.194	138.571	0.970
15	360	0.200	142.857	1.000
16	420	0.200	142.857	1.000
17	480	0.200	142.857	1.000
18	600	0.200	142.857	1.000
19	720	0.200	142.857	1.000

Appendix E.21: Hydraulic data from port 7,3.

Sample no.	Time (min)	Absorbance	C(t) (ppm)	F(t)
1	0	0.000	0.000	0.000
2	2	0.000	0.000	0.000
3	15	0.000	0.000	0.000
4	30	0.000	0.000	0.000
5	60	0.001	0.714	0.005
6	90	0.001	0.714	0.005
7	120	0.008	5.714	0.042
8	150	0.018	12.857	0.094
9	180	0.040	28.571	0.209
10	210	0.064	45.714	0.335
11	240	0.139	99.286	0.728
12	270	0.162	115.714	0.848
13	300	0.177	126.429	0.927
14	330	0.181	129.286	0.948
15	360	0.191	136.429	1.000
16	420	0.191	136.429	1.000
17	480	0.191	136.429	1.000
18	600	0.191	136.429	1.000
19	720	0.191	136.429	1.000

Appendix E.22: Hydraulic data from port 8,1.

Sample no.	Time (min)	Absorbance	C(t) (ppm)	F(t)
1	0	0.000	0.000	0.000
2	2	0.000	0.000	0.000
3	15	0.000	0.000	0.000
4	30	0.000	0.000	0.000
5	60	0.000	0.000	0.000
6	90	0.010	7.143	0.050
7	120	0.046	32.857	0.229
8	150	0.125	89.286	0.622
9	180	0.176	125.714	0.876
10	210	0.183	130.714	0.910
11	240	0.201	143.571	1.000
12	270	0.187	133.571	0.930
13	300	0.186	132.857	0.925
14	330	0.176	125.714	0.876
15	360	0.180	128.571	0.896
16	420	0.183	130.714	0.910
17	480	0.190	135.714	0.945
18	540	0.198	141.429	0.985
19	600	0.195	139.286	0.970
20	720	0.201	143.571	1.000

Appendix E.23: Hydraulic data from port 8,2.

Sample no.	Time (min)	Absorbance	C(t) (ppm)	F(t)
1	0	0.000	0.000	0.000
2	2	0.000	0.000	0.000
3	15	0.000	0.000	0.000
4	30	0.000	0.000	0.000
5	60	0.000	0.000	0.000
6	90	0.004	2.857	0.020
7	120	0.039	27.857	0.199
8	150	0.081	57.857	0.413
9	180	0.135	96.429	0.689
10	210	0.149	106.429	0.760
11	240	0.177	126.429	0.903
12	270	0.184	131.429	0.939
13	300	0.190	135.714	0.969
14	330	0.191	136.429	0.974
15	360	0.183	130.714	0.934
16	420	0.195	139.286	0.995
17	480	0.196	140.000	1.000
18	540	0.196	140.000	1.000
19	600	0.196	140.000	1.000
20	720	0.196	140.000	1.000

Appendix E.24: Hydraulic data from port 8,3.

Sample no.	Time (min)	Absorbance	C(t) (ppm)	F(t)
1	0	0.000	0.000	0.000
2	2	0.000	0.000	0.000
3	15	0.000	0.000	0.000
4	30	0.000	0.000	0.000
5	60	0.000	0.000	0.000
6	90	0.005	3.571	0.027
7	120	0.023	16.429	0.126
8	150	0.049	35.000	0.269
9	180	0.084	60.000	0.462
10	210	0.110	78.571	0.604
11	240	0.111	79.286	0.610
12	270	0.125	89.286	0.687
13	300	0.130	92.857	0.714
14	330	0.132	94.286	0.725
15	360	0.150	107.143	0.824
16	420	0.153	109.286	0.841
17	480	0.163	116.429	0.896
18	540	0.178	127.143	0.978
19	600	0.177	126.429	0.973
20	720	0.182	130.000	1.000

Appendix E.25: Hydraulic data from port 9,1.

Sample no.	Time (min)	Absorbance	C(t) (ppm)	F(t)
1	0	0.000	0.000	0.000
2	2	0.000	0.000	0.000
3	15	0.000	0.000	0.000
4	30	0.000	0.000	0.000
5	60	0.000	0.000	0.000
6	90	0.016	11.429	0.080
7	120	0.126	90.000	0.627
8	150	0.154	110.000	0.766
9	180	0.179	127.857	0.891
10	210	0.191	136.429	0.950
11	240	0.198	141.429	0.985
12	270	0.190	135.714	0.945
13	300	0.186	132.857	0.925
14	330	0.190	135.714	0.945
15	360	0.189	135.000	0.940
16	420	0.189	135.000	0.940
17	480	0.196	140.000	0.975
18	540	0.201	143.571	1.000
19	600	0.201	143.571	1.000
20	720	0.201	143.571	1.000

Appendix E.26: Hydraulic data from port 9,2.

Sample no.	Time (min)	Absorbance	C(t) (ppm)	F(t)
1	0	0.000	0.000	0.000
2	2	0.000	0.000	0.000
3	15	0.000	0.000	0.000
4	30	0.000	0.000	0.000
5	60	0.000	0.000	0.000
6	90	0.012	8.571	0.058
7	120	0.087	62.143	0.420
8	150	0.132	94.286	0.638
9	180	0.165	117.857	0.797
10	210	0.171	122.143	0.826
11	240	0.175	125.000	0.845
12	270	0.187	133.571	0.903
13	300	0.188	134.286	0.908
14	330	0.181	129.286	0.874
15	360	0.191	136.429	0.923
16	420	0.192	137.143	0.928
17	480	0.195	139.286	0.942
18	540	0.204	145.714	0.986
19	600	0.199	142.143	0.961
20	720	0.207	147.857	1.000

Appendix E.27: Hydraulic data from port 9,3.

Sample no.	Time (min)	Absorbance	C(t) (ppm)	F(t)
1	0	0.000	0.000	0.000
2	2	0.000	0.000	0.000
3	15	0.000	0.000	0.000
4	30	0.000	0.000	0.000
5	60	0.000	0.000	0.000
6	90	0.012	8.571	0.061
7	120	0.048	34.286	0.242
8	150	0.041	29.286	0.207
9	180	0.043	30.714	0.217
10	210	0.051	36.429	0.258
11	240	0.058	41.429	0.293
12	270	0.070	50.000	0.354
13	300	0.131	93.571	0.662
14	330	0.116	82.857	0.586
15	360	0.127	90.714	0.641
16	420	0.154	110.000	0.778
17	480	0.170	121.429	0.859
18	540	0.190	135.714	0.960
19	600	0.185	132.143	0.934
20	720	0.198	141.429	1.000

Appendix E.28: Hydraulic data from port 10,1.

Sample no.	Time (min)	Absorbance	C(t) (ppm)	F(t)
1	0	0.000	0.000	0.000
2	2	0.000	0.000	0.000
3	15	0.000	0.000	0.000
4	30	0.000	0.000	0.000
5	60	0.000	0.000	0.000
6	90	0.000	0.000	0.000
7	120	0.016	11.429	0.079
8	150	0.109	77.857	0.540
9	180	0.158	112.857	0.782
10	210	0.183	130.714	0.906
11	240	0.181	129.286	0.896
12	270	0.182	130.000	0.901
13	300	0.174	124.286	0.861
14	330	0.176	125.714	0.871
15	360	0.179	127.857	0.886
16	390	0.183	130.714	0.906
17	420	0.186	132.857	0.921
18	480	0.194	138.571	0.960
19	540	0.196	140.000	0.970
20	600	0.193	137.857	0.955
21	720	0.202	144.286	1.000

Appendix E.29: Hydraulic data from port 10,2.

Sample no.	Time (min)	Absorbance	C(t) (ppm)	F(t)
1	0	0.000	0.000	0.000
2	2	0.000	0.000	0.000
3	15	0.000	0.000	0.000
4	30	0.000	0.000	0.000
5	60	0.000	0.000	0.000
6	90	0.000	0.000	0.000
7	120	0.009	6.429	0.045
8	150	0.073	52.143	0.367
9	180	0.136	97.143	0.683
10	210	0.164	117.143	0.824
11	240	0.177	126.429	0.889
12	270	0.183	130.714	0.920
13	300	0.186	132.857	0.935
14	330	0.185	132.143	0.930
15	360	0.193	137.857	0.970
16	390	0.199	142.143	1.000
17	420	0.199	142.143	1.000
18	480	0.192	137.143	0.965
19	540	0.195	139.286	0.980
20	600	0.199	142.143	1.000
21	720	0.199	142.143	1.000

Appendix E.30: Hydraulic data from port 10,3.

Sample no.	Time (min)	Absorbance	C(t) (ppm)	F(t)
1	0	0.000	0.000	0.000
2	2	0.000	0.000	0.000
3	15	0.000	0.000	0.000
4	30	0.000	0.000	0.000
5	60	0.000	0.000	0.000
6	90	0.000	0.000	0.000
7	120	0.000	0.000	0.000
8	150	0.008	5.714	0.042
9	180	0.011	7.857	0.057
10	210	0.022	15.714	0.115
11	240	0.057	40.714	0.297
12	270	0.133	95.000	0.693
13	300	0.122	87.143	0.635
14	330	0.137	97.857	0.714
15	360	0.163	116.429	0.849
16	390	0.166	118.571	0.865
17	420	0.186	132.857	0.969
18	480	0.192	137.143	1.000
19	540	0.192	137.143	1.000
20	600	0.191	136.429	0.995
21	720	0.192	137.143	1.000

Appendix E.31: Hydraulic data from port 11,1.

Sample no.	Time (min)	Absorbance	C(t) (ppm)	F(t)
1	0	0.000	0.000	0.000
2	2	0.000	0.000	0.000
3	15	0.000	0.000	0.000
4	30	0.000	0.000	0.000
5	60	0.000	0.000	0.000
6	90	0.000	0.000	0.000
7	120	0.000	0.000	0.000
8	150	0.009	6.429	0.046
9	180	0.044	31.429	0.227
10	210	0.109	77.857	0.562
11	240	0.153	109.286	0.789
12	270	0.167	119.286	0.861
13	300	0.177	126.429	0.912
14	330	0.177	126.429	0.912
15	360	0.174	124.286	0.897
16	390	0.173	123.571	0.892
17	420	0.171	122.143	0.881
18	480	0.187	133.571	0.964
19	540	0.187	133.571	0.964
20	600	0.186	132.857	0.959
21	720	0.194	138.571	1.000

Appendix E.32: Hydraulic data from port 11,2.

Sample no.	Time (min)	Absorbance	C(t) (ppm)	F(t)
1	0	0.000	0.000	0.000
2	2	0.000	0.000	0.000
3	15	0.000	0.000	0.000
4	30	0.000	0.000	0.000
5	60	0.000	0.000	0.000
6	90	0.000	0.000	0.000
7	120	0.000	0.000	0.000
8	150	0.022	15.714	0.115
9	180	0.072	51.429	0.375
10	210	0.126	90.000	0.656
11	240	0.163	116.429	0.849
12	270	0.164	117.143	0.854
13	300	0.172	122.857	0.896
14	330	0.171	122.143	0.891
15	360	0.181	129.286	0.943
16	390	0.177	126.429	0.922
17	420	0.188	134.286	0.979
18	480	0.192	137.143	1.000
19	540	0.192	137.143	1.000
20	600	0.192	137.143	1.000
21	720	0.192	137.143	1.000

Appendix E.33: Hydraulic data from port 11,3.

Sample no.	Time (min)	Absorbance	C(t) (ppm)	F(t)
1	0	0.000	0.000	0.000
2	2	0.000	0.000	0.000
3	15	0.000	0.000	0.000
4	30	0.000	0.000	0.000
5	60	0.000	0.000	0.000
6	90	0.000	0.000	0.000
7	120	0.000	0.000	0.000
8	150	0.011	7.857	0.062
9	180	0.043	30.714	0.243
10	210	0.064	45.714	0.362
11	240	0.094	67.143	0.531
12	270	0.115	82.143	0.650
13	300	0.119	85.000	0.672
14	330	0.118	84.286	0.667
15	360	0.129	92.143	0.729
16	390	0.136	97.143	0.768
17	420	0.153	109.286	0.864
18	480	0.167	119.286	0.944
19	540	0.177	126.429	1.000
20	600	0.174	124.286	0.983
21	720	0.177	126.429	1.000

Appendix E.34: Hydraulic data from port 12,1.

Sample no.	Time (min)	Absorbance	C(t) (ppm)	F(t)
1	0	0.000	0.000	0.000
2	2	0.000	0.000	0.000
3	15	0.000	0.000	0.000
4	30	0.000	0.000	0.000
5	60	0.000	0.000	0.000
6	90	0.000	0.000	0.000
7	120	0.000	0.000	0.000
8	150	0.023	16.429	0.117
9	180	0.091	65.000	0.464
10	210	0.127	90.714	0.648
11	240	0.142	101.429	0.724
12	270	0.155	110.714	0.791
13	300	0.158	112.857	0.806
14	330	0.161	115.000	0.821
15	360	0.166	118.571	0.847
16	390	0.169	120.714	0.862
17	420	0.184	131.429	0.939
18	480	0.187	133.571	0.954
19	540	0.192	137.143	0.980
20	600	0.192	137.143	0.980
21	720	0.196	140.000	1.000

Appendix E.35: Hydraulic data from port 12,2.

Sample no.	Time (min)	Absorbance	C(t) (ppm)	F(t)
1	0	0.000	0.000	0.000
2	2	0.000	0.000	0.000
3	15	0.000	0.000	0.000
4	30	0.000	0.000	0.000
5	60	0.000	0.000	0.000
6	90	0.000	0.000	0.000
7	120	0.000	0.000	0.000
8	150	0.038	27.143	0.201
9	180	0.107	76.429	0.566
10	210	0.131	93.571	0.693
11	240	0.160	114.286	0.847
12	270	0.169	120.714	0.894
13	300	0.177	126.429	0.937
14	330	0.170	121.429	0.899
15	360	0.187	133.571	0.989
16	390	0.189	135.000	1.000
17	420	0.189	135.000	1.000
18	480	0.189	135.000	1.000
19	540	0.189	135.000	1.000
20	600	0.189	135.000	1.000
21	720	0.189	135.000	1.000

Appendix E.36: Hydraulic data from port 12,3.

Sample no.	Time (min)	Absorbance	C(t) (ppm)	F(t)
1	0	0.000	0.000	0.000
2	2	0.000	0.000	0.000
3	15	0.000	0.000	0.000
4	30	0.000	0.000	0.000
5	60	0.000	0.000	0.000
6	90	0.000	0.000	0.000
7	120	0.000	0.000	0.000
8	150	0.037	26.429	0.185
9	180	0.035	25.000	0.175
10	210	0.050	35.714	0.250
11	240	0.052	37.143	0.260
12	270	0.064	45.714	0.320
13	300	0.095	67.857	0.475
14	330	0.096	68.571	0.480
15	360	0.123	87.857	0.615
16	390	0.135	96.429	0.675
17	420	0.172	122.857	0.860
18	480	0.174	124.286	0.870
19	540	0.189	135.000	0.945
20	600	0.187	133.571	0.935
21	720	0.200	142.857	1.000

Appendix E.37: Hydraulic data from port 13,1.

Sample no.	Time (min)	Absorbance	C(t) (ppm)	F(t)
1	0	0.000	0.000	0.000
2	2	0.000	0.000	0.000
3	15	0.000	0.000	0.000
4	30	0.000	0.000	0.000
5	60	0.000	0.000	0.000
6	90	0.000	0.000	0.000
7	120	0.000	0.000	0.000
8	150	0.009	6.429	0.047
9	180	0.036	25.714	0.189
10	210	0.082	58.571	0.432
11	240	0.139	99.286	0.732
12	270	0.156	111.429	0.821
13	300	0.166	118.571	0.874
14	330	0.158	112.857	0.832
15	360	0.167	119.286	0.879
16	390	0.170	121.429	0.895
17	420	0.171	122.143	0.900
18	480	0.173	123.571	0.911
19	540	0.173	123.571	0.911
20	600	0.179	127.857	0.942
21	720	0.190	135.714	1.000

Appendix E.38: Hydraulic data from port 13,2.

Sample no.	Time (min)	Absorbance	C(t) (ppm)	F(t)
1	0	0.000	0.000	0.000
2	2	0.000	0.000	0.000
3	15	0.000	0.000	0.000
4	30	0.000	0.000	0.000
5	60	0.000	0.000	0.000
6	90	0.000	0.000	0.000
7	120	0.000	0.000	0.000
8	150	0.012	8.571	0.061
9	180	0.070	50.000	0.357
10	210	0.112	80.000	0.571
11	240	0.158	112.857	0.806
12	270	0.163	116.429	0.832
13	300	0.178	127.143	0.908
14	330	0.183	130.714	0.934
15	360	0.178	127.143	0.908
16	390	0.184	131.429	0.939
17	420	0.180	128.571	0.918
18	480	0.192	137.143	0.980
19	540	0.192	137.143	0.980
20	600	0.185	132.143	0.944
21	720	0.196	140.000	1.000

Appendix E.39: Hydraulic data from port 13,3.

Sample no.	Time (min)	Absorbance	C(t) (ppm)	F(t)
1	0	0.000	0.000	0.000
2	2	0.000	0.000	0.000
3	15	0.000	0.000	0.000
4	30	0.000	0.000	0.000
5	60	0.000	0.000	0.000
6	90	0.000	0.000	0.000
7	120	0.000	0.000	0.000
8	150	0.004	2.857	0.021
9	180	0.016	11.429	0.086
10	210	0.014	10.000	0.075
11	240	0.119	85.000	0.636
12	270	0.060	42.857	0.321
13	300	0.091	65.000	0.487
14	330	0.103	73.571	0.551
15	360	0.128	91.429	0.684
16	390	0.139	99.286	0.743
17	420	0.158	112.857	0.845
18	480	0.167	119.286	0.893
19	540	0.184	131.429	0.984
20	600	0.187	133.571	1.000
21	720	0.187	133.571	1.000

Appendix E.40: Hydraulic data from port 14.

Sample no.	Time (min)	Absorbance	C(t) (ppm)	F(t)
1	0	0	0	0
2	2	0	0	0
3	30	0.008	5.714285714	0.041450777
4	60	0.002	1.428571429	0.010362694
5	90	0.004	2.857142857	0.020725389
6	120	0.002	1.428571429	0.010362694
7	150	0.007	5	0.03626943
8	180	0.026	18.57142857	0.134715026
9	210	0.055	39.28571429	0.284974093
10	240	0.103	73.57142857	0.533678756
11	270	0.143	102.1428571	0.740932642
12	300	0.141	100.7142857	0.730569948
13	330	0.141	100.7142857	0.730569948
14	360	0.155	110.7142857	0.803108808
15	390	0.16	114.2857143	0.829015544
16	420	0.166	118.5714286	0.860103627
17	480	0.175	125	0.906735751
18	540	0.184	131.4285714	0.953367876
19	600	0.186	132.8571429	0.96373057
20	720	0.193	137.8571429	1

Appendix F: Hydraulic data from heat and chemical tracer experiment on unplanted laboratory-scale HSSF CW.

Appendix F.1: Hydraulic data from heat tracer

Time (min)	Inlet (deg C)	Outlet (deg C)	Delta T_{out}	$F(t)=deltaT_{out}/deltaT_{out,max}$
0		26.0	0.0	0.000
2		26.0	0.0	0.000
4		26.0	0.0	0.000
6		26.2	0.0	0.000
8		28.9	2.9	0.103
10	51.5	32.8	6.8	0.241
12	52.6	36.1	10.1	0.358
14	53.1	38.3	12.3	0.436
16	53.6	40.2	14.2	0.504
18	53.6	41.9	15.9	0.564
20	54.3	43.5	17.5	0.621
22	53.8	44.9	18.9	0.670
24	53.7	46.0	20.0	0.709
26	54.0	47.1	21.1	0.748
28	54.3	48.0	22.0	0.780
30	54.8	48.7	22.7	0.805
32	54.8	49.4	23.4	0.830
34	54.7	50.0	24.0	0.851
36	54.5	50.5	24.5	0.869
38	54.9	51.0	25.0	0.887
40	54.8	51.4	25.4	0.901
42	54.6	51.8	25.8	0.915
44	54.5	52.0	26.0	0.922
46	55.2	52.2	26.2	0.929
48	55.0	52.4	26.4	0.936
50	55.3	52.5	26.5	0.940
52	55.1	52.7	26.7	0.947
54	55.3	52.7	26.7	0.947
56	55.4	52.8	26.8	0.950
58	54.5	52.9	26.9	0.954
60	54.4	53.0	27.0	0.958
62	53.4	53.1	27.1	0.961
64	51.8	53.1	27.1	0.961

Appendix F.2: Hydraulic data from chemical tracer

Time (min)	Absorbance	C(t) (ppm)	F(t)
0	0.005	3.571	0.016
2	0.006	4.286	0.020
4	0.002	1.429	0.007
6	0.066	47.143	0.216
8	0.144	102.857	0.472
10	0.188	134.286	0.616
12	0.214	152.857	0.702
14	0.232	165.714	0.761
16	0.235	167.857	0.770
18	0.251	179.286	0.823
20	0.260	185.714	0.852
22	0.266	190.000	0.872
24	0.267	190.714	0.875
26	0.278	198.571	0.911
28	0.280	200.000	0.918
30	0.284	202.857	0.931
32	0.289	206.429	0.948
34	0.291	207.857	0.954
36	0.288	205.714	0.944
38	0.295	210.714	0.967
40	0.294	210.000	0.964
42	0.294	210.000	0.964
44	0.290	207.143	0.951
46	0.296	211.429	0.970
48	0.293	209.286	0.961
50	0.298	212.857	0.977
52	0.297	212.143	0.974
54	0.302	215.714	0.990
56	0.298	212.857	0.977
58	0.299	213.571	0.980
60	0.299	213.571	0.980
62	0.299	213.571	0.980
64	0.301	215.000	0.987
Inlet	0.305	217.857	